Juan Luis Bernal Wormull

The speleothem record of Ostolo and mewdukilo caves (Navarra, NE Spain): Present day cave dynamics and paleoclimatic reconstruction since las deglaciation

Director/es
Moreno Caballud, Ana

Universidad
Zaragoza
1542

Tesis Doctoral

THE SPELEOTHEM RECORD OF OSTOLO AND MEWDUKILO CAVES (NAVARRA, NE SPAIN): PRESENT DAY CAVE DYNAMICS AND PALEOCLIMATIC RECONSTRUCTION SINCE LAS DEGLACIATION
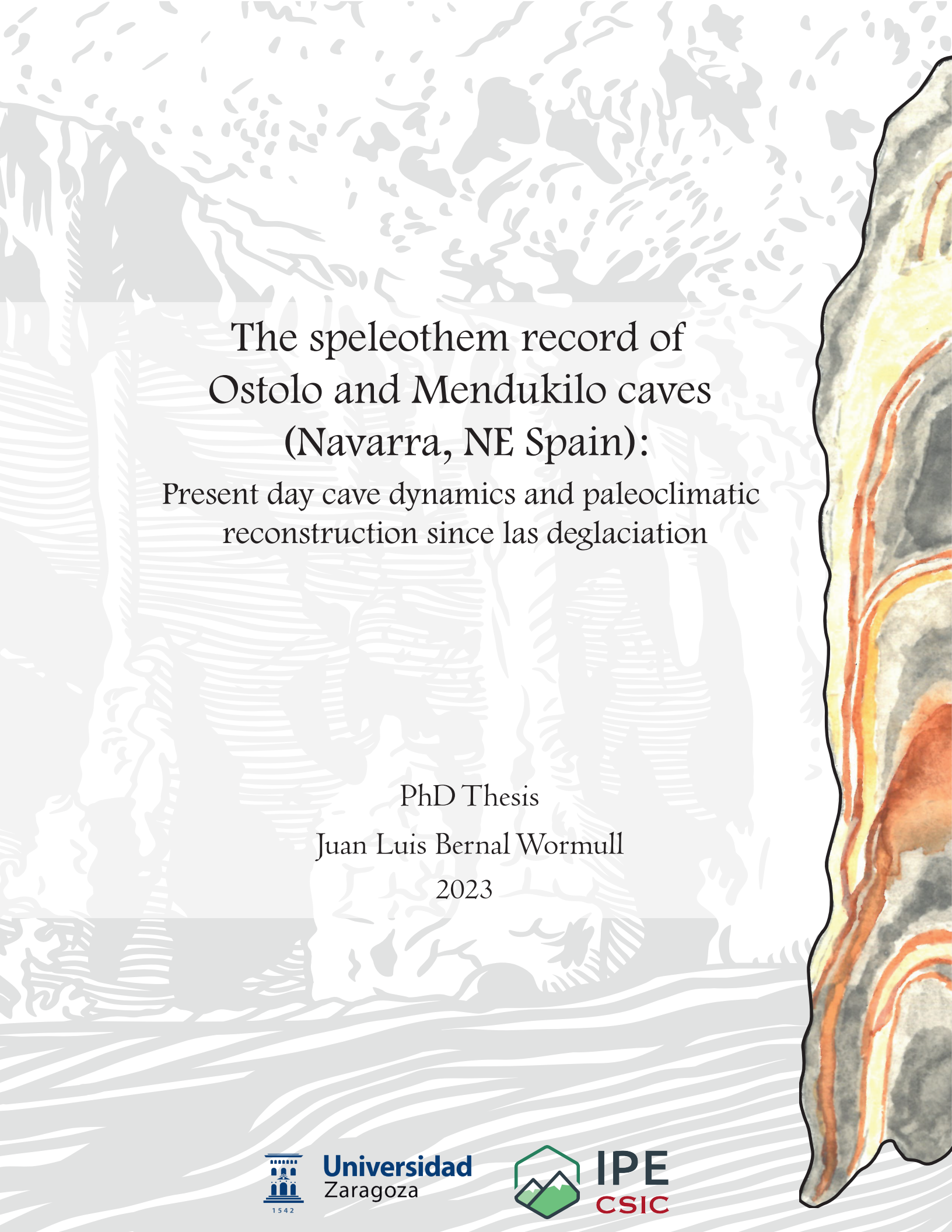
Autor

Juan Luis Bernal Wormull

Director/es

Moreno Caballud, Ana

UNIVERSIDAD DE ZARAGOZA
Escuela de Doctorado

Programa de Doctorado en Geología

2023

The speleothem record of Ostolo and Mendukilo caves (Navarra, NE Spain):

Present day cave dynamics and paleoclimatic reconstruction since las deglaciation

PhD Thesis

Juan Luis Bernal Wormull

2023

Universidad Zaragoza

IPE CSIC

UNIVERSIDAD DE ZARAGOZA

PhD DISSERTATION

The speleothem record of Ostolo

and Mendukilo caves (Navarra, NE Spain):

Present day cave dynamics and paleoclimatic

reconstruction since the last deglaciation

Author: Juan Luis Bernal Wormull

Supervisor: Ana Moreno Caballud (Instituto Pirenaico de Ecología-CSIC)
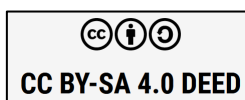
Tutor: Cinta Osácar (Universidad de Zaragoza)

The speleothem record of Ostolo and Mendukilo caves (Navarra, NE Spain): Present day cave dynamics and paleoclimatic reconstruction since the last deglaciation

Tesis doctoral defendida por Juan Luis Bernal-Wormull dentro del programa de doctorado en Geología, y dirigida por Ana Moreno Caballud (IPE-CSIC).

Grupo de Paleoambientes Cuaternarios
Departamento de Procesos Geoambientales
y Cambio Global
Instituto Pirenaico de Ecología (IPE-CSIC)
Consejo Superior de investigaciones Científicas
Avda. Montañana 1005 CP 50050
Zaragoza-España

La doctora Ana Moreno Caballud, con DNI 73200233D, investigadora del Instituto Pirenaico de Ecología (IPE-CSIC), en calidad de directora de la tesis de doctorado de Juan Luis Bernal Wormull.

Certifica:

Que Juan Luis Bernal Wormull, con NIE Y4930378C, ha realizado bajo mi dirección el trabajo que, para optar al grado de Doctor en Geología, presenta con el título:

"The speleothem record of Ostolo and Mendukilo caves (Navarra, NE Spain): Present day cave dynamics and paleoclimatic reconstruction since the last deglaciation".

Que el trabajo constituye un avance científico inédito y significativo en la temática tratada, cumple con los requisitos necesarios y se ajusta a los objetivos establecidos en el Plan de Investigación aprobado por la Comisión Académica del programa de Doctorado en Geología.

Y para que así conste, firmo la presente Certificación en Zaragoza el 10 de Octubre de 2023 para los efectos que sean oportunos.

Dra. Ana Moreno Caballud

Agradecimientos

"I wanted to tell everyone that without the support of all of you, this thesis would not have existed. It is true that people did not have much faith in me, but I believe that in life nothing is impossible hueón, not one hueá, nothing hueón." - Modified inspirational phrase from N. Massu (2009), during the Davis Cup series in which the Chilean team faced Austria.

––––––––––

Cierro aquí esta gran etapa de cinco años de mi vida en la cual la superación y el agotamiento se entremezclan. Quiero empezar agradeciendo a mi supervisora Ana Moreno quien me ha acompañado y ha sido imprescindible en este largo camino, aportando toda la ayuda necesaria (y más) para llevar a cabo cada uno de los complicados pasos durante la tesis. Gracias por la confianza, la paciencia y por lo que hemos aprendido juntos a lo largo de estos últimos años. Gracias también a Cinta Osacar, mi tutora de parte de la universidad y que siempre me ha ayudado en todo lo posible. Me gustaría también dar unas pequeñas palabras de agradecimiento a Carlos Sancho, quien me acompaño como tutor en los primeros pasos de este camino, siempre fue muy atento con mi tema de estudios y que hoy ya no está con nosotros. Quisiera extender este importante agradecimiento a toda la gente que conforma (o han conformado) al grupo Paleo-IPE del Instituto Pirenaico de Ecología, en donde hay gente con una calidad humana entrañable, los cuales me apoyaron y ayudaron durante todos estos años. Agradecer a Jana, Ixeia, Miguel Bartolomé, Carlos, Reyes, Graciela, Penélope, Blas, Elena, Jorge, Marcel, Miguel Sevilla, María, Iván, Raquel, Inés, Josu. A los recién llegados a este grupo (Irene, Javi, Kilian), mucho ánimo y que sepan que están en buenas manos. Dentro de las grandes personas que he conocido en Paleo-IPE me gustaría destacar a Héctor Romanos que fue un gran amigo y compañero. No hay día trabajando en su ex despacho que no recuerde los grandiosos días de amistad que vivimos juntos, salud al viento hermano.

Durante el trabajo de campo me gustaría agradecer a Martin Arriolabengoa, siempre dispuesto a colaborar y animado de ir a las cuevas. Sin él, ninguno de los innumerables trabajos de campo en las cuevas de Mendukilo y Ostolo podrían haberse llevado cabo. Fueron muchos días de exploración, muestreo y monitorización de los cuales aprendí muchísimo. ¡Muchas gracias, Martín! También agradecer a todas las otras personas que me ayudaron muchísimo en el campo y que fueron claves para conocer bien ambas cuevas: E. Iriarte; I. Altzuri; K. Sanchez; M. Larburu; A. Govillar.

Gracias Eneko y Arantza por recibirme en sus respectivas universidades (Universidad de Burgos y Universidad del País Vasco respectivamente) y ayudarme con las descripciones

i

petrográficas e isotópicas en las estalagmitas de ambas cuevas investigadas en esta tesis. Isa muchas gracias por la gran ayuda al debatir los artículos y la disposición de ayudar con análisis en las estalagmitas de Mendukilo en la Universidad de Barcelona. En la ayuda con los muestreos y sus respectivos análisis, me gustaría agradecer nuevamente a Ana, Miguel y Carlos, gracias a su experiencia y enseñanza pudimos entre todos obtener, y posteriormente analizar, miles y miles de muestras. Agradecido de Heather Stoll por la ayuda en el análisis de muestras de elementos traza y su disposición en la revisión de manuscritos sobre las estalagmitas de esta tesis. Thanks to Christoph Spötl and Yuri Dublyansky from the University of Innsbruck for offering me the possibility to use the laboratory of stable isotopes and fluid inclusions to run part of my samples. Likewise, thanks to Manuela, Charlotte, Gabriella, Gina, and Paul for helping me there. Likewise, I am in debt to Larry Edwards and to those I met at the University of Minnesota. Thank you so much for offering me the opportunity to work in your laboratory and other facilities. Many thanks to Hai Cheng and associates at Xi'an Jiaotong University for their help in receiving and dating several carbonate samples used in this thesis.

Jana muchas gracias por el apoyo mutuo que tuvimos durante estos años escribiendo la tesis, sin ti este proceso hubiera sido mucho más difícil de llevar. Un abrazo y gracias a Andrea, una persona muy fuerte y con quien salimos muchas veces fuera del instituto junto a Héctor. Ha sido increíble compartir esta fase de mi vida en Zaragoza con toda la demás gente del IPE: Fergus (un abrazo a María también), Dani (un abrazo a Ana igualmente), Clara, Ana Foronda, Natalia, Iván, Mónica, Pacho, Makki, Esteban, Fernando, Antonio, Melani, Alberto, Javi Fregola, Carmelo, Jesús, Xavi, Marta, César, Benito, Aurora, Félix, Héctor, María, Rodrigo, Francesco, Francesca, Alessandro, algún Javi o Xavi que me dejo, a todos los que han llegado hace poco y a los que se me ha pasado agregar aquí. Espero que nunca olviden mis enseñanzas haciendo parkour/balconing por Olite, los piscosours y que la dosis para empezar la fiesta siempre es con 2 chupitos y un cubata, lo básico. Nunca olvidare todos los juepinchos y el tour de bares rutinario por la ciudad. Los mejores antros donde compartí más de una vez con estos seres del averno son, fueron y serán: La Z, El Zorro (Q.E.P.D.), La Casa Magnética, La López y La Cucaracha. Nunca los olvidare.

También agradecer a todas las personas con las que he compartido piso en Zaragoza y con quienes me han dado grandes momentos para recordar en estos últimos 5 años: Alberto, Fran, Isa, Víctor, Elena, Melissa, Dia. Muchas gracias por la compañía. I will never forget my two-month stay in Minnesota. Thank you very much Laurie and Phyllis for hosting me and taking me to see beautiful things inside and outside the city. The state fair was crazy! I had never eaten that much in a single day, and the beers there were incredible.

Agradecer a la federación aragonesa de espeleología y a toda la gente que formo parte de los cursos de iniciación y formación en la disciplina. Me la pase muy bien durante los cursos, los chupitos de pacharán y lo aprendido en espeleología no se me olvidara nunca. Espero poder de

alguna forma retribuir con estos conocimientos en mi país en el futuro. Un fuerte agradecimiento a todos los chilenos (o los que se sienten así) por Zaragoza, dando la pelea y representando de la manera correcta el sueño de un Chile mejor (justo) que tenemos todos.

Un fuerte abrazo a mi familia en Chile, que siempre se acuerdan de mí y que me han apoyado en este proyecto de estudiar en el extranjero durante tantos años. A mi madre y mis dos hermanos, lo siento por tantos años de ausencia y gracias por el apoyo incondicional. Solo he de decirles que ha valido la pena en mi formación profesional y para crecer mucho como persona. A todos mis amigos en Chile muchísimas gracias: Tomas, Pedro, Nacho, Saimon, Ñafe. Nunca olvidare las partidas de Smash y las noches de vicio en el Tibia, sobre todo durante las trasnochadas de la pandemia. A los demás excompañeres de mi curso del colegio también muchas gracias y que sepan que les extraño a todes mucho. A mis amigis que ahora están en España muchísimas gracias por todo lo que compartimos por Barcelona o Madrid: Rorro, Joaquín y Sofí.

Mi más sentido agradecimiento a la Feña. Fuera de toda la gente del IPE, ella es la que más me acompaño (no solo durante estos 5 años de tesis) y que siempre me apoyo (aunque mucho de ese tiempo fue a la distancia) durante la tesis. Que buenos momentos pasamos viviendo juntos aquí en Zaragoza, viendo animes (no sé cuántos nos vimos juntos en 2022, pero yo este 2023 llevo 73 en total), comiendo papitas y pasando calores/fríos extremos (Ciudad qlia). Es con ella con quien me siento yo mismo y espero que podamos seguir sobrellevando las dificultades y alegrías de la vida misma por más tiempo. *Aishiteru*

Abstract

Reconstructing past climate variations from cave speleothems has roots in a major challenge we face as a society today: the current climate emergency. While there is scientific consensus regarding the anthropogenic origin of global warming, sizeable uncertainties persist concerning the potential impacts of increasing temperatures on our planet and society. The investigation of past climatic changes, particularly those that occurred quickly, such as glacial terminations and Holocene rapid climate changes, provides the most appropriate means of obtaining climate scenario data analogous to our current climatic state.

This Thesis specifically addresses the study of the Ostolo and Mendukilo caves (Navarra, NE Spain) with a focus on comprehending the present cave dynamics and reconstructing the paleoclimatic conditions since the last deglaciation, based on a multi-proxy analysis of their speleothems. Ostolo (248 m above sea level) and Mendukilo (750 m above sea level) caves are found in the easternmost region of the Cantabrian Mountain range (Basque Mountains) in the Western Pyrenees near the Cantabrian coast. Ostolo cave is 631 m long, with a vertical extent of 39 m, and has a single entrance formed by a narrow passage (approximately 0.5 – 1 m wide) that is permanently flooded with water, making access and monitoring during rainfall impossible. The cave passages display a lengthy network of branches, with discernible paragenetic processes and sediments resulting from river erosion filling the channels. In contrast, Mendukilo cave is a popular destination for tourists, spanning 869 m in length with a 59 m vertical extension. The cave is presently experiencing vadose conditions, and its morphology is defined by gravitational breakdown features, namely roof and wall collapses, which have obliterated the morphological characteristics of previous speleogenic phases.

The investigation of the present dynamics within caves encompasses the collection of precipitation, drip water, and farmed calcite samples. In the instance of Ostolo cave, despite continuous monitoring being impeded by the challenges encountered when accessing it, the analyses of $\delta^{18}O$ values in dripwater and on precipitated carbonate indicate no seasonal variation, while carbonate precipitation occurs throughout the year. Mendukilo cave has been monitored continuously from 2018 to 2021, demonstrating that changes in the precipitation levels affect the $\delta^{18}O$ and $\delta^{13}C$ values in carbonate samples on an interannual scale, although the seasonal impact is less pronounced.

Several stalagmites from the Ostolo and Mendukilo caves were sampled, dated, and geochemically analyzed to obtain high-resolution paleoclimate information from those excellent archives. Three speleothems from Ostolo cave (OST1, OST2, and OST3) were dated using the U/Th method at a high resolution in intervals that present a speleothem petrography suitable for paleoclimatic interpretations. These dating results allow the generation of age models and a series

of stable oxygen isotopes that cover a large part of the last deglaciation and the onset of the Holocene. These $\delta^{18}O$ series are robustly replicated, and their variations when abrupt climatic changes arise correlate very well with other records from the rest of Europe and the Greenland ice cores. This allows, together with the results of monitoring inside the cavity, the interpretation that the $\delta^{18}O$ signal stored in these stalagmites is directly influenced by the temperature changes that occurred during the different abrupt changes of the last deglaciation. Indeed, depleted $\delta^{18}O$ values were observed during the cold Greenland stadials (GS), and enriched values were observed during warm Greenland interstadials (GI), indicating a dominant control of air temperature in this signal. In addition to the effect of temperature, the $\delta^{18}O$ series of these speleothems is influenced by changes in the isotopic composition of the humidity source that affects these caves (e.g., meltwater released into the North Atlantic Ocean as a consequence of the discharge of massive ice sheets in the northern hemisphere during Heinrich Event 1).

The speleothem record from Mendukilo cave consists of four stalagmites (MEN-2, MEN-3, MEN-4, and MEN-5) extracted from the same gallery, composed of calcite, and with a similar petrography. The $\delta^{13}C$ composite record from Mendukilo cave, in conjunction with the trace element series, allowed us to determine that higher (lower) $\delta^{13}C$ values are related to colder (warmer) intervals and/or drier (wetter) environments with reduced (improved) soil respiration and vegetation productivity. However, the $\delta^{18}O$ composite record of the speleothems captured an annual signal, which was mainly influenced by the amount of rainfall and changes in the isotopic composition of the ocean. These interpretations for both composites, together with those of trace elements, allow us the identification and reconstruction of millennial-scale climate changes previously observed in other records from the region during last 13 kyr, such as the Holocene thermal maximum and neoglaciation. The Mendukilo oxygen isotope composite also records short-lived events associated with major disturbances in the North Atlantic deep-water circulation, and sometimes as a result of meltwater intrusion.

A new series of stable isotopes was defined based on the δD values from the analysis of fluid inclusions of Ostolo and Mendukilo stalagmites. The δD fluid inclusion values for the Holocene and other warm periods were similar to those of the present-day dripping waters at each cave. In contrast, δD values were more negative during GS-1 and GS-2.1a. Monitoring work (rainfall isotopes, dripwater isotopes, and temperature) allows defining a transfer function to convert the δD values of fluid inclusions to quantitative temperature values and to create a composite fluid inclusion paleotemperature record for both caves (OM-FIT). The OM-FIT record adds new and the first non-biogenic evidence for rapid temperature transitions during the last deglaciation and the Holocene period, accompanied by the identification of the most pronounced abrupt events that occurred during the last 16.5 thousand years in northern Iberia.

Resumen

Abordar la reconstrucción de la variación climática pasada a través de los espeleotemas de cuevas responde a uno de los mayores retos a los que nos enfrentamos como sociedad hoy en día, que es la emergencia climática. Aunque actualmente existe un consenso científico sobre la causa antrópica del reciente calentamiento global, las incertidumbres sobre las consecuencias previstas del aumento de la temperatura en nuestro planeta y en nuestra sociedad siguen siendo grandes. El estudio de los cambios climáticos del pasado, en particular los que se produjeron con rapidez, como las terminaciones glaciares y los cambios climáticos rápidos del Holoceno, se presenta como la mejor forma de obtener datos de escenarios climáticos comparables a nuestra situación climática actual.

La presente tesis aborda el estudio de las cuevas de Ostolo y Mendukilo (Navarra, NE de España) con el foco puesto en la comprensión de la dinámica actual en el interior de las cavidades y en la reconstrucción paleoclimática desde la última deglaciación a partir de su registro espeleotémico (últimos 16.000 años). La Cueva de Ostolo (248 m s.n.m.) y la de Mendukilo (750 m s.n. m.) están situadas en la parte más oriental de la Cordillera Cantábrica (Montañas Vascas), Pirineo Occidental. Morfológicamente, la cueva de Ostolo tiene una longitud de 631 m y una extensión vertical de 39 m y una única entrada formada por un pasaje corto y estrecho que, puesto que coincide con una salida de agua permanente, imposibilita el acceso y la monitorización continuada. Las galerías de la cueva son ramificadas y alargadas, y aparecen morfologías diagnósticas de procesos paragenéticos, a la vez que sedimentos fluviokársticos rellenan los conductos. Por otro lado, Mendukilo es una cueva turística con una longitud total de 869 metros y una extensión vertical de 59 metros, que se encuentra actualmente en condiciones vadosas. Está afectada por procesos de ruptura gravitacional (colapso de techo y paredes) que eliminan las morfologías asociadas con fases espeleogenéticas anteriores.

El estudio de la dinámica actual dentro de las cuevas, incluyendo muestreos de lluvia, de agua de goteo y de precipitados de calcita, permite conocer el funcionamiento de los procesos que influyen en la formación del registro espeleotémico. En el caso de la cueva de Ostolo, los trabajos de monitorización no se pudieron realizar de forma continuada, pero se mostró que los valores de $\delta^{18}O$ en el agua de goteo y el carbonato precipitado no presentan variación estacional y que el carbonato precipita a lo largo de todo el año. La cueva de Mendukilo sí que presenta una monitorización continua durante 2018-2021 que ha permitido determinar el papel de la cantidad de lluvia en los valores isotópicos ($\delta^{18}O$ y $\delta^{13}C$) en el carbonato precipitado.

Varias estalagmitas de ambas cuevas se muestrearon, dataron y fueron analizadas geoquímicamente para obtener registros paleoclimáticos de alta resolución a partir de estos excelentes archivos. Tres espeleotemas de la cueva de Ostolo (OST1, OST2 y OST3), datados

mediante el método de U/Th a alta resolución, abarcan gran parte de la última deglaciación y el inicio del Holoceno. Las series de $\delta^{18}O$, replicadas de un modo muy robusto, presentan una excelente correlación con otros registros del resto de Europa y Groenlandia permitiendo así obtener, junto con los resultados de monitorización en el interior de la cavidad, una señal precisa de la variación de temperatura asociada a los diferentes cambios bruscos de la última deglaciación. Además del efecto de la temperatura, las series $\delta^{18}O$ de estos espeleotemas están influidas por cambios en la composición isotópica de la fuente de humedad que afecta a estas cuevas, siendo notable este proceso durante la descarga masiva de icebergs en el hemisferio norte en el evento Heinrich 1.

El registro de espeleotemas de la cueva de Mendukilo consta de cuatro estalagmitas (MEN-2, MEN-3, MEN-4 y MEN-5) extraídas de la misma galería, compuestas de calcita y con una petrografía similar. El registro compuesto de $\delta^{13}C$ de la cueva Mendukilo, junto con las series de elementos traza, nos permite determinar que los valores más altos (más bajos) de $\delta^{13}C$ están relacionados con intervalos más fríos (más cálidos) y/o más secos (más húmedos) con una respiración del suelo y una productividad de la vegetación baja (alta). Por otro lado, el registro de $\delta^{18}O$ de los espeleotemas capturó una señal anual, que está modificada, principalmente, por la cantidad de lluvia y por cambios en la composición isotópica del océano. Estas interpretaciones nos permiten reconstruir e identificar los cambios climáticos a escala milenaria observados en otros registros de la región durante el Younger Dryas hasta principios del Holoceno tardío (eg. últimos 4000 años), como el máximo térmico del Holoceno y la Neoglaciación. Además, los eventos de corta duración asociados con perturbaciones importantes en la circulación de aguas profundas del Atlántico Norte y, a veces, como resultado de la intrusión de agua de deshielo, se pudieron identificar y caracterizar su magnitud en la cueva de Mendukilo.

Gracias al análisis de inclusiones fluidas de las estalagmitas de Ostolo y Mendukilo se obtuvieron nuevos registros climáticos desde la última deglaciación que pudieron ser interpretados, de un modo cuantitativo gracias a una función de transferida definida a partir de los trabajos de monitorización. Así, los valores de δD en inclusiones fluidas para el Holoceno y otros periodos cálidos fueron comparables a los actuales de goteos en cada cueva. Por el contrario, los valores de δD son más negativos durante periodos fríos, como el Younger Dryas o el evento de Heinrich 1. El registro compuesto de paleotemperatura calculado para ambas cuevas (OM-FIT) representa la primera evidencia no biogénica de las transiciones rápidas de temperatura durante la última desglaciación y el Holoceno en el noreste peninsular.

Content

List of Figures

List of tables

Abbreviations

a.s.l	Above sea level
IP	Iberian Peninsula
AMOC	Atlantic meridional overturning circulation
SST, SSS	Sea surface temperature and salinity, respectively
NGRIP	North Greenland Ice Core Project
BP	Before present
VSMOW	Vienna Standard Mean Ocean Water
VPDB	Vienna Pee Dee Belemnite standard
PCP	Prior calcite precipitation
IRD	Ice-rafted debris
HTM	Holocene thermal maximum
LGM	Last glacial maximum
OD	Oldest Dryas
B-A	Bølling-Allerød
YD	Younger Dryas
HS1	Heinrich Stadial 1
HE1	Heinrich Event 1
GS, GI	Greenland Stadial and Interstadial, respectively
$\delta^{18}O_{sw}$	Ratio of oxygen stable isotopes of sea water
$\delta^{18}O_v$	Ratio of oxygen stable isotopes of vapor
$\delta^{18}O_r, \delta D_r$	Ratio of oxygen (O) and hydrogen (D) stable isotopes of rainfall
$\delta^{18}O_d, \delta D_d$	Ratio of oxygen (O) and hydrogen (D) stable isotopes of dripwater
$\delta^{18}O_p, \delta^{13}C_p$	Ratio of oxygen (O) and carbon (C) stable isotopes of farmed calcite
$\delta^{18}O_c, \delta^{13}C_c$	Ratio of oxygen (O) and carbon (C) stable isotopes of speleothems
FI	Fluid inclusion
$\delta^{18}O_{FI}, \delta D_{FI}$	Ratio of oxygen (O) and hydrogen (D) stable isotopes of fluid inclusions
OST, MEN	Ostolo and Mendukilo samples, respectively
kyr	Thousand years
pCO_2	Partial pressure of carbon dioxide
LMWL, GMWL	Local and Global meteoric water line, respectively
MIS	Marine isotope stage
MAAT	Mean annual air temperature

Chapter I

Introduction

I.1   Motivation

Caves occur everywhere on our planet, from the tropics to high latitudes, from below sea level to mountain settings, and in karst or non-karst systems. Cave morphologies provide clues to their formation mechanisms, and their iconic mineralogical features—stalagmites and stalactites—carry a wealth of paleoenvironmental information encoded in their geochemistry, petrography and mineralogy (Feinberg & Johnson, 2021). Recent work demonstrates a striking improvement in our ability to decode these paleoenvironmental proxies, and dramatic geochronological advances enable higher-resolution records that extend further back in geologic time (Fairchild & Baker, 2012). Cave research addresses an ever-increasing range of geoscience problems: establishing the timing and mechanisms of climate change (Wong & Breecker, 2015), archaeology and anthropology (El-Shenawy et al., 2018), providing high-quality continuous records of the direction and relative paleointensity of the geomagnetic field (Jaqueto et al., 2022), and finding information about paleofire events (Campbell et al., 2023), among others.

The development of techniques for precise and accurate U–Th dating on small amounts of samples and the progress made in determining the different environmental factors that control the several proxy parameters that can be used (singly or in combination) to interpret changing environments or climates are the most important factors that have allowed speleothem science to become prominent in recent years (Edwards et al., 1987; Fairchild & Baker, 2012; Hoffmann et al., 2007; Wong & Breecker, 2015). Innovative trace element records (e.g., Sliwinski et al., 2023), clumped isotopes (e.g., Kato et al., 2023), and fluid inclusions (e.g., Weissbach et al., 2023) are among the newest climate proxies being progressively applied to refine speleothem-based paleoclimatic interpretations and to gain novel insights into past climatic and environmental dynamics.

All these improvements in speleothem science over the last two decades have been demonstrated in the impressive paleoclimate records around the world, where more than 500 speleothem datasets have been published to date, 70% of which have been published since 2007 and compiled in the SISAL database (Atsawawaranunt et al., 2018). Great examples of such records can be found in Europe (Boch et al., 2011; Drysdale et al., 2007, 2009; Genty et al., 2010; McDermott et al., 2001; Meyer et al., 2008; Spötl et al., 2006, 2008; Spötl & Mangini, 2002), Near East (Bar-Matthews et al., 1999; Burns et al., 2002, 2003; Fleitmann et al., 2007, 2009), North and South America (Asmerom et al., 2010; Cruz et al., 2005, 2009; Lachniet, 2004; Medina-Elizalde et al., 2010; Medina-Elizalde & Rohling, 2012; Polyak & Asmerom, 2001), Asia (Cheng et al., 2006, 2009, 2016; Yuan et al., 2004) and Southwest Pacific (Treble et al., 2003, 2005; Webb et al., 2014; Williams et al., 2005).

In the case of the Iberian Peninsula (IP), a climatic transition area between the Atlantic and the Mediterranean and subtropical to middle-latitude climate gradients, few speleothem studies

were available during that time. Pioneering studies focused mainly on the present-day cave dynamics and the alteration of speleothem textures and geochemical signals in the search to provide paleoclimatic interpretations along the Iberian setting (Alonso-Zarza & Martín-Pérez, 2008; Durán Valsero et al., 1999; Jiménez De Cisneros et al., 2003; Martín-Chivelet et al., 2006, 2007; Muñoz et al., 2009; Muñoz & Sancho, 2008; Muñoz-García et al., 2004, 2007; Vesica et al., 2000). These efforts to understand the isotopic signal in spelothems gave rise to the elaboration of the first records with paleoclimatic reconstructions equipped with U-Th dating at a high chronological resolution (Domínguez-Villar et al., 2008, 2009; Dorale et al., 2010; Hodge et al., 2008; Moreno et al., 2010).

During the past and current decades, studies on speleothems have diversified into the use of new climatic and paleoenvironmental indicators. These studies have focused on the application of new paleoclimatic proxies (Cáceres et al., 2017; Cruz et al., 2015a, 2015b; Jiménez de Cisneros et al., 2020, 2023; Lopez-Elorza et al., 2021; Martín-Chivelet et al., 2011, 2017; Martín-García et al., 2014, 2019; Muñoz-García et al., 2016; Stoll et al., 2013) that allow paleoclimatic interpretations to be carried out on a shorter time scale (e.g., Stoll et al., 2015) and to identify climatic factors that affect the paleoclimatic records within the Iberian region (Walczak et al., 2015). The identification and characterization of different periods has also been possible, and the Blake geomagnetic excursion has been identified in speleothems of the Cantabrian Range (Osete et al., 2012; Rossi et al., 2014), whereas in other studies, the Younger Dryas has been clearly identified (Baldini et al., 2015; Rossi et al., 2018). Holocene speleothem records in the IP revealed paleohydrological anomalies (Budsky et al., 2019; Thatcher et al., 2020) and the Atlantic Ocean's important role in shaping centennial-scale oscillations (Domínguez-Villar et al., 2017; Smith et al., 2016). A compilation of speleothem records from northern Spain has highlighted the role of rainfall seasonality (Baldini et al., 2019).

The "Quaternary Paleoenvironments and Global Change" group of the Pyrenean Institute of Ecology-CSIC (IPE), together with the University of Zaragoza, have put their efforts into understanding the current dynamics inside different caves of the IP to understand the processes that control the rainfall isotopic features and calcite precipitation, with the goal of providing an interpretation of the paleoclimatic signal of the speleothem records during the last glacial maximum (LGM), the last deglaciation, and the Holocene. The first efforts, around 2009-2010, focused on the northern IP and the Iberian Range, specifically in the Pindal cave (Asturias) (Moreno et al., 2010), Ortigosa de Cameros (La Rioja) (Muñoz et al., 2009; Osácar et al., 2014), and Molinos caves (Teruel) (Moreno et al., 2017; Moreno et al., 2014a; Muñoz et al., 2015). The increase in the number of works that include $\delta^{18}O$ isotopic records in stalagmites of the IP, which presents a complex topography and varied weather regimes (influenced by Atlantic and Mediterranean climates), prompted the collection of rainwater samples from different regions within the IP during that time, for later study the high spatial variability of the $\delta^{18}O$ rainfall signal

($\delta^{18}O_r$) and the multiple (and sometimes overlapping) processes determining its temporal variation from multiple stations, across northern IP all the way to the Balearic Islands, with the purpose of improving the interpretation of oxygen isotope stalagmite paleorecords (Moreno et al., 2021).

In 2011, new cave alternatives were sought in the Pyrenees, beginning studies in the Seso cave, which was selected for a PhD thesis. In the conclusions of this work (Bartolomé, 2016), the paleoclimate of the last 13 kyr in this region was reconstructed, accompanied by extensive monitoring and a detailed description of the speleogenesis of Seso cave (Bartolomé et al., 2012, 2015a). Additionally, analysis of different proxies in stalagmites from Seso Cave provided robust evidence of the existence of two different phases in GS-1 in terms of the hydrological response of terrestrial environments (Bartolomé et al., 2015b). Simultaneously, new records of speleothems were discovered, and monitoring campaigns began in caves located in the south-central Pyrenees. To this day, these campaigns seek innovative methods for monitoring caves and show how a combined interpretation of clastic and speleothem lithofacies is critical for elucidating landscape evolution and surface-groundwater paleohydrological changes in northern Iberia during the Last glacial cycle (Bartolomé et al., 2021). In contrast, analysis of ice deposits from the Pyrenees provides unique insights into the processes leading to the formation of cryogenic carbonates and sulfates (Bartolomé et al., 2023; Bartolomé et al., 2015c). This study represents the first report of such speleothems on the IP (Bartolomé et al., 2015c) and now allows for a better understanding of mountain permafrost evolution in the Monte Perdido massif and Pyrenees in general (Bartolomé et al., 2023).

In 2012, following the work on stalagmites in caves from the IP, the Ejulve cave was selected as a likely candidate to investigate past climate variations for a PhD thesis in an environment largely influenced by the Mediterranean compared to the Pyrenean caves. The preliminary results in the cave focused on analyzing the geomorphology, present-day hydrology and precipitates, cave environmental parameters, and investigating the potential of the speleothems in the cave in the reconstruction of past climates (Pérez-Mejías, 2013). Between 2013-2016, extensive monitoring of Ejulve Cave began, and many speleothems were dated. Unlike the Seso and Molino caves, which mostly cover the Holocene and part of the last deglaciation, the Ejulve speleothems cover older periods, such as termination III (T-III) during the transition from MIS 8 to MIS 7 (Pérez-Mejías et al., 2017), the end of the interglacial and glacial inception during MIS 5 (Pérez-Mejías et al., 2019a), and several stadials and interstadials during MIS 4 and MIS 3 (Pérez-Mejías, 2019; Pérez-Mejías et al., 2019a). This record also allowed defining the terrestrial response to abrupt events (T-III and Heinrich event 6; Pérez-Mejías, 2019) for the first time in this region. The four years of monitoring inside the Ejulve Cave were very useful in identifying the factors affecting the isotopic composition of rainfall, dripwater, and farmed calcite to better understand and accurately interpret these speleothems (Pérez-Mejías et al., 2018). In addition, the different hydrogeomorphic stages of speleogenesis in the phreatic environment of the Ejulve cave are also

defined through the study of morphologies and deposits, together with regional geomorphology and hydrothermal observations (Pérez-Mejías et al., 2019b). At the same time, stalagmites from Meravelles cave (Tarragona, NE Spain) were also sampled. An absolute-dated record from this cave provides ages for two key events throughout the Oldest Dryas (onset of cold conditions and discharge of icebergs during Heinrich Event 1) (Pérez-Mejías et al., 2021).

In 2017, a new monitoring campaign begins at the "Las Güixas" touristic cave in Villanúa (central Pyrenees), where oxygen and hydrogen isotopes composition ($\delta^{17}O_r$, $\delta^{18}O_r$, and δD_r) of rainwater were measured and subsequently correlated with meteorological parameters (Giménez et al., 2021). This new dataset of oxygen and hydrogen isotopes of rainfall is now helpful to fully understand the influence of atmospheric features on isotopic rainfall composition at local and regional scales, and can be highly useful for further interpretation of paleoclimate records based on isotopic data (Giménez et al., 2021).

With this prior knowledge in working with speleothems from the Iberian Peninsula, new IP cave exploration campaigns were carried out in 2018 in a different context to those mentioned above. This is how a total of five caves (Goicoetxe, Arrikrutz, Haitzea, Mendukilo, and Ostolo) are explored in the Basque Country and Navarra (north and northeast of the IP), with the intention of evaluating both the Atlantic and Mediterranean influences in new speleothermic records. Furthermore, this was a good opportunity to start a thesis that connects the previously mentioned results from the Pyrenees with those from Cantabria, in an area of Spain where higher spelotemic growth rates could be expected due to the higher amount of rainfall compared to much of the IP. Preliminary dating and isotopic results in stalagmites hint at the great potential of these caves for future high-resolution and continuous paleoclimatic works during the last deglaciation and the Holocene, especially those corresponding to the Mendukilo and Ostolo caves. This is how a greater number of stalagmites were collected at the end of the same year, and a seasonal monitoring campaign began in both caves for the elaboration of this PhD thesis. Hence, these stalagmites offer the possibility to study some abrupt changes that are barely identified in other records and provide new insights into the Iberian climate evolution on millennial to centennial time scales since the Greenland stadial 2.1 until the present day, with a very high temporal resolution. Additionally, with the intention of developing new techniques in speleothem analysis, during–2020-2022 the stalagmites were sampled and analyzed for fluid inclusions with the main aim, for the first time in the region, of determining changes (not only qualitative but also quantitative) in the temperature evolution that occurred since the last deglaciation in the IP. Therefore, the results presented in this thesis have not only regional but also global importance due to the significant climatic teleconnections (e.g., changes in the North Atlantic Sea surface and the Atlantic meridional overturning circulation (AMOC) triggers changes in precipitation in the IP).

I.2   Research goals

The main objective of this dissertation is to provide high-resolution paleoclimate records to reconstruct the abrupt climatic changes of the last 16.5 thousand years before the present (kyr BP; present = 1950) through the multi-proxy study of accurately dated stalagmites from the Ostolo and Mendukilo caves. This objective is accompanied by an understanding of the present-day dynamics of both caves related to the environmental conditions in which the carbonate that gives rise to speleothems currently precipitates. Additionally, we sought to quantitatively reconstruct the temperature changes that accompany the short-lived climate shifts that have occurred since the last deglaciation. The specific objectives in relation to the main results of this thesis (Chapters IV, V, and VI) are detailed below.

1. **The Ostolo cave speleothem record:**

    1.1 Evaluate the present-day dynamics inside the cave and analyze the factors that control $\delta^{18}O_r$ in farmed calcite $\delta^{18}O$ ($\delta^{18}O_p$).

    1.2 Identify petrographic changes in the speleothem records.

    1.3 Establish accurate absolute chronologies using the U/Th method.

    1.4 Elaborate the age models and perform $\delta^{18}O$ series for each speleothem ($\delta^{18}O_c$).

    1.5 Understand the processes that explain the $\delta^{18}O_c$ variability in the samples from this cave. Then compare this stable isotope series with other records (terrestrial, marine, ice cores, etc.) inside and outside the IP.

2. **The Mendukilo cave speleothem record:**

    2.1 Evaluate the present-day dynamics inside the cave and analyze the factors that control $\delta^{18}O_r$ to $\delta^{18}O_p$ and $\delta^{13}C_p$.

    2.2 Identify petrographic changes in the speleothem records.

    2.3 Establish accurate absolute chronologies using the U/Th method.

    2.4 Elaborate the age models and perform $\delta^{18}O_c$, $\delta^{13}C_c$, and trace element composite series.

    2.5 Understand the processes that explain the $\delta^{18}O_c$, $\delta^{13}C_c$, and trace element variability in the samples from this cave. Then compare this stable isotope series with other records (terrestrial, marine, ice cores, etc.) inside and outside the IP.

3. **Temperature reconstruction since the last deglaciation:**

    3.1 Perform δD series from the analysis of stalagmite fluid inclusions in speleothems (δD_{FI}) in both caves.

    3.2 Quantify the paleotemperature changes with the generation of a transfer function for the fluid-inclusion isotope data.

    3.3 Compare this quantitative temperature reconstruction with other records (terrestrial, marine, ice cores, etc.) inside or outside the IP.

I.3   Research strategy

Each cave system has unique characteristics and the processes that dominate the isotopic signal cannot be extrapolated from one cavity to another. This suggests that each cave has a different sensitivity to climatic conditions, which may ultimately affect the climatic information recorded in speleothems. Taking this into consideration, knowing the present-day dynamics within the cave is of first order of relevance to having a sufficient degree of reliability in subsequent paleoclimatic reconstructions from speleothems; in other words, current conditions are key to understanding those of the past. Therefore, the first point of this thesis is to summarize the regional conditions in which both caves are located (Chapter II) and to describe the climatic signal stored in the speleothems, which has been interpreted from the **monitoring work inside each cavity** (sections IV.4.1 and V.4.1).

Paleoclimatic interpretations of stalagmites require several prior analyses. The first is to determine the mineralogical and **petrographic** (sections IV.4.2 and V.4.2) changes throughout each sample, which can provide information on the conditions under which the stalagmites grow and change during the precipitation process. Indeed, some of the different arrangements in which carbonate crystals grow in stalagmites (speleothem fabrics) may clearly be indicative of quasi-equilibrium precipitation conditions (Frisia & Borsato, 2010). The next step is to generate precise and reliable **age models** (sections IV.4.3 and V.4.2) that characterize the speleotemic growth and age of each stalagmite. The precision of U-Th dating depends directly on the initial concentration of uranium and the external detrital thorium incorporated. The elaboration of age models allows us to make **isotopic** (sections IV.4.3 and V.4.3) **and trace element** (sections V.4.3) **series** for each speleothem in the search for future paleoclimatic interpretations and identify abrupt climatic changes. Prior to this, it is relevant to determine whether the conditions under which carbonate precipitates are in isotopic equilibrium. A good method to determine whether this is accurate is to replicate the isotopic data of two or more stalagmites. The latter has been the strategy to follow in geochemical sampling of stalagmites from both caves.

The isotopic series mentioned above cannot be used alone in the **interpretation of past paleoenvironmental changes** (sections IV.5 and V.5). Records of past environmental change need to follow a multiproxy approach and be compared with different paleorecords (e.g., ice and marine cores, pollen, and chironomids) to determine whether our data exhibit a signal seen previously in other areas. Furthermore, effective evaluation of these records should be carried out (if possible) at different geographic (local to global) and temporal scales (annual to millennial). Paleoclimatic interpretations can be accompanied by quantitative temperature data from the isotopic analysis of **fluid inclusions** (Chapter VI) trapped in speleothems. After the analysis of these inclusions, δD_{FI} values can be transmuted into temperature with the help of the present monitoring work for each cave and the isotope concentration of rainfall within the study region,

accompanied by the definition of a transfer function that allows for the calculation of paleotemperatures in comparison with those currently present in the study area.

The present dissertation is structured as follows: The **Introduction** (Chapter I), including the objectives of the research, the steps followed to reach these objectives (research strategy), a brief description of the climatic conditions from the last deglaciation to the present, accompanied by a compilation of several relevant records to characterize the Northern Hemisphere paleoclimatically, and a state-of-the-art of the discipline focused on the potential of speleothem records to perform paleoclimatic inferences. The following chapters present the **study area** (Chapter II) and the **methodology** used during this Thesis (Chapter III). From this chapter onwards, the main part of the dissertation is dedicated to the results and discussion to achieve the goals explained above, starting with the paleoclimatology inferences, at millennial and centennial scales, of **Ostolo cave during the last deglaciation period** (Chapter IV, based on Bernal-Wormull et al., 2021) and **Mendukilo cave during the Holocene** (Chapter V, based on Bernal-Wormull et al., 2023), followed by quantitative paleotemperature reconstructions in both caves using **fluid inclusion analysis** (Chapter VI). The dissertation concludes with the last chapter, the **Epilogue** (Chapter VII), which highlights the **conclusions** of the study and the **future perspectives** that have emerged from the completion of this dissertation research.

I.4   Climate since last deglaciation

On the broadest scale, the rate at which energy is received from the sun and the rate at which it is lost to space determine the equilibrium temperature and climate of Earth. Climate variability can be defined as variations in the mean state of temperature, precipitation, and atmospheric circulation on spatial and temporal scales, beyond individual weather events (Bond et al., 2001). Internal variability arises because of complex (often nonlinear) internal processes within the atmosphere-ocean-biosphere-cryosphere system (Deser et al., 2012; Olonscheck & Notz, 2017) or forced external variability in response to changes in natural or anthropogenic forcing (Foster & Rahmstorf, 2011). Temporarily, the closest we can get to best exemplify internal variability at millennial scales is the last deglaciation/glacial termination, which is characterized by being a transition from full glacial conditions (ice age) to warm interglacials characterized by global warming and sea level rise due to changes in continental ice volume (Barker & Knorr, 2021). In addition, several episodes of large and rapid sea-level rise and abrupt climate change have produced regional climate signals superimposed on those associated with global warming (Clark et al., 2012). This contrasts with the present interglacial period, the Holocene, which has conventionally been viewed as climatically stable, with little evidence of abrupt millennial-scale climatic shifts that characterize glacial periods. Over the last 100 years, there has been a clear example of external climate variability owing to anthropogenic forcing (deMenocal et al., 2000). As mentioned in Chapter I, this thesis focuses on the internal variability of the climate during the last deglaciation and the Holocene (specifically the last 16.5 kyr BP) in the North Atlantic, and evaluates the abrupt changes that occur during these periods.

I.4.1   From the end of the Last glacial maximum to Younger Dryas

During the interval of global warming from the end of the Last Glacial Maximum (LGM) approximately 19 kyr to the early Holocene 11 kyr BP, virtually every component of the climate system underwent large-scale changes, sometimes at extraordinary rates, as the world emerged from the last ice age (Fig. 1.1; Clark et al., 2012; Shakun et al., 2012). This dramatic global change was triggered by changes in insolation, with associated changes in ice sheets (Fig. 1.1), greenhouse gas concentrations, sea-level rise, and other amplifying feedbacks that produced distinctive regional and global responses (Clark et al., 2012). Actual observations and transient global climate model simulations support the conclusion that an antiphase hemispheric temperature (Fig. 1.2A) response (bipolar seesaw response between the northern and southern hemispheres) to ocean circulation changes in the strength of the Atlantic meridional overturning circulation (AMOC) superimposed on global in-phase warming driven by increasing CO_2 concentrations is an explanation for much of the temperature change at the end of the most recent ice age (Monnin et al., 2001; Shakun et al., 2012); Fig. 1.2A).
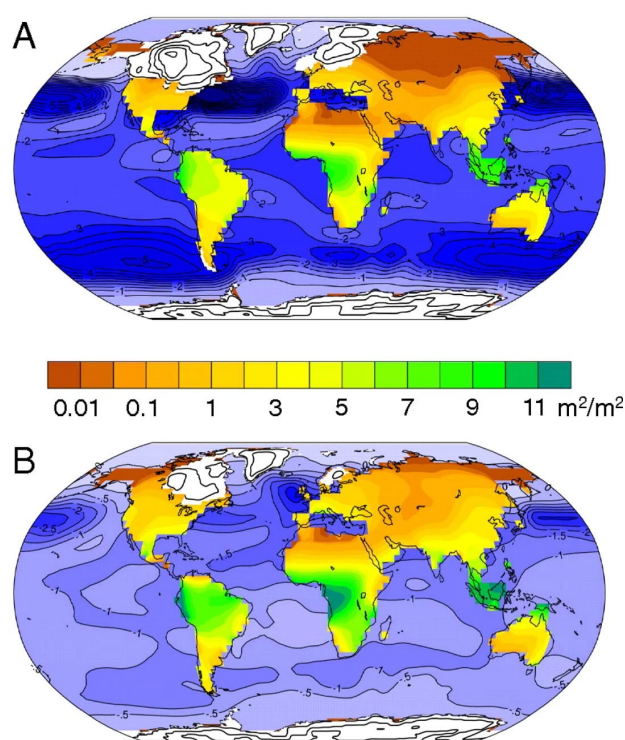
Fig 1.1. *A) Climate simulation of the Last Glacial Maximum 21,000 years ago using the National Center for Atmospheric Research Community Climate System Model (Liu et al., 2009). Sea-surface temperatures are anomalies relative to the control climate. Continental ice sheets (1,000-m contours) (Peltier, 2004) and leaf area index (a representation of vegetation cover) were simulated by the model (scale bar shown). B) Same as A, except 11,000 years ago. Extracted from Clark et al. (2012).*

The global temperature stack and transient modelling point to CO_2 as a key mechanism of global warming during the last deglaciation (Fig. 1.2A). Furthermore, an interhemispheric seesawing of heat (related to AMOC variability) suggests that these internal heat redistributions explain the lead of the southern hemispheric temperature over CO_2, while the global temperature was in phase with or slightly lagged CO_2. Additionally, the global proxy database compiled by Shakun et al. (2012) (purple line, Fig.1.2A) suggests that parts of the northern mid-to high-latitudes were the first to warm after the LGM, which could have initiated the reduction in the AMOC, which may have ultimately caused the increase in CO_2 concentration.

During the LGM, the $\delta^{18}O$ values in Greenland (Fig. 1.2B) were much lower than what we know today, and temperatures were approximately 15 °C lower (Kindler et al., 2014). Climate reconstructions from European pollen records, which account for the effects of lower atmospheric CO_2, indicate winter cooling of 5–15 °C across Europe, with the greatest cooling occurring in the western part (Clark et al., 2012).
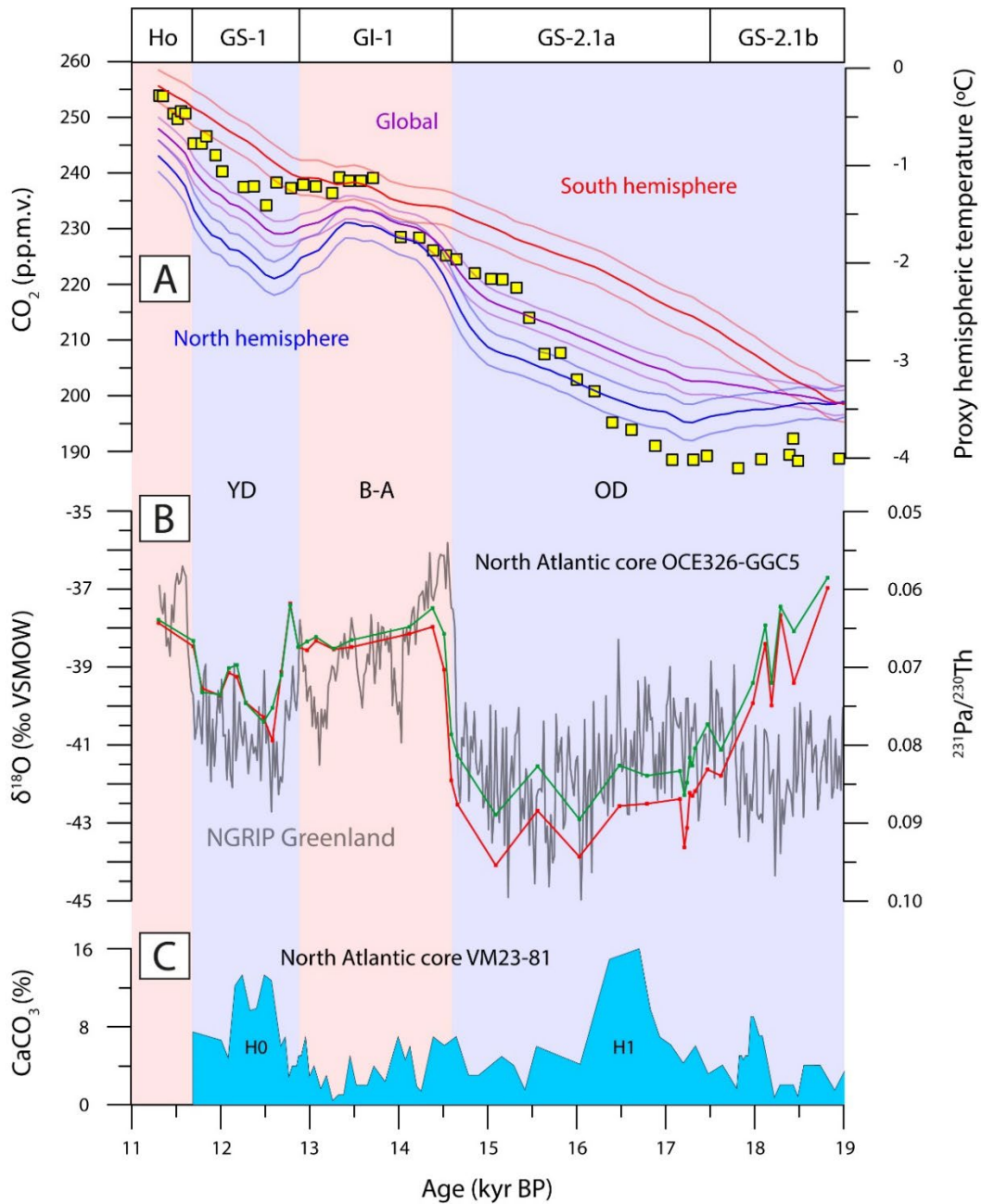
Fig 1.2. *Some of the records to visualize the global climatic evolution during the end of the LGM and throughout the last deglaciation period. A) Atmospheric CO₂ concentration (yellow squares) and the global (purple), Northern Hemisphere (blue) and Southern Hemisphere (red) proxy temperature stacks (with 1s uncertainties) as deviations from the early Holocene (11.5–6.5 kyr ago) mean (Monnin et al., 2001; Shakun et al., 2012). B) North Atlantic sediment core OCE326-GGC5 ²³¹Pa/²³⁰Th (McManus et al., 2004) as an indicator of deep water overturning and the NGRIP Greenland record (Rasmussen et al., 2014) as a proxy for Greenland climate. C) Record of ice-rafted detrital carbonate from North Atlantic core VM23-81 identifying times of Heinrich events 1 and 0 (Bond et al., 1999).*

Termination of the LGM was marked by a slight increase in temperature and precipitation (Goñi et al., 2000; Nebout et al., 2009), followed by a cool and dry Oldest Dryas (OD) stadial from approximately 17.5 to 14.7 kyr when European vegetation returned to its glacial state (Fletcher et al., 2010; Fletcher & Sánchez Goñi, 2008). At ~20–18 kyr, ice retreat induced by warming started in Fennoscandia, resulting in enhanced freshwater fluxes into the North Atlantic, provoking a sea level rise of approximately 2 m in the Nordic Seas (Álvarez-Solas et al., 2011). The discharges of the Fleuve Manche paleoriver, interpreted by means of turbidite deposits, increased drastically at ~18.3 kyr and were clearly more intense compared to the beginning of the deglaciation at ~20 kyr (Toucanne et al., 2008). Such freshwater fluxes turn the ocean into a new state of weakened AMOC that precipitates the onset of HS-1 (Heinrich Stadial 1, considered the marine equivalent of the OD in Europe; Álvarez-Solas et al., 2011; Bond et al., 1999; Denton et al., 2010). Indeed, $^{231}Pa/^{230}Th$ suggests that the net AMOC decreased below the LGM strength at nearly all depths during the OD (Fig. 1.2B). One of the most prominent deglacial events of the Northern Hemisphere, associated with the OD, is Heinrich Event 1 (HE1 or H1, ~17.5 to 16 kyr). This natural phenomenon, in which large groups of icebergs broke off from the Laurentide Ice Sheet and traversed the Hudson Strait into the North Atlantic, caused vast quantities of freshwater to be added to the North Atlantic (Fig. 1.2C; Álvarez-Solas et al., 2011). Such inputs of cold and fresh water may well have altered the density-driven, thermohaline circulation patterns of the ocean thus causing global climate fluctuations (Bond et al., 1999; Denton et al., 2010) (Fig. 1.3A). During the main phase of IRD discharges of HS1, the AMOC in the North Atlantic was already weakened (Ng et al., 2018). This large volume of meltwater from the icebergs (cold and freshwater) entered the Mediterranean, decreasing its salinity and reducing its thermohaline circulation in less than 1000 years (Sierro et al., 2005). Such an event could have triggered the decrease in precipitation, as interpreted from the analysis of $\delta^{18}O_c$ speleothem record in eastern Iberia (Pérez-Mejías et al., 2021).

At the Bølling-Allerød (B-A or BA) warm period (~14.7 to 12.9 kyr), temperatures increased rapidly (Fig. 1.3B) by 3–5°C across western Europe (Heiri et al., 2014a; Renssen & Isarin, 2001) and Greenland (9 ± 3 °C) (Severinghaus & Brook, 1999) with the reactivation of the AMOC (Fig. 1.2B). These surface air temperature changes exhibit a bipolar seesaw when comparing both hemispheres between the B-A and HE1 time periods (Fig. 1.3B), but a more symmetric warming over the LGM (Fig. 1.3C). B-A is clearly registered in proxy records from the Greenland ice sheets, such as $\delta^{18}O$ (Fig. 1.2B; Rasmussen et al., 2014) and $\delta^{15}N$ data (Kindler et al., 2014). This is also true for European oxygen isotope lake records (Grafenstein, 1999; Taylor et al., 1993). All these data suggest a very rapid transition from glacial to interglacial climate conditions, possibly within a few decades (Rasmussen et al., 2014; Severinghaus & Brook, 1999).
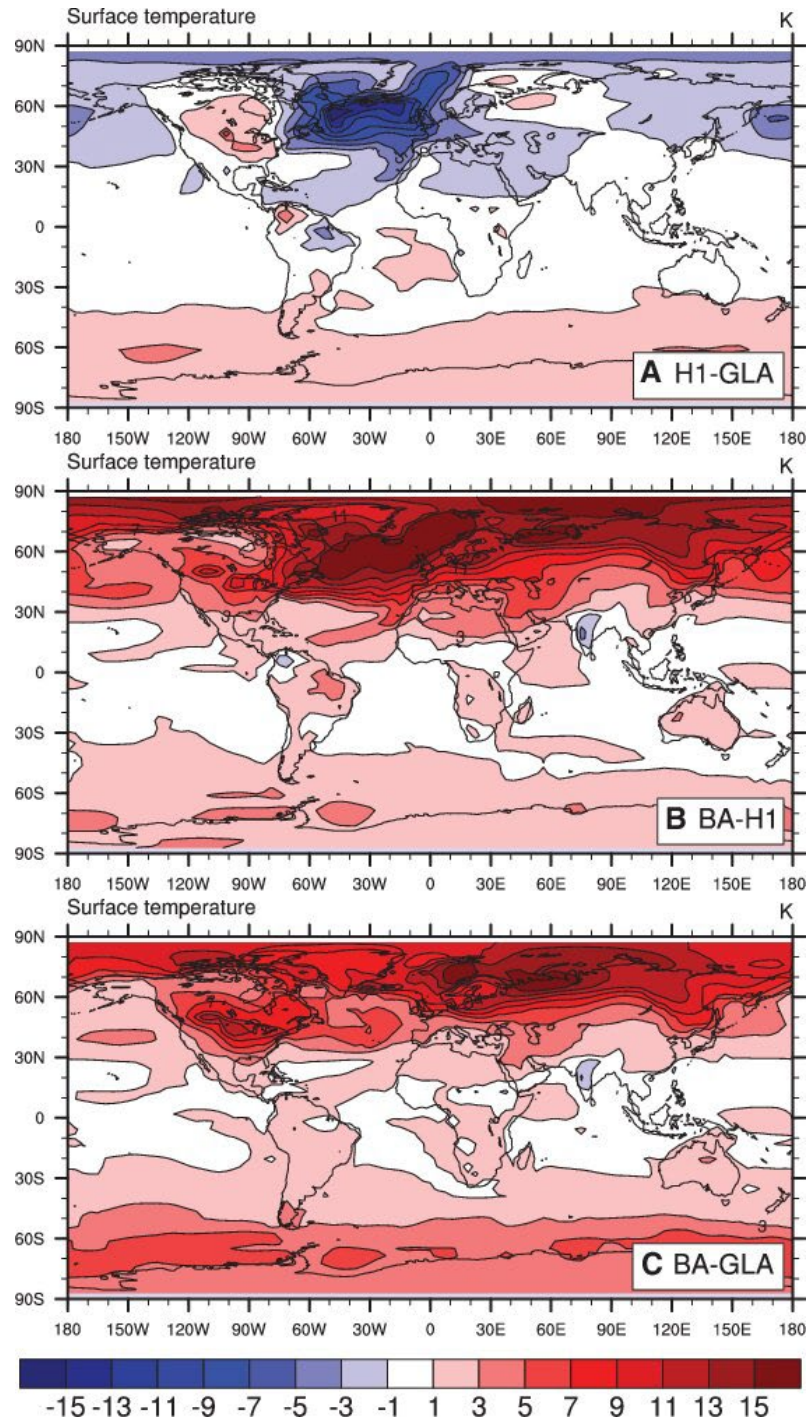
Fig 1.3.   *Surface air temperature changes (in °C). A) Heinrich Event 1(H1, ~17 kyr) temperature anomaly from the glacial state (GLA, 19 kyr); B) Bølling-Allerød (BA, ~14.5 kyr) temperature anomaly from H1; and C) BA temperature anomaly from GLA. The H1 temperature response exhibits a bipolar seesaw; the BA warming is dominated by maximum warming at northern high latitude over H1 (B), but exhibits a more symmetric warming over the glacial state (C). Extracted from Liu et al. (2009).*

Subsequent cooling at the start of the Younger Dryas (YD) cold event (~12.9 to 11.7 kyr, Greenland stadial 1) ranged between 5 and 10 °C in Europe and 10 ± 4 °C in Greenland (Grachev & Severinghaus, 2005; Isarin & Bohncke, 1999; Kindler et al., 2014). This temperature decrease resulted in a return to grassland communities in southern Europe and tundra in the north, while the ^{231}Pa/^{230}Th record (Fig. 1.2B) suggests only a partial weakening of the AMOC during the Younger Dryas, in contrast to the completed shutdown simulated during HS1. The YD ended abruptly in Europe approximately 11.7 kyr ago with a rapid temperature increase of approximately 4 °C, but varied latitudinally, with a greater increase in the north (Davis et al., 2003). AMOC changes, in conjunction with latitudinal shifts of the polar jet stream, had a major impact on the climatology of the regions around the North Atlantic, including the IP (Cacho et al., 2001; Naughton et al., 2016), a southern European region key to understanding Northern Hemisphere climate teleconnections, and where the climate (e.g., temperature) fluctuations of these abrupt events lack continuous, accurate, and high-resolution absolute chronologies in their scarce paleoclimatic records.

At the regional scale of the IP, glacier records from the Iberian Mountains, despite their discontinuous character and low resolution, indicate advances and retreats in phase with the well-known rapid temperature changes during the last deglaciation (García-Ruiz et al., 2016). Sea surface temperature (SST) records from marine sediments around Iberia (Cacho et al., 2001; Naughton et al., 2016; Rodrigues et al., 2010) reveal a last deglaciation evolution comparable to Greenland ice cores (Rasmussen et al., 2014); however, recent studies exposed large discrepancies between different records (Ausín et al., 2019) and also suggested that the SST proxies around Iberia are complicated by a seasonal component in the different proxies (Català et al., 2019). Additional regional paleoclimatic information is provided by well-dated lacustrine records (González-Sampériz et al., 2006; Morellón et al., 2009), which suggest cold and dry climates and large hydrological variability characterizing the end of the last glacial period in the IP (González-Sampériz et al., 2017) (Fig. 1.4).

At low, middle, and high altitudes in the Central Pyrenees and in the nearby Iberian range, lacustrine sequences also show remarkable changes in vegetation and hydrology during the different stages of the last deglaciation (Aranbarri et al., 2014; Gil-Romera et al., 2014; González-Sampériz et al., 2017; Pellicer et al., 2016; Vegas-Vilarrúbia et al., 2013). However, their resolution is insufficient to examine the fine-scale structure of the last deglaciation and, despite new Padul Lake record has presented a subdivision into several centennial-scale climatic phases (Camuera et al., 2021), still the chronology is not accurate enough to describe high-resolution changes.

An increasing number of speleothem records from Spain and southern France have provided new insights into the deglacial climate (Baldini et al., 2015; Bartolomé et al., 2015b; Genty et al., 2006; Moreno et al., 2010; Pérez-Mejías et al., 2021; Rossi et al., 2018). For example, a speleothem record from eastern Iberian allowed the identification of the onset of cold conditions that triggered the decay of vegetation during the OD and the discharge of icebergs during HE1, as inferred from $\delta^{18}O_c$ anomalies (Pérez-Mejías et al., 2021). A detailed study with a well-constrained chronology of a speleothem from Seso cave (Bartolomé et al., 2015b; Cheng et al., 2020) identified two phases within the YD: the first arid period and a relatively moister second one. However, none of these Iberian stalagmite records cover complete deglacial transitions at high resolution, and additionally, they differ with respect to the interpretation of $\delta^{18}O_c$ variability (Baldini et al., 2015; Genty et al., 2006; Moreno et al., 2010).
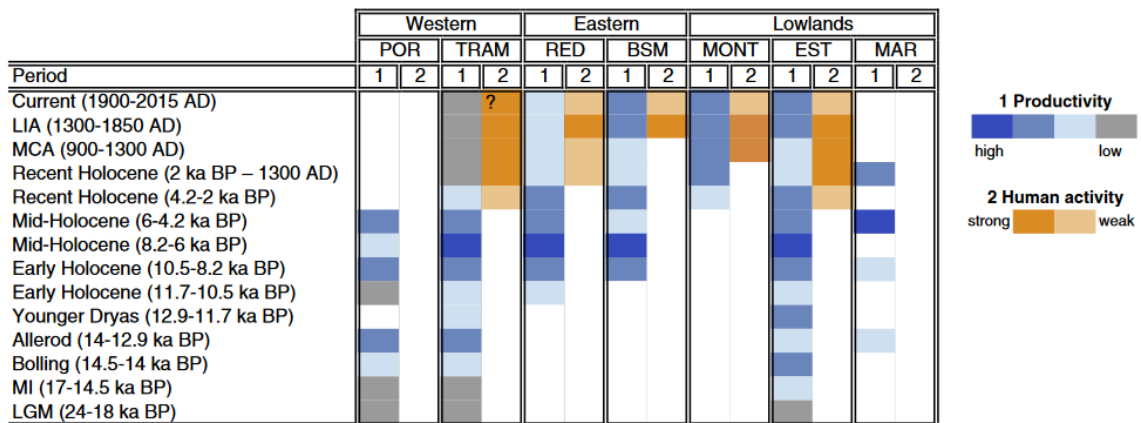
Fig 1.4. *Synthesis of environmental variation since the LGM to current times in the Central Pyrenees. Each column represents the qualitative value of (1) productivity and (2) human activity following the colour gradient in the legend. Lake sites are organized in western, eastern and lowlands attending at their relative latitudes and within these categories, attending at their altitudes. POR: El Portalet, TRAM: Tramacastilla, RED: Redon, BSM: Basa de la Mora, MONT: Montcortès, EST: Estanya, MAR: Marcelino. Extracted from González-Sampériz et al. (2017).*

16

I.4.2   The Holocene

The Holocene provides the opportunity to study the linked ocean–atmospheric dynamics shifts as the Earth system undergoes a transition from a world dominated by massive continental ice sheets to one where the ice sheet extent in the northern high latitudes and alpine regions was reduced (Mayewski et al., 2004). The climate throughout the Holocene has shown significant variability despite the ice core records from Greenland indicated very stable temperatures (Rasmussen et al., 2014) (Fig. 1.5A). Orbital variation has a pronounced impact on atmospheric circulation patterns and hence on Holocene temperature and/or precipitation patterns, although with considerable variability in magnitude and rate depending on different regions (Fig. 1.5B; Marcott et al., 2013) and climatic archives (Fig. 1.5C; Affolter et al., 2019; Kaufman et al., 2020; Kobashi et al., 2017; Marsicek et al., 2018; Mayewski et al., 2004; Smith et al., 2016).

At the onset of the Holocene, a period of rapid ice-sheet retreat and sea-level rise under interglacial climate conditions, summer insolation was maximized in the mid to high latitudes of the Northern Hemisphere (Mayewski et al., 2004), with pronounced impacts on climate and the landscape (e.g., thinning at the margins of the Greenland ice sheet; Vinther et al., 2009). Global and Northern Hemisphere temperature anomaly reconstructions (referenced to the 1961–1990 instrumental mean) during the Holocene (Marcott et al., 2013) allowed the identification of an early to middle Holocene Thermal Maximum (HTM; ~10 to 6 kyr BP) and a subsequent cooling trend as we approached the present (Fig. 1.5B). Northward heat transport in the Atlantic basin by the meridional overturning circulation (AMOC) may have weakened since the middle Holocene (Hoogakker et al., 2011), contributing to the strong cooling in the North Atlantic while dampening cooling in the mid- to high-latitude Southern Hemisphere (Fig. 1.5B) due to the bipolar seesaw (Broecker, 1998). On the other hand, climate models and new pollen-inferred temperature reconstructions (Fig. 1.5C) show evidence of lower temperatures during the early Holocene and continuous warming until approximately 2 kyr BP in the Northern Hemisphere (Marsicek et al., 2018), a temperature evolution that is supported by qualitative temperature records from Eurasia (Baker et al., 2017). These contradictory temperature evolution deduced from models and some proxy records is known as the Holocene temperature conundrum (Liu et al., 2014).
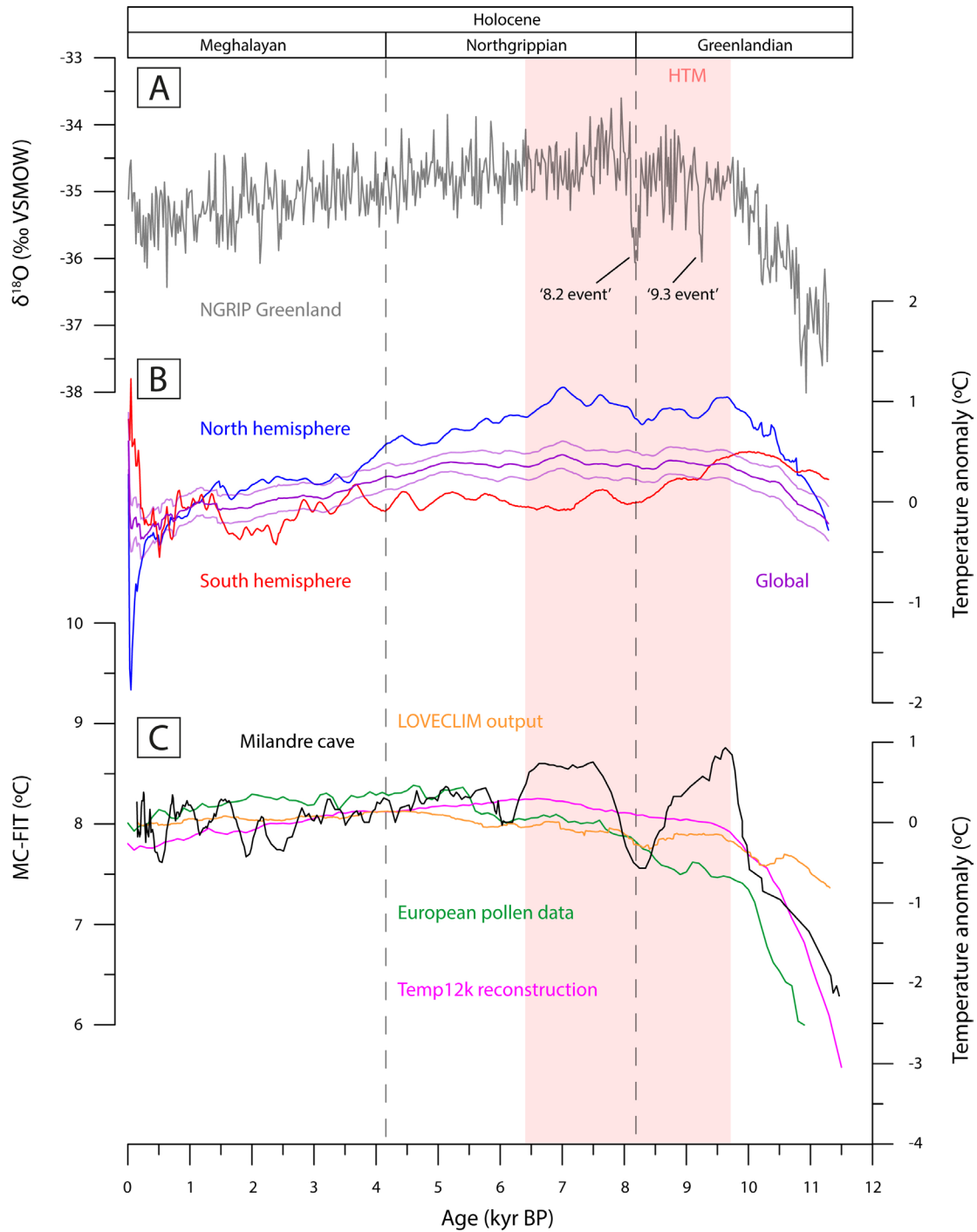
Fig 1.5. *Holocene temperature records. A) North Greenland Ice Core Project (NGRIP). B) Global (purple; with 1s uncertainties), Northern Hemisphere (blue), and Southern Hemisphere (red) proxy temperature stacks as deviations from the 1961 to 1990 instrumental mean (Marcott et al., 2013). C) European pollen record (Marsicek et al., 2018) (green), Switzerland MC-FIT (Affolter et al., 2019) (black), multi-method median global mean surface temperature reconstruction (Kaufman et al., 2020)(pink), and mid-latitude band (30–60°N) LOVECLIM (Kobashi et al., 2017)(orange) transient simulations of mean annual temperatures.*

The Milandre Cave Fluid Inclusion Temperature Record (MC-FIT) from Switzerland (Fig. 1.5C) adds new non-biogenic evidence for the occurrence of an HTM in central Europe and documents a significant temperature gradient between central and northeastern Europe (Affolter et al., 2019). The contradiction between this array of global cooling evidence and warming at high latitudes (Baker et al., 2017; Marsicek et al., 2018) sheds light on the influence of the Laurentide and Fennoscandian ice sheets that would act on high-latitude continental proxies, as modeled for summer temperatures (Renssen et al., 2009), while mid to low latitudes are less affected.

The hydrological responses during this period of rapid oceanic and atmospheric changes at the Holocene onset, are even more complex and show a high spatial and temporal variability (Clark et al., 2012). In the Northern Hemisphere, although there is a general pattern of increase in humidity following arid conditions during the late glacial, differences are evident when comparing records from different latitudes and regions (Garcin et al., 2007; Magny et al., 2003; Magny & Bégeot, 2004). An example of this is the available paleoclimate reconstructions from the Mediterranean region, which show a progressive increase in humidity during the transition from late glacial to Holocene conditions, but interrupted by arid periods with variable intensity, timing, and temporal duration, in some cases restricted to the Younger Dryas and in other cases, extending into the first millennia of the Early Holocene (Magny et al., 2013; Moreno et al., 2012; Zielhofer et al., 2017). Indeed, well-dated, lacustrine, speleothem, and terrestrial pollen records from the IP spanning the Holocene onset and the Early Holocene (11.7-8 kyrs BP) show large hydrological fluctuations and landscape changes with a complex regional pattern in timing and intensity (González-Sampériz et al., 2017; Morellón et al., 2018; Moreno et al., 2017).

After this well-documented HTM, a dry tendency that mimics the long-term trend of decreasing values in summer insolation was also identified in different records from the IP. Generally dry conditions across much of Iberia between ca. 8 and 5 kyr BP are suggested by the northwest Iberian Cova de Arcoia (Railsback et al., 2011), the GAR-01 stalagmite (Baldini et al., 2019), stalagmites from caves in the Iberian range (Moreno et al., 2017), a sharp decrease in precipitation derived from the growth rates of 11 stalagmites on the Cantabrian coast (Stoll et al., 2013), and a composite record of six stalagmites from Buraca Gloriosa (BG) in western Portugal (Thatcher et al., 2020). Lake records from Spain (González-Sampériz et al., 2017; Jambrina-Enríquez et al., 2014; Moreno et al., 2011) and a pollen-based climate reconstruction from Mauri et al. (2015) support the increasingly dry conditions in Iberia during the middle Holocene. However, dry conditions were not reached at the same time at all sites. These proxy records suggest that during the mid-Holocene, aridity prevailed in both southern and northwestern Iberia, while moisture availability in the north was likely higher (probably controlled by the winter westerlies) than in southern Iberia, as reflected by the continuous growth of northern (Baldini et al., 2019) relative to southern stalagmites between ca. 8 and 5 kyr BP (Walczak et al., 2015). Climatic trend reconstruction of Holocene precipitation in the Mediterranean using an approach

based on both terrestrial and marine pollen records, along with a model–data comparison based on a high-resolution regional model, seems to corroborate a north–south division of precipitation regimes during the Holocene, with wet conditions in the south–central and eastern Mediterranean and dry conditions above 45°N during the early Holocene, whereas the opposite pattern dominated during the late Holocene (Fig. 1.6).
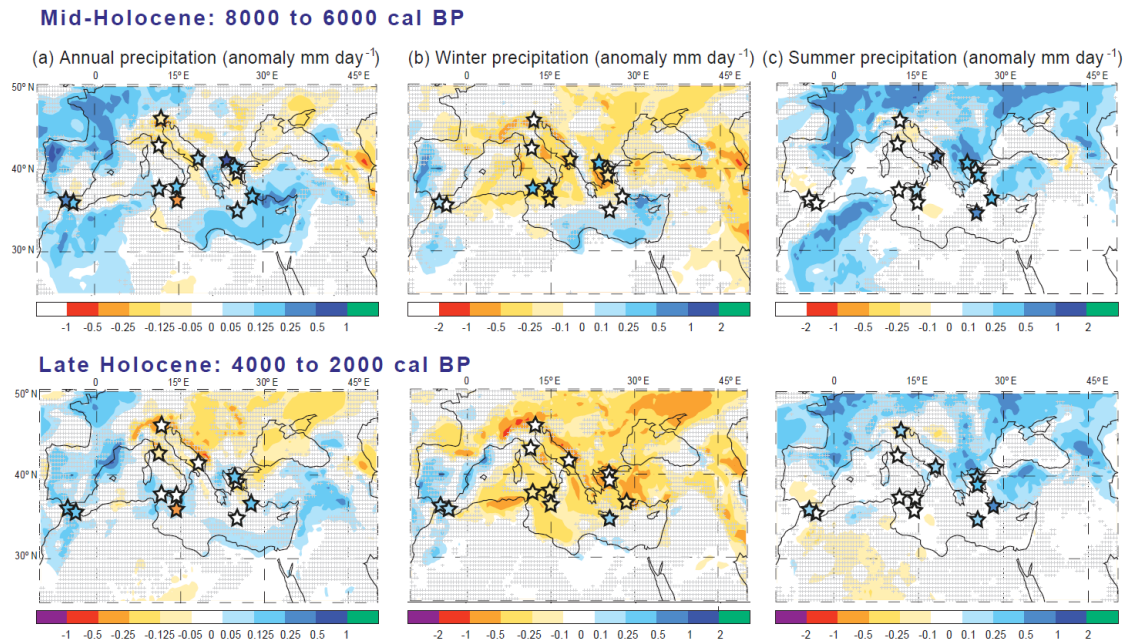
Fig 1.6. *Data–model comparison for mid- and late-Holocene precipitation, expressed in anomaly compared to the present day (mm day^{-1}). Simulations are based on a regional model (Brayshaw et al., 2010). Stars indicate Pollen-inferred climate estimates. A) Annual precipitation, B) winter precipitation (sum of December, January, and February precipitation), and C) summer precipitation (sum of June, July, and August precipitation). Extracted from Peyron et al. (2017).*

The Northern Hemisphere experienced widespread cooling starting at about 6.0-5.5 kyr BP, known as the Neoglacial period (Davis et al., 2009; Kumar, 2011). This cooling is known throughout Europe (e.g., Ilyashuk et al., 2011; Larocque-Tobler et al., 2010), and in the IP is documented by *Globigerina bulloides* Mg/Ca SST from the Alboran Sea (Català et al., 2019) and continental chironomid-based temperature reconstruction from la Basa de la Mora in central Pyrenees (Tarrats et al., 2018), among others. Glaciers began to expand around 6 kyr BP in both the southern (García-Ruiz et al., 2020) and northern (Gellatly et al., 1992) parts of the Pyrenees and Arctic-Alpine species such as *Dryas octopetala* spread (Leunda et al., 2019), simultaneously with the accumulation of ice in caves at high elevations in the central Pyrenees (Sancho et al., 2018). This cooling trend is also consistent with the most important change in depositional

processes in Basa de la Mora (González-Sampériz et al., 2017) and a decreasing trend in pine pollen content in Estanilles (Pérez-Obiol et al., 2012), indicating a likely downward movement of the treeline and the expansion trend of *Juniperus* in Pyrenean lake records (González-Sampériz et al., 2017).

Despite being climatically more stable than the last deglaciation, the Holocene is not free of abrupt climate changes (Crombé, 2018; Wang et al., 2013). One of the main challenges for reconstructing the paleoclimate during an abrupt event is the lack of precise and accurate high-resolution records (e.g., marine sediment chronologies can be hampered by the uncertainties in the radiocarbon reservoir correction). The 8.2 kyr event (Fig. 1.5A) was the strongest cold event in the Holocene and had a significant effect on climate (Alley & Agustsdottir, 2005; Bond, 1997). Currently, most studies agree that the decrease in the AMOC was the cause of the 8.2 kyr event (Barber et al., 1999; Li et al., 2012; Törnqvist & Hijma, 2012). An alternative cause, freshwater outburst from the collapsing ice saddle over Hudson Bay, has also been proposed (Gregoire et al., 2012; Matero et al., 2017). This event was a period of abrupt cooling of 1–3 °C across large parts of the Northern Hemisphere (Fig. 1.7) and is most clearly captured in Greenland ice-core records, where it is reported as a cold and dry anomaly lasting ∼ 160 years, from 8.25 ± 0.05 until 8.09 ± 0.05 kyr (Thomas et al., 2007) defined by a sharp decrease in $\delta^{18}O$ (of more than 1 ‰; Fig. 1.5A).
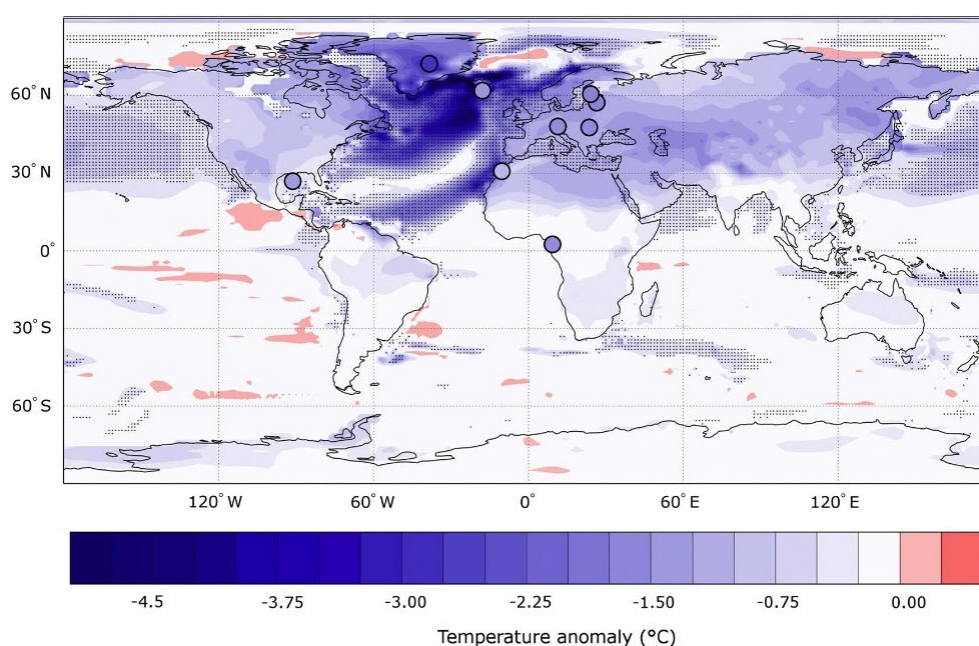
Fig 1.7. *Maximum annual surface temperature change during the 8.2 kyr event. The upper ocean temperature (top 164 m) is shown for marine regions and surface air temperature is shown over continents. The overlain filled circles show geological reconstructions (Morrill et al., 2013) of surface air temperature and upper ocean mean temperature anomalies associated with the 8.2 ka event. Extracted from Matero et al. (2017).*

The 8.2 kyr event has been recorded in numerous archives across Europe (Alley & Agustsdottir, 2005; Morrill et al., 2013) and in the IP (Baldini et al., 2019; Domínguez-Villar et al., 2009; Kilhavn et al., 2022; Pérez-Sanz et al., 2013).

During the early Holocene, there were other cold events, like the one at 9.3 kyr (Fleitmann et al., 2008; Fletcher et al., 2013; Haas et al., 1998; Rasmussen et al., 2007) present in the NGRIP record of Greenland (Fig. 1.5A). Analyses have shown that this cold event was accompanied by corresponding freshwater pulses (Magny et al., 2007; Teller et al., 2002), indicating that its mechanisms might be the same as that of the 8.2 kyr event. Abrupt events during the mid and late Holocene were unrelated to freshwater pulses in the North Atlantic because by that time the Laurentide ice sheet had melted completely (Mayewski et al., 2004). One of the most outstanding events during this period is the 4.2 kyr event, which is reported to have occurred in many regions around the world – although it is focused around the Mediterranean - and was generally characterized by dry and cool climatic conditions (Mayewski et al., 2004). The 4.2 kyr was defined as the chronological divider between the warmer middle Holocene and the cooler late Holocene (after ~4.2 kyr) (Walker et al., 2019). More importantly, this "4.2 kyr Event" was reported to have played important roles in the collapses of three of the four major ancient civilizations (i.e., Ancient India, Ancient Egypt, and Mesopotamia) (deMenocal et al., 2000; deMenocal, 2001; Drysdale et al., 2006; Perry & Hsu, 2000; Staubwasser et al., 2003; Weiss et al., 1993; Weiss & Bradley, 2001). Given that the northern North Atlantic is a key region for the formation of deepwater, which has consequences for the overall global oceanic circulation, the absence of a strong global signal of an abrupt climatic event at 4.2 kyr BP suggests that it is unlikely that the North Atlantic Ocean circulation played a driving role (Bradley & Bakke, 2019). The cause of the 4.2 kyr BP event must be sought elsewhere in terms of direct radiative forcing (possibly due to explosive volcanic events or earth surface aerosols resulting from aridity or solar forcing). Currently, none of these possibilities provides a compelling argument; the alternative is that the observed changes (and other mid- and late-Holocene events) were a consequence of internal climate system variability (Bradley & Bakke, 2019), perhaps modulated by the overall decline in summer radiation across the Northern Hemisphere due to orbital changes, which are generally considered the cause of neoglaciation in the late Holocene.

I.5   Speleothems as paleoclimate archives

Moore (1952) was one of the pioneers in defining the term "speleothems" (from the Greek: spelaion, cave; thema, deposit) given the need to specify mineral deposits that grow inside caverns. The different possible forms that calcareous speleothems can take when growing made the scientific community think, at first, that it would be very complex to obtain records about the past from them (Franke, 1965). However, scientific efforts carried out during the last decades have established speleothems, almost always composed of calcite or aragonite, as one of the most precious resources in the task of understanding the conditions (local, regional, and global) of the formation of different environments and the climate on the surface land in the past (Fairchild et al., 2006; Fairchild & Baker, 2012). This 'conditions' mean not only the local context (soil, vegetation, landscape instability and climate), but also the regional to global patterns of change that characterize former environments and climates (Fig. 1.8).
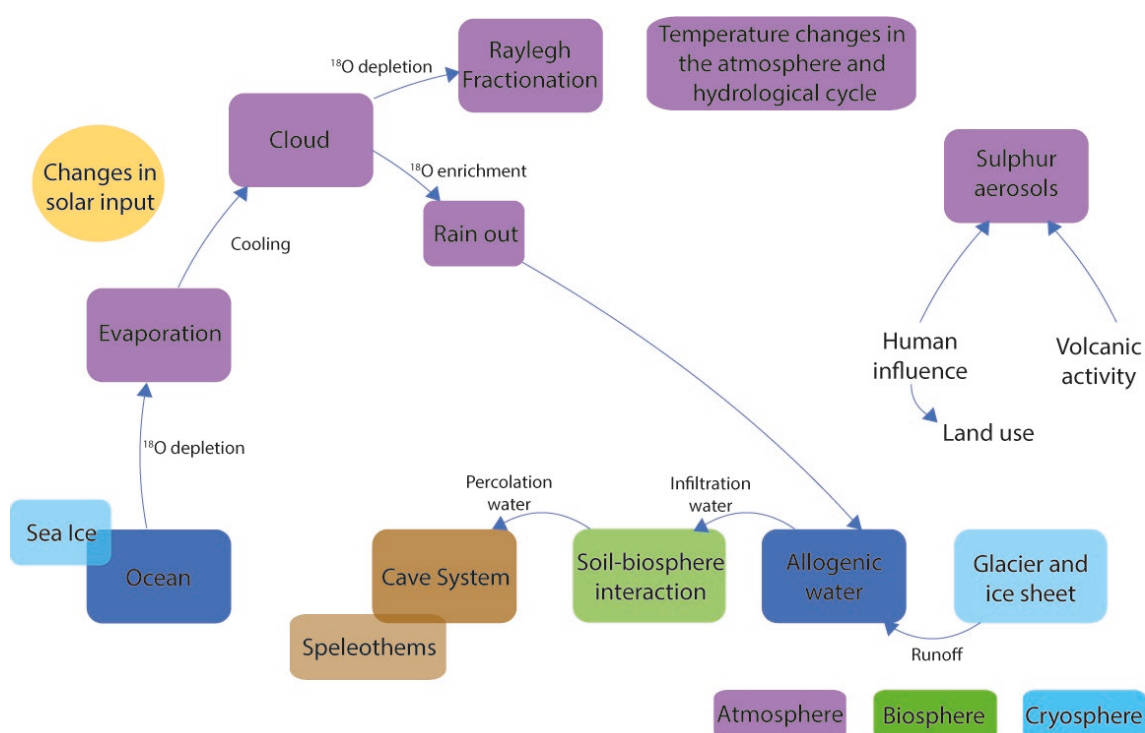
Fig 1.8.   *Speleothems as underground recorders of signals related to parameters of the external Earth system. Edited from Fairchild et al. (2006).*

Calcareous speleothems are divided into different types of formations, but only three of them have current utility in the generation of climatic records (Fairchild & Baker, 2012; Frisia & Borsato, 2010; Hill & Forti, 1997): deposits that grow by dripping water inside a cavity (dripstones), such as stalactites and stalagmites; continuous deposits that form between thin layers of water on the surfaces of caves (flowstones); and crystalline deposits that form underwater

within a cavity. In relation to dripstone-type deposits, stalagmites are more useful as paleoclimatic records in relation to stalactites because their internal structure is much simpler and allows for several observations that represent different periods of time in the past (time series) that form along it in a sub-vertical direction (Baker et al., 1998; Dreybrodt, 1988, 1999; Kaufmann, 2003). The first step in the study of stalagmites is to cut one across the main growth axis. This allows the visualization of the macroscopic characteristics of these speleothems, such as their visible lamination, growth hiatuses, and the main growth axis (Fig. 1.9). Fairchild & Baker (2012) summarized the potential of speleothem records as follows:

> The common occurrence of continuous episodes of growth, thousands of years in duration, and the preservation of information representing timescales from days up to a million years.
> The excellent chronologies that can be obtained by U-series dating.
> Speleothems contain several proxy parameters recorded at very high resolution that can be used singly or in combination.
> They are widespread in inhabited continental areas, so their records have direct relevance to regional climates and environments and may also contribute to archaeological investigations.
> Speleothems are physically and chemically robust and relatively protected from erosion.

Speleothem deposits are controlled not only by the distribution, quantity, and chemistry of water percolating through the karstic aquifer (a property strongly influenced by the surface geomorphology and macroclimate) but also by the cave's peculiar microclimate, which in turn is controlled by cave geometry, aquifer properties, and external microclimates (Fairchild et al., 2007). Therefore, the interpretation of the different proxies to be used in stalagmite records (e.g., isotope records) must be accompanied by a geomorphological description of the cave and an understanding of the present-day dynamics inside it.

I.5.1   How do we date them?

The most widely applicable radiometric technique for dating calcareous speleothems is U-Th disequilibrium dating (^{230}Th-^{234}U-^{238}U), which can be used for a timescale of a few years (limited by the determination of ^{230}Th) to approximately 500-600 kyr (Edwards et al., 1987), although the precision declines beyond 400 kyr. Uranium is soluble and incorporated, via groundwater, into $CaCO^3$ as uranyl ions (UO_2^{2+}), whereas Th is practically insoluble and so will be incorporated into speleothems only with non-carbonate phases (organic matter, colloidal material, and sediments). The fundament of the U-Th method relies on the decay of ^{238}U through two short-lived intermediate daughter isotopes to ^{234}U and the decay of ^{234}U to ^{230}Th (Cheng et al., 2000). The rapid technological evolution from alpha-spectrometry to thermal ionization mass

spectrometry (TIMS) (Edwards et al., 1987) and multicollector inductively coupled plasma mass spectrometry (MC-ICP-MS) has dramatically increased the resolution and precision of dating systems (Cheng et al., 2013). The sample size decreased from 10–100 g (alpha-spectrometry) to 10–500 mg (TIMS and MC-ICP-MS), and the precision (2σ) in the ^{230}Th analyses improved markedly (Cheng et al., 2013; Goldstein & Stirling, 2003). Precision is limited mainly by primary ^{238}U concentration (variable over several orders of magnitude in different carbonate samples) and the contamination by external Th ('detrital' Th), this offers analytical challenges but can be overcome with sufficient knowledge of primary ^{230}Th/^{232}Th ratios (Edwards et al., 2003; Richards & Dorale, 2003).
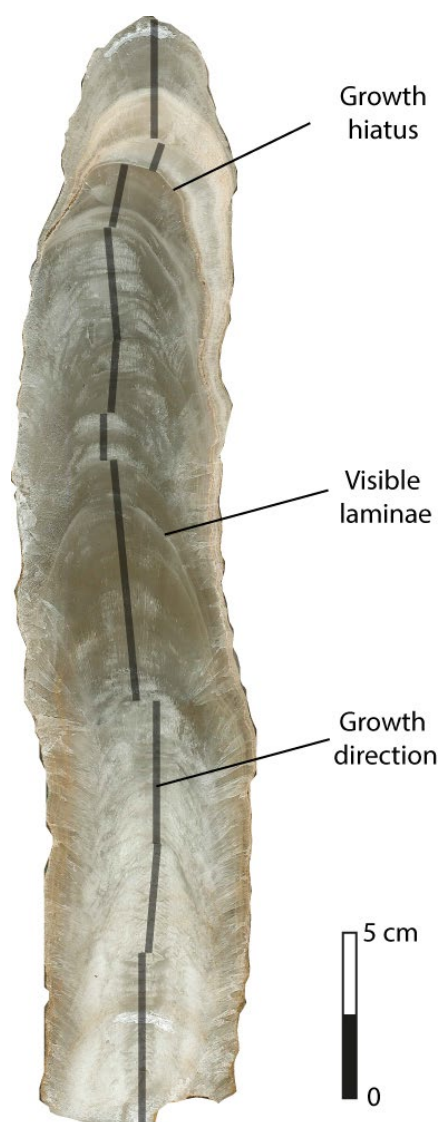
Fig 1.9. *Cross-section through a stalagmite (OST2, Ostolo cave) illustrating visible growth layers (laminae) and the shifting position of the growth axis (growth direction), which represents the ideal position to generate the most continuous time series.*

New algorithms (e.g., StalAge) have been designed to construct speleothem age models. Algorithms use U-series ages and their corresponding age uncertainty for modelling and also include stratigraphic information to further constrain and improve the age models of dated speleothems. Currently, these algorithms are applicable to problematic datasets that include outliers, age inversions, hiatuses, and large changes in the growth rate (Scholz & Hoffmann, 2011). Other techniques for dating stalagmites and improving age models include interval dating by counting the annual layers (e.g., Domínguez-Villar et al., 2009) and ^{14}C dating (Lechleitner et al., 2016), the latter is limited by uncertainty over the percentage of dead carbon and organic matter from the soil in a given sample incorporated during growth (Genty et al., 2001). For samples older than 500 kyr, low-precision ages can be obtained from paleomagnetic methods (Osete et al., 2012), electron-spin resonance (Grün, 1989), and ^{234}U/^{238}U disequilibrium (Ludwig et al., 1992). New improvements in reaching older periods at high resolution using the U-Pb method with low Pb concentrations exist, but some correction problems remain unsolved (Hellstrom & Pickering, 2015; Woodhead & Pickering, 2012).

I.5.2   Stable isotopes as proxies for past environments and climates

Stable isotope studies have formed a major type of geochemical investigation into speleothems (Fairchild et al., 2006; Harmon et al., 2004; Lachniet, 2009; McDermott, 2004). The signal of stable isotopes undergoes many phase changes that control its pathway (through the atmosphere, hydrosphere, soil, and epikarst zone), which are finally recorded in stalagmites. These phase changes are known as fractionation, in which one isotope of a certain element is favored in relation to another in relation to the difference in its atomic weight. The fractionation of these isotopes can be carried out in equilibrium or kinetics (Dansgaard, 1964). Variations in the ^{18}O/^{16}O and ^{13}C/^{12}C ratios in calcite speleothems ($\delta^{18}O_c$ and $\delta^{13}C_c$) can provide important information about the terrestrial paleoclimate (if deposition occurs under equilibrium conditions) because variations in their internal chemical and isotopic compositions are determined by the environmental conditions at the time of deposition (Harmon et al., 2004), and they tend to behave as geochemically closed systems (e.g., Gascoyne, 1992; Schwarcz, 1986). Speleothem deposition frequently occurs under conditions of isotopic equilibrium; however, in most cave systems, equilibrium isotopic fractionation is modified by kinetic effects (Mickler et al., 2004) resulting from factors such as high supersaturation of the water (Kim & O'Neil, 1997) and outgassing and evaporation (Gonzalez & Lohmann, 1988). Fortunately, two features of the cave environment facilitate the use of stable isotopes in paleoclimatic reconstruction. First, cave air temperatures remain relatively constant throughout the year, and are similar to the mean annual air temperature of the region above the cave. Second, in cool temperate regions, cave air is characterized by high humidity levels (typically 95–99%), minimizing evaporation, which might otherwise cause

kinetic isotope fractionation (McDermott, 2004) that may modify the original climatic signal. In this section, the processes that affect $\delta^{18}O$ and $\delta^{13}C$ are summarized.

I.5.2.1 The $\delta^{18}O$ signal

The first steps in the fractionation of $\delta^{18}O$ occur within the atmosphere-hydrosphere interaction (Fig. 1.10). When ocean water ($\delta^{18}O_{sw}$) evaporates, it prefers to release the oxygen isotope with the lowest atomic mass; therefore, the concentration of the light isotope increases in the vapor phase ($\delta^{18}O_v$). On the other hand, the condensation of this vapor in the atmosphere in the form of rainwater ($\delta^{18}O_r$) will prefer to incorporate heavier atomic weight isotopes in the liquid phase (greater $\delta^{18}O$ in rain). This last step, which is directly dependent on temperature, is known as Rayleigh fractionation or distillation (Kendall & Caldwell, 1998). This $\delta^{18}O$ fractionation process can be conducted within different contexts and climatic conditions in the atmosphere as well as in the hydrosphere (Fig. 1.10); therefore, it is of fundamental importance in any paleoenvironmental or climatic work to consider the following effects (or a combination of them) in the $\delta^{18}O$ fractionation:

> *Temperature effect (T):* As mentioned above, fractionation is temperature dependent (Dansgaard, 1964; Lachniet, 2009). For example, colder climates allow more condensation and carry out significant fractionation of $\delta^{18}O$ (e.g., Baker et al., 2019).

> *Altitude effect:* At higher altitudes, precipitation is more depleted in heavy isotopes than at lower elevations (Clark and Fritz, 1997; Dansgaard, 1964; Kendall & Caldwell, 1998). A negative stable isotope altitude gradient is expected in this case (e.g., Kong & Pang, 2016).

> *Amount effect (P):* There is a strong correlation between the depletion of heavy isotopes and the amount of rain (Lachniet, 2009). Therefore, $\delta^{18}O$ decreases when the amount of rain increases (e.g., Moreno et al., 2014b).

> *Source effect:* This effect considers that air masses derived from different moisture sources have distinct $\delta^{18}O$ values (Lachniet, 2009) based on regional differences in $\delta^{18}O$ and temperature in the oceans (e.g., LeGrande & Schmidt, 2006, 2008).

> *Continental effect:* $\delta^{18}O$ decreases with increasing distance from the main moisture source (Dansgaard, 1964), proving the importance of moisture loss from an air mass during the passage of extensive territories (e.g., Lachniet et al., 2007).

> *Ice volume effect (V_{ice}):* Because evaporation of ocean water preferentially removes light stable isotopes into the vapor, $\delta^{18}O_{sw}$ will increase as the volume of freshwater stored on the continents as ice increases (Lachniet, 2009). The increase in ice volume accounts for an approximately 1.0–1.2 per mil enrichment in $\delta^{18}O_{sw}$ of the global ocean at the Last Glacial Maximum relative to today (e.g., Shah et al., 2013).

> *Seasonality effect:* During different seasons, a region can experience strong changes in precipitation and/or temperature, such that the relative proportions of summer and winter and their related changes in moisture sources may result in abrupt variations in $\delta^{18}O$ values on different paleoclimate time scales (Denton et al., 2005). Changes in seasonality also apply to different air mass trajectories and dominant synoptic patterns of precipitation (e.g., Baldini et al., 2019; Moreno et al., 2014b).

> *Evaporation effect:* Recycled continental moisture that returns to the atmosphere due to the evaporation of water from soils, lakes, and rivers exhibits high $\delta^{18}O$ values (Koster et al., 1993; Rozanski et al., 1993).
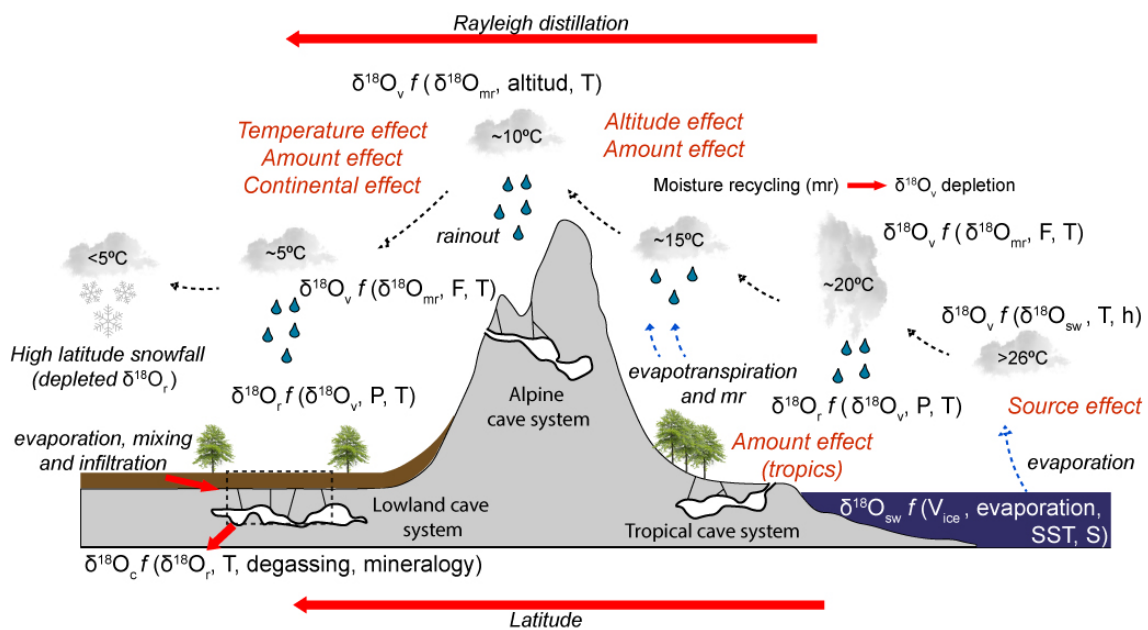
Fig 1.10. *Diagram illustrating the fundamental processes affecting $\delta^{18}O$ in the hydrological cycle relevant to speleothem paleoclimatology. The dominant controls are based on variations in temperature and relative humidity, which influence the $\delta^{18}O$ values through various processes and phase changes in the ocean, atmosphere, hydrosphere, soil, and epikarst zones, and finally in speleothem $CaCO_3$ ($\delta^{18}O_r$). See the text for further details. In the Figure, f indicates it is a function of the listed variables, and h indicates the relative humidity. Extracted and modified from Lachniet (2009) and Baker (2014).*

As we have seen, the effects that rainwater can suffer in terms of $\delta^{18}O$ fractionation are varied. This does not end there, since when the water contacts the soil, the epikarst, and the cave environment, there are other new effects to consider (Fig. 1.10):

> *Evaporation:* Evaporation and subsequent higher $\delta^{18}O$ values of the infiltrating waters can occur in the soil, epikarst, and inside the cave (Fairchild et al., 2006). Regions with arid climates are associated with the greatest evaporative enrichment. Most caves lacking large openings to the surface are characterized by relative humidity values at or near 100%, but the $\delta^{18}O$ value of drip water ($\delta^{18}O_d$) may be increased by evaporation in caves with low relative humidity, low air circulation, and long residence time of the water on a stalactite or stalagmite tip (Fairchild & Baker, 2012).

> *Infiltration and mixing:* Fractionation can result from the mixing of various infiltrating waters, with soil moisture typically having less $\delta^{18}O$ variability than precipitation (Tang & Feng, 2001). In some cases, such mixing appears to be rapid and occurs near the surface (Cruz et al., 2005). Infiltration of lower $\delta^{18}O$ waters may be favored in climates with intense precipitation concentrated in time, or with selective infiltration biased to the winter rainy season, resulting in lower $\delta^{18}O_d$ than the weighted mean precipitation (Lachniet, 2009).

> *Rate discharge:* $\delta^{18}O_d$ variability can be observed within the same cave, attending to the drip rate discharge between different drips (Lachniet, 2009).

> *CO^2 degassing:* Kinetic fractionation is associated with incomplete or rapid reactions in which the equilibrium between phases is not maintained, such as during fast and/or extensive CO^2 degassing (Hendy, 1971).

> *Carbonate mineralogy:* Stalagmites are usually formed by calcite and/or aragonite. These two differ in their fractionation factors, giving rise to the fact that aragonite usually has higher $\delta^{18}O_c$ values than calcite at the same formation temperature (Frisia et al., 2002).

I.5.2.2   The $\delta^{13}C$ signal

The $\delta^{13}C_c$ values can provide information on climate and vegetation conditions (e.g., Fohlmeister et al., 2020; McDermott, 2004) but still it is difficult to attribute individual processes as the driving force behind $\delta^{13}C_c$ variations (Griffiths et al., 2012). The $\delta^{13}C$ signal is less affected by evaporative effects than $\delta^{18}O$ when the water contacts the soil, epikarst, and cave environment (Fairchild et al., 2006). However, $\delta^{13}C$ may also be affected by other kinetic factors.

> *Type and density of vegetation:* The $\delta^{13}C$ composition of soil gas CO^2 is influenced by the type and density of vegetation above the cave (Fohlmeister et al., 2020), depending on the dominant photosynthetic pathway (e.g., C3 or C4 plants) and the soil respiration

29

rate by changes in vegetation cover. For densely vegetated cave environments with high soil air pCO_2, soil water mirrors the soil air C isotopic composition, and a certain offset is mainly induced by isotope fractionation effects (Fohlmeister et al., 2020).

> *Soil gas CO_2:* Soil gas CO_2 is dissolved in percolating meteoric water, introducing a temperature-dependent fractionation effect on $\delta^{13}C$. This acidic water dissolves the underlying host rock carbonate until the solution reaches equilibrium with Ca^{2+}. Dissolution can occur under "open" conditions, where enough gaseous CO_2 is available in the soil or karst to allow for complete carbon exchange with the dissolved inorganic carbon species, or under "closed" conditions, where no gaseous CO_2 is present and carbon exchange is absent (Hendy, 1971). Intermediate conditions generally prevail in natural systems, as often only a limited amount of gaseous CO_2 is available (e.g., Genty et al., 1998; Rudzka et al., 2011).

> *CO_2 degassing:* Once the water solution reaches the cave atmosphere with a lower partial pressure of CO_2 (pCO_2), CO_2 begins to degas from the solution, triggering $CaCO_3$ precipitation. This process is accompanied by temperature-dependent carbon isotope fractionation processes.

> *Prior calcite precipitation:* Carbonate precipitation occurring before reaching the apex of the stalagmite is known as prior calcite precipitation (PCP). This effect produces high $\delta^{13}C$ values unrelated to changes in vegetation type or intensity. The degree of PCP usually depends on two parameters: A) the pCO_2 gradient between the water and the gaseous phase, and B) the length of the period the water is in contact with the cave air before dripping (Stoll et al., 2022a).

I.5.3 Trace element partitioning: Additional paleoenvironmental information

The use of trace-element concentrations (e.g., Mg, Sr, Ba, Y, Cu, Zn, and U) as paleoclimate and paleoenvironmental proxies is becoming a standard practice in speleothem reconstruction (Fairchild & Treble, 2009; Griffiths et al., 2010; Regattieri et al., 2016). The use of trace elements allows to corroborate the paleoenvironmental interpretations obtained from other proxies (e.g., $\delta^{18}O$ and $\delta^{13}C$) and provides additional information that can be used to unravel seasonal variability and paleohydrology in speleothem chemistry. Examples include the use of trace element concentrations as proxies for precipitation (Baldini et al., 2002; Vansteenberge et al., 2020; Wang et al., 2001), soil processes (Borsato et al., 2007; Treble et al., 2003), changes in sediment supply (Regattieri et al., 2016), and changes in atmospheric input (anthropogenic, volcanic-derived aerosols, and volcanic ash fall events) (Frisia et al., 2005a; Jamieson et al., 2015). In principle, three groups of transport and incorporation of trace elements into $CaCO_3$ can be distinguished.

> Those that are present in fluid or solid inclusions within the $CaCO_3$ (e.g., Y, Zn, Cu). In cases where solid inclusions are introduced by high flows, the distribution of such elements can be hydrologically significant.

> Those that are incorporated interstitially on a molecular scale in $CaCO_3$ (e.g., PO_4, Na, and F in calcite). Typically, these components are preferentially incorporated at growth defects and tend to be more abundant where crystals have more defects, which is related to either the rate or style of growth.

> Those that substitute Ca or CO_3 in the $CaCO_3$ lattice (e.g., Mg, Sr, Ba, U, and SO_4).

The sources of trace elements include aeolian particles, dry and wet atmospheric deposition, bedrock, superficial sediment deposits, inorganic soil constituents, and elements recycled via the soil biota (Fairchild & Treble, 2009). Atmosphere is only a subordinate source for trace elements. However, Sr isotope signals have been shown to be related to the supply of aeolian dust in speleothems, and sea salt aerosols in wet atmospheric deposition can be an important source for certain trace species in karst waters, sometimes including Mg or Sr, where the bedrock supply is limited (Baker et al., 2000; Fairchild et al., 2000). Temporal changes in sulfate in drip water can be linked to changes in atmospheric pollutants (Spötl et al., 2005), and this can be captured in speleothems under favorable circumstances (Frisia et al., 2005a). Despite the above exceptions, the primary sources of calcium and most trace elements in speleothems are the bedrock and overlying regolith, including bedrock fragments in the soil, and dissolution is focused in the zone where pCO_2 is at a maximum.

Fairchild et al. (2000) noted that during periods of low flow (longer water-rock and/or water-soil contact times), PCP could preferentially remove Ca from dripwaters, elevating the ratios of alkali metals (Mg/Ca, Ba/Ca, and Sr/Ca). This means that given the constant partitioning of these trace elements into speleothems, periods of low flow would be recorded by high Mg/Ca, Ba/Ca, and Sr/Ca ratios (Stoll et al., 2012). PCP is dependent on the drip interval, but also on seasonal variations in cave pCO2, which can change the amount of calcite precipitated on cave ceilings and result in variations in dripwater Mg/Ca, Sr/Ca, and Ba/Ca ratios (Mattey et al., 2010). Although seasonal covariation of Mg/Ca, Sr/Ca, and Ba/Ca and amplified signals due to PCP are expected, the interpretation of trace element concentrations of speleothems has proven to be considerably more complex (Stoll et al., 2012). This is because some stalagmites exhibit anticorrelation between Mg/Ca and Sr/Ca (and Ba/Ca) at seasonal and interannual scales. Deviations from the expected PCP control may reflect variations in the partitioning coefficients of Sr (or Ba) (Stoll et al., 2012). Increased Sr with a higher growth rate or saturation state has been widely observed in non-cave analog laboratory experiments (Lorens, 1981; Tang et al., 2008; Tesoriero & Pankow, 1996). According to Nielsen et al. (2013), the magnitude of the

growth rate dependence depends on the forward and reverse reaction rates, which are sensitive to the temperature and solution chemistry.

I.5.4 Stalagmite fabric types

When analyzing the geochemistry of a stalagmite to obtain a paleoclimatic interpretation, petrographic descriptions of the stalagmite time series are crucial, especially where proxies such as stable isotopes and trace elements are fundamental for understanding past climate changes (Fairchild & Baker, 2012; Frisia, 2015). The spatial orientation of crystallites (the smallest crystals that form composite crystals) and their relationships are called *speleothem fabrics* (Frisia et al., 2000). Fabrics provide valuable information on post-depositional phenomena (diagenesis) such as phase transformations (aragonite to calcite), aggrading neomorphism (Frisia, 1996), and dissolution and re-precipitation processes, which may alter the original geochemical signal. Petrographic observations should not be confined solely to the identification of diagenesis, particularly when U-series dating is problematic (Hoffmann et al., 2009; Lachniet et al., 2012; Ortega et al., 2005). Stalagmite fabrics have been most comprehensively studied and classified by Frisia & Borsato (2010), updating (Frisia et al., 2000). Currently, studies are still looking for a system that allows the construction of a fabric time series comparable to geochemical time series (Frisia, 2015). Calcite shows a large variety of morphologies, but known speleothem fabrics can be grouped into a few broad categories: columnar, dendritic, micrite, microsparite, and mosaic calcite (cf. Frisia & Borsato, 2010). For simplicity, only the fabrics described later in this work are summarized below (Fig. 1.11).

I.5.4.1 Columnar

The columnar calcite proper (C) consists of crystals with the c axis commonly at 90–60° to the substrate (Fig. 1.11A), unit extinction, and length fast, with a length-to-width ratio < 6:1 (Frisia et al., 2000). Acute and equant rhombohedra are the predominant individual crystal forms (Dickson, 1993). In temperate climate settings, C fabric forms under relatively constant discharge, low (up to 0.35) calcite supersaturation state (SIcc), low Mg concentration in dripwater (Mg/Ca ratio < 0.3), and negligible presence of particulate and/or organic colloids. When the crystals form a compact aggregate with welded crystal boundaries, where the inter-crystalline porosity is not discernible under an optical microscope, the fabric becomes columnar compact. When the intercrystalline boundaries are marked by the presence of linear inclusions or pores, the fabric is columnar open (Co). Because columnar compact and columnar open fabrics result from growth processes that imply a combination of low/high drip rates and high/low degassing, the C isotope ratios in the two types may be modified by kinetics. Given the common low Mg/Ca ratio range

measured to date in their parent waters (0 to 0.3), trace element variability may likely reflect impurities trapped within intercrystalline spaces in the open type.

I.5.4.2 Columnar elongated

Elongated columnar (Ce) is composed of crystals with a length-to-width ratio of 6:1 (Fig. 1.11B), most commonly 2 up to 60 mm long, and 0.2 up to 5 mm wide (Frisia, 2015). In certain cases, these figures can exceed, particularly where stalagmites do not show visible interfaces and renucleation phenomena. The elongated columnar fabric is the result of preferential growth of the acute rhombohedron. Elongated columnar type forms from constant drip, with similar SIcc but higher Mg/Ca ratios (>0.3) than for columnar compact and open.

I.5.4.3 Columnar microcrystalline

The columnar microcrystalline fabric (Cm) is characterized by polycrystals with a length-to-width ratio < 6:1, highly irregular intercrystalline boundaries (Fig. 1.11C), uniform extinction, and punctuated by inter- and intra-crystalline microporosity (Frisia et al., 2000). Cm is typical in speleothems, showing laminae rich in organic colloidal particles and fed by a variable drip rate (cf. Frisia et al., 2000). The notable difference from the typical columnar fabric is the highly irregular crystal boundaries, which developed because of the presence of foreign particles that favored the formation of crystal defects. Cm has serrated boundaries, and because of the composite nature of each individual with uniform extinction, some of the "crystallites" of adjacent polycrystals crosscut each other, creating areas where the extinction is different from that of the cross-cut individual. The presence of intracrystalline porosity and impurity-rich layers results in the opaque and milky appearance of Cm type in the polished hand specimen with visible "flame-like" polycrystals.

I.5.4.4 Dendritic

The Dendritic (D) fabric is composed of branching polycrystals (Fig. 1.11D), with each branch consisting of stacked rhombohedra (Frisia, 2015). Under the optical microscope, two branches form an angle of ca. 90º, and are inclined of ca. 45º relative to the substrate (V-shaped aspect). In the hand specimen, fabric D is characterized by a milky, opaque appearance due to high intercrystalline porosity, related to the voids, which may then be sites where particles, impurities, or fluid inclusions are trapped. Fabric D may be the result of bio-influenced mineralization (Banks et al., 2010). Frisia et al. (2000) documented that the development of D fabrics required variable discharge, enhanced CO_2 degassing and a slightly higher SIcc (up to 0.4) than the C fabrics. In paleoclimate studies, the best strategy for sampling when speleothems show

D fabric is to compare geochemical time series in two coeval specimens from the same cave with diverse stalagmite morphologies.
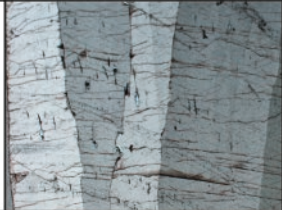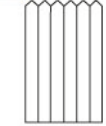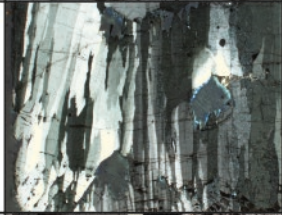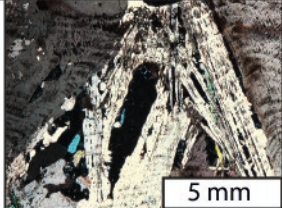
A		Columnar (C)	Relatively slow and constant drip; low impurity content.
B		Columnar elongated (Ce)	Drip rate > than in C.
C		Columnar microcrystalline (Cm)	Variable drip rate (seasonal); drip/flow carrying colloidal particles.
D		Dendritic (D)	Variable drip rate; strong degassing; presence of particles/foreign ions; bio-influenced precipitation. 5 mm

Fig 1.11. *Summary of calcite speleothem fabrics described in stalagmites in this thesis. Their symbols, codes, and known environmental parameters that underpin their development are also described. The diagrams and descriptions of each fabric were modified from those in Frisia (2015).*

I.5.5   Fluid inclusions in stalagmites: A thermometer for paleoclimate research

Although $\delta^{18}O_c$ records are of great value for understanding paleoclimate, their interpretation remains difficult because they can be influenced by several and sometimes competing climatic and non-climatic factors (Lachniet, 2009), such as changes in seasonality of rainfall, varying cave air temperatures, and evaporation. To overcome this uncertainty, the oxygen and hydrogen isotopic compositions of water in fluid inclusions in speleothems ($\delta^{18}O_{FI}$ and δD_{FI}) are important hydroclimate proxies, because they provide information on the isotopic compositions of rainwater in the past (Dublyansky & Spötl, 2009; Fleitmann et al., 2003; Genty et al., 2002; Harmon et al., 1979; Labuhn et al., 2015; McDermott, 2004; Schwarcz et al., 1976). Moreover, because isotopic differences between fluid inclusion water and host calcite provide

information on past isotopic fractionation factors, they are also useful for quantitative estimation of past temperature changes (Demény et al., 2016; Genty et al., 2002; McGarry et al., 2004; Meckler et al., 2015; Uemura et al., 2016). Fluid inclusion water isotopes can be measured using different analytical techniques (Affolter et al., 2014; Arienzo et al., 2013; Dublyansky & Spötl, 2009; Vonhof et al., 2006) and three fluid inclusion-based paleotemperature reconstruction approaches (Demény et al., 2021; Uemura et al., 2020), which are briefly described below.

> *Combined analyses of hydrogen and oxygen isotope ratios performed directly on H_2O from the sample*: Analyses of stable isotope compositions of inclusion-hosted water, combined with the determination of the oxygen isotope composition of the host carbonate produce carbonate-water oxygen isotope fractionation values that in turn can be used to calculate formation temperatures, when fractionation-temperature relationships are applied (Schwarcz et al., 1976; Uemura et al., 2016). However, studies that apply these analyses do not usually use measured carbonate and $\delta^{18}O_{FI}$ compositions to calculate formation temperatures (Demény et al., 2021). This is partly because (i) extensive diagenetic alteration due to post-entrapment fractionation processes can deteriorate the original $\delta^{18}O_{FI}$ composition; (ii) site-specific carbonate-water oxygen isotope fractionation may also complicate the interpretation of calculated temperatures; and (iii) uncertainty derived from differences in various calcite-water oxygen isotope fractionation equations affects all of the paleotemperature calculations that apply oxygen isotope compositions of calcite and water.

> *Use of the δD_{FI} to calculate the $\delta^{18}O_{FI}$ value:* δD_{FI} is determined for the extracted fluid inclusion, and the $\delta^{18}O_{FI}$ is calculated using the local or global meteoric water line (the relationship between hydrogen and oxygen isotope compositions of meteoric waters). As the $\delta^{18}O_{FI}$ composition is calculated and carbonate is measured, the formation temperature is given as above. This approach has two major uncertainties: (i) knowledge of the local meteoric water line equation, which is valid in the time period studied, and (ii) selection of the carbonate-water oxygen isotope fractionation equation.

> *Based solely on δD_{FI} composition:* This third approach uses the composition-temperature relationship determined for the research area (Affolter et al., 2019). The advantage of this method is that it relies on a relatively simple and robust analytical method. The composition-temperature relationship is estimated only from recent monitoring activities, and the approach is best applied in settings where δD_r and $\delta^{18}O_r$ are driven by the surface temperature (Demény et al., 2021).
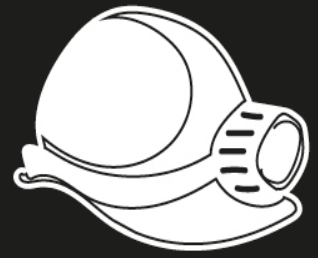
Chapter II

Study area

This thesis focuses on the study of two cavities: Mendukilo and Ostolo caves. Both cavities, about 30 km away from each other, are found within the northern zone of the province of Navarra, northern Spain (Fig. 2.1).
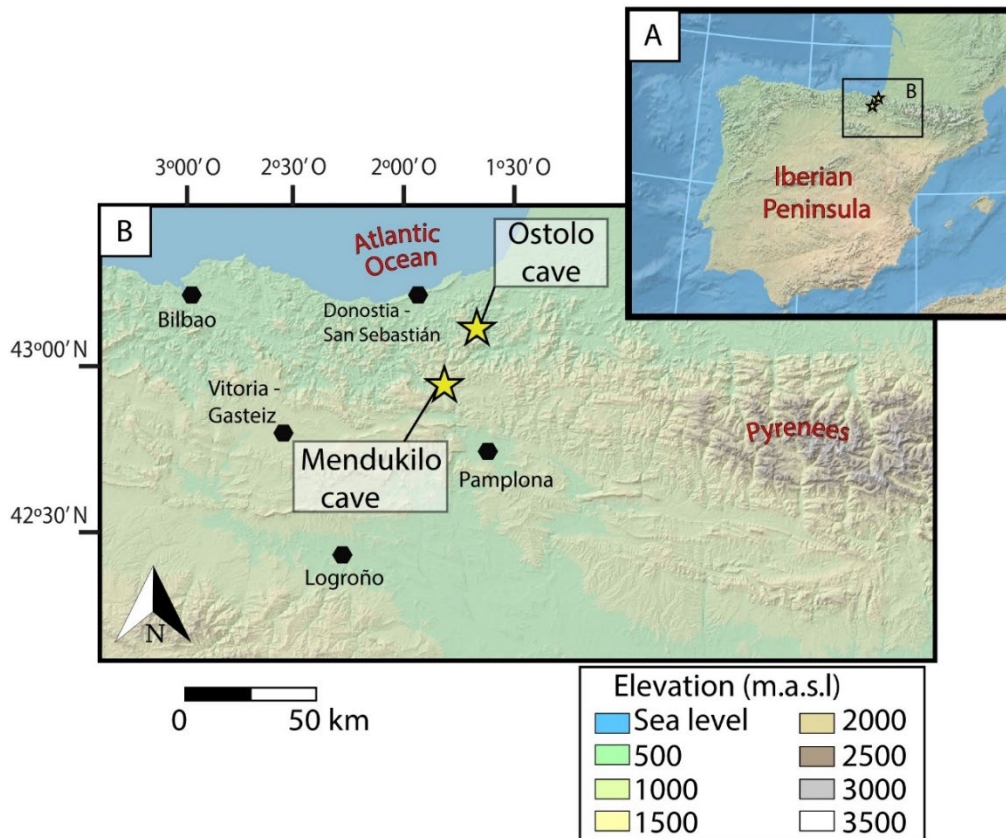
Fig 2.1. *A) Elevation map of the Iberian Peninsula that demarks the B) location of the study area in the NE of Iberia. Yellow stars indicate the locations of both caves, and black pentagons indicate the main cities nearby.*

Ostolo cave is located at 248 m a.s.l. in the Bidasoa River valley (43°11'16''N, 1°43'56''W) near Arantza village (1 km south), which is located in the easternmost part of the Cantabrian Mountain range (Basque Mountains), Western Pyrenees (Fig. 2.1). Although these mountains have a moderate altitude, they are areas with very high relief, sometimes exceeding 1,000 m. Even though the cave is quite close to the principal road that connects with Arantza village, access to the cave is covered by abundant vegetation, and the terrain is steep.

Mendukilo cave is 750 m a.s.l. on the lands of the Astitz Council (Larraun Valley, Navarra), on the slopes of the eastern part of the Sierra de Aralar (42°58'25"N, 1°53'45"W), and 40 km from the Cantabrian coast (Fig. 2.1). This is a tourist cave located at a site of community importance (SCI). The cave opens at the Oyanábal mountain, just 1.5 km west of the town of Astiz and 3.5 km south of Lekunberri.

II.1 Geological context

In regional terms, the Mendukilo and Ostolo caves are located at the eastern boundary of the Basque-Cantabrian basin (BCB) (Fig. 2.2). The BCB is a major geological entity initiated as a peri-cratonic rift related to the Mesozoic opening of the North Atlantic/Gulf of Biscay (Ábalos, 2016). It experienced extensive faulting and high subsidence rates during the Cretaceous and was inverted during Tertiary compression related to the alpine orogeny (García-Mondéjar et al., 1996; Gómez et al., 2002; Rat, 1988). Currently, the BCB is considered a segment of the Pyrenean system (e.g., Tugend et al., 2014), which extends with an E – W trend from the Mediterranean border between France and Spain to the western end of the North Iberian margin. This segment connects two major geographical features: the Pyrenees Mountains and Cantabrian Mountains. The BCB eastern boundary is loosely related to the long-debated geographical termination of the Western Pyrenees (cf. Lamare et al., 1952; Olagüe, 1951). The geology of the area near Mendukilo cave is composed of reef limestone (Fig. 2.2), with fossil content from the Lower Cretaceous (Urgonian, Albian-Aptian). The strata have a variable dip between 20° and 45° to the south-southwest. This arrangement is in accordance with the north flank of an east-west direction syncline in the area. On the other hand, Ostolo cave is located in the outcrops of the pre-Mesozoic Basque Massifs (Fig. 2.2), representing the geological limit of the eastern BCB. The outcropping rocks correspond to the Carboniferous shallow-marine limestones of the Cinco Villas Massif.

II.2 Climate and vegetation

The climate outside Mendukilo cave is temperate with cool summers (west coast maritime climate following the Köppen-Geiger classification). Rain, fog, and drizzles are abundant, making this area one of the rainiest locations in Spain (1365 mm of annual precipitation; Fig. 2.3). Rainfall is concentrated in fall, winter, and spring, and temperatures are mild without reaching extreme values, reflecting the proximity of the Atlantic Ocean. The surroundings of the cave are composed of small karstic mountain plateaus and dolines, with meadows in the highest parts and forests of beech, oak, and abundant moss covering the slopes. Soils are well-developed, rich in clay, and usually less than 50 cm in thickness. On the other hand, Ostolo cave is in a region characterized by an oceanic climate (temperate oceanic climate type of the Köppen-Geiger climate classification) with a dominant influence of the Atlantic, with temperate summers (18-20°C average), rain distributed throughout the year, and no dry season (Fig. 2.3). The average annual rainfall is significant and greater than that in Mendukilo cave, exceeding 2000 mm. The mean annual temperature outside the cave is close to 13 °C. The vegetation in the cave area is a dense forest mainly composed of oak (Quercus robur and Quercus pyrenaica), alder (Alnus glutinosa), and beech (Fagus sylvatica). Atlantic-type polycultures, dry farming, mowing meadows, ferns (Pteridophyta), and heaths (Ericaceae) are abundant.
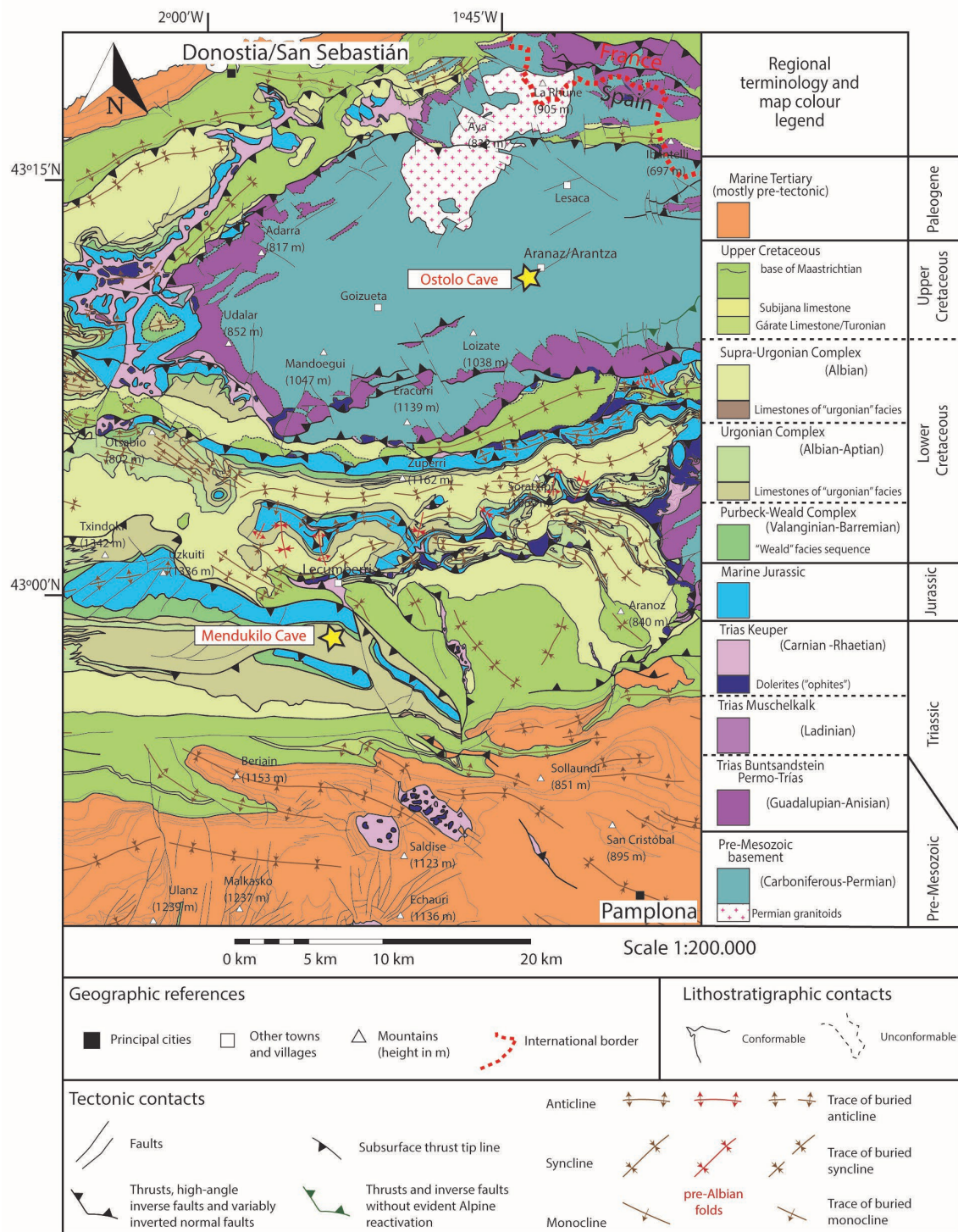
Fig 2.2. *Geological map of the study area marking the location of the Mendukilo and Ostolo caves (yellow stars). Modified from Ábalos (2016).*
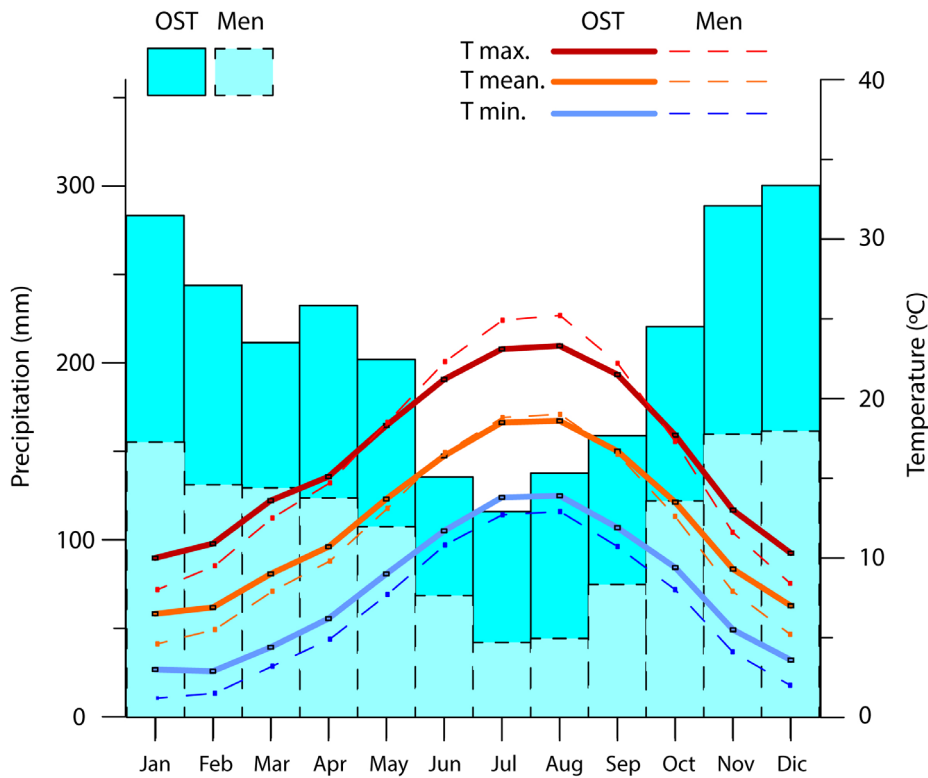
Fig 2.3. *Climate diagrams of Mendukilo (Men) and Ostolo (OST) caves. Diagram summarizes monthly precipitation and temperature of the Altsasu-Alsasua (located 24 km away from the Mendukilo cave site; data interval: 1921-2021) and Artikutza (located 6 km away from the Ostolo cave site; data interval: 1931-2018) weather stations. Light blue bars: monthly precipitation; blue line: minimum average monthly temperature (T min.); orange line: mean average monthly temperature (T mean.); red line: maximum average monthly temperature (T max.). Data source: Government of Navarre.*

II.3 Geomorphology of the caves

II.3.1 Mendukilo cave

The cave has a total passage length of 869 m and vertical extension of 59 m (Fig. 2.4) and has been enabled for tourist visits (Fig. 2.5.A). This has been carried out by prioritizing its conservation (50% of the rooms have been left unconditional) and reducing the impacts with removable structures (Aguirre, 2008). More than 10 years before the start of the monitoring campaigns for this work, the cave was continuously monitored (CO_2 temperature, etc.) through the installation of three indoor climatic stations (and one outside) in the rooms that can be visited (period 2006-2010; Otero, 2009); however, registration has ceased due to lack of maintenance.

Formed in bedded limestones of the Lower Cretaceous, there is a close relationship between the geometry and development of the cave galleries with the main fault lines of the area,

42

stratification, and fractures of the rocky massif (Fig. 2.5.B). The cave shows a descending morphology and consists of seven main rooms (Entrance Hall, Intermediate gallery, Laminosin gallery, Los Lagos gallery, Dragon gallery, Guerrero and Caballo gallery's). Los Lagos and Guerrero galleries are the only ones that are not regularly visited by tourists during the year (Fig. 2.4). The cave is currently in vadose conditions, and its morphology is characterized by gravitational breakdown features (roof and wall collapse), which eliminate morphological features associated with earlier speleogenetic phases. The entrance, Entrance Hall and Intermediate gallery have been modified during show cave development. Speleothem deposition is abundant in the Laminosin gallery, Los Lagos gallery, Dragon gallery, Guerrero gallery, and Caballo gallery (Fig. 2.5.C and 2.5.D). Most of the drip sites are active throughout the year. The main gours and pools (Fig. 2.5.D) are filled with water in autumn, winter, and spring, and are typically dry in summer.
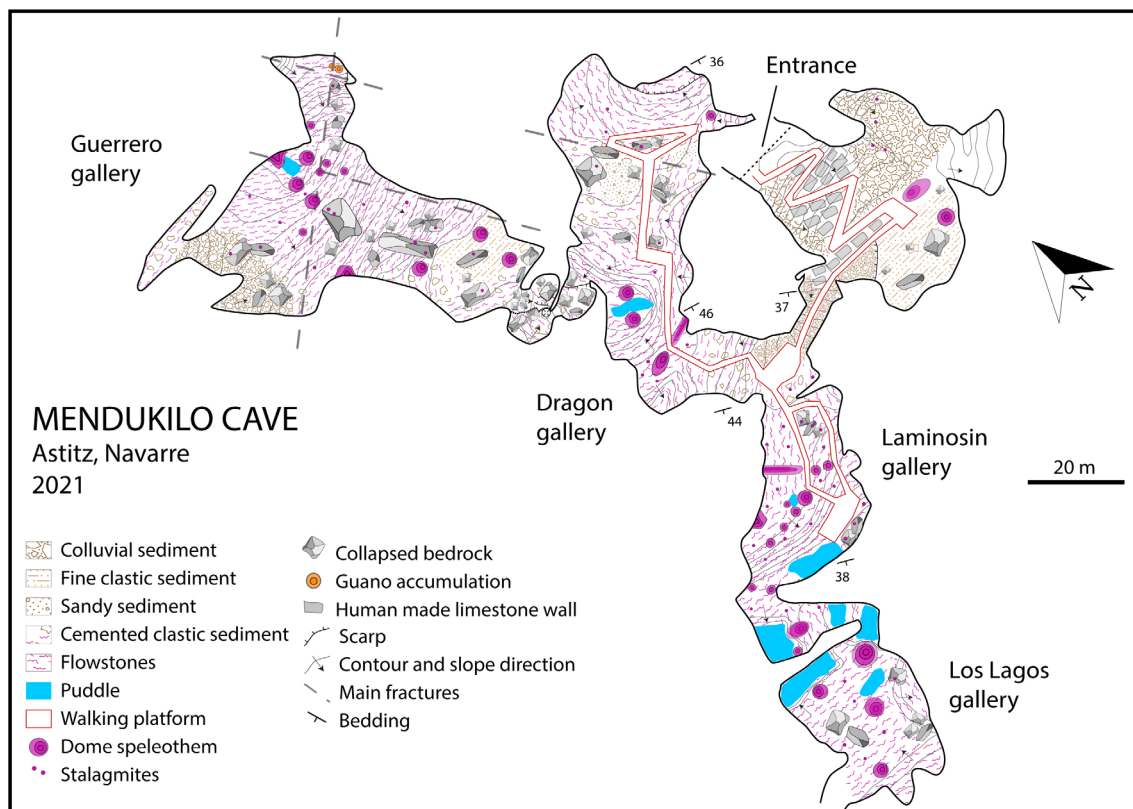
Fig 2.4. *Geomorphology map of Mendukilo cave and its different galleries.*
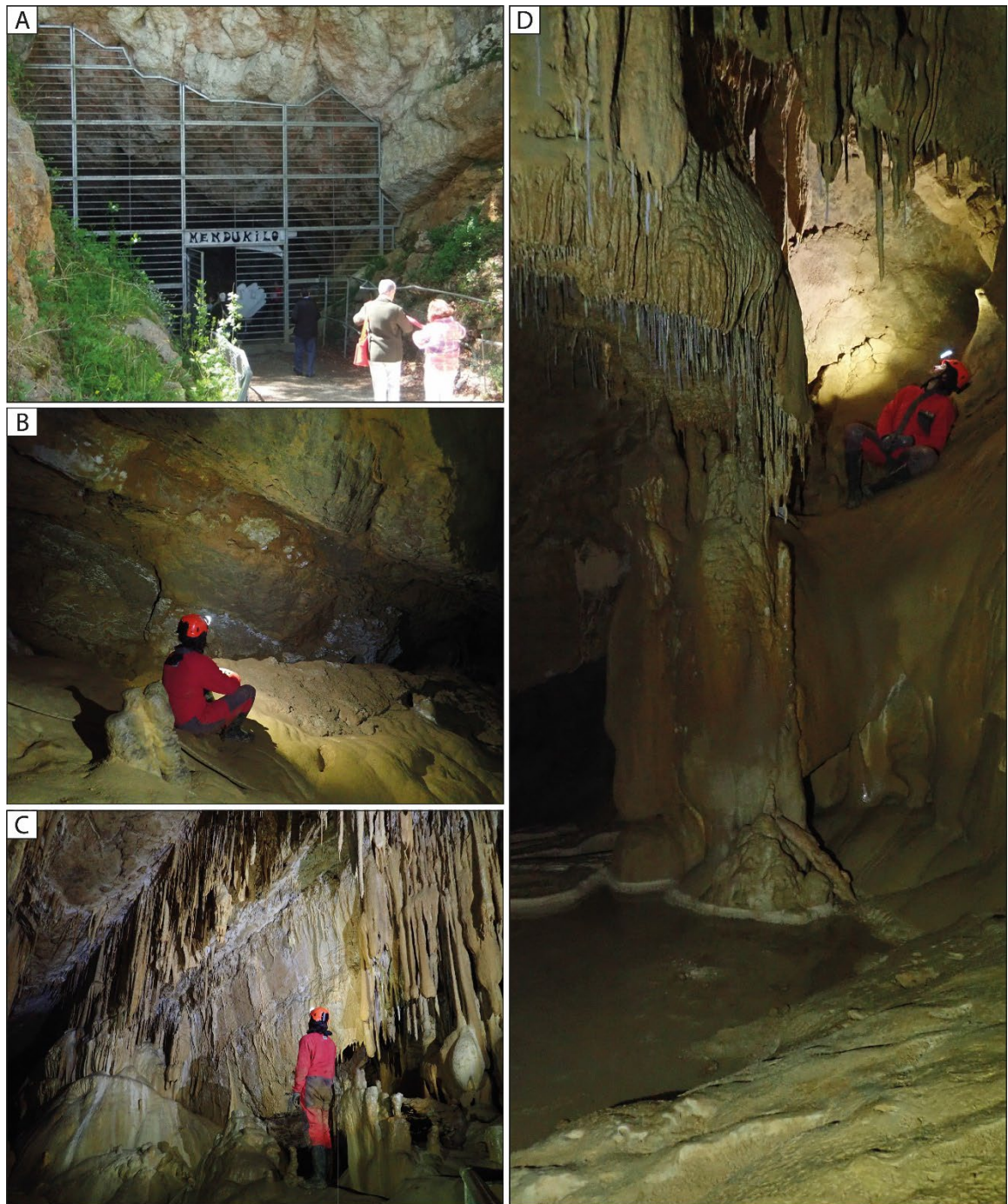
Fig 2.5. *A) Entrances of the touristic Mendukilo cave. B) Clear stratification planes inside the cave (Laminosin gallery). C) Fracture zones promoting the growth of speleothems with active drips (Dragon gallery). D) Formation of speleothems accompanied by the presence of gours filled with water (Guerrero gallery).*

II.3.2 Ostolo cave

The cave is 631 m long and has a vertical extent of 39 m (Fig. 2.6). The only entrance, located 14 m above the Arantza River, is formed by a short (0.5 – 1 m) and narrow passage (~1 m) with a permanent water outflow (Fig. 2.7.A), making access and monitoring during rainy days impossible (which is quite common because of the high frequency of rainfall). The cave passages exhibit an elongated branchwork pattern, where diagnostic morphologies of paragenetic processes, such as roof pendants, ceiling channels, anastomotic bedding planes, and fluviokarstic sediments filling the conduits, are present (Fig. 2.7.B). Currently, the cavity is vadose, and it is entirely traversed by a stream that exits through the entrance. In the deepest part of the cavity two small tributaries emerge from different impassable openings. The initial part of the stream bed is characterized by allochthonous and autochthonous conglomerate sediments. In the middle part, these sediments begin to display a layer of speleothem flowstone above, and in the final section, only an active speleothem flowstone base is evident until it becomes a travertine formation at the entrance. In the middle part of the cave and at gallery confluence zones, gravitational processes such as roof collapses and colluvial deposits from the upper conduits and fluvial terraces predominate (Fig. 2.7.C). Throughout the conduit, ancient fluvial deposits are exposed on the sides, some of them related to the paragenetic stage of the cave (Fig. 2.7.D). Finally, it is worth mentioning the presence of ophitic dikes that intrude the bedrock along the cave.
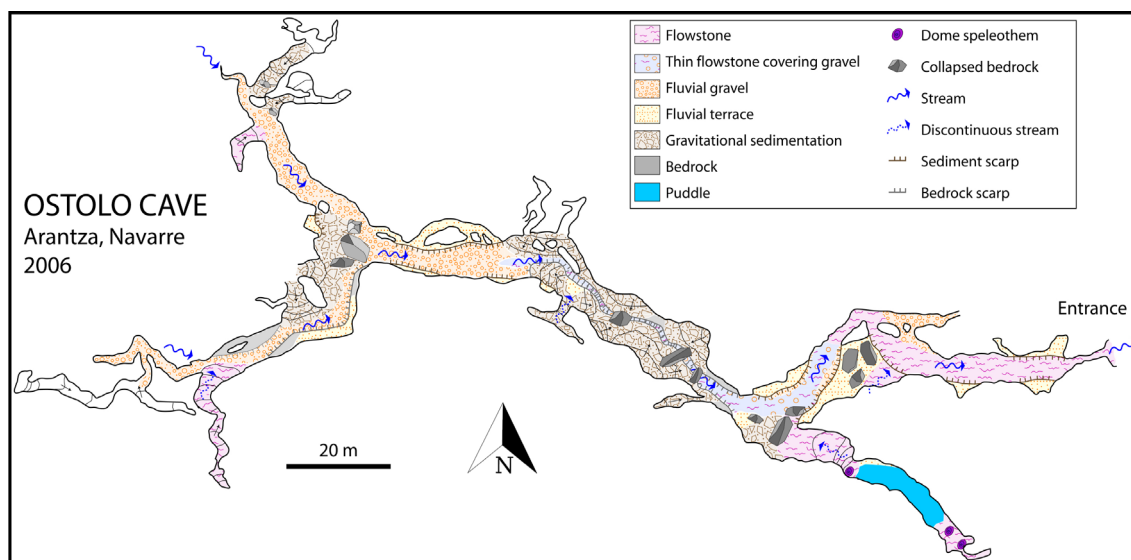
Fig 2.6. *Geomorphological map of Ostolo cave. Cave survey map courtesy of Santzez, K., Garcia, C., Ferreira, C., and del Cura, N. (Aranzadi Speleological Group).*
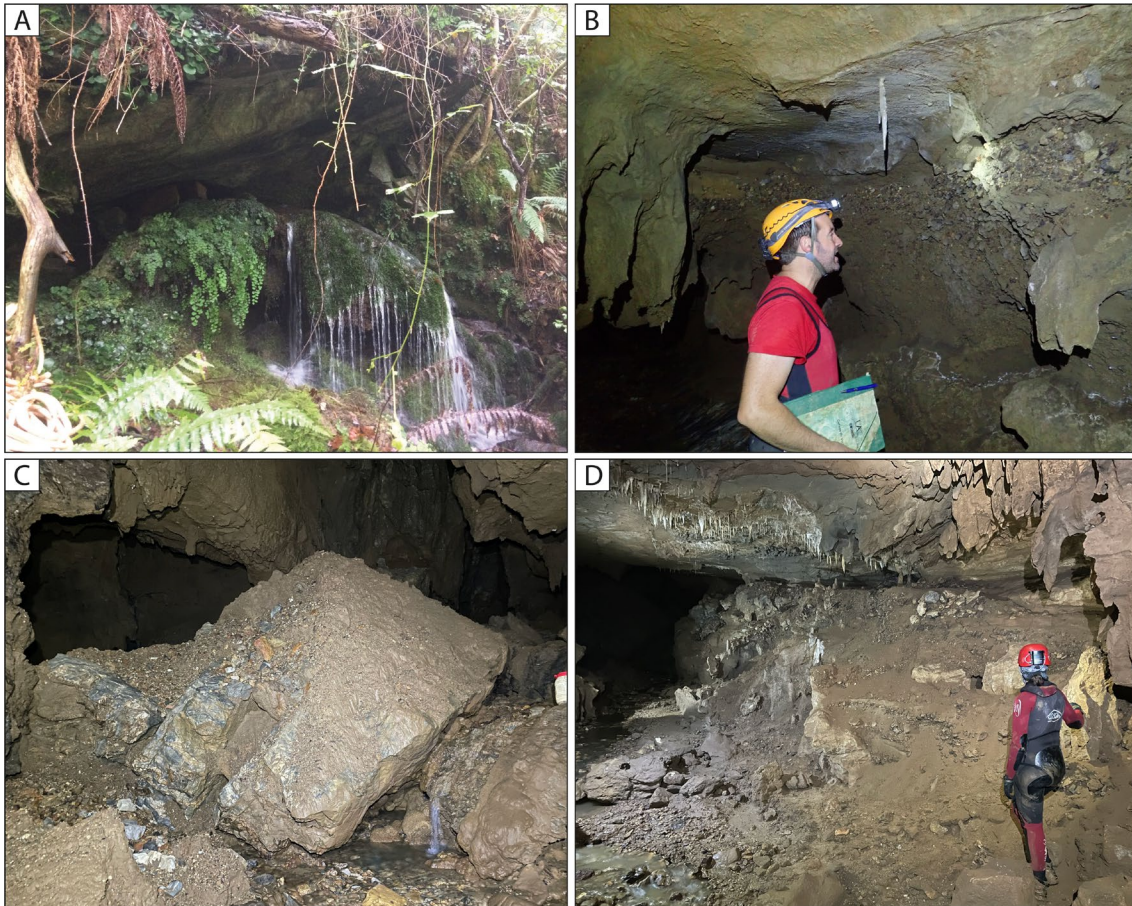
Fig 2.7. *A) Narrow entrance at Ostolo cave with continuous water outflow. B) Morphologies of paragenetic processes and sediment deposits inside the cave. C) Roof collapses and colluvial deposits near the main river. D) Terraced alluvial sediments crossed by the river.*

Chapter III

Methodology

To meet the objectives set out in this thesis (Chapter I), a multidisciplinary study was conducted, following a methodology that mainly consisted of fieldwork, laboratory analysis, record interpretation and comparison with other sites (Fig. 3.1) to characterize abrupt climatic changes in the past.
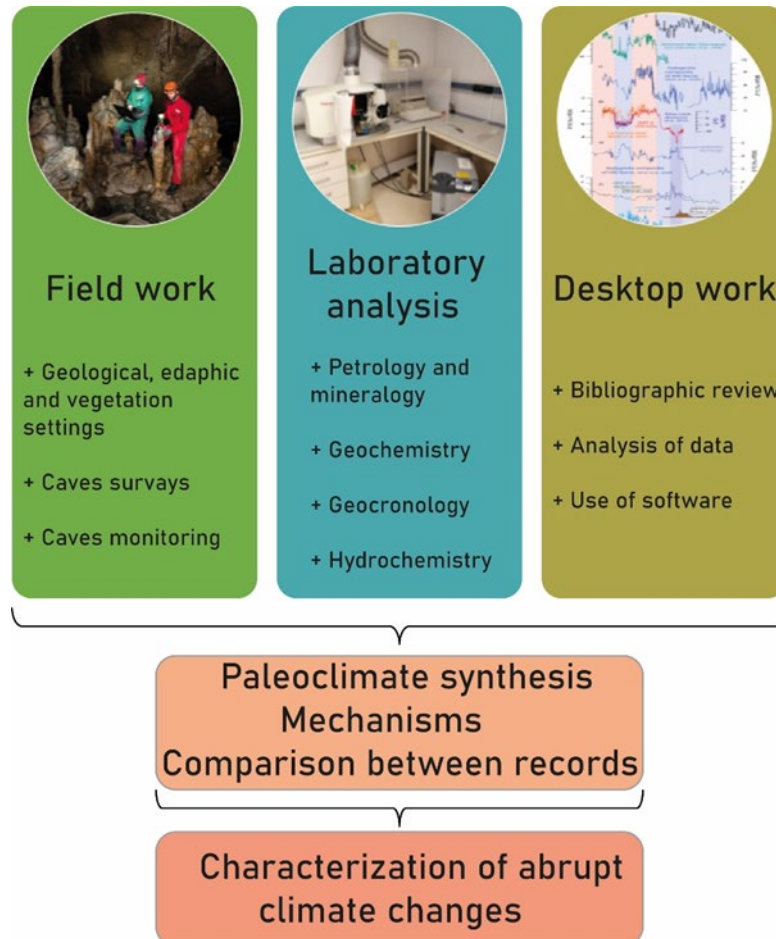
Fig 3.1. *Conceptual diagram of the methodology followed in this work.*

III.1 Field work

III.1.1 Geological, edaphic and vegetation setting

The first steps in the field work consisted of data collection outside the caves on two main topics: (i) general identification of stratigraphic, geochemical, structural, and geomorphological aspects of the study areas, and (ii) a detailed characterization of the soils and the predominant type of vegetation cover above and around the caves.

III.1.2 Cave surveys and speleothem sampling

The second stage in the field work is carried out inside the caves and consists of (i) describing, in general terms, the different morphologies and sedimentary characteristics of the cavities (Fig. 3.2.A and C) and elaborate a geomorphological map of the caves (see Section II.3), and (ii) sampling bedrock and stalagmites with or without an active drip above them (Fig. 3.2.B and D).

Fig 3.2. *Images of the interior and sampling of stalagmites from both caves. A) Inside Mendukilo cave, it is possible to appreciate a great variety of speleothems and B) several stalagmites with active drippings are sampled. On the other hand, C) the Ostolo cave presents a permanent water flow and a large amount of accumulation of fluviokarstic sediments, D) from which the stalagmites of this work are extracted (most without the presence of active dripping).*

III.1.3 Monitoring

Ostolo and Mendukilo caves were monitored seasonally between 2018 and 2021. Much of the surveys, sampling, and measurement of environmental variables in the Ostolo cave are limited by its difficult access (large amount of water outlet during the entire year). Environmental parameters were measured, and samples were obtained using the following techniques:

- **Variables inside the cave**

  > *Cave-air temperature*, leaving a HOBO® U23 pro v2 temperature data logger in different galleries of the caves to obtain continuous records.

  > *Cave-air pCO_2*, measured seasonally in different cave chambers (near drip sampling points) using a pSense Portable CO_2 meter (model AZ-0001).

  > *Drip discharge*, was measured manually at each drip sampling point (drips/s). Additionally, pluviometers (RAIN-O-MATIC-HOBO attached with a HOBO data logger UA-003-64) were installed inside Mendukilo cave to record changes in drip rates continuously over time (Fig. 3.3.A).
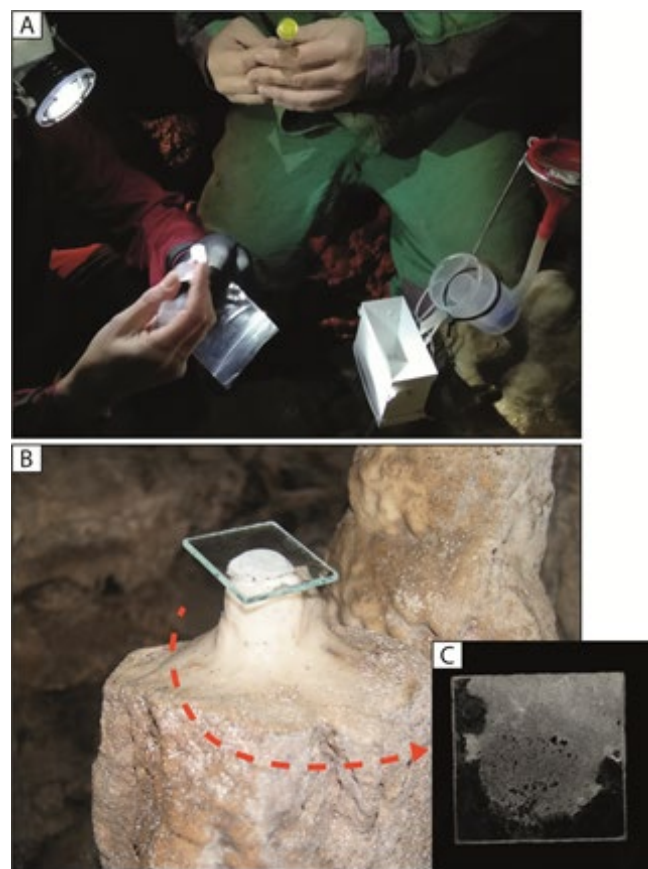
Fig 3.3. *Illustration detailing the sampling method for A) dripping water and B) farmed calcite inside the caves. In image A), it is possible to see how the water, which accumulates during the last days in a container modified for this function, is extracted with a syringe and then poured into 5 ml vials. In both caves, there were farmed calcite sampling points under drippings from which the water and their dripping rate were also sampled, or from which only a glass plate was left. C) Glass plate with a sample of farmed calcite accumulated during the entire season.*

- **Sampling for isotopic analysis**

> *Rainfall samples* were collected from the University of the Basque Country (Bilbao), an area with an Atlantic source of rainfall. Rainfall samples from Las Güixas cave in Villanúa (Huesca) were also used in this Thesis (Giménez et al., 2021).

> *Dripwaters* were sampled at each drip point of interest inside the caves between 2018 and 2021. Dripwaters were sampled twice per season in 5 ml vials (filled, capped, and refrigerated until analyses; Fig. 3.3.A). $\delta^{18}O_d$ and δD_d were analyzed.

> *Farmed carbonate* recovered seasonally over glass plates (Fig. 3.3.B and C). $\delta^{18}O_p$ and $\delta^{13}C_p$ were analyzed.

III.2 Laboratory work

Among the samples analyzed in this work, we found two main types: (i) dripwaters, farmed carbonates, and rainfall samples obtained from the monitoring campaigns, and (ii) carbonate powder samples and thin sections extracted from speleothems taken from the caves. All the stalagmites were sectioned along their central growth axis to obtain a pair of slabs per speleothem, which were subsequently polished prior to sampling at the Servicio General de Apoyo a la Investigación-SAI of the University of Zaragoza. One slab per speleothem was used for chronological, isotopic, and trace element analyses, while thin slides for pethrographic characterization and fluid inclusion analysis were performed on the other half of each stalagmite.

III.2.1 Petrography

Petrographic analyses, to identify the presence of hiatuses and examine the fabric changes along the speleothems, are carried out at the University of Burgos using a petrographic microscope to analyze thin sections of each one of the stalagmites described in this thesis. These thin sections were obtained at the Servicio General de Apoyo a la Investigación-SAI of the University of Zaragoza. The different fabrics and the construction of the petrographic record*s* followed the methodology described by Frisia (2015), Frisia et al. (2000), and Frisia & Borsato (2010).

III.2.2 Geochronology

All the powder samples, which were then analyzed for dating using the U/Th method, were sampled with a handheld drill and a tungsten carbide drill bit. The strategy to better approach the process of obtaining U/Th dates in each stalagmite consisted of four sampling/dating steps: (i) Obtain a sample from the base and the top of each speleothem and date them; (ii) continue to

increase the number of samples in an equidistant way (e.g., every 5 cm) along the main growth axis in stalagmites that cover age ranges of interest; (iii) if a hiatus is thought to be present visually, a sample is obtained from before and immediately after this drastic change in the appearance of the records; and (iv) focus on a large number of dates on intervals of drastic changes that are visualized in the preliminary isotopic results. All this is important at the moment of identifying hiatuses, periods of growth rate changes, and obtaining detailed results during time intervals of greater interest in meeting the objectives of this thesis with fewer sampling and dating analyses.

The amount of carbonate powder sampled varied between 0.02 and 0.2 g. This depends in the U concentration present in the stalagmite (if it is known), but if this value is unknown or there is not enough information about the cave, the amount of sample extracted was 0.2 g to make sure that the later chemical preparation can be carried out. The U/Th method consists on two main processes: (i) extraction and separation of the U and Th from the carbonate samples following a chemical procedure with strict hygiene and safety precautions, and (ii) the measure and quantification of this isotopes. The chemical procedure consisted of the following steps:

- The samples were weighed in Teflon beakers (previously cleaned in a meticulous process that included the use of aqua regia).
- The carbonate powder was then dissolved in ultrapure 7N HNO_3.
- The solution was then spiked with a standardized laboratory solution of ^{229}Th-^{233}U-^{236}U, based on the amount of uranium in the sample (if known). If this value is unknown, it is always better to use a low-spike solution.
- A few drops of perchloric acid ($HCLO_4$) were added to eliminate as many organic compounds as possible and balance the spike solution.
- The samples were then dried down on hot plates.
- A few drops of 2N HCl were added to remove Ca, and then a couple of drops of Fe solution were added.
- Approximately 10 drops of ammonium hydroxide (NH_4OH) were added, and the samples were centrifuged at several stages to precipitate Fe together with other elements (including Th and U).
- The precipitate was exposed to 14N HNO_3 and dried. It was then re-dissolved in 7N HNO_3.
- The U and Th of the solution were separated by passing it through columns filled with an anion exchange resin after filling them several times with 7N HNO_3 (Fig. 3.4.A). Th was removed from the column by adding 2N HCL and U was separated using Milli-Q water.

- In the last step, the U and Th samples were exposed to various acids (14N HNO₃) and dried on a hotplate to subsequently dissolve the final precipitate in a very dilute ICP solution (14N HNO₃ + Milli-Q + HF).

The analyzes and quantification of the U and Th isotopes were performed using a MC-ICP-MS (Thermo-Finnigan Neptune) at the University of Xi'an (Xi'an, China) and the University of Minnesota (Minneapolis, USA) (Fig. 3.4.B), following a previously described methodology (Cheng et al., 2013). To calculate the corrected ages in conjunction with the decay constant (Cheng et al., 2013), an initial ^{230}Th/^{232}Th atomic ratio of $4.4 \pm 2.2 \times 10^{-6}$ was used. All isotopes were measured with Faraday cups, except for ^{230}Th and ^{234}U, which were analyzed by a secondary electron multiplier (SEM). A total of 102 dates were selected to cover the time interval proposed in the objectives of this thesis (last 16.5 kyr BP). Age models were obtained using StalAge (Scholz & Hoffmann, 2011). The age uncertainties were low for the stalagmites of both caves, approximately ±48 and ±52 years in stalagmites from Ostolo and Mendukilo, respectively.
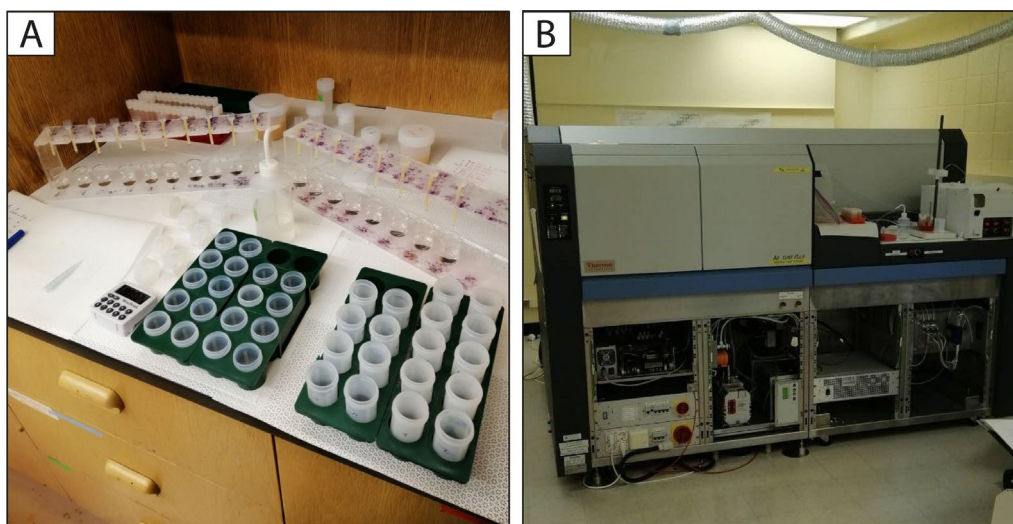
Fig 3.4. *(A) Separation of U and Th in the solution by passing them through columns filled with an anion-exchange resin. (B) Neptune MC-ICP-MS.*

III.2.3 Stable isotopes in water samples

III.2.3.1 Rainfall samples

Sampling was conducted between July 2018 and February 2021, and 144 rain events were sampled. Rainfall was sampled every rainy day, following the protocol described in Moreno et al., (2014b). The stable isotopic compositions of these samples were analyzed using cavity ring-down spectroscopy (PICARRO L2130-i) at the Pyrenean Institute of Ecology (Zaragoza).

The results are reported in per mil with respect to Vienna Standard Mean Ocean Water (VSMOW), and the reproducibility of the measurements was typically 0.1‰ for $\delta^{18}O_r$ and 0.5‰-1‰ for δD_r.

III.2.3.2 Dripwater samples

A total of 104 drip water samples from both caves (89 from Mendukilo cave and 15 in the case of Ostolo) were analyzed for $\delta^{18}O_d$ and hydrogen δD_d isotope composition via cavity ring-down spectroscopy (PICARRO L2130-I; Fig. 3.5) at the Pyrenean Institute of Ecology (Zaragoza). The results are reported in per mil with respect to Vienna Standard Mean Ocean Water (VSMOW), and the reproducibility of the measurements was typically 0.1‰ for $\delta^{18}O_d$ and 0.5‰-1‰ for δD_d.

Fig 3.5.   *PICARRO L2130-i for stable isotopes in water sample analysis.*

III.2.4 Stable isotopes in farmed calcite

A total of 51 samples of farmed carbonate (49 from Mendukilo cave and 2 in the case of Ostolo) and two samples of bedrock were collected in the present thesis. Farmed carbonate precipitated on glass plates and powder samples from bedrock were analyzed for oxygen and carbon isotopes ($\delta^{18}O_p$ and $\delta^{13}C_p$, reported as ‰ with respect to the Vienna Pee Dee Belemnite standard). Part of the isotopic analyses were analyzed at the University of Innsbruck (Austria) using a Thermo Fisher Delta V Plus linked to a GasBench II, following the methodology described in Spötl (2011). The long-term reproducibility (1 sigma) of $\delta^{18}O_p$ is 0.08‰, and 0.06‰ for $\delta^{13}C_p$ (Spötl, 2011). The rest of the samples were analyzed at the Iso TOPIK Laboratory (University of Burgos) and the University of Barcelona, following similar procedures and equipment.

III.2.5 Stable isotopes in stalagmite carbonate samples

The strategy in the sampling and subsequent isotopic analysis of the different stalagmites generally consisted of two steps: (i) A first low-resolution analysis (samples every 1-5 mm; Fig. 3.6.A), and (ii) a posterior improvement of the resolution (samples every 0.3 -1 mm) in selected areas of the stalagmites with more interest attending to the age model and probability to cover abrupt events (Fig. 3.6.B). A total of 2685 samples for $\delta^{18}O_c$ and $\delta^{13}C_c$ analyses were collected from the different stalagmites of both caves. Isotopic analyses were performed at the University of Innsbruck using a ThermoFisher Delta V Plus linked to a GasBench II (Fig. 3.6.C), following the methodology described in Spötl (2011). The long-term reproducibility (1 sigma) of the $\delta^{18}O_c$ analyses is 0.08‰ and 0.06‰ for $\delta^{13}C_c$ (Spötl, 2011). All values are reported as per mil with respect to the Vienna Pee Dee Belemnite standard (VPDB).
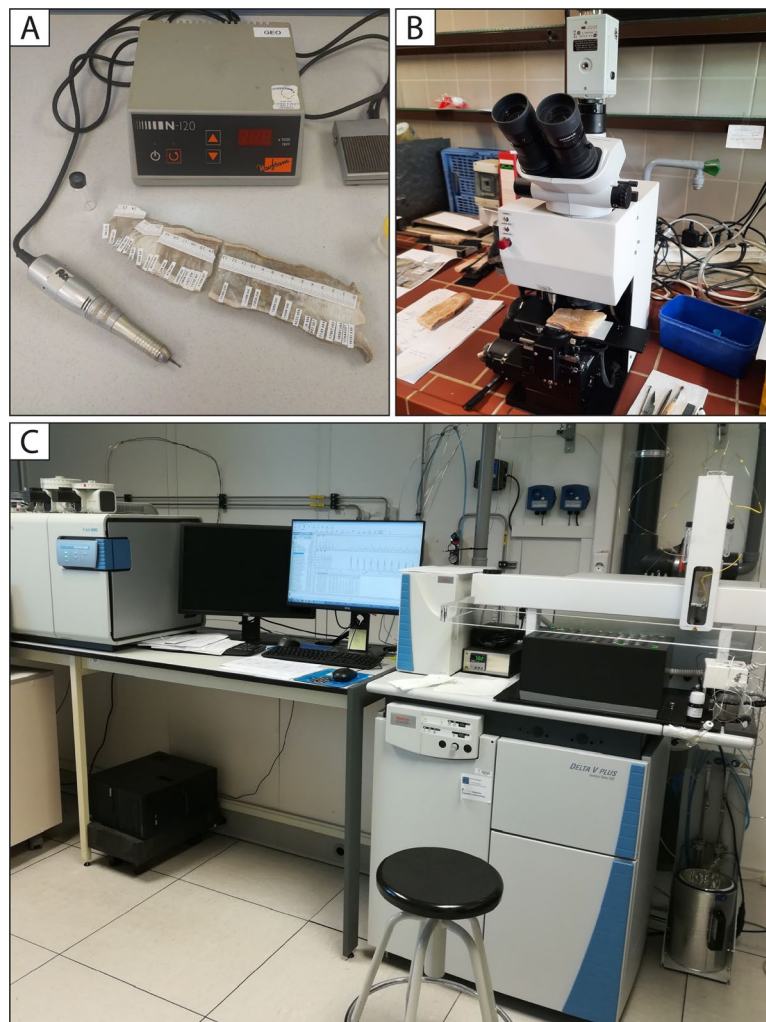
Fig 3.6. *Procedures for isotopic analysis. A) Low-resolution sampling. B) High-resolution sampling. C) Thermo Fisher Delta V Plus linked to a GasBench II, University of Burgos.*

III.2.6 Trace elements

A total of 637 carbonate samples were analyzed for trace elements. 267 of this samples (Mendukilo stalagmites), sampled every 5 mm, were measured for Mg/Ca and Sr/Ca ratios at ETH Zurich (Agilent QQQ 8800), using a standardized approach similar to that reported in Stoll et al. (2022b). The analysis of the other 370 samples (Ostolo stalagmites), sampled every 1 mm, were performed in the IPE-CSIC laboratories with an ICP-OES (Thermo Scientific iCAP DUO 6300) using molar ratios of Mg in relation to Ca.

Fig 3.7. *ICP-OES (Thermo Scientific iCAP DUO 6300), IPE laboratory.*

III.2.7 Fluid inclusions

The stable isotopic composition of stalagmite fluid inclusion water was analyzed using a Delta V Advantage isotope ratio mass spectrometer following crushing and high-temperature conversion as described by Dublyansky & Spötl (2009), which is summarized below:

- Intervals of interest in the stalagmite were cut according to the required weight using a saw to cut rock (Fig. 3.8.A).
- A carbonate sample was placed inside the crusher (Fig. 3.8.B). Subsequently, the crusher was assembled, placed in an aluminum block (Fig. 3.8.C), and then connected to two carrier-gas ports and thrust bearings (Fig. 3.8.D).
- The subsample of the carbonate crystal was crushed, releasing fluid inclusions as water vapor (Fig. 3.8.D; Fig. 3.9; Fig. 3.10.A).

- Water vapor was transported by the carrier gas (Fig. 3.10.B) from the crusher to the cryo-focusing cell (Fig. 3.9; Fig. 3.10.C). Here, the steam was frozen (Fig. 3.10.C; Fig. 3.10.D), and then quickly heated to transport it to the reactor (Fig. 3.9; Fig. 3.10.E).

- Molecular hydrogen and carbon monoxide, which evolved from water through reaction with glassy carbon at 1400 °C in a thermal combustion/elemental analyzer reactor (TC/EA), were separated (Fig. 3.10.E).

- Molecular hydrogen was analyzed using mass spectrometry (Fig. 3.10.F).
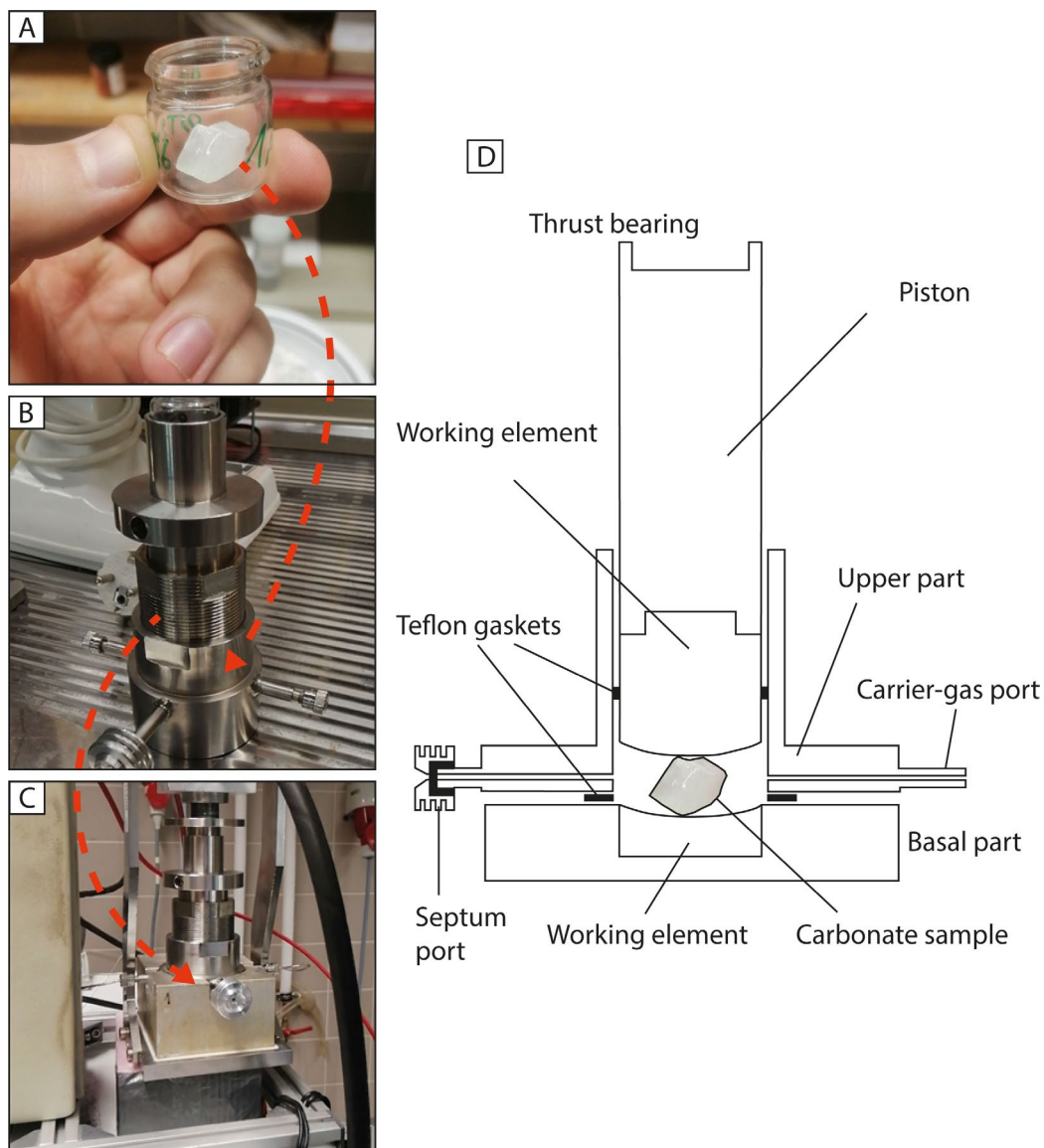
Fig 3.8. *Preparation of carbonate samples before crushing. A) After cutting the sample, it was weighed, B) placed inside the crusher, and later the assembled crusher was installed above an aluminum heater block that was connected to two carrier-gas ports. D) Schematic drawing of the assembled crusher (extracted and modified from Dublyansky & Spötl, 2009).*
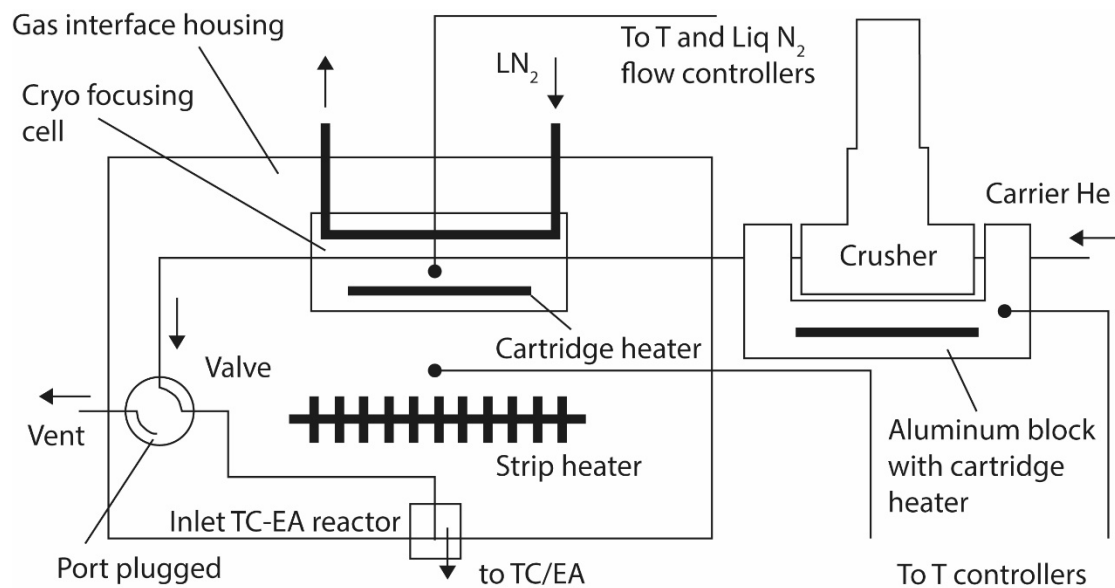
Fig 3.9. *Setup of the fluid-inclusion extraction line (extracted and modified from Dublyansky & Spötl, 2009). The purified He carrier gas enters the crusher, which is then placed in an aluminum block heater. The water released by crushing is transported into the cryo-focusing cell mounted inside the heated gas-interface housing. The high-temperature four-port two-way valve directs the gas flow either to the vent or to the inlet port of the high-temperature conversion unit. The temperature in the aluminum heater block and the interface housing is controlled by two microstats (lines with dots indicate temperature sensors).*

A total of 356 carbonate crystal subsamples (0.3 to 2.5 g) were crushed and subsequently analyzed for fluid inclusions. 69 subsamples correspond to Ostolo stalagmites and the other 287 to Mendukilo samples. δD_{FI} values are reported in per mil relative to Vienna Standard Mean Ocean Water (VSMOW). The average long-term precision of replicate measurements of our in-house calcite standard is 2.4 ‰ for δD for water amounts between 0.2 and 1 μL.

Fig 3.10. *Illustration of different steps and devices necessary for the analysis of fluid inclusions used in this study. (A) The sample inside the crusher was pulverized at a high temperature, releasing water from the fluid inclusion that was transported through the He carrier (He comes from a (B) cylinder connected to the crusher) to the cryofocusing cell inside the (C) gas interface housing, which was at very low temperatures owing to the contribution of (D) LN$_2$. The sample was rapidly heated to very high temperatures and transported to (E) TC/EA, where molecular hydrogen and carbon monoxide were separated. Finally, molecular hydrogen was analyzed using a (F) Delta V Advantage isotope ratio mass spectrometer.*

Chapter

IV

Last deglaciation to the Holocene onset: Ostolo cave record

IV.1 Introduction

Major and abrupt changes in the Atlantic Meridional Overturning Circulation (AMOC) during the last deglaciation were responsible for redistributing heat on a planetary scale, and are believed to have triggered ocean CO_2 degassing, leading to the end of the last glacial period (Muschitiello et al., 2019; Skinner et al., 2010). These AMOC changes, in conjunction with latitudinal shifts in the polar jet stream, had a major impact on the climatology of the regions around the North Atlantic, including the Iberian Peninsula (Cacho et al., 2001; Naughton et al., 2016), a southern European region key to understanding Northern Hemisphere climate teleconnections. Sea surface temperature (SST) records from marine sediments around Iberia (Cacho et al., 2001; Rodrigues et al., 2010) show an evolution comparable to the event structure defined in Greenland ice cores (Rasmussen et al., 2014). However, recent studies have revealed large discrepancies between different records (Ausín et al., 2019) and have also suggested that the SST proxies around Iberia are complicated by a seasonal component (Català et al., 2019).

Glacier records from the Iberian Mountains despite their discontinuous character and low resolution, indicate advances and retreats in phase with well-known rapid temperature changes (García-Ruiz et al., 2016). Additional regional paleoclimatic information is provided by well-dated lacustrine records (González-Sampériz et al., 2006; Morellón et al., 2009); however, their resolution is insufficient for examining the fine-scale structure of the last deglaciation. Increasing numbers of speleothem records from Spain and southern France have provided new insights into the deglacial climate (Baldini et al., 2015, 2019; Bartolomé et al., 2015b; Genty et al., 2006; Moreno et al., 2010; Rossi et al., 2018). However, none of these records cover the complete deglacial transition at high resolution, and they differ with respect to the interpretation of $\delta^{18}O_c$ variability (Baldini et al., 2015; Genty et al., 2006; Moreno et al., 2010).

In this study, we present an oxygen isotope record of three stalagmites from the Ostolo cave in the Western Pyrenees covering the critical time interval from 18.5 to 10.5 kyr BP. This new replicated record provides an opportunity to examine the climate response in southern Europe to rapid AMOC changes at a high resolution. We show that centennial-scale climate changes during the last deglaciation captured by the precisely dated Ostolo stalagmites were identical within dating uncertainties to the well-known pattern recorded by northern high-latitude ice cores.

IV.2 Cave setting

Ostolo cave (43°11′16″N, 1°43′56″W, 248 m above sea level [a.s.l.]) is located in the Basque Mountains, Western Pyrenees, northern Spain (Fig. 4.1). The mountains receive ∼2000 mm/yr of rain, and the average annual temperature is 13.5 °C. The cave is ∼22 km from the Atlantic Ocean and is developed in Carboniferous limestones. The total passage length of the cave

is 631 m and shows a vertical extent of 39 m. The entrance is formed by a short and narrow passage with permanent water outflow (Fig. 4.2).
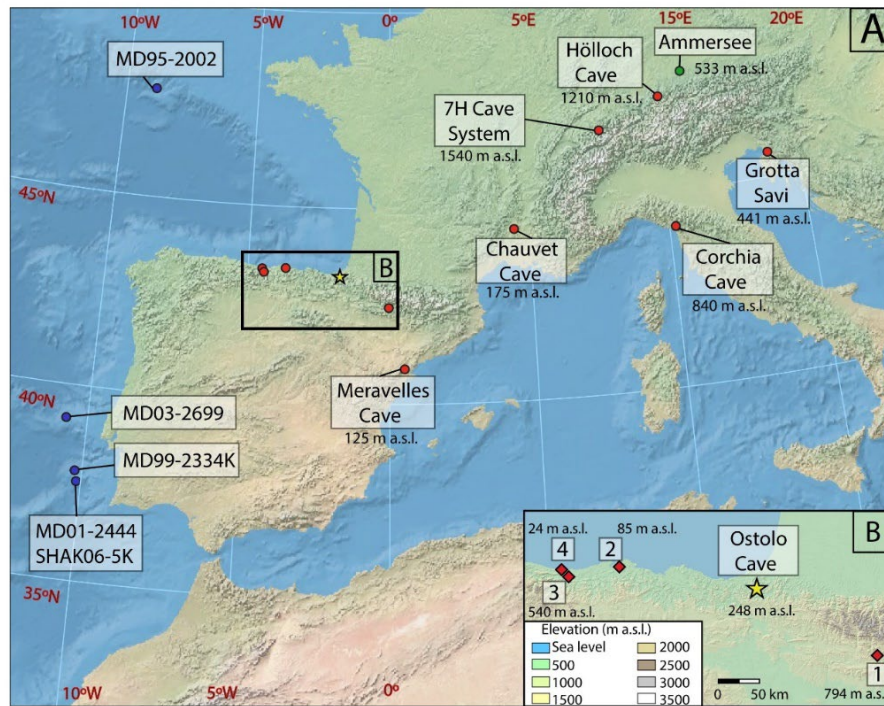
Fig 4.1. *A) Location of Ostolo cave (yellow star) and other sites mentioned in the text. B) Caves with last deglaciation stalagmite records in N Iberia: 1. Seso Cave; 2. Kaite Cave; 3. La Garma Cave; 4. El Soplao Cave; 5. Pindal Cave.*

IV.3 Methods

Inside the cave, temperature variations are continuously monitored, and samples of dripping water (five different drip sites) and farmed calcite (one drip site) are collected on each visit to the cave. The number of samples is not extensive and continuous because of the difficulties of entering the cave during rainy periods, which are quite frequent in any season of the year in the area. Dripwaters from different seasons (15 samples) were analyzed for $\delta^{18}O_d$ and δD_d using cavity ring-down spectroscopy (PICARRO L2130-i) at the Pyrenean Institute of Ecology (Zaragoza). The results are reported in per mil with respect to Vienna Standard Mean Ocean Water (VSMOW), and the reproducibility of the measurements was typically 0.1‰ for $\delta^{18}O_d$ and 0.5‰-1‰ for δD_d. Two samples of farmed calcite from only one gallery with active calcite precipitation inside the cave were analyzed for oxygen ($\delta^{18}O_p$) and carbon ($\delta^{13}C_p$) isotopes using an isotope ratio mass spectrometer (ThermoFisher Delta V Plus linked to a GasBench II) at the Iso TOPIK Laboratory (University of Burgos) and reported as ‰ with respect to the VPDB. The first sample corresponds to a year of farmed calcite (2018-2019), while the second sample was maintained during the winter and spring months, from December 2019 to July 2020.
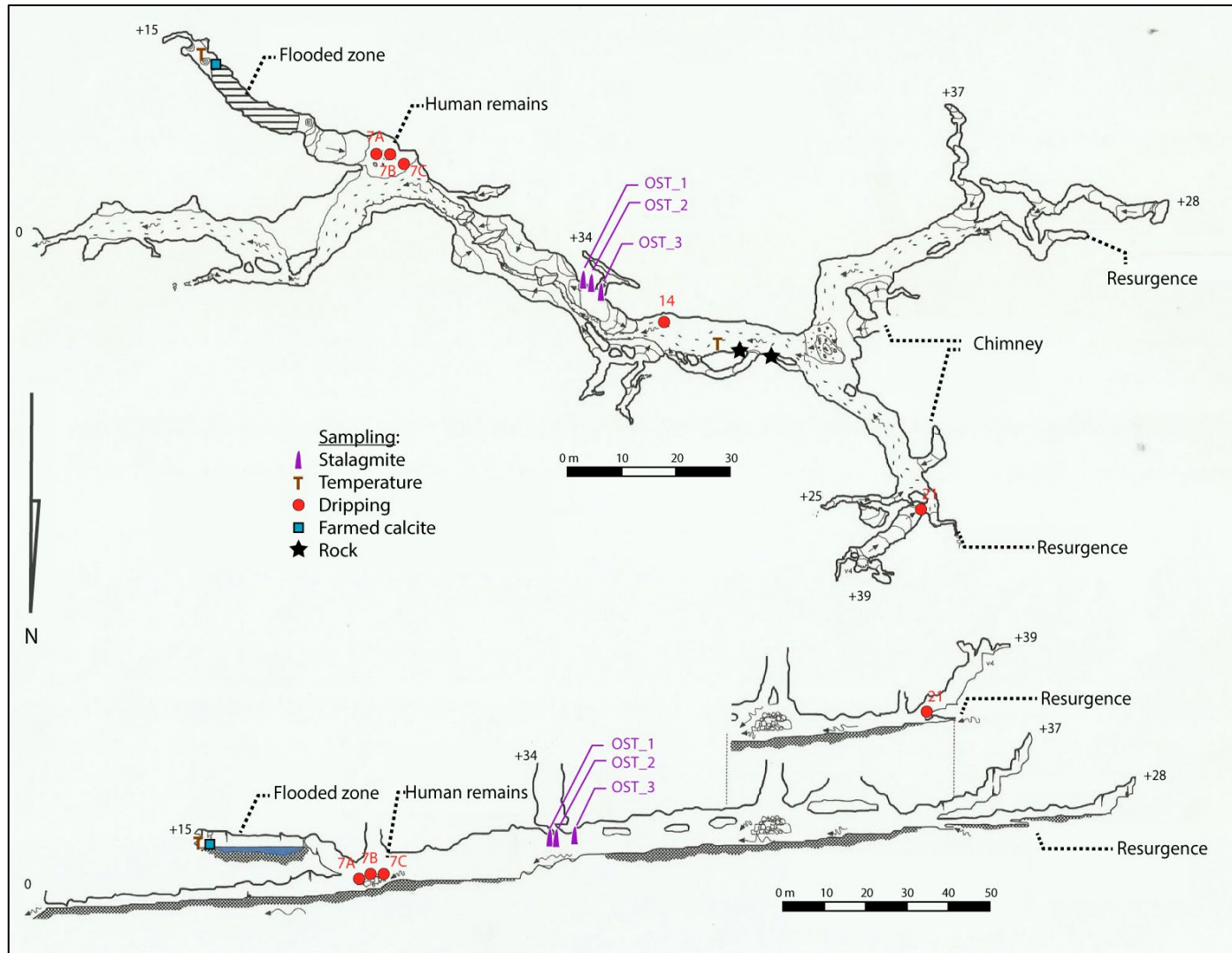
Fig 4.2. *Plan view and vertical section of Ostolo cave. The locations where speleothems were extracted are marked in red (OST1, OST2, and OST3). Sites where host rock, drip water, and farmed calcite were sampled and the air temperature was logged are marked. Cave survey map courtsey of Santzez, K., Garcia, C., Ferreira, C., and del Cura, N. (Aranzadi Speleological Group).*

Three stalagmites (OST1, OST2, and OST3) were collected under non-active drips inside Ostolo cave (Fig. 4.2) and were sectioned along their central growth axis to obtain a pair of slabs per stalagmite, which were subsequently polished. One slab was used for chronological and isotopic analyses, whereas petrological analyses (thin sections) were performed on the other half. To identify the presence of hiatuses and examine textural changes along the three speleothems, 46 thin sections were prepared (17 in OST1, 16 in OST2, and 13 in OST3) and analyzed using optical microscopy. The code for the different fabrics and the construction of a petrographic log (Frisia, 2015) is simplified and follows Muñoz-García et al. (2016).

A total of 78 powder samples were collected for U-Th dating from the three stalagmites (15 samples of OST1, 43 of OST2, and 20 of OST3). The samples were taken with a handheld drill and a tungsten carbide drill bit. The analyses were performed using a MC-ICP-MS (Thermo-Finnigan Neptune) at the University of Xi'an and the University of Minnesota, following previously described methods (Cheng et al., 2013). Age models are built using StalAge (Scholz & Hoffmann, 2011). In contrast, 1234 $\delta^{18}O_c$ samples were collected along the central axis at 300 μm increments for OST2 and OST3. In the case of OST1, the samples were taken at 5 mm increments. Isotopic analyses were performed in the University of Innsbruck, using a ThermoFisher Delta V Plus linked to a GasBench II, following the methodology described in Spötl (2011). The long-term reproducibility (1 sigma) of the $\delta^{18}O_c$ analyses is 0.08‰ (Spötl, 2011). All values are reported as $\delta^{18}O_c$ 'per mille' (‰) with respect to the Vienna Pee Dee Belemnite standard (VPDB). The $\delta^{18}O_c$ values were corrected for the ice-volume effect following Bintanja et al. (2005).

IV.4 Results

IV.4.1 Monitoring

The $\delta^{18}O_d$ values (Table 4.1) are very stable during the year (with values that vary between -6.09 and -6.58‰). The differences within summer values (July 2020) and winter or fall values (Sept 2019 and Jan 2020) is small (0.2 – 0.3‰). $\delta^{18}O_d$ and δD_d of the stream at the cave entrance are -6.87‰ and -40.3‰, respectively (sampled in the fall of 2018). The farmed calcite results indicate similar values of $\delta^{18}O_p$ (-5.06‰ for the annual sample and -4.94‰ for the second sample). Calcite precipitation occurs throughout the year, at least at present-day.

Drip sample	$\delta^{18}O_d$ (‰)	δD_d (‰)
OST 7A September 2019	-6,53	-39,39
OST 7A January 2020	-6,58	-40,46
OST 7A July 2020	-6,40	-39,24
OST 7B September 2019	-6,47	-39,18
OST 7B January 2020	-6,47	-39,44
OST 7B July 2020	-6,31	-38,24
OST 7C September 2019	-6,58	-40,40
OST 7C January 2020	-6,43	-39,57
OST 7C July 2020	-6,30	-38,37
OST 14 September 2019	-6,32	-38,11
OST 14 January 2020	-6,30	-38,16
OST 14 July 2020	-6,40	-38,62
OST 21 September 2019	-6,24	-37,55
OST 21 January 2020	-6,48	-39,43
OST 21 July 2020	-6,09	-37,14

Table 4.1. *Ostolo cave drip water samples analyzed to determine the variations of $\delta^{18}O_d$ and δD_d from five different drip sites (7A, 7B, 7C, 14 and 21) in three different cave galleries, including the one where the stalagmites analyzed in this study were obtained.*

IV.4.2 Petrography

All the stalagmites are composed of calcite, and the predominant fabric is the columnar elongate (Ce) type (Fig. 4.3) made of crystals with a length to width ratio of 6:1, most commonly 2 up to 60 mm long, and 0.2 up to 5 mm wide (Fig. 4.3.B, C and D). This great variability in the length/width ratio of the fabrics of the Ostolo stalagmites makes it necessary to distinguish between two Ce fabrics. Columnar elongated 1 (Ce1) corresponds to a fabric with crystals less than 10 mm in length and 1 mm in width (Fig. 4.3.B and D). In contrast, the fabric with crystals of length greater than 10 mm and width greater than 1 mm is described as columnar elongated 2 (Ce2; Fig. 4.3.C). Other fabrics present in these stalagmites are compact columnar (C) and microcrystalline columnar (Cm) types (Fig. 4.3.B and Fig. 4.3.E respectively).
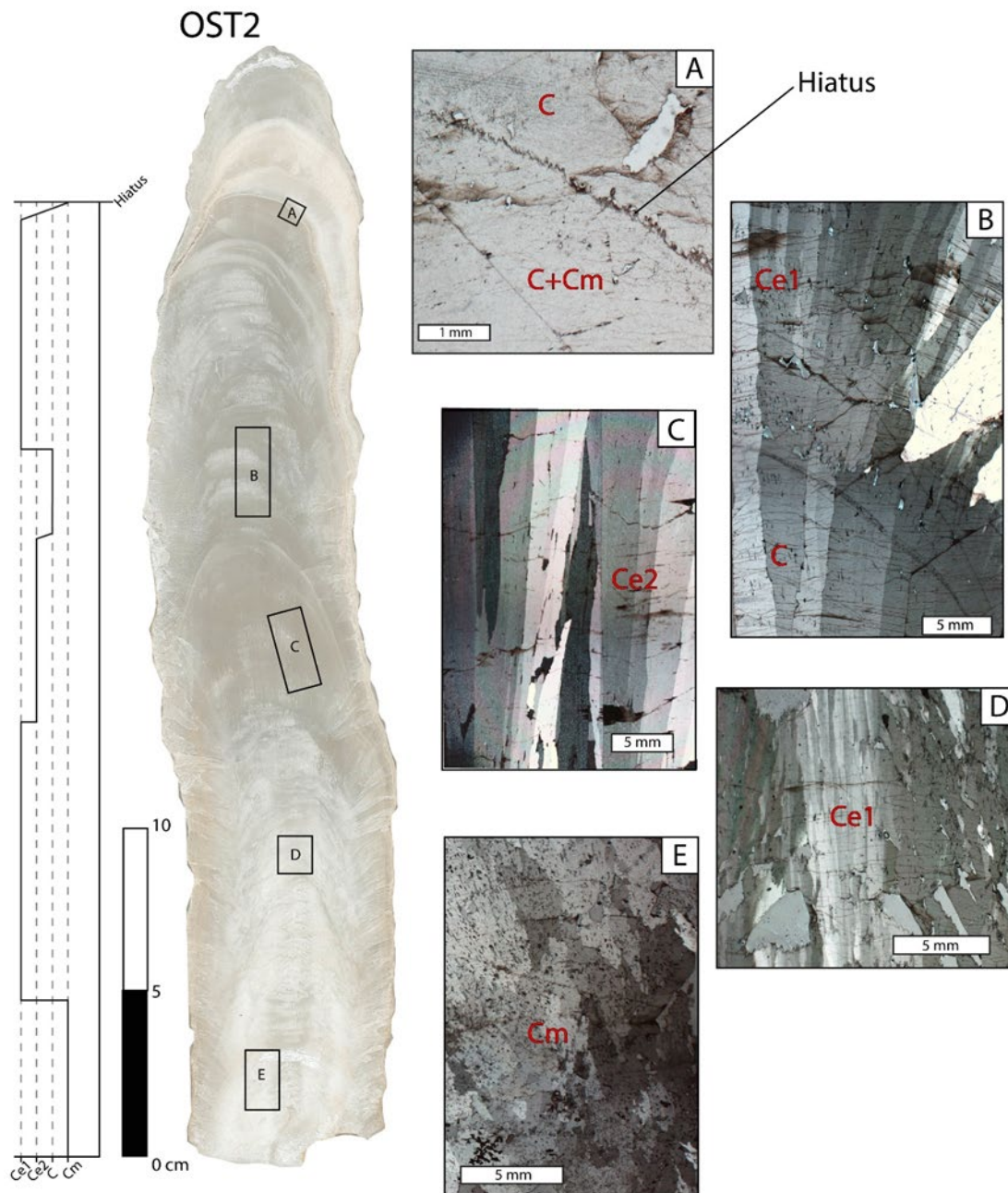
Fig 4.3. *Slab of stalagmite OST2 and its microstratigraphic log (left side) showing changes in the type of fabric (Cm, columnar microcrystalline; C, columnar compact; Ce, columnar elongated [1 and 2]). Photomicrographs of the thin sections are shown on the right side. A) Hiatus in the upper area (serrated form), marking the base of the Holocene. B) Compact columnar fabric changes to an elongated one (columnar elongated, Ce1). C) Columnar elongated fabric with wide crystals (Ce2). D) Columnar elongated fabric with small, thin, and elongated crystals (Ce1). E) Microcrystalline fabric (Cm) with small crystals and irregular intercrystalline boundaries. Image A was taken in plane-polarized light, and images B-E were taken in cross-polarized light.*

To simplify the petrographic characterization and build a microstratigraphic log, only the OST2 stalagmite is described in this work (Fig. 4.3), since OST3 presents at least three important discontinuities in its growth (hiatus?) and OST1 show high porosity and is frequently made up of a mixture of fabrics such as Cm and Ce1, which complicate the petrographic description. The microstratigraphic log shows that the basal zone of OST2 (the first 12 cm), quite porous and with a whiter tonality, presents a Cm fabric that later evolves to a Ce1 type (Fig. 4.3.D and E). Later, the predominant fabric is Ce2 evolving to C towards the top (Fig. 4.3.B and C). Finally, the stalagmite once again presents a more porous appearance, and the predominant fabric is Ce1, which becomes C and Cm at the top (just before the discontinuity; Fig. 4.3.A and B).

IV.4.3 Chronology and stable isotopes

The uranium content of these stalagmites is extraordinarily high, ranging from 10 to 80 ppm. Despite this, these high uranium content values are not observed in the rocks of the cave, which have a much lower concentration of U (200-300 ppb). This high uranium content in the stalagmites, together with the low values of ^{232}Th, resulted in highly precise U-Th dates (Table 4.1). Depth-age models show a common growth period during the last deglaciation in OST1 and OST2 (from 18.5 to 10.5 kyr BP), interrupted by two hiatuses in OST3 during part of Greenland Stadial (GS) 2.1a and GS-1 (Fig. 4.4).

The $\delta^{18}O_c$ profiles, corrected for global ice-volume changes during this time (Fig. 4.5), show a high degree of correlation among the three stalagmites (Fig. 4.4). A large $\delta^{18}O_c$ isotopic amplitude of more than 5‰ is common for OST1 and OST2, with more negative values (−5‰ to −8.9‰) during GS-1 and GS-2.1 and less negative values (up to −3.4‰) during Greenland Interstadial (GI) 1 and the onset of the Holocene. OST3 did not grow during the intervals of the most negative $\delta^{18}O_c$ values covered by the other two stalagmites, and hence shows a smaller range (<3‰). The oldest parts of the three stalagmites from 18.7 to 16.8 kyr BP, composed of microcrystalline fabric (Fig. 4.3), yielded inconsistent $\delta^{18}O_c$ values as well as age reversals (Fig. 4.4 and 4.6). Therefore, these basal parts were not included in this study.

Sample	Depth (mm)	^{238}U (ppb)	^{232}Th (ppt)	$^{230}Th/^{232}Th$ (atomicx10^{-6})	$\delta^{234}U*$ (measured)	$^{230}Th/^{238}U$ (activity)	$\delta^{234}U_{initial}**$ (corrected)	^{230}Th age*** (yr BP)
OST1-325	37	10581 ±21	1069 ±45	16335 ±685	-1.9 ±1.4	0.1001 ±0.0004	-2 ±1	11449 ±52
OST1-315	47	11717 ±22	658 ±41	30632 ±1918	-3.5 ±1.3	0.1043 ±0.0004	-4 ±1	11987 ±51
OST1-305	57	17152 ±33	1535 ±50	20714 ±677	-4.7 ±1.3	0.1124 ±0.0004	-5 ±1	13000 ±49
OST1-294	68	18945 ±37	871 ±43	40784 ±2006	-10.3 ±1.4	0.1137 ±0.0004	-11 ±1	13244 ±49
OST1-275	87	4872 ±7	479 ±14	20443 ±609	-6.2 ±1.6	0.1219 ±0.0005	-7 ±2	14195 ±70
OST1-245	117	17305 ±35	296 ±39	114524 ±15177	-12.4 ±1.6	0.1189 ±0.0004	-13 ±2	13926 ±53
OST1-210	152	13436 ±27	658 ±41	40454 ±2531	-8.0 ±1.6	0.1202 ±0.0004	-8 ±2	14014 ±57
OST1-150	212	12432 ±29	292 ±10	89161 ±2977	-8.9 ±1.5	0.1269 ±0.0004	-9 ±2	14875 ±52
OST1-120	242	18287 ±36	1154 ±46	34379 ±1359	-8.8 ±1.5	0.1316 ±0.0005	-9 ±2	15467 ±63
OST1-112	250	25553 ±52	1166 ±46	47967 ±1880	-11.5 ±1.4	0.1328 ±0.0004	-12 ±1	15663 ±56
OST1-95	267	24754 ±50	4390 ±97	12652 ±281	-9.8 ±1.5	0.1361 ±0.0004	-10 ±2	16051 ±57
OST1-60	302	16651 ±34	1148 ±45	34136 ±1354	-12.9 ±1.8	0.1428 ±0.0005	-14 ±2	16970 ±69
OST1-40	322	18546 ±37	525 ±40	86759 ±6662	-10.1 ±1.5	0.1490 ±0.0005	-11 ±2	17724 ±69
OST1-25	337	16911 ±34	2623 ±66	16019 ±405	-9.8 ±1.5	0.1507 ±0.0005	-10 ±2	17934 ±67
OST1-0	362	13945 ±26	5698 ±122	6334 ±136	-9.1 ±1.4	0.1570 ±0.0005	-10 ±1	18727 ±75

Table 4.2. **(Continue on the following pages).** ^{230}Th dating results (2σ error) of the Ostolo stalagmites. U decay constants: λ_{238} = 1.55125x10^{-10} (Jaffey et al., 1971) and λ_{234} = 2.82206x10^{-6} (Cheng et al., 2013). Th decay constant: λ_{230} = 9.1705x10^{-6} (Cheng et al., 2013). *$\delta^{234}U$ = ([$^{234}U/^{238}U$]$_{activity}$ − 1) x 1000. **$\delta^{234}U$ initial was calculated based on ^{230}Th age (T), i.e., $\delta^{234}U$ initial = $\delta^{234}U_{measured}$ x $e^{\lambda234xT}$. Corrected ^{230}Th ages assume the initial $^{230}Th/^{232}Th$ atomic ratio of 4.4 ± 2.2 x10^{-6}. Those are the values for a material at secular equilibrium, with the bulk earth $^{232}Th/^{238}U$ value of 3.8. The errors are arbitrarily assumed to be 50%. ***BP stands for "Before Present" where the "Present" is defined as the year 1950 A.D. Outliers are marked in red.

Sample	Depth (mm)	^{238}U (ppb)	^{232}Th (ppt)	$^{230}Th/^{232}Th$ (atomic x10^{-6})	$\delta^{234}U*$ (measured)	$^{230}Th/^{238}U$ (activity)	$\delta^{234}U_{initial}**$ (corrected)	^{230}Th age*** (yr BP)
OST2-272	47	5535 ±6	243 ±9	35821 ±1328	-3.1 ±1.2	0.0953 ±0.0003	-3 ±1	10885 ±41
OST2-258	60.5	8665 ±11	467 ±12	30290 ±785	-3.0 ±1.2	0.0990 ±0.0002	-3 ±1	11335 ±31
OST2-249	69	11260 ±21	900 ±43	20961 ±1005	-2.7 ±1.1	0.1016 ±0.0004	-2.8 ±1.2	11643 ±49
OST2-247	72	7320 ±11	517 ±12	23749 ±540	-3.2 ±1.3	0.1016 ±0.0002	-3 ±1	11655 ±31
OST2-244	75	6525 ±12	891 ±43	12251 ±594	-3.0 ±1.2	0.1014 ±0.0005	-3.1 ±1.3	11625 ±66
OST2-235	84	18403 ±36	1298 ±47	23934 ±875	-5.2 ±1.2	0.1024 ±0.0005	-5.3 ±1.3	11774 ±62
OST2-230	89	15824 ±31	1078 ±45	24977 ±1039	-3.1 ±1.2	0.1032 ±0.0004	-3.2 ±1.2	11844 ±46
OST2-222	96	25413 ±52	1275 ±47	33859 ±1246	-6.9 ±1.3	0.1031 ±0.0003	-7 ±1	11877 ±42
OST2-215	104	10442 ±16	365 ±10	50260 ±1383	-5.7 ±1.3	0.1066 ±0.0002	-6 ±1	12299 ±33
OST2-204	113	6619 ±12	268 ±39	44587 ±6509	-7.1 ±1.3	0.1096 ±0.0005	-7 ±1	12690 ±66
OST2-202	115.5	5139 ±6	333 ±9	28084 ±742	-7.0 ±1.1	0.1104 ±0.0002	-7 ±1	12780 ±31
OST2-200	117	13287 ±25	3513 ±81	6911 ±161	-7.8 ±1.3	0.1108 ±0.0004	-8 ±1	12840 ±52
OST2-183	135	6584 ±9	612 ±15	20511 ±505	-12.3 ±1.4	0.1156 ±0.0003	-13 ±1	13507 ±42
OST2-170	149	7862 ±12	539 ±12	28933 ±654	-11.3 ±1.2	0.1203 ±0.0003	-12 ±1	14082 ±37
OST2-159.5	159.5	12707 ±17	672 ±25	38115 ±1416	-20.6 ±1.2	0.1222 ±0.0003	-21 ±1	14466 ±40
OST2-158	161	9151 ±13	1084 ±28	17173 ±452	-13.1 ±1.4	0.1234 ±0.0003	-14 ±1	14499 ±43
OST2-156	163	19858 ±27	979 ±28	41481 ±1201	-12.7 ±1.3	0.1241 ±0.0003	-13 ±1	14580 ±38
OST2-154	164	5790 ±9	1390 ±29	8642 ±178	-7.8 ±1.4	0.1258 ±0.0003	-8 ±1	14714 ±40
OST2-152	167	8433 ±12	1573 ±38	11215 ±270	-10.3 ±1.5	0.1269 ±0.0003	-11 ±2	14888 ±49
OST2-150	169	8896 ±11	879 ±26	21355 ±633	-14.4 ±1.4	0.1280 ±0.0003	-15 ±1	15100 ±45
OST2-148	171	786 ±1	68 ±3	24705 ±975	-13.0 ±1.5	0.1290 ±0.0004	-14 ±2	15213 ±53
OST2-146.5	172.5	12232 ±16	803 ±24	32498 ±986	-14.5 ±1.5	0.1294 ±0.0003	-15 ±2	15289 ±43

Sample	Depth (mm)	^{238}U (ppb)	^{232}Th (ppt)	$^{230}Th/^{232}Th$ (atomicx10^{-6})	$\delta^{234}U*$ (measured)	$^{230}Th/^{238}U$ (activity)	$\delta^{234}U_{initial}**$ (corrected)	^{230}Th age*** (yr BP)
OST2-145	174	17536 ±24	482 ±16	78095 ±2640	-12.2 ±1.5	0.1303 ±0.0003	-13 ±2	15360 ±43
OST2-135	181	11553 ±23	1234 ±46	20411 ±769	-11.5 ±1.5	0.1323 ±0.0005	-12 ±2	15595 ±64
OST2-121	197	18919 ±20	1023 ±26	41362 ±1044	-12.0 ±1.2	0.1357 ±0.0002	-13 ±1	16041 ±39
OST2-118	200	7313 ±11	316 ±8	51897 ±1345	-11.9 ±1.3	0.1362 ±0.0003	-12 ±1	16104 ±42
OST2-114	204	24161 ±33	2136 ±50	25557 ±596	-12.1 ±1.2	0.1370 ±0.0003	-13 ±1	16217 ±43
OST2-102	216	25136 ±61	981 ±21	58713 ±1237	-11.7 ±1.3	0.1389 ±0.0004	-12 ±1	16454 ±55
OST2-85	233	28309 ±64	1106 ±23	59173 ±1252	-10.5 ±1.4	0.1402 ±0.0004	-11 ±1	16594 ±53
OST2-77	241	49254 ±106	967 ±44	119564 ±5404	-13.1 ±1.2	0.1424 ±0.0004	-14 ±1	16926 ±60
OST2-67	251	50487 ±102	1387 ±52	84878 ±3166	-9.7 ±1.2	0.1414 ±0.0004	-10 ±1	16733 ±59
OST2-55	262	57952 ±137	2679 ±67	52051 ±1308	-12.1 ±1.4	0.1459 ±0.0005	-13 ±2	17363 ±68
OST2-48	269	48084 ±78	2060 ±54	56423 ±1473	-10.5 ±1.1	0.1466 ±0.0004	-11 ±1	17416 ±52
OST2-40	277	80882 ±200	2557 ±65	78544 ±2006	-12.1 ±1.4	0.1506 ±0.0005	-13 ±2	17972 ±69
OST2-36	281	48396 ±89	1426 ±49	80626 ±2790	-9.0 ±1.1	0.1441 ±0.0004	-9 ±1	17068 ±58
OST2-31	286	4247 ±5	179 ±4	56335 ±1187	-12.2 ±1.3	0.1444 ±0.0002	-13 ±1	17168 ±36
OST2-26	291	32110 ±52	1838 ±48	41318 ±1088	-9.4 ±1.3	0.1434 ±0.0004	-10 ±1	16990 ±53
OST2-21	296	33914 ±74	1436 ±49	56448 ±1920	-11.2 ±1.3	0.1450 ±0.0004	-12 ±1	17227 ±61
OST2-15	302	40468 ±86	874 ±43	111812 ±5486	-12.6 ±1.3	0.1464 ±0.0004	-13 ±1	17434 ±61
OST2-10	307	35554 ±56	2941 ±67	29666 ±675	-10.9 ±1.3	0.1488 ±0.0004	-11 ±1	17716 ±55
OST2-5	312	76332 ±186	4690 ±103	39563 ±873	-11.8 ±1.5	0.1474 ±0.0005	-12 ±2	17554 ±72
OST2-3	314	50122 ±100	1516 ±54	79603 ±2819	-9.1±1.1	0.1460 ±0.0005	-10 ±1	17317 ±62
OST2-1	318	31476 ±86	1016 ±22	78800 ±1736	-11.1±1.6	0.1542 ±0.0005	-12 ±2	18434 ±71

Sample	Depth (mm)	^{238}U (ppb)	^{232}Th (ppt)	$^{230}Th/^{232}Th$ (atomic $\times 10^{-6}$)	$\delta^{234}U*$ (measured)	$^{230}Th/^{238}U$ (activity)	$\delta^{234}U_{initial}**$ (corrected)	^{230}Th age*** (yr BP)
OST3-162	98	5433 ±6	1674 ±34	4805 ±99	-1.9 ±1.3	0.0898 ±0.0002	-2 ±1	10203 ±32
OST3-157	103	7662 ±15	2644 ±54	4541 ±92	-3.0 ±1.7	0.0951 ±0.0003	-3 ±2	10849 ±38
OST3-151	108	6483 ±10	496 ±11	20719 ±478	-5.1 ±1.4	0,0961 ±0.0003	-5 ±1	11011 ±36
OST3-145	115	7115 ±14	485 ±14	23515 ±659	-4.2 ±1.8	0,0972 ±0.0003	-4 ±2	11132 ±41
OST3-138	123	9366 ±18	404 ±12	37557 ±1092	-1.6 ±1.6	0,0982 ±0.0003	-2 ±2	11225 ±37
OST3-122	138	12031 ±26	464 ±12	42498 ±1068	-2.3 ±1.6	0,0995 ±0.0003	-2 ±2	11383 ±38
OST3-100	160	12122 ±27	1570 ±33	12782 ±267	-2.8 ±1.7	0,1004 ±0.0003	-3 ±2	11498 ±40
OST3-94	165	6989 ±10	7901 ±159	1621 ±33	-6.3 ±1.4	0,1111 ±0.0003	-7 ±1	12833 ±45
OST3-70	189	7804 ±13	506 ±13	29520 ±732	-7.1 ±1.6	0,1162 ±0.0003	-7 ±2	13504 ±42
OST3-60	199	9862 ±18	604 ±15	32049 ±793	-9.0 ±1.6	0,1191 ±0.0003	-9 ±2	13899 ±45
OST3-47	212	17283 ±40	503 ±12	69356 ±1722	-9.1 ±1.5	0,1225 ±0.0004	-9 ±2	14323 ±52
OST3-41	218	21422 ±47	1065 ±23	46071 ±989	-6.4 ±1.5	0,1389 ±0.0004	-7 ±2	16356 ±56
OST3-32	227	22636 ±55	5894 ±119	9121 ±186	-5.7 ±1.5	0,1441 ±0.0005	-6 ±2	16993 ±67
OST3-25	234	30498 ±89	891 ±20	81869 ±1802	-6.4 ±1.7	0,1451 ±0.0005	-7 ±2	17145 ±69
OST3-17	242	54150 ±115	878 ±43	151284 ±7394	-9.2 ±1.2	0,1487 ±0.0004	-10 ±1	17667 ±62
OST3-10	249	47540 ±398	3865 ±86	29216 ±656	-13.9 ±3.3	0,1441 ±0.0013	-15 ±3	17158 ±180
OST3-9	250	42178 ±86	1100 ±45	98238 ±4021	-10.1 ±1.2	0,1554 ±0.0004	-11 ±1	18551 ±63
OST3-5	254	26192 ±53	1994 ±56	32258 ±913	-6.5 ±1.3	0,1489 ±0.0004	-7 ±1	17643 ±61
OST3-0	259	29186 ±74	1460 ±30	50200 ±1042	-7.6 ±1.4	0,1523 ±0.0005	-8 ±2	18101 ±69
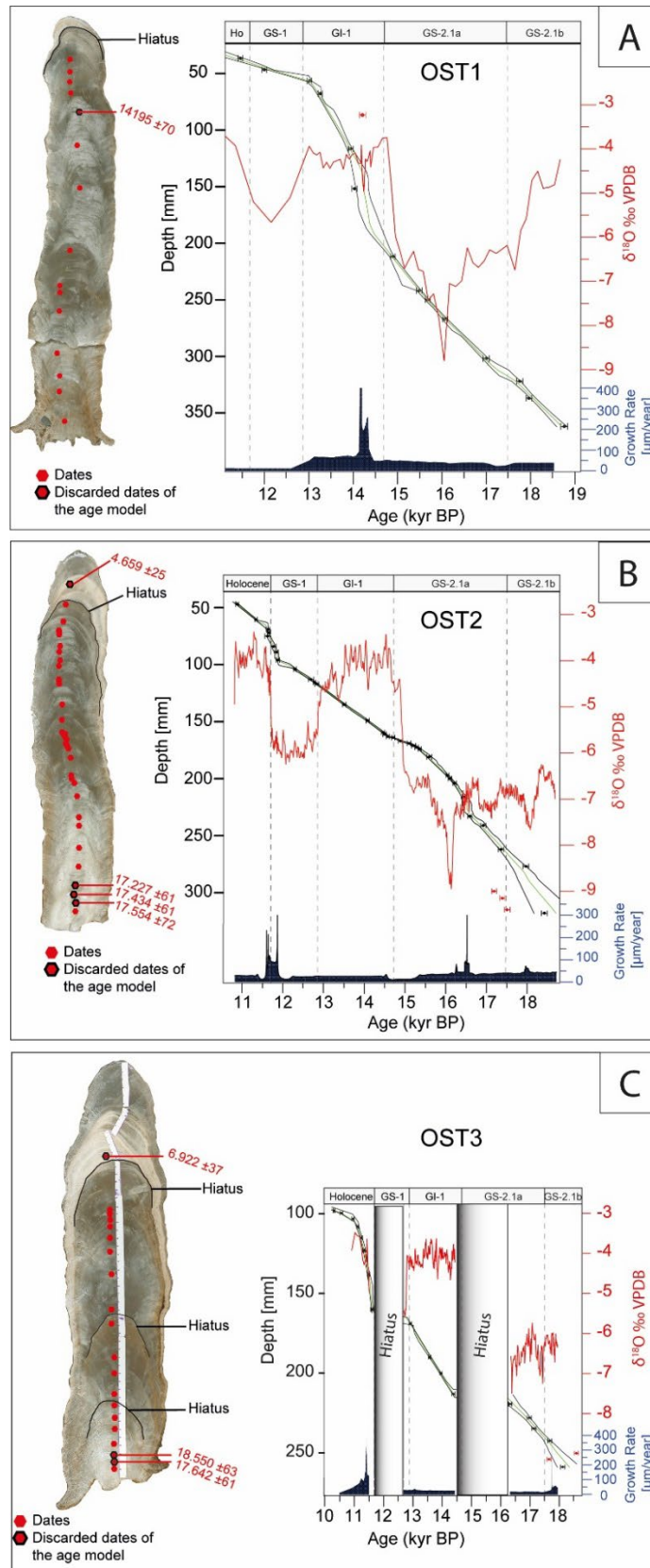
Fig 4.4. *Depth-age models (gray lines and black dots with error bars), $\delta^{18}O_c$ data (red), and growth rate (light blue) of three stalagmites from Ostolo cave. A) OST1, B) OST2, and C) OST3. Red dots mark outliers.*
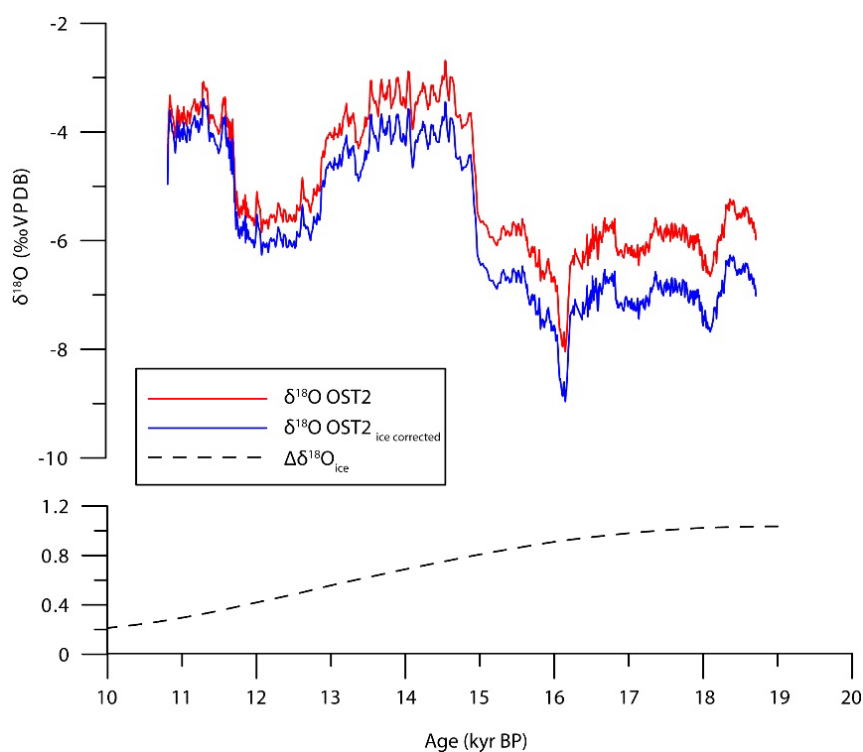
Fig 4.5. *The $\delta^{18}O_c$ record of OST2 corrected for the global ice-volume effect, following Bintanja et al. (2005).*

IV.5 Discussion

IV.5.1 Interpretation of the $\delta^{18}O$ Signal of the Ostolo cave record

Rainfall monitoring surveys in the Central Pyrenees indicate that the values of $\delta^{18}O_r$ show a dependence on temperature equivalent to 0.47‰–0.52‰/°C (Bartolomé et al., 2015b). This dependence is only partially offset by the empirical value of isotope fractionation during calcite precipitation (−0.18‰/°C; Tremaine et al., 2011). Thus, present-day $\delta^{18}O_r$ data may provide semiquantitative constraints on temperature changes during the last deglaciation, supported by the correlation between recent $\delta^{18}O_c$ data and instrumental temperature records in the Pyrenees (Bartolomé et al., 2015b). The uncertainty in this reconstruction is large. The monitoring of the cave indicates that the $\delta^{18}O_d$ values do not present a clear seasonality (Table 4.2), indicating that the signal has been homogenized in the epikarst with a small winter/summer difference (0.2 – 0.3‰) to be considered as a response to seasonal temperature changes. Additionally, for the time interval under consideration, global ice-volume changes affected the $\delta^{18}O_{sw}$ value. Therefore, the Ostolo $\delta^{18}O_c$ measurements were corrected for global ice-volume changes (Fig. 4.5) to better evaluate the contributions of other factors to the $\delta^{18}O_c$ signal.

Previously published speleothem $\delta^{18}O_c$ data from Europe have often been interpreted as temperature records (Frisia et al., 2005b; Moseley et al., 2020). The high degree of similarity between the Ostolo $\delta^{18}O_c$ record and Greenland ice cores (Fig. 4.6), other $\delta^{18}O_c$ cave records dependent on changes in temperature of the region (Fig. 4.7), and the lacustrine $\delta^{18}O$ record from Ammersee (Grafenstein, 1999; Fig. 4.8) confirms that the Ostolo $\delta^{18}O_c$ record mainly reflects regional (North Atlantic) air temperature trends. The variation of $\delta^{18}O_c$ in some cave records from northern Spain and southern France has been attributed to changes in the precipitation amount, seasonality, or variable moisture sources (Baldini et al., 2019; Genty et al., 2006; Moreno et al., 2010; Rossi et al., 2018). Nevertheless, the $\delta^{18}O_c$ amplitude is much smaller in these records (1‰–3‰) than in Ostolo cave stalagmites (~5‰), and the patterns are different (Fig. 4.7). The record from El Pindal Cave in NW Iberia (Fig. 4.7) shows a constant and less clear signal, which makes it difficult to identify drastic changes during the last deglaciation. In this case, and in the speleothem record from Chauvet Cave (Genty et al., 2006) in southern France (Fig. 4.7), the complexity of competing factors (temperature vs. precipitation) makes it difficult to obtain unambiguous information from $\delta^{18}O_c$ values. Hence, most interpretations are based on other geochemical indicators, such as $\delta^{13}C_c$ (Moreno et al., 2010). It is worth noting that both El Pindal and Chauvet records display more negative $\delta^{18}O_c$ values during warm/wet interstadials, thus pointing to the potential role of precipitation (note the reversed y-axis for a better comparison in Fig. 4.7). Therefore, we propose that these differences in the $\delta^{18}O_c$ amplitude likely reflect the distance of Ostolo cave from the coast and its altitude compared with coastal caves. This interpretation is supported by the 7H cave system (1540 m a.s.l.; Luetscher et al., 2015) and Hölloch cave (1210 m a.s.l.; Li et al., 2020) records from the Alps, where the $\delta^{18}O_c$ data sets reflects a temperature signal with similar amplitude as in the Ostolo stalagmites (Fig. 4.7 and 4.8), while Mediterranean $\delta^{18}O_c$ records in Italy present greater difficulties at the time of temperature interpretations (Fig. 4.7).

Although air temperature likely played a dominant role in controlling $\delta^{18}O_c$, other processes such as changes in seasonality may also have had an influence, as has been suggested for speleothems from La Garma cave (northern Iberia; Baldini et al., 2019), where similar $\delta^{18}O_c$ values were found during warm periods in the Holocene and during the cold Younger Dryas (YD). In the Ostolo stalagmites, the $\delta^{18}O_c$ signal is coherent with air temperature changes throughout the entire deglaciation. Current Ostolo cave data show stable annual temperature conditions (13–14 °C) that match the annual mean air temperature outside the cave (13.5 °C), while modern carbonate precipitation occurs year-round. Thus, in principle, seasonal temperature changes are not required to interpret $\delta^{18}O_c$ variations in the studied speleothems.
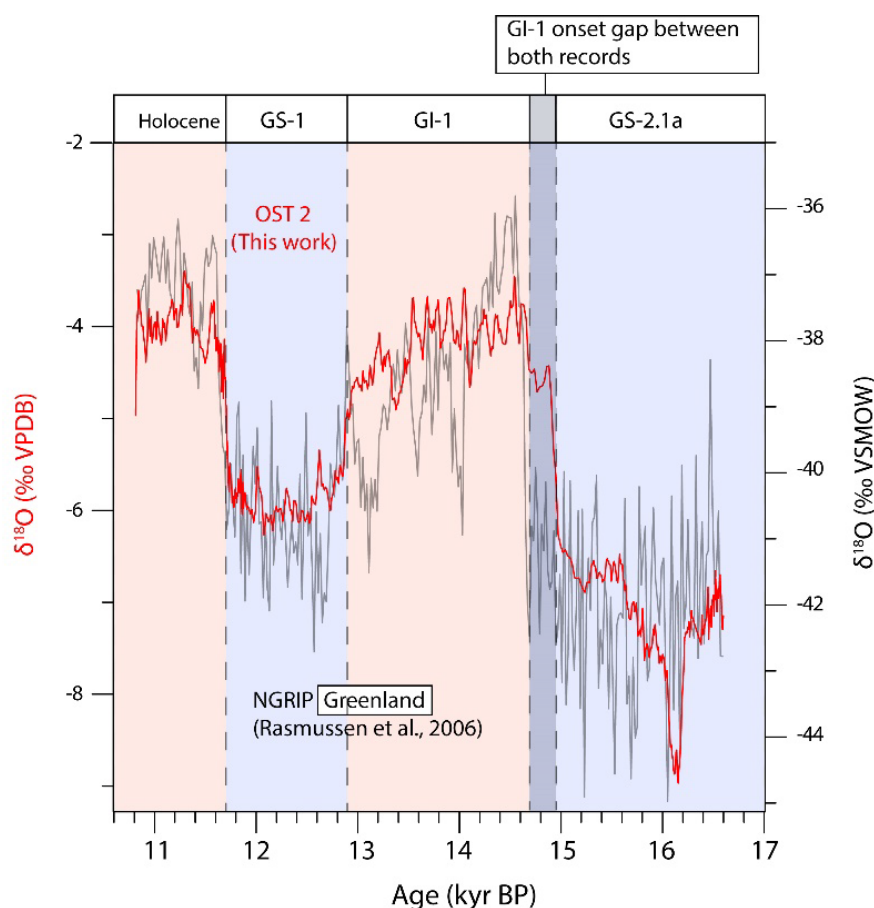
Fig 4.6. *Detailed comparison of the δ¹⁸O records from NGRIP (Rasmussen et al., 2014) and Ostolo (OST2) cave for the last deglaciation. The time gap between both records in the onset of GI-1 is highlighted by a gray column.*

Fig 4.7. *(Next page) (a) Ostolo δ¹⁸O_c records compared to other speleothems records for the last deglaciation. (b) δ¹⁸O_c record of Seso Cave, Pyrenees (Cheng et al., 2020); (c) GAR-01 δ¹⁸O_c record form La Garma Cave (micromilled samples and laser ablation (orange dots) spots - Baldini et al., 2015); (d) δ¹⁸O_c from the southern France (Genty et al., 2006) and (e) northern Iberia (Moreno et al., 2010); (f) δ¹⁸O_c from Meravelles Cave, NE Spain (Pérez-Mejías et al., 2021); (g) δ¹⁸O_c from the southern Germany (Li et al., 2020); (h) The δ¹⁸O_c record of the 7H cave system, Switzerland (Luetscher et al., 2015); (i) The δ¹⁸O_c from Grotta Savi (SV1 record), NE Italy (Frisia et al., 2005b); (j) δ¹⁸O_c from Grotta Antro del Corchia, central Italy (Zanchetta et al., 2007). Note that the y-axis amplitude is the same in all records. The y-axis is reversed for Chauvet, El Pindal, Meravelles, Corchia, and Savi speleothems (combined effect of temperature and precipitation) to facilitate comparison with records from the Alps and the Pyrenees (which are temperature dominated).*
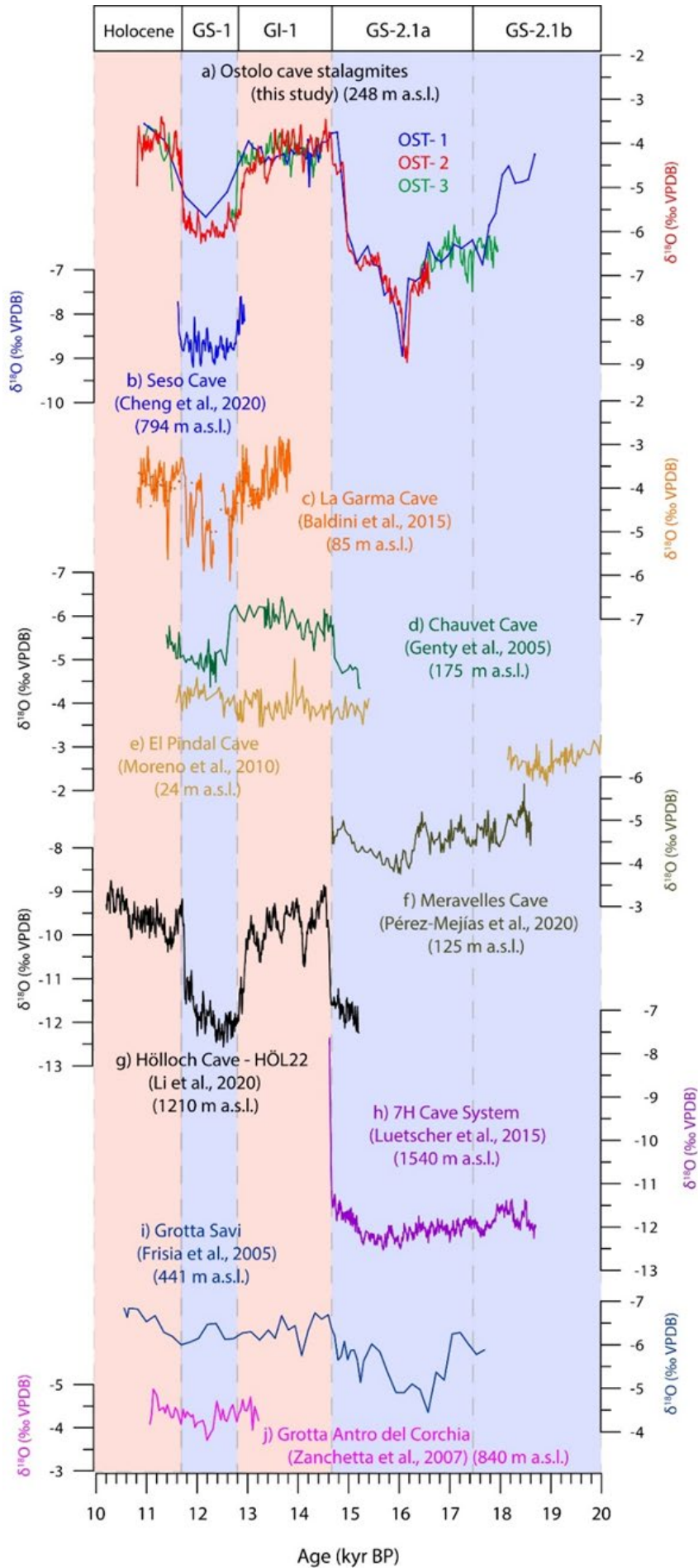
In addition to the temperature effect, we also invoke changes in the isotopic composition of the moisture source to explain the negative excursion in the Ostolo $\delta^{18}O_c$ record during Heinrich event 1 (HE1) at 16.5–16.0 kyr BP, reaching values as low as −8.9‰. This light excursion was synchronous with the deposition of ice-rafted debris in the northern Bay of Biscay (Eynaud et al., 2012; Fig. 4.8). Meltwater released into the North Atlantic Ocean as a consequence of massive discharge from the Northern Hemisphere ice sheets resulted in a cooling and decrease of the isotopic composition of seawater by 1‰–1.2‰ (Voelker et al., 2009). We propose that this oceanic isotopic change was transported via moisture to the study area and recorded by the Ostolo stalagmites as a negative $\delta^{18}O_c$ excursion, capturing the meltwater signal at ca. 16.1 kyr BP. This freshening during HE1 has been observed in $\delta^{18}O$ records from the Atlantic Ocean (MD99–2334 core; Fig. 4.1; Skinner & Shackleton, 2006) and in sea surface salinity (SSS) reconstructions in the Bay of Biscay (MD95–2002 core; Eynaud et al., 2012; Fig. 4.8). Similarly, the meltwater signal was captured, although at much smaller amplitude, in the $\delta^{18}O_c$ record from Meravelles cave in northeastern Spain (Pérez-Mejías et al., 2021; Fig. 4.7), supporting our interpretation of the episodic contribution of a major change in the moisture source composition to the Ostolo $\delta^{18}O_c$ record.

Fig 4.8. *(Next page) Regional synthesis of terrestrial and marine records of the last deglaciation: (a) North Greenland Ice Core Project (NGRIP; Rasmussen et al., 2006); (b) $\delta^{18}O$ of ostracods from Ammersee, Germany (Grafenstein, 1999); (c) $\delta^{18}O_c$ of stalagmites HÖL22 and HÖL1 from Hölloch cave (Li et al., 2020); (d) $\delta^{18}O_c$ of stalagmite from Ostolo (OST-2, red), Seso (blue) and La Garma caves (orange); (e) $\delta^{18}O$ from Globigerina bulloides of marine core MD99-2334K (green, Skinner & Shackleton, 2006); (f) Sea surface salinity (SSS) reconstruction derived from planktonic foraminifera (Eynaud et al., 2012); and (g) Ice-rafted debris (IRD) record from MD95–2002, northern Bay of Biscay (Eynaud et al., 2012). VPDB—Vienna Peedee belemnite standard; VSMOW—Vienna standard mean ocean water; GS—Greenland Stadial; GI—Greenland Interstadial.*
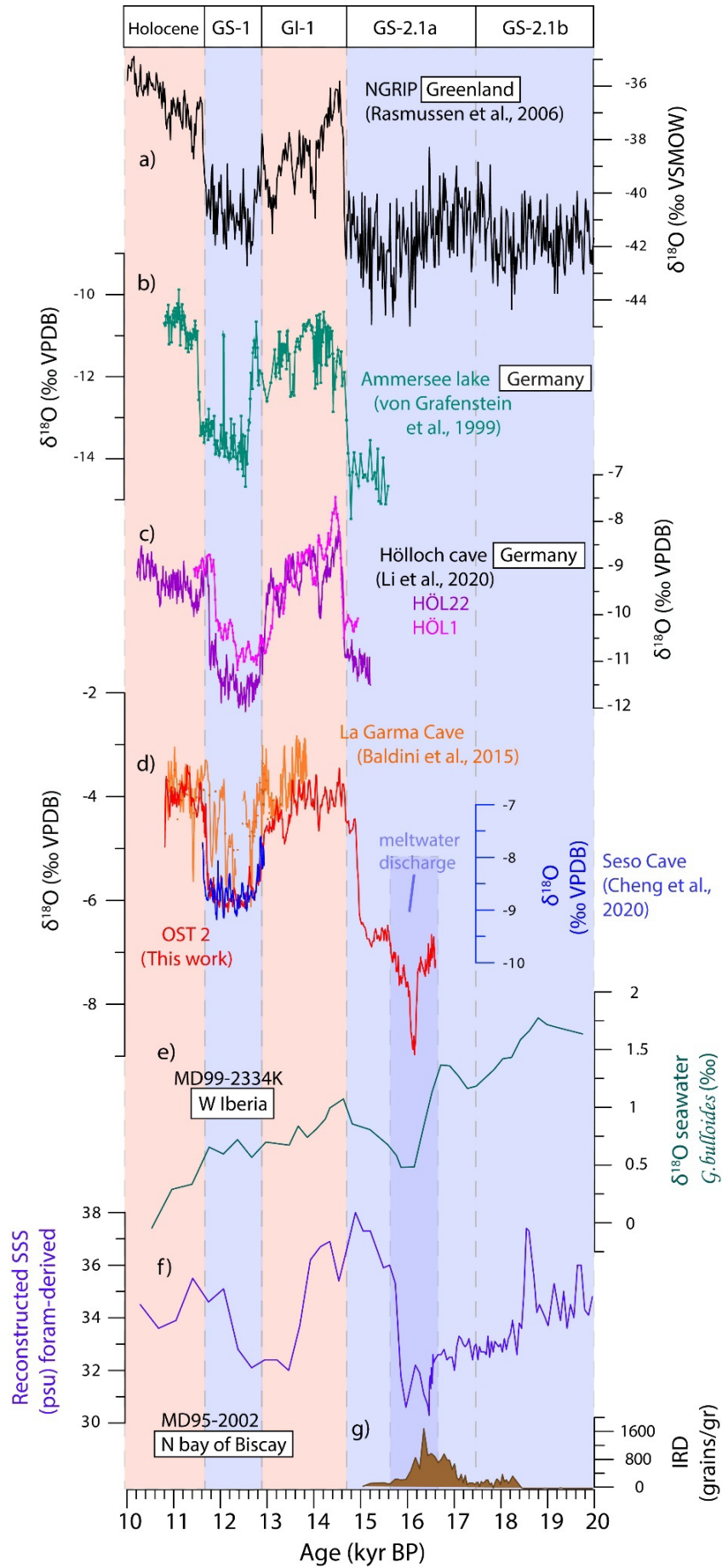
IV.5.2 Evolution of the δ¹⁸O Signal During the Last Deglaciation in Northern Iberia

The replicated $\delta^{18}O_c$ record from Ostolo cave covers the interval from 16.8 to 10.5 kyr BP. (Fig. 4.9). After the negative spike at 16.2–16.0 kyr BP associated with HE1, $\delta^{18}O_c$ values show a progressive increase from −8.9‰ to −6.7‰ between 16 and 15 kyr BP. The end of the meltwater contribution could explain the drastic isotopic increase at 16 kyr BP, but not the progressive increase lasting until 15 kyr BP. In contrast, the NGRIP record $\delta^{18}O$ values during GS-2.1a do not show any significant trend. An early warming trend during the pre-Bølling millennium has been recorded by $\delta^{15}N$ data from Greenland (Buizert et al., 2018) and in a terrestrial record in central Europe (Bolland et al., 2020). We suggest that this early warming of the northern circum-Atlantic realm and adjacent regions could also have been present in southern Europe.
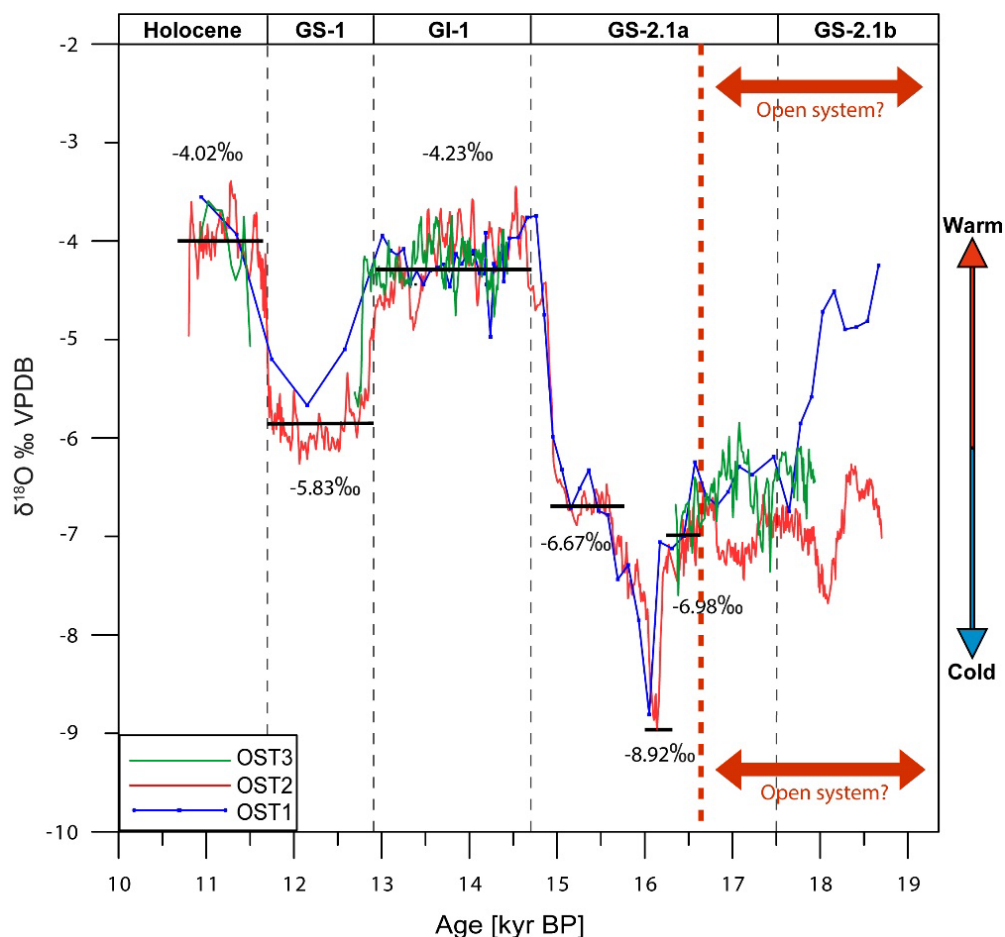
Fig 4.9. *Replicated δ¹⁸Oc data of three stalagmites from Ostolo cave. The average values of OST2 are indicated for each stage of the last deglaciation (black horizontal lines). Note that the record prior to 16.8 kyr BP was not included in this study (see text).*

The onset of GI-1 in the Ostolo stalagmites (Fig. 4.9) is marked by heavier $\delta^{18}O_c$ values at 14.938 ± 0.040 kyr BP. This sharp change is almost synchronous with the onset of GI-1 recorded by Greenland ice cores at 14.642 ± 0.186 kyr BP. (Rasmussen et al., 2014). The difference of 296 yr is almost included in the dating uncertainties of both records (Fig. 4.6). Nevertheless, the low error in the Ostolo dates (± 40 yrs) together with the well-constrained age model (constrained by nine dates allowing a robust age model for this part of the sequence) may serve to assess the chronology of the onset of GI-1. The mean $\delta^{18}O_c$ amplitude of 2.43‰, varying from −6.67‰ to −4.23‰, could represent a temperature change of roughly 7.5 °C in less than 50 yr, based on the present-day temperature dependence of $\delta^{18}O_r$. These values are also consistent with the 5–6 °C SST warming during GI-1 recorded in marine cores from the Iberian margin (e.g., MD01–2444 core [Martrat et al., 2007]; core MD03–2699 [Rodrigues et al., 2010]; Fig. 4.1).

Between 12.9 and 12.8 kyr BP, a $\delta^{18}O_c$ decrease by 1.6‰ marks the onset of GS-1 in Ostolo (Fig. 4.9). This important change is equivalent in amplitude to a high-resolution stalagmite $\delta^{18}O_c$ record from Seso cave (Central Pyrenees; Bartolomé et al., 2015b; Cheng et al., 2020), showing similar dating uncertainties (between 30 and 60 yr; Fig. 4.10). This change could reflect a temperature decrease of ∼5 °C, which agrees with rapid cooling recorded by speleothems from the European Alps (around 4–5 °C; Li et al., 2020) and the Jura Mountains (around 4.3 ± 0.8 °C; Affolter et al., 2019). These data are also in agreement with the decrease in SST of around 4 °C offshore Iberia at 12.9 kyr BP (Rodrigues et al., 2010).

A comparison of $\delta^{18}O_c$ values for GS-1 (−5.83‰) and GS-2.1a (−6.87‰) (Fig. 4.9) suggests colder temperatures during GS-2.1a, which is in agreement with Greenland ice cores (Buizert et al., 2018). This interpretation is consistent with the cessation of growth in stalagmites from El Pindal and Villars caves (Genty et al., 2006; Moreno et al., 2010), reduced sedimentation rates, and lower lake levels during GS-2.1a in northern Spain (Morellón et al., 2009). GS-2.1a period was likely the coldest one of the last deglaciation on a regional scale.

An abrupt change in $\delta^{18}O_c$ occurred at the end of GS-1 (11.72 ± 0.06 kyr BP), reaching values at the beginning of the Holocene (−4.02‰) like those at the onset of GI-1 (−4.23‰). However, the amplitude of change from GS-2.1a to GI-1 (∼3.5‰) was larger than that from GS-1 to the Holocene (∼1.8‰; Fig. 4.9). The similarity of the values suggests that both warm intervals were characterized by a comparable regional climate. Coherently, SST reconstructions around Iberia indicate similar temperatures during GI-1 and the Holocene (Ausín et al., 2019; Skinner & Shackleton, 2006). Future quantitative constraints on the regional temperatures during the Holocene and GI-1 onset, e.g., by fluid inclusion isotope analyses, would be required to precisely estimate this described evolution.
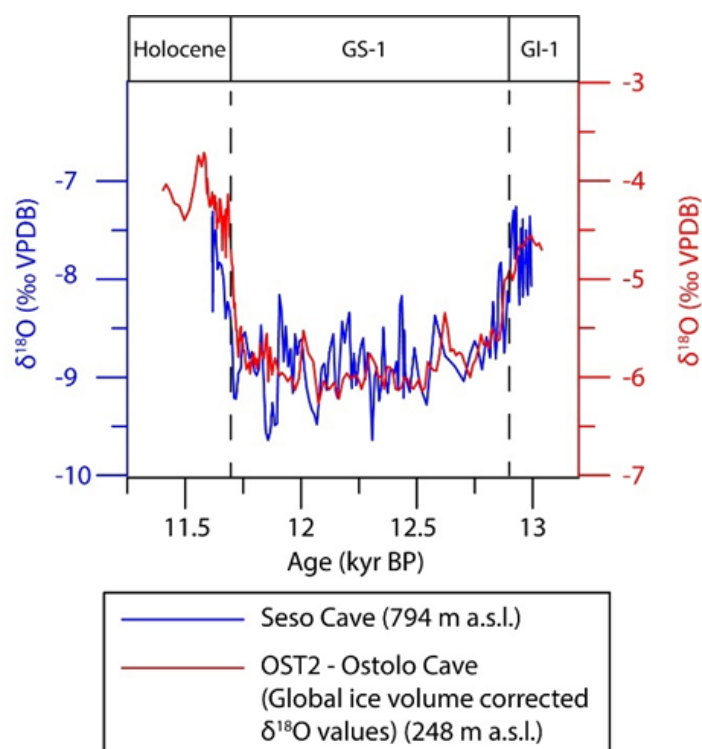
Fig 4.10. *A detailed comparison of the $\delta^{18}O_c$ record from Seso cave (Cheng et al., 2020) and the global ice volume corrected $\delta^{18}O_c$ of Ostolo cave (OST2) at GS-1.*

IV.6 Conclusion

The $\delta^{18}O_c$ record from Ostolo cave provides a unique opportunity to accurately date the abrupt millennial-scale climate oscillations of the last deglaciation for the first time in southern Europe. Light $\delta^{18}O_c$ values were observed during stadials (GS-1 and GS-2.1a), and heavier values were observed during warm events (GI-1 and Holocene), thus indicating a dominant air temperature control on this signal. An exceptional light $\delta^{18}O_c$ excursion centered at 16.2–16.0 kyr BP is interpreted to reflect the major phase of HE1 iceberg melting reaching the Iberian Peninsula, which drastically changed the $\delta^{18}O$ composition of regional precipitation. The exceptional high quality of the Ostolo chronology and its clear $\delta^{18}O_c$ signal support a deglacial ocean-atmosphere connection that rapidly transferred high-latitude changes toward southern Europe.
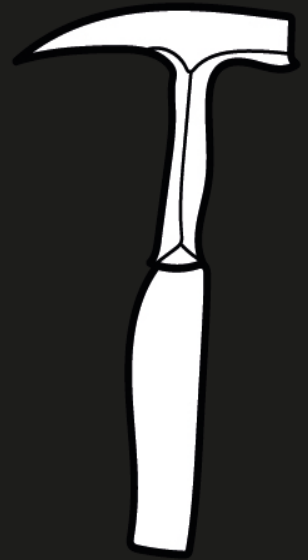
Chapter V

Since the YD to present day: Mendukilo cave record

V.1 Introduction

The transition from the cold and dry Younger Dryas to the early Holocene was one of the most rapid warming events on a global scale. This warming was associated with a resumption of the Atlantic Meridional Overturning Circulation (AMOC) (McManus et al., 2004). In the North Atlantic, the onset of the Holocene was punctuated by short cold periods due to variable meltwater input. At latitudes below 45ºN, including the Mediterranean region, deglacial warming was influenced by orbitally driven changes (Renssen et al., 2009) that modulated Holocene hydroclimate variability. The general evolution from wetter to drier climatic conditions between the early and late Holocene throughout southern Europe (Roberts et al., 2019) is consistent with the long-term change in insolation, and hence, it is influenced by seasonality (Wanner et al., 2008). In fact, the Holocene Mediterranean climate has been traditionally divided into three intervals according to water availability: (i) a first part characterized by humid conditions (11.7-7.0 kyr BP), (ii) the mid-Holocene with increased hydroclimatic variability but in general higher temperatures (7.0-5.5 kyr BP), and (iii) a decrease in humidity since ~5.5 kyr BP associated with the onset of the current Mediterranean-type climate (Jalut et al., 2009; Magny et al., 2011). In the case of the Iberian Peninsula, which is influenced by two contrasting climate regimes (Atlantic and Mediterranean), the hydroclimate evolution during the deglacial warming and the Holocene was characterized by a strong regional heterogeneity (e.g., Carrión et al., 2010). Thus, the observed changes in continental records (lake sediments and speleothems) (e.g., González-Sampériz et al., 2017; Morellón et al., 2018; Moreno et al., 2017) in Iberia are not consistent in space or time with the simplified picture outlined for the Mediterranean region leading to apparent contradictions in temperature and precipitation reconstructions that need to be understood on a regional scale. Different records in the region have highlighted that the sometimes contradictory pattern of climate proxy results may be due to seasonality changes in rainfall (Baldini et al., 2019; Morellón et al., 2009; Moreno et al., 2017; Walczak et al., 2015), potentially associated to shifts in the position and strength of the Azores High.

Northern Iberia shows large environmental changes along a W-E transect controlled by altitude and proximity to the ocean, resulting in a large temperature and humidity variability during the Holocene (Finné et al., 2019). For example, the Holocene vegetation and climate succession reconstructed from lakes and peatbogs in NW Iberia and the Eurosiberian region (excluding eastern Iberia) reveals the traditional Holocene regional tripartite pattern (Allen et al., 1996; López-Merino et al., 2012; Moreno et al., 2011): Lake records from the Pyrenees show a progression from a dominantly Atlantic pattern in the western sector (González-Sampériz et al., 2006) to a significant Mediterranean imprint in the central region (Pérez-Sanz et al., 2013). Consistently, lake records present in the central-southern region of the pre-Pyrenees show a delay in the onset of wet conditions (9.5 kyr BP) and a decrease in humidity after 5-4.5 kyr BP (Morellón

et al., 2009), a pattern that is supported by terrestrial proxies obtained from western Mediterranean marine records (Fletcher et al., 2013; Frigola et al., 2007). Several Holocene speleothem records have also been obtained from caves in northern Spain, but some are discontinuous (e.g., Serra do Courel; Railsback et al., 2011) or do not cover the entire interglacial (Martín-Chivelet et al., 2011; Rossi et al., 2018). In general, orbital forcing clearly exerted a first-order control on speleothem growth, as shown by an increase in the relative abundance of speleothems in the early Holocene (Stoll et al., 2013). Holocene speleothem records have also revealed the important role of the Atlantic Ocean in shaping centennial-scale oscillations (Domínguez-Villar et al., 2017; Smith et al., 2016), while a compilation of speleothem records from northern Spain has highlighted the role of rainfall seasonality (Baldini et al., 2019).

Here, we present four new stalagmites collected from Mendukilo cave in northern Iberia, which provide a well-replicated, high-resolution, and continuous record of the northern Iberian climate from the beginning of the Younger Dryas to present-day. Stable isotopes, combined with trace elements and supported by a detailed monitoring of the cave, allow reconstructing temperature and amount of rainfall during the last 12,700 years, thus addressing the role of different mechanisms in causing centennial-scale oscillations, such as the 8.2 kyr event. The new data is discussed in both site-specific and regional contexts, together with other published records from the Atlantic margin of Europe, thus offering new insights into the Iberian climate evolution on millennial to centennial timescales since the Younger Dryas.

V.2 Site description

Mendukilo cave is located at 750 m a.s.l. and 40 km from the Cantabrian coast (Fig. 5.1A and B) in a site of community importance within the lands of the Astitz council (Larraun valley, Navarra), on the slopes of the eastern part of the Sierra de Aralar (42º58'25''N, 1º53'45''W; Fig. 5.1B). The cave developed within reef limestones of Lower Cretaceous age (Urgonian, Albian-Aptian) at the eastern boundary of the Basque-Cantabrian basin. The climate of this region is temperate with cool summers (west coast maritime climate following the Köppen-Geiger classification). Rain, fog, and drizzles are abundant, making this area one of the rainiest locations in Spain (1365 mm of annual precipitation). Rainfall is concentrated in fall, winter, and spring, and temperatures are mild without reaching extreme values, reflecting the proximity of the Atlantic Ocean. The surroundings of the cave are composed of small karstic mountain plateaus and dolines, with meadows in the highest parts and forests of beech, oak, and abundant moss covering the slopes. Soils are well developed, rich in clay, and usually less than 50 cm in thickness.
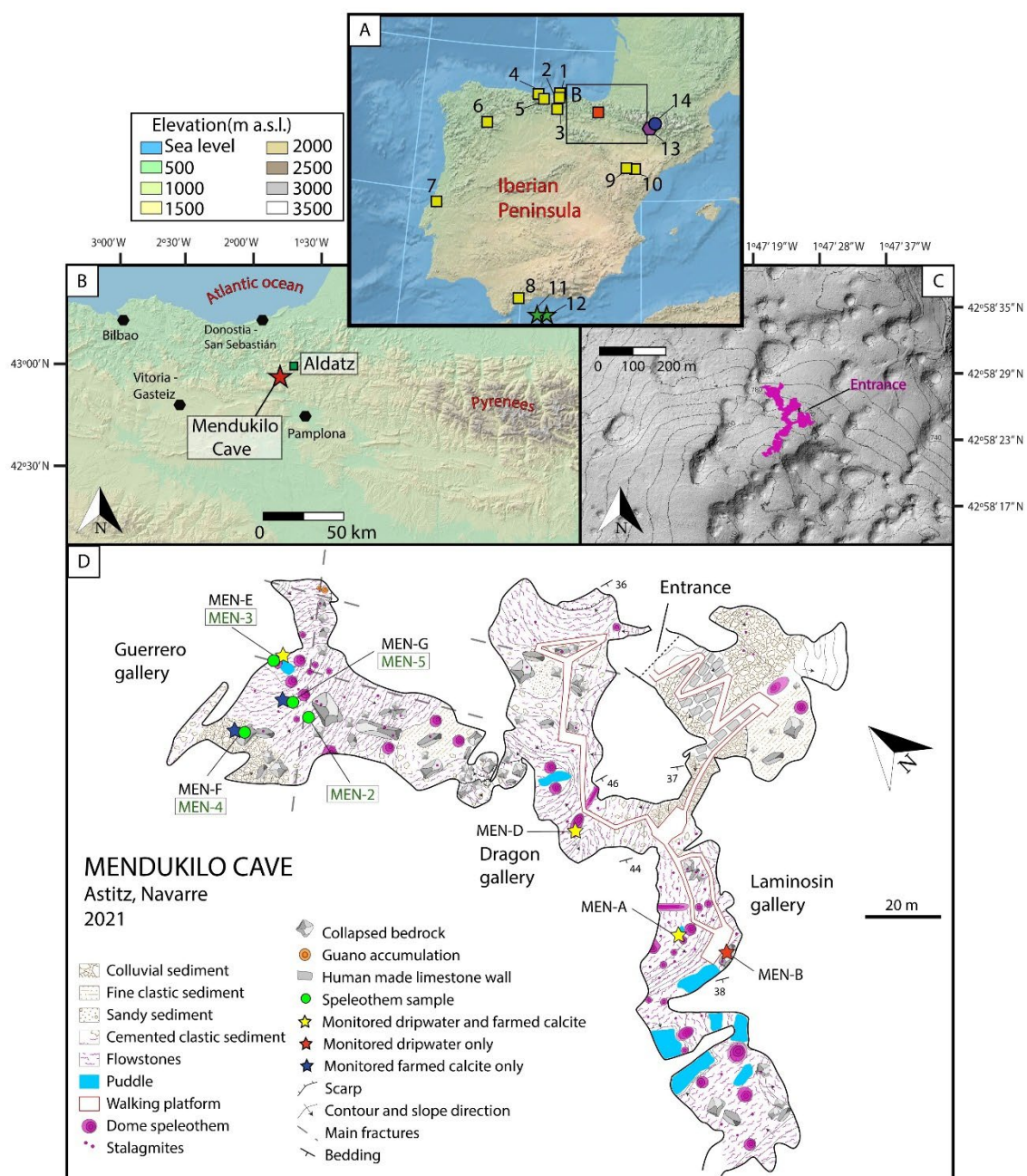
Fig 5.1. *Location of Mendukilo cave (red square) and other records of the Iberian Peninsula cited in this work (yellow squares = cave sites; green stars = marine records; purple hexagon = lake record; blue circle = ice cave): [1] La Garma Cave; [2] Cueva de Asiul; [3] Kaite Cave; [4] El Pindal Cave; [6] El Soplao Cave; [7] Cova de Arcoia; [8] El Refugio Cave; [9] Ejulve Cave; [10] Molinos cave; [11] ODP976; [12] ALB-2; [13] Basa de la Mora lake; [14] A294 Ice Cave. B) Regional setting with the location of the cave (red star), meteorological station (yellow square, where the temperature and rainfall databases for this study were obtained) and nearby major cities (black hexagons). C) Digital elevation model and plan view of the cave (pink). D) Geomorphological map of Mendukilo cave showing locations of dripwater and speleothem samples.*

93

The cave shows a descending morphology and consists of seven main rooms (Entrance hall, Intermediate gallery, Laminosin gallery, Los Lagos gallery, Dragon hall, Guerrero and Caballo gallery's) (Fig. 5.1C and D). The total passage length is 869 m and the vertical extension is 59 m. Its geometry is controlled by a NW-SE- and NE-SW-oriented fracture network. The cave is currently in the vadose zone, and its morphology is characterized by gravitational breakdown features (roof and wall collapse). The entrance, Entrance Hall and Intermediate gallery have been modified during show cave development. Speleothem deposition is abundant in the Laminosin gallery, Los Lagos gallery, Dragon hall, Guerrero gallery and Caballo gallery. Most drip sites are active throughout the year. The main gours and pools are filled with water in autumn, winter, and spring, and are typically dry in summer.

V.3 Methods

V.3.1 Rainfall monitoring

To explore the relationship between the isotopic composition of rainfall ($\delta^{18}O_r$ and δD_r) and the climate parameters outside the cave, rainwater was sampled at the University of the Basque Country (Bilbao), an area with a mainly Atlantic source of rainfall and 95 km away from Mendukilo cave (Fig. 5.1). Sampling was conducted between July 2018 and February 2021, and 144 rain events were sampled. The stable isotopic compositions of these samples were analyzed using cavity ring-down spectroscopy (PICARRO L2130-i) at the Pyrenean Institute of Ecology (Zaragoza). The results are reported in per mil with respect to Vienna Standard Mean Ocean Water (VSMOW), and the reproducibility of the measurements was typically 0.1‰ for $\delta^{18}O_r$ and 0.5‰-1‰ for δD_r. The isotopic results were compared with the air temperature measured at the Bilbao airport meteorological station on the day of the respective rain event (Supp. Material Fig. 8.1).

V.3.2 Cave monitoring: sampling and analyses

Mendukilo cave was monitored on a seasonal basis for temperature, humidity, pCO_2, dripwater composition, and farmed carbonates from 2018 to 2021. Cave-air temperature and relative humidity were recorded using HOBO® U23 pro v2 data loggers in three different galleries (Laminosin, Dragon hall and Guerrero; Fig. 5.1D). Additionally, pCO_2 was measured using a pSense Portable CO_2 meter (model AZ-0001) at the same sampling points. Precipitation and temperature data obtained from the Aldatz meteorological station, located 5 km northeast of Mendukilo cave (Fig. 5.1B), were used for comparison.

Dripwater samples were obtained from four different drip sites (MEN-A, MEN-B, MEN-D, and MEN-E; Fig. 5.1D) and four pluviometers (RAIN-O-MATIC-HOBO coupled with a HOBO

data logger UA-003-64) were used to monitor the drip rate (Fig. 5.1D). All dripwater samples were analyzed for oxygen ($\delta^{18}O_d$) and hydrogen (δD_d) isotope composition via cavity ring-down spectroscopy (PICARRO L2130-i) at the Pyrenean Institute of Ecology (Zaragoza). The results are reported in per mil with respect to Vienna Standard Mean Ocean Water (VSMOW), and the reproducibility of the measurements is typically 0.1‰ for $\delta^{18}O$ and 0.5‰-1‰ for δD.

Farmed carbonate precipitated on glass plates (at drip sites MEN-A, MEN-D, and MEN-E and additionally at MEN-F and MEN-G sites without drip monitoring) was analyzed for oxygen and carbon isotopes ($\delta^{18}O_p$ and $\delta^{13}C_p$, reported as ‰ with respect to the Vienna Pee Dee Belemnite (VPDB) standard). The samples were recovered seasonally. The MEN-E, MEN-F, and MEN-G monitoring sites coincide with the locations of the stalagmites examined in this study (MEN-3, MEN-4, and MEN-5, respectively; MEN-2 was not beneath an active drip site). The first batch of isotopic analyses (7 samples) was analyzed at the University of Innsbruck (Austria) using a ThermoFisher Delta V Plus linked to a GasBench II, following the methodology described in Spötl (2011). The long-term reproducibility (1 sigma) of $\delta^{18}O_p$ is 0.08‰, and 0.06‰ for $\delta^{13}C_p$ (Spötl, 2011). The rest of the samples were analyzed at the Iso TOPIK Laboratory (University of Burgos; 29 samples) and at the University of Barcelona (10 samples) following similar procedures and identical equipment.

V.3.3 Mendukilo stalagmites: petrography, trace elements and stable isotope analyses

Four stalagmites were collected from the Guerrero gallery (Fig. 5.1D), a deep gallery around 200 m from the cave entrance. Except for MEN-2, these stalagmites were located underneath active drips fed by different fracture networks and dripping conditions (section V.4.1). The stalagmites were cut parallel to their growth axis, and the central segment of the slab of each speleothem was sampled for U-Th dating, stable isotopes, and major and trace elements. In MEN-3 and MEN-4, the opposite slab was used to obtain thin sections for a petrographic study. MEN-4 is macroscopically very similar to MEN-2 and MEN-5; thus, these last two stalagmites were not petrographically analyzed.

A total of 1451 samples for $\delta^{18}O_c$ and $\delta^{13}C_c$ analyses were obtained along the central axis at 1 mm increments from stalagmites MEN-2, MEN-3, MEN-4, and MEN-5. Isotopic analyses were performed at the University of Innsbruck, using a ThermoFisher Delta V Plus linked to a GasBench II, following the methodology described in Spötl (2011). The long-term reproducibility (1 sigma) of the $\delta^{18}O_c$ analyses is 0.08‰ and 0.06‰ for $\delta^{13}C_c$ (Spötl, 2011). All values are reported as per mil with respect to the Vienna Pee Dee Belemnite standard (VPDB).

In addition to the isotope samples, 267 carbonate samples were analyzed for trace elements. Samples were taken at 5 mm intervals and measured for Mg/Ca and Sr/Ca ratios at ETH Zurich

(Agilent QQQ 8800) using a standardization approach similar to that reported in Stoll et al. (2022b).

V.3.4 U-Th dating and age model development: integration into a composite record

A total of 41 powder samples were drilled for uranium-series dating from distinct growth layers along the central growth axis of each speleothem using a handheld drill and a tungsten carbide drill bit. After chemical separation, U and Th isotope measurements were performed using a MC-ICP-MS (Thermo-Finnigan Neptune Plus) at the University of Xi'an and the University of Minnesota (USA), following a previously described methodology (Cheng et al., 2013). To calculate corrected ages, an initial $^{230}Th/^{232}Th$ atomic ratio of 4.4 ± 2.2 x 10^{-6} was used.

The individual age model for each stalagmite was obtained using the StalAge software (Scholz & Hoffmann, 2011). Subsequently, the individual isotope profiles of the four stalagmites were integrated into a single one (MEN composite record) using the software Iscam (Fohlmeister, 2012). This program looks for the highest correlation between two or more dated proxy signals within age uncertainties using a linear interpolation between adjacent U-Th dates. Two composite records have been constructed by applying the $\delta^{13}C_c$ and then the $\delta^{18}O_c$ data from the different stalagmites of the Mendukilo cave. The isotopic values between the different stalagmites in the overlapping intervals correlate well with each other in each of the composites ($\delta^{13}C_c$ and $\delta^{18}O_c$), but finally it has been decided to use the $\delta^{13}C_c$ composite (and the resulting age model) throughout this work, since it presents a greater variability in its isotopic values over the last 13 kyr BP. Finally, the age model that produced the highest coherence (applying a smoothing of 100 years) was selected and subsequently the data from other proxies of this work ($\delta^{18}O_c$ and trace elements) have been assigned a chronology based on this new $\delta^{13}C_c$ composite age model.

V.4 Results

V.4.1 Monitoring

The average annual rainfall in the area (1921-2021) is 1365 mm. Rainfall amount during the monitored years shows an important interannual variability, with a decreasing annual amount from 2019 (1931 mm) to 2020 (1371 mm) (Fig. 5.2A). Drip data (November 2018 to May 2021) reveal that the MEN-D and MEN-E drip sites were continuously dripping. They show a lower drip-rate variability between different seasons compared to the MEN-A and MEN-B drip sites, which tend to almost cease in summer (Fig. 5.2B). Episodes of highest drip rates per day recorded by the MEN-A and MEN-B loggers correlate with periods of intense daily (>50 L/m^2) and monthly rainfall (winter and fall in 2019, Fig. 5.2A). Drip sites MEN-A, MEN-B and MEN-D are

fed by low discharge seasonal drips with a medium to high variability, with a maximum discharge rate of 2.49 ml min^{-1}, 0.15 ml min^{-1} and 0.17 ml min^{-1} and a coefficient of variation of 134, 90 and 59, respectively (following Smart & Friederich (1987), Supp. Material Fig. 8.2). On the other hand, MEN-E is fed by seepage flow (low variability, coefficient of variation of 21), showing the lowest maximum discharge rate of 0.06 ml min^{-1}. In the case of drips without drip rate monitoring (MEN-F and MEN-G) they have been categorized as continuous drips (not seasonal) in the different monitoring campaigns inside the cave and with an apparent similar behavior between MEN-E and MEN-D drips. The classification of drips based on discharge rate and coefficient of variation has been shown to be useful to discern its influence on the isotopic composition of the dripwater and of the farmed calcite (Pérez-Mejías et al., 2018).

The air temperature inside Mendukilo cave varies between 8.4 and 9.2 ºC during the year, i.e., 3.4 ºC lower than the mean annual surface air temperature in the monitored years (11.8-12.6 ºC, Aldatz meteorological station) showing a delay of about 10-14 days in relation to variations in surface temperature (Fig. 5.2C and D). Only the temperature sensor installed in the Guerrero room, far from the entrance, recorded a constant temperature (9.1-9.2 ºC). pCO$_2$ values follow the seasonal temperature pattern inside the cave, being higher in summer and lower in winter.

For the studied period, $\delta^{18}O_d$ and δD_d values for the four drip sites range from -8.7 to -7.3‰ and -53.8 to -42.0‰, respectively. The mean $\delta^{18}O_d$ values for these drip sites are between -7.6‰ (MEN-D and MEN-E) and -8.0‰ (MEN-A and MEN-B) and, in general, winter values are lower than summer values (Fig. 5.2F). Considering the average values for all drip sites during summer (-7.6‰) and winter (-8.1‰), the average seasonal variability is 0.5‰. Adding to this variability, a slight trend towards less negative values is observed between 2018 and 2021, associated with a decreasing amount of rainfall, as described above. The exception is the MEN-E drip site, which fed the MEN-3 stalagmite and records a stable drip rate that does not respond to seasons or rain events and shows a low isotopic variability (Fig. 5.2). The seasonality recorded in the dripwaters (low variability) values was also observed in rainfall (high variability; Supp. Material Fig. 8.1), although it was much more reduced in dripwaters due to homogenization once water enters the epikarst.

Fig 5.2. **(Next page)** *Monitoring results from Mendukilo cave from November 2018 to May 2021. A) Daily and monthly precipitation outside the cave (Aldatz meteorological station). B) Drip rate of the different sampling points inside the cave. C) Daily surface average temperature outside the cave. D) Cave temperature and E) CO$_2$ concentration at the Laminosin (light blue line and dots), Dragon (grey line and dots) and Guerrero (blue line and dots) galleries. F) Dripwater $\delta^{18}O_d$ composition of the different drip sites. G) $\delta^{18}O_p$ and H) $\delta^{13}C_p$ values of farmed calcite for the different monitoring sites (see Fig. 8.2 in the Supp. Material for more information).*
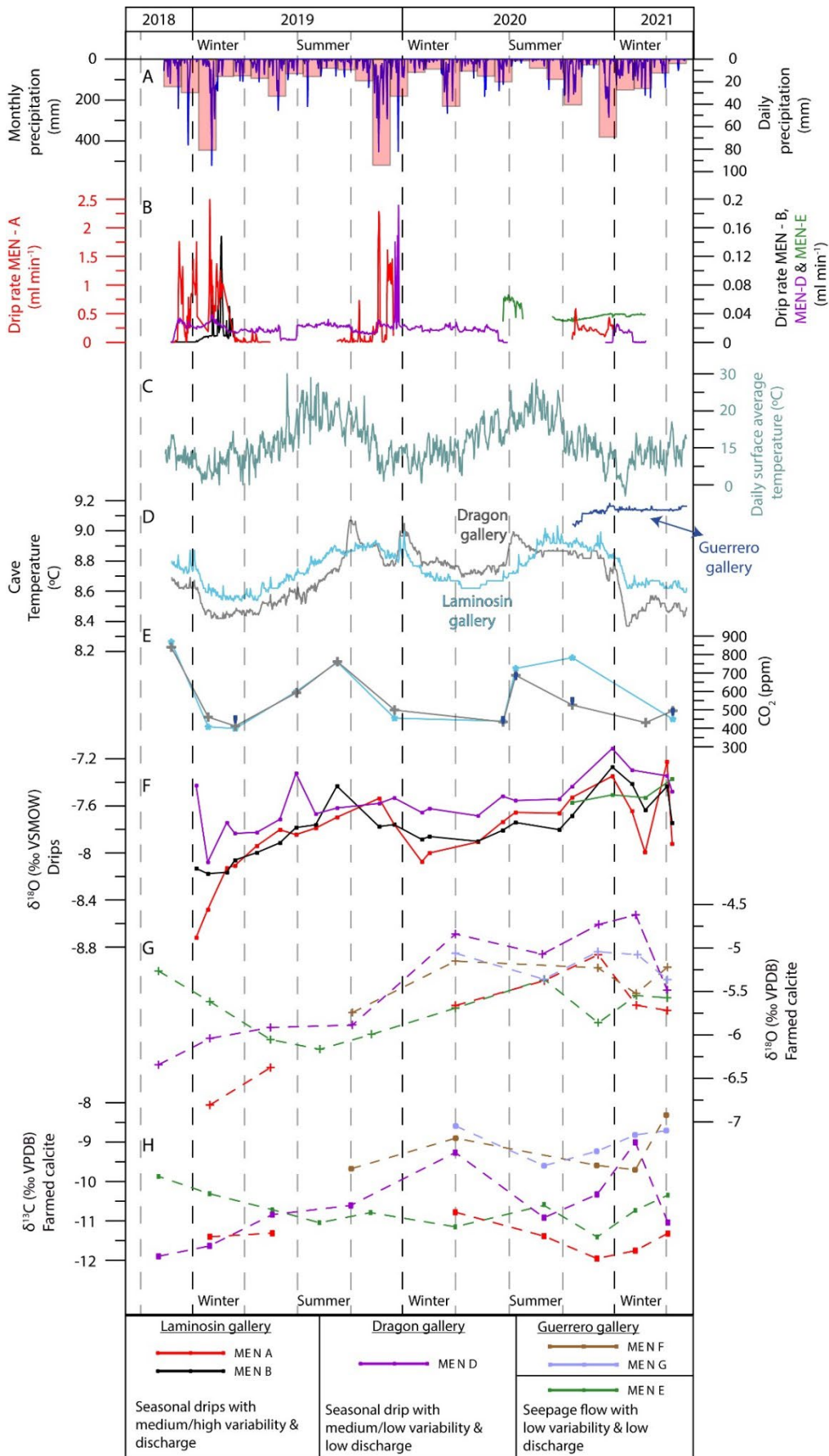
Carbonate precipitated on glass slides all year round, and the $\delta^{18}O_p$ and $\delta^{13}C_p$ values range from -6.8‰ to -4.6‰ and from -12.0‰ to -8.3‰, respectively (five different sampling points, Fig. 5.2G and H). Except for drips MEN-E, MEN-F, and MEN-G, farmed calcite results show a tendency towards less negative values (statistically significant for $\delta^{18}O_p$) during the second half of 2020 and the first part of 2021 (mean $\delta^{18}O_p$ -5.3‰) compared to the period 2018-2020 (mean $\delta^{18}O_p$ -6.3‰; Fig. 5.2G). Comparing $\delta^{18}O_d$ with $\delta^{18}O_p$ of each drip site shows that calcite precipitated close to isotopic equilibrium. Thus, the amount of rainfall is likely influencing $\delta^{18}O_p$ on an interannual scale, but the seasonal impact is less pronounced. This seems to be true for $\delta^{13}C_p$ as well, although the MEN-D drip site shows seasonal variability in the 2020-2021 time interval, where the highest $\delta^{13}C_p$ values coincide with low pCO_2, thus suggesting enhanced degassing and possible prior calcite precipitation (PCP). An interesting feature is that $\delta^{13}C_p$ shows less negative values for the seepage drip and nearby drips of the same cave gallery (MEN-F and MEN-G) in comparison to faster drips (Fig. 5.2H).

V.4.2   Petrography, chronology and stable isotopes of the Mendukilo stalagmites

Stalagmites MEN-2 (31.0 cm), MEN-4 (25.6 cm), and MEN-5 (61.0 cm) consist of coarsely crystalline calcite and are macroscopically homogeneous without any signal of recrystallization. They are made of columnar fabric, lack growth hiati, and do not exhibit macroscopically visible laminae (Fig. 5.3A). Stalagmite MEN-3 (28.0 cm) is an exception, showing a more porous, columnar microcrystalline fabric passing into a dendritic type at the base (the first 4.0 cm) as well as close to the top (between 18.5 and 28.0 cm from the base - Fig. 5.3A). According to Frisia (2015), this transition suggests a change from a relatively slow and constant discharge to more variable drip rates.

U-Th dating revealed that these four stalagmites grew continuously over different intervals of the Holocene and Younger Dryas (YD). Taken together, they continuously cover the entire Holocene and the YD (i.e., since 12.8 kyr BP) with a good overlap (Fig. 5.3): MEN-2 grew between 12.8 and 6.3 kyr BP, MEN-3 between 6.0 and 0 kyr BP, MEN-4 covers the last 3.0 kyr, and MEN-5 spans the last 8.8 kyr (Table 5.1). The dating of the base and top parts of stalagmite MEN-3 was challenging given the change in petrography (see above; Table 5.1). Measured U concentrations in Mendukilo stalagmites range between 73 and 350 ppb, and the measured $^{230}Th/^{232}Th$ activity ratio varies between 20 and 9500 (Table 5.1).
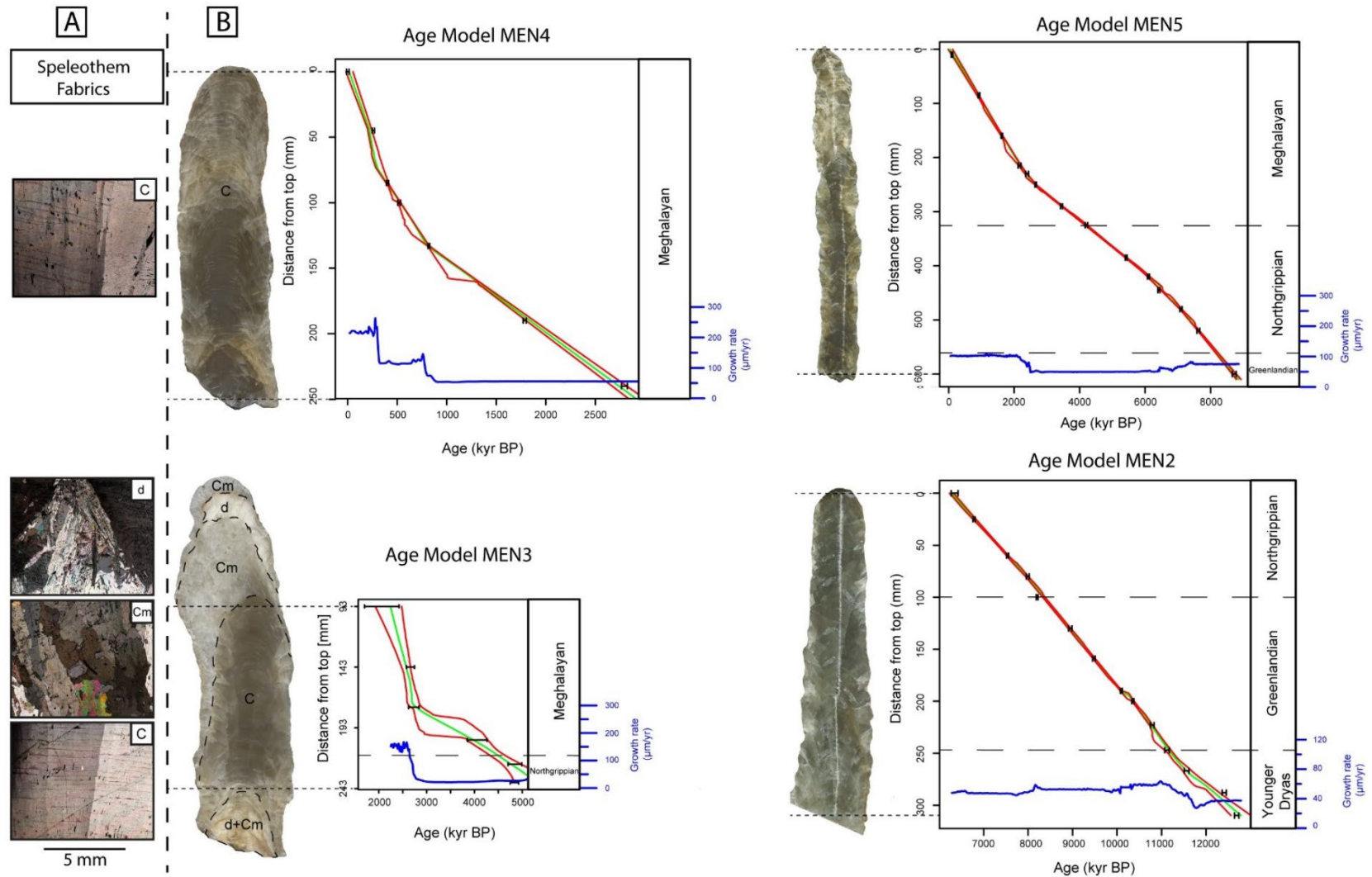
Fig 5.3. *A) Thin sections showing the main fabrics of stalagmites MEN-4 (columnar fabric [C]) and MEN-3 (transition between columnar, columnar microcrystalline [Cm], and dendritic [d] fabrics). B) Dating results (black dots with error bars) and age models of the four stalagmites (green line) with their corresponding error limits (red lines) obtained using StalAge. Changes in growth rate (blue line) are also indicated.*

100

Sample	Depth (mm)	^{238}U (ppb)	^{232}Th (ppt)	$^{230}Th/^{232}Th$ (atomic x10^{-6})	$\delta^{234}U$* (measured)	$^{230}Th/^{238}U$ (activity)	$\delta^{234}U_{initial}$** (corrected)	^{230}Th age*** (yr BP)
MEN5-600	10	137.3 ±0.2	49 ±1	115 ±16	545.5 ±1.9	0.0025 ±0.0003	546 ±2	101 ±24
MEN5-525	85	128.4 ±0.2	65 ±2	460 ±17	551.2 ±1.7	0.0142 ±0.0004	553 ±2	925 ±29
MEN5-450	160	134.6 ±0.2	61 ±1	868 ±23	526.0 ±1.8	0.0237 ±0.0003	528 ±2	1627 ±24
MEN5-395	215	108.9 ±0.2	70 ±2	810 ±24	546.9 ±1.7	0.0316 ±0.0006	550 ±2	2165 ±42
MEN5-380	230	99.9 ±0.3	185 ±4	314 ±8	555.0 ±4.1	0.0353 ±0.0005	559 ±4	2395 ±45
MEN5-360	250	124.9 ±0.1	91 ±2	876 ±20	555.9 ±1.8	0.0387 ±0.0003	560 ±2	2658 ±24
MEN5-320	290	124.5 ±0.1	114 ±2	912 ±20	583.1 ±1.5	0.0505 ±0.0003	589 ±1	3447 ±27
MEN5-285	325	136.5 ±0.2	283 ±6	489 ±10	584.5 ±1.8	0.0616 ±0.0004	592 ±2	4208 ±39
MEN5-225	385	172.4 ±0.2	222 ±4	1005 ±21	584.5 ±1.7	0.0783 ±0.0003	594 ±2	5419 ±26
MEN5-190	420	156.1 ±0.2	160 ±3	1435 ±30	611.4 ±1.7	0.0892 ±0.0004	622 ±2	6102 ±31
MEN5-165	445	154.3 ±0.3	147 ±3	1604 ±34	591.7 ±2.4	0.0925 ±0.0004	603 ±2	6419 ±33
MEN5-130	480	128.0 ±0.1	185 ±4	1157 ±24	588.5 ±1.8	0.1017 ±0.0004	600 ±2	7093 ±34
MEN5-90	520	142.6 ±0.2	142 ±3	1794 ±39	580.1 ±2.0	0.1083 ±0.0005	593 ±2	7624 ±43
MEN5-10	600	163.4 ±0.2	143 ±3	2336 ±58	591.1 ±1.7	0.1240 ±0.0008	606 ±2	8723 ±61

Table 5.1. **(Continue on the following pages).** ^{230}Th dating results (2σ error) of the Mendukilo stalagmites. U decay constants: λ_{238} = 1.55125x10^{-10} (Jaffey et al., 1971) and λ_{234} = 2.82206x10^{-6} (Cheng et al., 2013). Th decay constant: λ_{230} = 9.1705x10^{-6} (Cheng et al., 2013). *$\delta^{234}U$ = ([$^{234}U/^{238}U$]$_{activity}$ − 1) x 1000. **$\delta^{234}U$ initial was calculated based on ^{230}Th age (T), i.e., $\delta^{234}U$ initial = $\delta^{234}U_{measured}$ x $e^{\lambda_{234}xT}$. Corrected ^{230}Th ages assume the initial $^{230}Th/^{232}Th$ atomic ratio of 4.4 ± 2.2 x10^{-6}. Those are the values for a material at secular equilibrium, with the bulk earth $^{232}Th/^{238}U$ value of 3.8. The errors are arbitrarily assumed to be 50%. ***BP stands for "Before Present" where the "Present" is defined as the year 1950 A.D.

Sample	Depth (mm)	^{238}U (ppb)	^{232}Th (ppt)	$^{230}Th/^{232}Th$ (atomicx10^{-6})	$\delta^{234}U^*$ (measured)	$^{230}Th/^{238}U$ (activity)	$\delta^{234}U_{initial}^{**}$ (corrected)	^{230}Th age*** (yr BP)
MEN4-245	0	199.8 ±0.2	108 ±2	39 ±6	711.7 ±2.0	0.0013 ±0.0002	712 ±2	3 ±13
MEN4-200	45	237.6 ±0.3	90 ±2	224 ±8	674.6 ±1.7	0.0052 ±0.0002	675 ±2	260 ±11
MEN4-160	85	283.1 ±0.4	150 ±3	235 ±6	714.5 ±2.0	0.0076 ±0.0001	715 ±2	403 ±11
MEN4-145	100	257.0 ±0.9	177 ±4	227 ±6	713.9 ±3.6	0.0095 ±0.0002	715 ±4	521 ±14
MEN4-112	133	286.6 ±0.2	126 ±3	525 ±12	713.8 ±1.9	0.0140 ±0.0001	716 ±2	820 ±10
MEN4-55	190	209.0 ±0.2	143 ±3	691 ±15	687.2 ±1.8	0.0287 ±0.0002	691 ±2	1787 ±16
MEN4-5	240	142.7 ±0.2	281 ±6	372 ±8	692.0 ±2.3	0.0444 ±0.0003	698 ±2	2793 ±30
MEN3-185	96	73.3 ±0.1	1357 ±27	23 ±1	79.4 ±1.7	0.1340 ±0.0003	80 ±2	2062 ±363
MEN3-140	141	75.5 ±0.1	193 ±4	176 ±6	77.6 ±1.5	0.0273 ±0.0007	78 ±2	2661 ±85
MEN3-102	179	97.7 ±0.2	496 ±10	93 ±2	75.3 ±2.4	0.0286 ±0.0005	76 ±2	2732 ±110
MEN3-75	206	77.8 ±0.3	792 ±16	69 ±2	77.3 ±3.8	0.0427 ±0.0006	78 ±4	4059 ±205
MEN3-55	226	76.9 ±0.1	484 ±10	128 ±3	74.2 ±1.8	0.0490 ±0.0007	75 ±2	4848 ±143
MEN3-43	238	102.2 ±0.2	373 ±8	218 ±5	73.8 ±1.9	0.0482 ±0.0005	75 ±2	4839 ±88

Sample	Depth (mm)	^{238}U (ppb)	^{232}Th (ppt)	$^{230}Th/^{232}Th$ (atomicx10^{-6})	$\delta^{234}U^*$ (measured)	$^{230}Th/^{238}U$ (activity)	$\delta^{234}U_{initial}^{**}$ (corrected)	^{230}Th age*** (yr BP)
MEN2-310	0	201.6 ±0.3	1349 ±27	262 ±5	826.4 ±1.9	0.1064 ±0.0003	841 ±2	6346 ±78
MEN2-285	25	229.4 ±0.2	111 ±2	3797 ±80	826.3 ±1.7	0.1118 ±0.0004	842 ±2	6782 ±24
MEN2-250	60	209.3 ±0.2	169 ±3	2546 ±52	840.4 ±1.7	0.1248 ±0.0003	859 ±2	7538 ±22
MEN2-230	80	242.4 ±0.6	76 ±2	6853 ±149	830.0 ±2.7	0.1312 ±0.0005	849 ±3	7991 ±34
MEN2-210	100	290.9 ±0.3	82 ±2	7867 ±168	825.0 ±1.7	0.1340 ±0.0003	844 ±2	8201 ±21
MEN2-180	130	237.4 ±0.5	446 ±9	1297 ±26	847.5 ±2.3	0.1479 ±0.0005	869 ±2	8947 ±38
MEN2-151	159	297.6 ±0.6	93 ±2	8221 ±174	846.2 ±2.2	0.1558 ±0.0004	869 ±2	9479 ±29
MEN2-120	190	318.8 ±0.3	312 ±6	2814 ±57	862.1 ±1.5	0.1671 ±0.0003	887 ±2	10097 ±22
MEN2-110	200	252.8 ±0.2	139 ±3	5174 ±106	873.0 ±1.7	0.1720 ±0.0003	899 ±2	10355 ±22
MEN2-87	223	288.0 ±0.5	130 ±3	6614 ±138	902.0 ±2.3	0.1817 ±0.0006	930 ±2	10791 ±42
MEN2-63	247	292.3 ±0.6	98 ±2	9418 ±201	951.8 ±2.6	0.1919 ±0.0008	982 ±3	11122 ±53
MEN2-43	267	322.6 ±0.8	174 ±4	6129 ±127	964.1 ±3.1	0.2005 ±0.0008	996 ±3	11563 ±53
MEN2-22	288	349.6 ±0.5	261 ±5	4735 ±97	965.5 ±2.1	0.2145 ±0.0007	1000 ±2	12408 ±47
MEN2-0	310	277.7 ±0.4	1094 ±22	912 ±18	950.2 ±1.8	0.2181 ±0.0005	985 ±2	12688 ±52

Each of the MEN stalagmite age models have fairly low uncertainty of the corrected ages ranging between 0.005 and 0.250 kyr BP (the average error of the MEN-2, MEN-4, and MEN-5 age models are 0.055, 0.041, and 0.040 kyr BP, respectively). In the case of MEN-3 the errors are larger fluctuating between 0.060 and 0.800 kyr BP (average error of 0.212 kyr BP). Average growth rates of MEN-3 (145 mm/yr) and MEN-4 (224 mm/yr) are higher than for MEN-2 (68 mm/yr) and MEN-5 (77 mm/yr), indicating higher speleothem growth rates during the late Holocene in this cave compared to the YD and early Holocene (Fig. 5.3).

The $\delta^{18}O_c$ and $\delta^{13}C_c$ values of the four stalagmites range from -6.3 to -4.3‰ and from -10.4 to -4.4‰, respectively, with similar amplitudes in the overlapping intervals (Supp. Material Fig. 8.3 and Fig. 8.4). This replication supports the use of these isotopic profiles as reliable proxy records. The only exception is the upper part of stalagmite MEN-3, which differs markedly from MEN-4 and MEN-5 in its stable isotope values (Supp. Material Fig. 8.3 and Fig. 8.4). Given the fact that this part of MEN-3 also shows a different type of calcite fabric, we excluded this part.

V.4.3   Composite record from Mendukilo cave

The MEN composite generated with Iscam for both $\delta^{13}C_c$ and $\delta^{18}O_c$ isotopic records covers the last 12.7 kyr BP with an average growth rate of 130 mm/yr. The $\delta^{13}C_c$ composite record shows values between -9.5 and -4.5‰ (MEN$_{\delta13C\ mean}$ = -6.6‰; MEN$_{\delta13C\ STD}$ = 0.8‰; Fig. 5.4). In the case of $\delta^{18}O_c$, the values are characterized by a lower amplitude and variability, ranging from -6.3 to -4.3‰ (MEN$_{\delta18O\ mean}$ = -5.4‰; MEN$_{\delta18O\ STD}$ = 0.3‰; Fig. 5.4). For the composite, we included the stalagmites from the youngest to the oldest one to maximize the correlation coefficient. The $\delta^{13}C_c$ correlation between MEN-3 and MEN-4 is high (r = 0.97), but they only intersect at a gap of about 0.5 kyr; when adding MEN-5, the correlation decreases (r = 0.37), reflecting poor interrelation in the overlapping intervals of stalagmites MEN-5, MEN-4, and MEN-3 during the last 3 kyr (Supp. Material Fig. 8.3 and Fig. 8.4). Thus, paleoclimatic interpretations for the last 3 kyr should be viewed with caution. Finally, when combining this composite with the MEN-2 record, the final correlation is very high (r = 0.91). The MEN composite data contains results from mathematical interpolation; therefore, abrupt variations in the MEN composite should be treated and interpreted with caution and always considering the isotopic (Supp. Material Fig. 8.3 and Fig. 8.4) and trace element (Supp. Material Fig. 8.5 and Fig. 8.6) records of each stalagmite separately.

The composite record produced by Iscam shows that the YD starts with opposite trends when comparing both isotopic records (Fig. 5.4). The $\delta^{13}C_c$ values increase (from -6.7 to -5.6‰) and those of $\delta^{18}O_c$ decrease (from -4.6 to -5.2‰) at the onset of the YD. The values remain stable during the YD, and at its end, the $\delta^{13}C_c$ values gradually decrease (from -5.6 to -7.8‰) while the $\delta^{18}O_c$ values increase abruptly (from -5.2‰ in the YD to -4.3‰ at 11.6 kyr BP), reaching the highest values of the entire record at the YD-Holocene transition (Fig. 5.4).
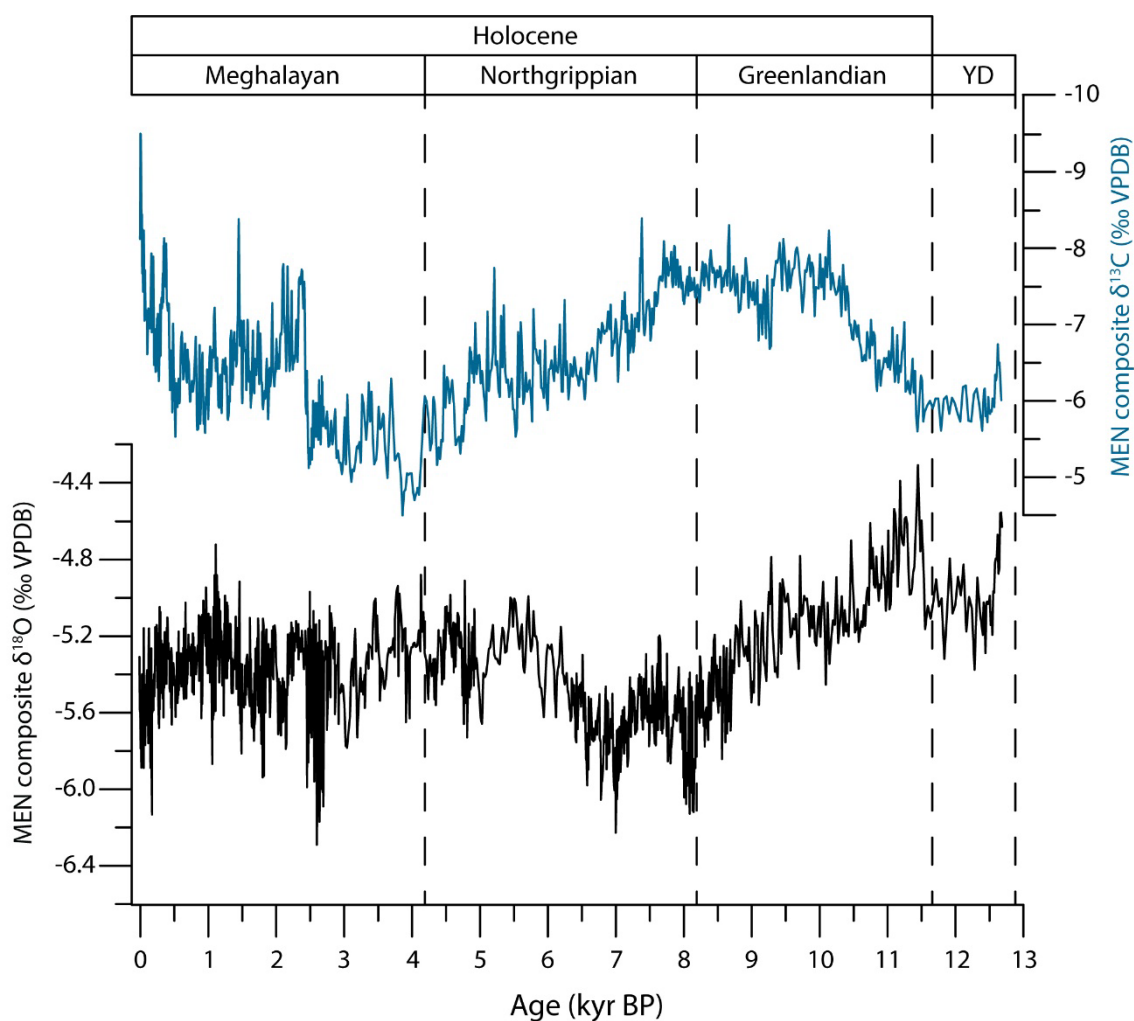
Fig 5.4. *Mendukilo isotope composites for δ¹³Cᶜ (upper panel; note inverted y-axis) and δ¹⁸Oᶜ (lower panel) for the last 13 kyr obtained using Iscam combining four stalagmites. The Holocene division follows Walker et al. (2019).*

The MEN composite $\delta^{13}C_c$ data show a significant trend towards more negative values during the first part of the Greenlandian, from -6.0‰ at 11.7 kyr BP to -8.1‰ at 10 kyr BP (Fig. 5.4). Afterwards, the values remain stable, only interrupted by a short interval of higher values between 9.3 and 9.1 kyr BP. The highest $\delta^{18}O_c$ values of the composite are present in the early Greenlandian and show a trend towards lower values (as the $\delta^{13}C_c$ record) but lasting until the end of the Greenlandian (from -5.0‰ at 11.68 kyr BP to -5.7‰ at 8.23 kyr BP). During the Northgrippian (8.2-4.2 kyr BP) the $\delta^{13}C_c$ record shows a progressive trend towards higher values: from -8.0‰ at 7.9 kyr BP to -4.8‰ at 4.1 kyr BP (Fig. 5.4). During the first part of the Northgrippian (8.2-6.5 kyr BP) the $\delta^{18}O_c$ values are very negative and increase in the second part (mean 5.2‰ between 6.5 and 4.2 kyr BP). The lowest $\delta^{18}O_c$ values of the MEN composite record are present by extreme values of -6.3‰ at 7.0 and 8.1 kyr BP. The $\delta^{18}O_c$ variability during the

Meghalayan (4.2 kyr BP to present) is small and lacks a trend. $\delta^{13}C_c$ profile shows the highest values from 4.2 to 2.5 kyr BP, but by comparing the $\delta^{13}C_c$ values of the composite with those of stalagmites MEN-3 and MEN-5 it is possible to detect that there is a distortion in the former during the time interval of 4.2 and 3.5 kyr BP. This over-exaggeration of the $\delta^{13}C_c$ data in the composite is clearly an artifact of the mathematical algorithm, so that interpretations at millennial and centennial scales during that time interval must take into consideration the $\delta^{13}C_c$ values shown by stalagmites MEN-3 and MEN-5 separately from the composite. The MEN $\delta^{13}C_c$ composite shows a rapid shift towards lower isotope values at 2.5 kyr BP (Fig. 5.4).

Mg/Ca ranges between 0.40 and 1.60 mmol/mol (Supp. Material Fig. 8.5) and shows greater variations in trends among the four stalagmites. Sr/Ca measured in the four stalagmites show similar temporal patterns and are spanning the same range of values (0.12-0.06 mmol/mol) (Supp. Material Fig. 8.6). Sr/Ca values are low during the YD and increase during the Greenlandian, reaching high values around 10 kyr BP. This is followed by a decreasing trend until 3.5 kyr BP and an increasing trend until modern conditions. Sr/Ca is anticorrelated with $\delta^{13}C_c$ at the millennial time scale (correlation coefficient -0.37, n = 1288, p ≪ 0.01) (Supp. Material Fig. 8.7). The Ba/Ca ratio of the MEN composite shows strong similarities with Sr/Ca, but correlation among the four stalagmites is less good, so we only use Sr/Ca to compare with other proxies. In particular, the trends during the last 3000 years are not well replicated among the four speleothems and thus not considered for discerning the climate signal. We also assess the potential effect of in-cave processes, such as PCP, on the $\delta^{13}C_c$ record, looking for the most robust proxy trends associated to more constant Mg/Ca ratios of the MEN-5 stalagmite (Supp. Material Fig. 8.8).

V.5 Discussion

V.5.1 Controls on MEN geochemical proxy data

Trace elements in speleothems are useful paleoclimate indicators in caves where seasonal and long-term changes in water balance result in large and systematic change in Mg/Ca, Sr/Ca, and Ba/Ca in dripwater associated with PCP during the dry season (Fairchild & Treble, 2009). In Mendukilo stalagmites, Mg/Ca and Sr/Ca show a contrasting pattern (Supp. Material Fig. 8.5 and Fig. 8.6), indicating that PCP cannot be the dominant control on both ratios. One explanation could be a significant non-bedrock source of Mg or Sr which varied temporally. In caves very close to the coast, such as Pindal Cave with galleries 200 m from the sea cliff, marine aerosols can be a significant source of Mg in the Holocene (Moreno et al., 2010). However, in the cave of Mendukilo, 50 km from the Atlantic coast and at 750 m elevation, surrounded by mountain ranges of higher altitude, a dominant marine aerosol contribution of Mg is not expected, and temporal changes in Mg/Ca are unlikely to reflect changes in marine aerosol Mg delivery. An alternative

explanation for the differences in Mg and Sr could be decoupled temporal changes in the partitioning coefficient of either Sr or Mg. Many studies have documented variations in the Sr partitioning coefficient driven by calcite growth rate (Lorens, 1981; Nielsen et al., 2013; Tan et al., 2014; Tang et al., 2008; Tesoriero & Pankow, 1996), and this is a common explanation for the decoupling of Mg/Ca and Sr/Ca in stalagmites (Stoll et al., 2012; Warken et al., 2018). We observe that Sr/Ca in Mendukilo stalagmites positively correlates with growth rate (correlation coefficient = 0.55, n = 1288, p ≪ 0.01) deduced from the U-Th age models (Supp. Material Fig. 8.7), suggesting that growth rate contributed to the Sr/Ca variations. Consequently, we infer that Sr/Ca may be driven by the growth rate effect superimposed on PCP, whereas Mg/Ca may reflect temporal variations in PCP. In fact, Sr/Mg of stalagmites allows isolating the correlation between Sr/Ca and growth rate (Supp. Material Fig. 8.9). Since stalagmites fed by different drip routes may have different sensitivities to PCP, Mg/Ca of coeval stalagmites may not covary, as is the case in this study. In contrast, the existence of common drivers of dripwater saturation by soil pCO_2 may lead to more reproducible variations in growth rate and Sr/Ca.

$\delta^{13}C_c$ is regulated by both soil/vegetation processes as well as in-cave processes. The $\delta^{13}C_d$ of DIC in dripwater is initially set by the $\delta^{13}C$ of soil CO_2, which is more negative when the soil pCO_2 is high under warm and moist conditions which favor high heterotrophic and autotrophic respiration. The $\delta^{13}C_d$ of DIC in dripwater may be modified slightly during carbonate dissolution, but the low dead carbon percentage in most recent stalagmites, including those from Northern Iberia, suggests that dissolution commonly occurs in open systems and the impact on the $\delta^{13}C$ of DIC is limited (Lechleitner et al., 2021). In the cave or karst cavities, the coupled processes of degassing and PCP can generate a significant positive shift in $\delta^{13}C$ of DIC before the water reaches the stalagmite. The modern $\delta^{13}C_p$ for the high drip location (-11 to -12‰) is in the range of $\delta^{13}C$ expected for CO_2 in soils with a dominant C3 vegetation in a warm and humid climate (Lechleitner et al., 2021), potentially affected by only limited PCP. The modern $\delta^{13}C_p$ for the seepage location (MEN-E) and other nearby drips of the same gallery (MEN-F and G) are less negative (-9 to -10‰) and these drips may have experienced some degassing and PCP and/or a greater extent of precipitation from the arriving drip (in situ PCP), and/or a more closed dissolution regime. Seasonal changes in $\delta^{13}C_p$ at higher and intermediate drip rate sites may reflect seasonal variations in soil pCO_2 or in the significance of PCP. Drip rate monitoring and farmed calcite data suggest that the MEN composite record is not seasonally biased but rather reflects continuous year-round deposition. Continuous calcite deposition is also supported by the columnar fabric and the absence of visible laminae as well as the lack of dissolution features (i.e., the dripwater was always supersaturated with respect to calcite).

Long-term changes in $\delta^{13}C_c$ values are rather unrelated to the Mg/Ca pattern in the MEN stalagmites. For example, in the $\delta^{13}C_c$ MEN5 record, the main long-term trends exhibit similar Mg/Ca ratios (low Mg/Ca variability between the different $\delta^{13}C_c$ larger anomalies; Supp. Material

Fig. 8.8). Therefore, the temporal trends in $\delta^{13}C_c$ are most likely driven unaffected by PCP, although the seepage drips may be characterized by some PCP. We suggest that the long-term trends in $\delta^{13}C_c$ are driven by climatic processes controlling soil pCO_2, i.e., soil temperature and soil moisture. Some studies suggest that the temperature component dominates over soil pCO_2, such during MIS 3 and 4 in Villars cave in SW France (Genty et al., 2006) and during the last deglaciation in El Pindal cave in NW Spain (Moreno et al., 2010). Comparison of the Mendukilo composite $\delta^{13}C_c$ record with paleotemperature reconstructions from Pyrenean lakes (e.g., Tarrats et al., 2018) and SST records (Català et al., 2019; Martrat et al., 2014) supports a temperature influence at millennial scale (Fig. 5.5). Therefore, higher (lower) $\delta^{13}C_c$ values are arguably linked to colder (warmer) and/or dryer (wetter) intervals with reduced (enhanced) soil respiration and vegetation productivity. We note that the inverse correlation between $\delta^{13}C_c$ and Sr/Ca in the MEN stalagmites (Supp. Material Fig. 8.7), while opposite to the trend expected from PCP control, is consistent with the expected relationship of low $\delta^{13}C_c$ in warm and humid periods of high soil CO_2, which also lead to higher dripwater oversaturation and higher growth rates, promoting higher Sr/Ca.

Variation in the dripwater and $\delta^{18}O_c$ record may reflect changes in $\delta^{18}O_{sw}$ of the surface ocean in the moisture source area, as well as changes in the atmospheric processes which together affect the fractionation of $\delta^{18}O$ in the hydrological cycle between the ocean and rainfall over the cave. Over the time period covered by the MEN record, marine records confirm a significant change of $\delta^{18}O_{sw}$ between 13 and 8 kyr (Català et al., 2019; Peck et al., 2006; Skinner & Shackleton, 2006), but smaller variations since 8 kyr (Supp. Material Fig. 8.10). This change in seawater composition is likely a significant component of the long-term trend in MEN $\delta^{18}O_c$ between 11.5 and 8.5 kyr. Short-term changes in seawater composition, not captured by the low-resolution $\delta^{18}O_{sw}$ may also contribute to variation in MEN $\delta^{18}O_c$, and in the subsequent section we discuss how these may be distinguished from changes due changing isotope fractionation in the hydrological cycle.

For a constant sea-surface composition, event-scale monitoring of the isotopic composition of $\delta^{18}O_r$ in different areas of the Iberian Peninsula constrains some of the drivers of hydrological fractionation (Giménez et al., 2021; Moreno et al., 2014b, 2021). Air temperature, together with the amount of precipitation, accounts for less than 40% of the variability of $\delta^{18}O_r$ in the transect across the northern Iberian Peninsula all the way to the Balearic Islands. Rather, the synoptic-scale atmospheric circulation plays the dominant role in determining the ranges, values and seasonal distribution of $\delta^{18}O_r$ (Moreno et al., 2021). In fact, the record of $\delta^{18}O_r$ in the northern coastal area of Iberia (Bilbao) during the last four years (Supp. Material Fig. 8.1) indicates a minor dependence on temperature (r = 0.20) and precipitation (r = 0.22; during days with >3 mm of rainfall). This contrasts with the significant correlation between $\delta^{18}O_r$ and air temperature in more inland and high-elevation settings of the Pyrenees (Giménez et al., 2021), where temperature

could be interpreted as dominating $\delta^{18}O_c$ records (Bartolomé et al., 2015b; Bernal-Wormull et al., 2021). In the northern coastal region, the seasonality of rainfall has been discussed as a potential driver of $\delta^{18}O_c$ (Baldini et al., 2019).

At the Mendukilo cave location, dripwater and farmed calcite provide a limited perspective and suggest that both $\delta^{18}O_d$ and $\delta^{18}O_p$ are lower during the rainy period of 2018-2019 than during the drier year of 2020-2021 (Fig. 5.2). This suggests that synoptic processes during a wet year may lead to lower $\delta^{18}O_c$. Monitoring and petrographic data thus suggest that the MEN $\delta^{18}O_c$ record captured an annual signal, which is primarily influenced by rainfall amount as well as by changes in the isotopic composition of the ocean during the first part of the record (13-8 kyr). A prominent feature of the MEN $\delta^{18}O_c$ composite record is a -0.71‰ anomaly (relative to the Holocene mean of -5.4‰) that repeats at 8.11 kyr BP and at 7.00 kyr BP (Fig. 5.4). During these time periods, neither $\delta^{13}C_c$ nor Mg/Ca show a negative shift as might be expected for increased rainfall, nor is did the growth rate increase. Thus, we propose that these two events of anomalously low $\delta^{18}O_c$ values are likely caused not by increased rainfall amount but rather record rapid and short-lived decreases in $\delta^{18}O_{sw}$ (e.g., Domínguez-Villar et al., 2009; García-Escárzaga et al., 2022; LeGrande & Schmidt, 2008; Matero et al., 2017).

Fig 5.5. *(Next page) Paleoenvironmental records from the Iberian Peninsula and Morocco covering the YD and the Holocene. A) Stacked record of normalized $\delta^{13}C_c$ stalagmite data from Kaite cave; Cueva del Cobre; Cueva Mayor from northern Iberia (Martín-Chivelet et al., 2011). B) $\delta^{13}C_c$ record of the SIR-1 speleothem from El Soplao cave in northern Iberia (Rossi et al., 2018). C) Summer insolation at 42°. D) $\delta^{13}C_c$ record of the BG speleothem from westernmost Iberia (Buraca Gloriosa Cave, Portugal) (Thatcher et al., 2020). Note that the amplitude of $\delta^{13}C_c$ axis in this record (high variability) is not the same compared to the rest of the Iberian stalagmite records. E) MEN $\delta^{13}C_c$ composite record (this work). F) Globigerina bulloides Mg/Ca SST (ALB-2;Català et al., 2019) compared with the alkenone SST (Martrat et al., 2014) from Western Mediterranean. G) Temperature record of the Basa de la Mora Lake in the Central Pyrenees based on chironomid data (Tarrats et al., 2018) H) $\delta^{18}O$ values of ostracod shells from Lake Sidi Ali (Morocco; Zielhofer et al., 2019). I) Dryas octopetala macrofossil abundance (Leunda et al., 2019) and J) phases of ice accumulation (Sancho et al., 2018) in the Armeña-A294 Ice Cave (Central Pyrenees). The Holocene is divided following Walker et al. (2019). The "4.2 and 9.2 events" are indicated by higher values in the MEN $\delta^{13}C_c$ composite record (this work).*
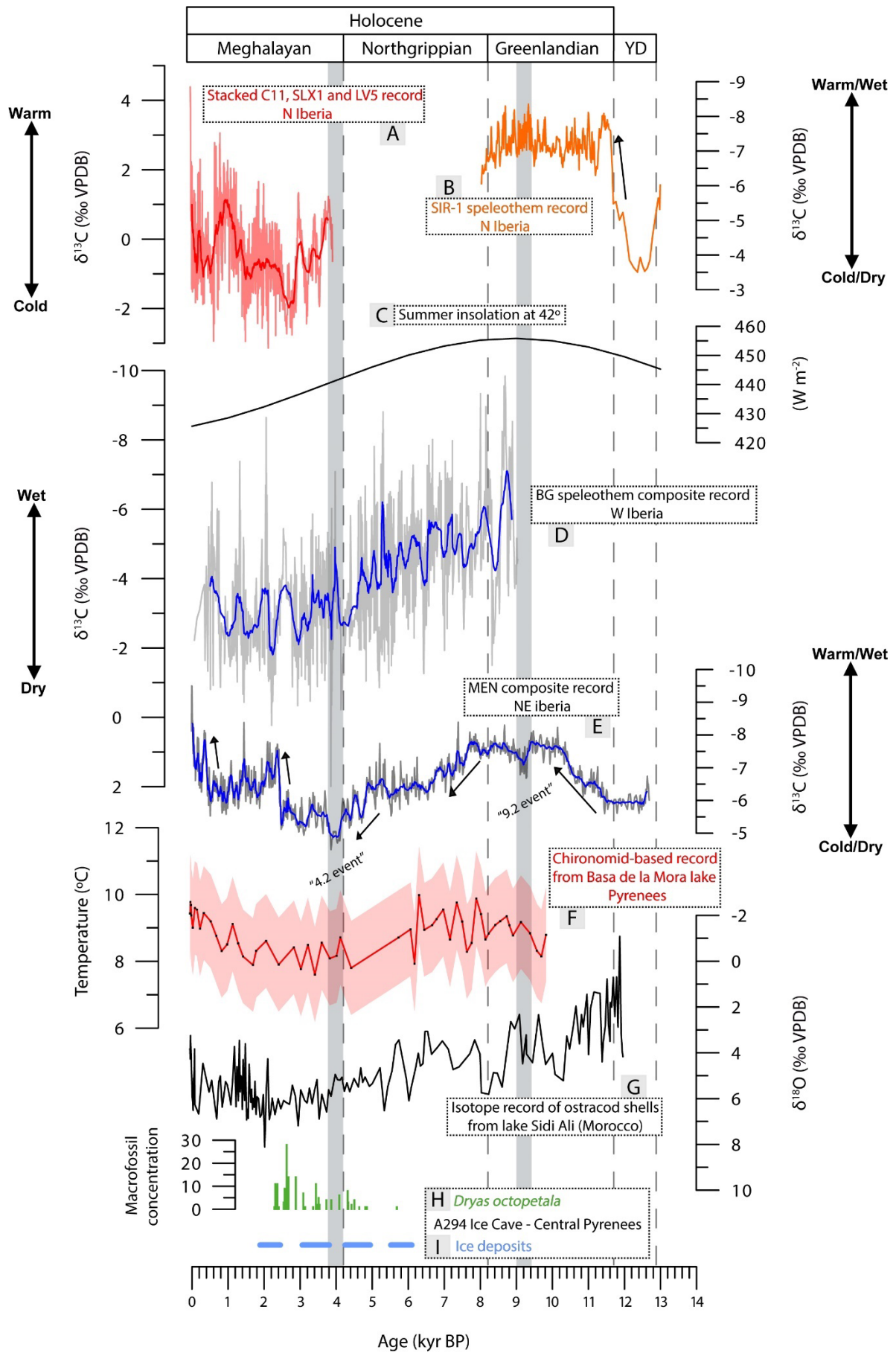
V.5.2 Climate variability reconstructed for northern Iberia during the YD and the Holocene

V.5.2.1 Younger Dryas

The YD was a cool and generally dry episode that likely resulted from a prolonged weakening of the Atlantic Meridional Overturning Circulation (AMOC) (Bakke et al., 2009; McManus et al., 2004). This event is precisely recorded in lake sediments (Gil-Romera et al., 2014; González-Sampériz et al., 2006; Leunda et al., 2017; Morellón et al., 2018) and speleothems (Baldini et al., 2019; Bernal-Wormull et al., 2021; Moreno et al., 2010; Rossi et al., 2018) from northern Iberia, confirming its cool and dry character in southwestern Europe. Moreover, a high-resolution Pyrenean speleothem provided evidence of two hydrological contrasting phases within the YD (Bartolomé et al., 2015b; Cheng et al., 2020) supporting previous observations from pollen in Iberian marine sediments (e.g., Chabaud et al., 2014; Fletcher et al., 2010; Nebout et al., 2009; Rodrigues et al., 2010). In Mendukilo cave, the lowest speleothem growth rates of the entire record were recorded during the YD (29-37 mm/yr), while the composite MEN $\delta^{13}C_c$ record (Fig. 5.4 and 5.5) shows higher values (-6.0‰) in relation to the average $\delta^{13}C_c$ value of the Greenlandian (-7.2‰). These data provide evidence of dry and cold conditions during the YD in this region which would have resulted in slow speleothem growth (low Sr/Ca ratio) and elevated $\delta^{13}C_c$ values. Similarly, mean values of the MEN $\delta^{18}O_c$ (Fig. 5.4) composite record are slightly lower (-5.0‰) than at the beginning of the Holocene (-4.7‰). As also observed by Baldini et al. (2019) in La Garma cave, YD $\delta^{18}O_c$ values in the Mendukilo record are not particularly different from other Holocene intervals where $\delta^{18}O_c$ values are even lower (e.g., $\delta^{18}O_c$ values of -5.8‰ at 7.87 kyr BP, compared to a value of -5.4‰ at 12.29 kyr BP). Baldini et al. (2019), using a Monte Carlo model applied to the GAR-01 $\delta^{18}O_c$ record, report that seasonal rainfall and temperature distribution account for 95% of the $\delta^{18}O_c$ variability and that the YD was characterized by dry and cool winters and wet summers. Thus, the $\delta^{18}O_c$ values recorded in Mendukilo during the YD are actually higher than expected if they were recording cold temperatures given the decrease in winter precipitation. Besides this combination of climate variables, those higher $\delta^{18}O_c$ values may be related to the higher $\delta^{18}O_{sw}$ values that characterize North Atlantic records in the YD (Supp. Material Fig. 8.10), thus enforcing the idea that the MEN record captured important changes in the isotopic composition of the North Atlantic Ocean.

Regarding the intra-YD variability, the MEN $\delta^{13}C_c$ composite suggests a quite stable YD in terms of soil and vegetation activity. On the contrary, the MEN $\delta^{18}O_c$ composite shows three different phases, in good correspondence with a simplified version of the three stages recorded by marine sediments (Naughton et al., 2019): (i) a cool/dry climate at the YD onset, (ii) a slightly

warmer (and wetter) phase at about 12.3 kyr BP, and (iii) a cool and dry (but quite unstable phase) just before the onset of the Holocene. The age model (Fig. 5.3B) precludes establishing the precise timing of these stages. The fact that this intra-YD variability is observed in the $\delta^{18}O_c$ but not in the $\delta^{13}C_c$ data may provide a hint to the season when most of the rain fell. If there was enough rainfall in the warm season (spring-summer, as proposed by Baldini et al. (2019)) to support vegetation growth and soil activity, then the $\delta^{13}C_c$ may have remained stable during the YD while the $\delta^{18}O_c$ values oscillated. Thus, a change in rainfall seasonality during the YD may explain the different patterns of carbon and oxygen isotopes from Mendukilo cave, as previously suggested for La Garma cave (Baldini et al., 2019). Similar ideas about the proxy expression of the YD seasonality may be reflected by SST proxies in Fig. 5.5F. Thus, SST obtained from Mg/Ca (Català et al., 2019) presents a much less pronounced temperature change during the YD than SST obtained from alkenones (Martrat et al., 2004).

V.5.2.2   Onset of the Holocene and the Greenlandian period

The onset of the Holocene has not been well captured by Iberian speleothems as most of them started to grow after 10-9.5 kyrs BP (Railsback et al., 2011; Stoll et al., 2013; Walczak et al., 2015), once optimum climatic conditions in terms of temperature and humidity were attained. Even so, there are few speleothem records in northern Spain that cover the climate transition between the YD and the Holocene (Baldini et al., 2015, 2019; Bernal-Wormull et al., 2021; Moreno et al., 2017; Rossi et al., 2018). In the case of Mendukilo cave, there is only one stalagmite, MEN-2, which started to grow just before the YD and continuously covers the Holocene until 6 kyr BP. Its $\delta^{13}C_c$ and $\delta^{18}O_c$ profiles show a slower transition until optimum conditions are reached (Fig. 5.4, Supp. Material Fig. 8.3, and Fig. 8.4). Thus, the MEN $\delta^{13}C_c$ isotope composite records a different signal at the Holocene onset compared to speleothems from NW Iberia, such as the SIR-1 speleothem from El Soplao cave (Rossi et al., 2018) (Fig.. 5.5B), a record that reflects an (hydro)climate signal as well as the MEN $\delta^{13}C_c$ composite between intervals of cold/dry or warm/wet conditions. In the case of SIR-1, the $\delta^{13}C_c$ values decrease quickly at the end of the YD and remain stable throughout the Greenlandian (Fig. 5.5B). On the other hand, the $\delta^{13}C_c$ profile in Mendukilo shows a gradual positive trend since the end of the YD, lasting until 10 kyr BP, when $\delta^{13}C_c$ values stabilize (Fig. 5.5E). This difference in the $\delta^{13}C_c$ signal of both records may be due the fact multiple studies show that Holocene humidity changes are locally variable and of contrasting sign between NW, eastern and southern Iberia (Morellón et al., 2018), allowing the Mendukilo record to be affected not only by a purely Atlantic signal, but rather a combination of a Mediterranean (where several records in the region show a delay in reaching Holocene optimum conditions) and Atlantic signal. Another possibility is that the hydrological imprint is predominant in the case of MEN stalagmites to the detriment of temperature, as in the case of SIR-1. Coherently, the $\delta^{18}O_c$ MEN record shows the least negative

values of the whole record at the onset of the Holocene, when temperatures were high but water availability was still low and $\delta^{18}O_{sw}$ still shows highly positive values (Supp. Material Fig. 8.10). The $\delta^{18}O_c$ values then gradually decrease until 8 kyr, which coincides not only with the change towards optimal conditions during the beginning of the Holocene, but also with a significant evolution of $\delta^{18}O_{sw}$ in marine records between 11 and 8 kyr BP (Supp. Material Fig. 8.10) as a result of meltwater pulses in the North Atlantic (Peck et al., 2006; Skinner & Shackleton, 2006) (Fig. 5.4). Another point to consider is that the relevant increase in temperature during the early Holocene must necessarily modify the $^{18}O/^{16}O$ fractionation in the cave, which could lead to a progressive but very significant decrease in the $\delta^{18}O_c$. Rainfall monitoring surveys in the Central Pyrenees indicate that $\delta^{18}O_r$ show a dependence of temperature equivalent to a temperature dependence on $\delta^{18}O_r$ of 0.47-0.52‰/°C (Bartolomé et al., 2015b). This dependence is only partially offset by the empirical change of the value of isotope fractionation during calcite precipitation (Tremaine et al., 2011). Therefore, attributing the progressive decline in $\delta^{18}O$ values purely to changes in fractionation does not seem feasible. Therefore, both isotopic records, together with Sr/Ca ratios and growth rates (which increase from 40 to 63 mm/yr; Fig. 5.3 and Supp. Material Fig. 8.7) support the model of a progressive change towards more humid conditions from the onset of the Holocene to 10.5-10.0 kyr BP, coinciding with the start of the Holocene Thermal Maximum at higher latitudes (Marcott et al., 2013). From 10 to 8 kyr BP, optimum conditions in terms of soil activity and vegetation development were attained around Mendukilo cave (Fig. 5.4). Regarding SST, that interval also correspond with the highest temperatures of the Holocene (Fig. 5.5F).

Morellón et al. (2018) compiled lake and speleothem records from Iberia covering the Holocene onset and observed two main patterns of spatial and temporal hydrological variability: i) Atlantic influenced sites located in the Northwest (e.g., Enol or Sanabria lakes, (Jambrina-Enríquez et al., 2014; Moreno et al., 2011) and speleothems from the Cantabrian coast (Stoll et al., 2013) are characterized by a gradual increase in humidity from the end of the YD to the mid Holocene, similarly to most North Atlantic records; and ii) continental and Mediterranean-influenced sites (e.g., Villarquemado or Estanya lake, Aranbarri et al., 2014; Morellón et al., 2009 and El Refugio cave; Walczak et al., 2015) show evidence of prolonged arid conditions of variable duration after the YD, followed by an abrupt increase in moisture at 10-9 kyr BP. Mendukilo cave, showing a gradual increase in moisture availability since the end of the YD, falls into the first category. This delay in reaching optimum temperature and humidity conditions during the Holocene agrees with the insolation change at this latitude, which reaches its maximum approximately at 10 kyr BP (Fig. 5.5C). Optimum humidity conditions in the MEN composite record are maintained between 10 and 7.8 kyr BP, contrary to what is seen in speleothems from the Mediterranean part which suggest an arid climate at that time (Budsky et al., 2019).

V.5.2.3   From the Northgrippian to the end of the Neoglacial cooling

The Northgrippian (8.2-4.2 kyr BP) was characterized by a gradual increase in the MEN $\delta^{13}C_c$, with centennial-scale oscillations, pointing to the end of optimum thermal and humidity conditions in the region (Fig. 5.4 and 5.5). This trend was accompanied by a decrease in growth rate of the MEN stalagmites (Fig. 5.3 and Supp. Material Fig. 8.7 and Fig. 8.9) while speleothem growth in southern Iberia stopped (Walczak et al., 2015). Generally dry conditions across much of Iberia between ca. 8 to 5 kyr BP are suggested by positive $\delta^{13}C_c$ excursions in the northwest Iberian Cova de Arcoia (Railsback et al., 2011), the GAR-01 stalagmite (Baldini et al., 2019), stalagmites from caves in the Iberian range growing during 8.5-4.8 kyr (Moreno et al., 2017) and a sharp decrease of precipitation derived from growth rates of 11 stalagmites on the Cantabrian coast (Stoll et al., 2013). Similarly, the long-term trend in carbon and oxygen isotopic variability of the composite record of six stalagmites from Buraca Gloriosa (BG) in western Portugal (Thatcher et al., 2020) suggests drier conditions from the middle to late Holocene as evidenced by increasing $\delta^{13}C_c$ and $\delta^{18}O_c$ values (Fig. 5.5D). Lake records from Spain (González-Sampériz et al., 2017; Jambrina-Enríquez et al., 2014; Moreno et al., 2011), a pollen-based climate reconstruction from Mauri et al. (2015), as well as a lacustrine $\delta^{18}O$ record from Morocco (Zielhofer et al., 2019, Fig. 5.5H) support increasingly dry conditions in Iberia and North Africa during the Northgrippian. This trend mimics the long-term trend of decreasing values in summer insolation (Fig. 5.5C). However, dry conditions were not reached at the same time at all sites. These proxy records suggest that during the mid-Holocene, aridity prevailed in both southern and north-western Iberia, while moisture availability in the north was likely higher (probably controlled by the winter westerlies) than in southern Iberia, reflected by the continuous growth of northern (Baldini et al., 2019; this work) relative to southern stalagmites between ca. 8 to 5 kyr BP (Walczak et al., 2015).

The Northern Hemisphere experienced widespread cooling starting at about 6.0-5.5 kyr BP, known as the Neoglacial period (Davis et al., 2009; Kumar, 2011). This trend is captured by the MEN $\delta^{13}C_c$ composite record (Fig. 5.5E) with a trend towards less negative values starting about 5.2 kyr BP. This cooling is known throughout Europe (e.g., Ilyashuk et al., 2011; Larocque-Tobler et al., 2010) and, regarding Iberian records, is documented by *Globigerina bulloides* Mg/Ca SST from the Alboran Sea (Català et al., 2019, Fig. 5.5F) and the continental chironomid-based temperature reconstruction from la Basa de la Mora in central Pyrenees (Tarrats et al., 2018, Fig. 5.5G). Glaciers began to expand around 6 kyr BP in both the southern (García-Ruiz et al., 2020) and the northern (Gellatly et al., 1992) part of the Pyrenees, and Arctic-Alpine species such as Dryas octopetala spread (Leunda et al., 2019, Fig. 5.5I) simultaneous with the accumulation of ice in caves at high elevation in the central Pyrenees (Sancho et al., 2018, Fig. 5.5J).

The onset of the Meghalayan at 4.2 kyr BP coincides with higher isotopic values in the MEN composite $\delta^{13}C_c$ record (Fig. 5.5E) in comparison with what was seen during the

Northgrippian period. This trend ends around 2.5 kyr BP, when a gradual amelioration led to the onset of a relatively warmer and/or humid interval, in agreement with the Basa de la Mora lake record (Fig. 5.5G) and the Mg/Ca SST marine records (Fig. 5.5F). Besides, the MEN $\delta^{18}O_c$ composite values stabilized around -5.2‰ 5 kyr BP ago (punctuated by centennial-scale oscillations), likely reflecting the combination of cold and dry conditions. Thus, cold and probably dry conditions prevailed in northern Iberia between the onset of Neoglacial at about 5-6 kyr BP and 2.5 kyr BP.

After 2.5 kyr BP, a gradual amelioration trend led to relatively warmer and/or humid conditions which lasted until ~1700 yr BP, as recorded by the $\delta^{13}C_c$ MEN composite and the increase in growth rate (Fig. 5.5 and Supp. Material Fig. 8.7). The last 2.5-3 kyr, however, are not well-resolved in the MEN record (Supp. Material Fig. 8.3) and climate inferences are less robust than for the earlier part of the record.

V.5.3   Abrupt climate changes during the Holocene

Although the $\delta^{18}O_c$ variability of the MEN record is small throughout the Holocene, as the case of most records in the region (Baldini et al., 2019; Domínguez-Villar et al., 2009; Smith et al., 2016), we identified four events of lower $\delta^{18}O_c$ values (at 8.2, 7.0-6.6, 5.5-4.8, and 2.8 kyr BP) that can be correlated within dating uncertainty with other cave records and compared with some of the Bond events, periods with increase of North Atlantic ice-rafted debris record in marine sediment cores (Bond et al., 2001) (stacked MC52, VM29-191, MC21 and GGC22 marine cores) (Fig. 5.6). These negative excursions along the Holocene MEN $\delta^{18}O_c$ composite curve (representing centennial-scale cold events) can be compared with maxima in the ice-rafted debris record (cold meltwater input at the north Atlantic) despite to different resolutions and probable uncertainties in both age models. Other abrupt hydroclimatic changes during the Holocene that have been identified in Iberian records occurred at 9.2 and 4.2 kyr BP (Baldini et al., 2019; Jiménez-Moreno et al., 2015; Mesa-Fernández et al., 2018; Walczak et al., 2015). These two events are not prominent in the $\delta^{18}O_c$ MEN record, but both are clearly expressed in the $\delta^{13}C_c$ record (Fig. 5.5). Those six Holocene events are discussed separately since their origin and signal is not the same.

V.5.3.1   The 9.2 kyr BP event

Between 8.9 and 9.3 kyr BP the MEN $\delta^{13}C_c$ composite values increase (amplitude of 1‰) coinciding with the '9.2 kyr event' (Fig. 5.5), as documented in many proxy records across the Northern Hemisphere (e.g., Fleitmann et al., 2008; Genty et al., 2006; Masson-Delmotte et al., 2005; Rasmussen et al., 2007). This event may reflect the effects of a meltwater pulse (Fleitmann et al., 2008). Indeed, a major $\delta^{18}O$ peak in the lake sediment record of Sidi Ali, Morocco (Zielhofer

et al., 2019), coincides with maxima in ice-rafted debris in the North Atlantic at 9.3 kyr BP (Bond, 1997). This prominent peak (Fig. 5.5H) corresponds to Bond event 6 (Bond, 1997; Bond et al., 2001). Mesa-Fernández et al. (2018) identified a short and relatively arid in the Laguna Hondera record (southern Iberian Peninsula) between ~ 9.6 and 9.0 kyr BP. As indicated above, this event is not reflected in the MEN composite $\delta^{18}O_c$ signal (not even in the $\delta^{18}O_c$ values of the MEN-2 stalagmite separately; Supp. Material Fig. 8.4) but in its $\delta^{13}C_c$ record. A possible explanation is that the drier conditions, documented for this period for the Iberian Peninsula by terrestrial (Baldini et al., 2019; Carrión, 2002; Iriarte-Chiapusso, 2016; Vegas et al., 2010) and marine records (Nebout et al., 2009), played a role in counteracting this MEN $\delta^{18}O$ composite signal, in a similar way to what we have seen in the $\delta^{18}O$ values of the MEN record during the cold and dry YD (Fig. 5.6A). Baldini et al. (2019) suggested arid summers between 9.3 and 8.9 kyr BP, roughly corresponding to our "9.2 kyr event", based on modelled seasonality data (Fig. 5.6D). This summer aridity suggests that a Mediterranean-type climate may have existed in northern Iberia at this time, which is also consistent with the northward shift of the westerlies (Walczak et al., 2015). This movement results in an increase in moisture observed in Scandinavia (Bakke et al., 2009) and a reduction of moisture in southern France (Genty et al., 2006; Wirth et al., 2013) and northern Iberia (Aranbarri et al., 2014; Railsback et al., 2011).

Fig 5.6. *(Next page) $\delta^{18}O$ records from the Iberian Peninsula showing evidence of abrupt climate change during the Holocene. A) MEN $\delta^{18}O_c$ composite (this work). B) $\delta^{18}O_c$ record of the BG speleothem from westernmost Iberia (Buraca Gloriosa Cave, Portugal) (Thatcher et al., 2020). C) $\delta^{18}O_c$ record of LV5 stalagmite from northern Iberia (Kaite Cave) (Domínguez-Villar et al., 2017). D) GAR-01 $\delta^{18}O_c$ record from northern Iberia (La Garma Cave) (Baldini et al., 2019). The vertical gray bars mark abrupt events within the Holocene. E) Combined and normalized Cueva de Asiul $\delta^{18}O_c$ data from northern Iberia (Smith et al., 2016). F) Ice-rafted debris (IRD) record based on hematite-stained grains of stacked MC52, VM29-191, MC21, and GGC22 cores from the subpolar North Atlantic (Bond et al., 2001). Note that the amplitude of $\delta^{18}O$ axis is not the same for the case of MEN composite record (low variability) in comparison with the rest of the $\delta^{18}O$ records.*
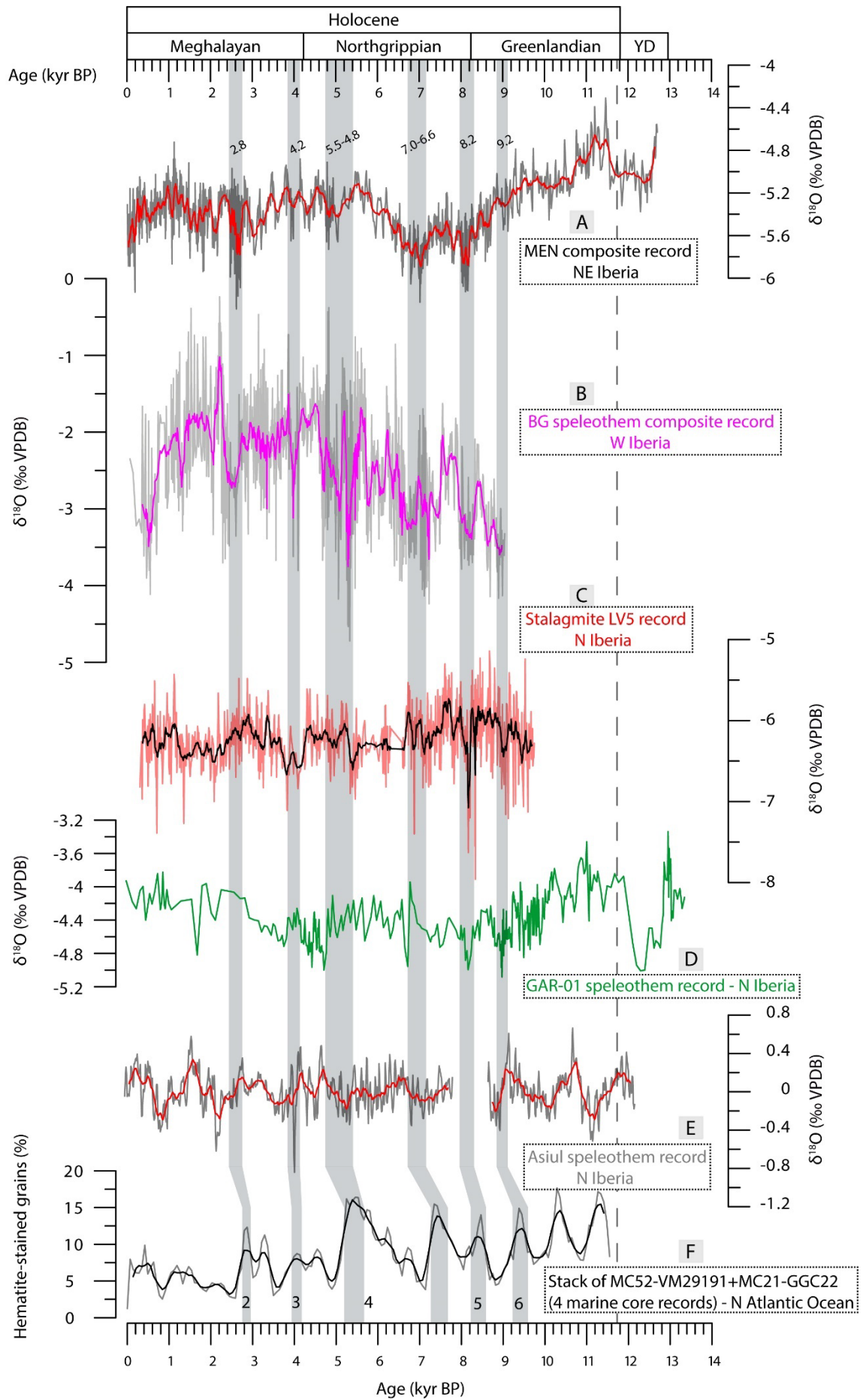
V.5.3.2   The 8.2 kyr BP event

One of the largest depletion in $\delta^{18}O_c$ values recorded by the MEN composite and stalagmites MEN-2 and MEN-5 occurred between 8.1 and 8.2 kyr BP (amplitude of 0.6‰) (Fig. 5.6A and Supp. Material Fig. 8.4), coinciding with the so-called '8.2 kyr event' (Alley et al., 1997). This larger depletion in the composite record presents a similar chronology and intensity in the $\delta^{18}O_c$ individual records of the MEN-2 and MEN-5 stalagmites (Supp. Material Fig. 8.4). Catastrophic meltwater during the '8.2 event' from Agassiz glacial lake dropped the North Atlantic isotope composition of the surface water by 0.4 ‰ (Carlson et al., 2008; Kleiven et al., 2008) that according to cooling of the North Atlantic region. This regional cooling is well described for this event (Alley & Agustsdottir, 2005; Ayache et al., 2018) and resulted in a fresh $\delta^{18}O_{sw}$ signal that was transferred into the precipitation of the region (LeGrande & Schmidt, 2008). Many Iberian speleothem captured a negative $\delta^{18}O_c$ anomaly during this time (Baldini et al., 2019; Benson et al., 2021; Domínguez-Villar et al., 2009; Kilhavn et al., 2022; Thatcher et al., 2020), possible growth hiatuses (e.g., Asiul Cave - ASR; El Soplao Cave - SIR-1) and even erosion events (e.g., Cova da Arcoia - ESP03), thus revealing a coherent regional response to this event. Thatcher et al. (2020) summarized hydroclimate data for Iberia between 8.8 and 8.0 kyr BP, signaling the difference between south and north (humid or variable) in relation to the central and westernmost (arid) zone of Iberia in terms of humidity. The 8.2 kyr event is pronounced in the MEN $\delta^{18}O_c$ composite record, in contrast to the 9.2 kyr BP event. The conditions in northern Iberia were therefore colder and with a contribution of freshwater from the North Atlantic in the negative signal of $\delta^{18}O_{sw}$. This allows the cold anomaly of the 8.2 kyr event to be clearly expressed in the MEN $\delta^{18}O_c$ record.

V.5.3.3   The 7.0-6.6 kyr and 5.5-4.8 kyr BP events

The next event of anomalously low $\delta^{18}O_c$ values occurred between 7.0 and 6.6 kyr BP (Fig. 5.6A and Supp. Material Fig. 8.4), with a very similar intensity as the one at 8.1 kyr BP (reaching values of -5.98 in the MEN-2 stalagmite, -6.33 in the $\delta^{18}O_c$ values of the MEN-5 stalagmite and -6.23‰ in the MEN $\delta^{18}O_c$ composite record). This event in MEN may be associated to meltwater pulse during the final demise of the Laurentide ice sheet, which disappeared at 7 kyr BP (Carlson et al., 2008) and correlates quite well with the BG speleothem record (Thatcher et al., 2020, Fig. 5.6B) and the LV5 record (Domínguez-Villar et al., 2009, Fig. 5.6C). Between 5.5 and 4.8 kyr BP, the stalagmites MEN-3 and MEN-5 (and the MEN $\delta^{18}O_c$ composite) shows small drops in $\delta^{18}O_c$, an event which is more evident in W Iberia (BG record; Thatcher et al., 2020) and NW African lakes (Sidi Ali $\delta^{18}O$ values; Zielhofer et al., 2019) reflecting the last part of Bond event 4 (Fig. 5.6F). Thatcher et al. (2020) argued that on a centennial scale, increased effective precipitation in westernmost Iberia, indicated by lower stalagmite $\delta^{13}C_c$ and $\delta^{18}O_c$ values, is evident at 7.5–7.1, 6.9–6.5, 6.4–6.0, 5.5-5.2 kyr BP at BG (Fig. 5.5D and 5.6B). However, those

events were identified as arid phases (7.5–7.0 and 5.5-5.0 kyr BP) in the FUENT-1 lacustrine sequence from central Iberia (Vegas et al., 2010) and in the Laguna Hondera record from southern Iberia (Mesa-Fernández et al., 2018). The fact that these short intervals are observed in several records within this region indicating humid conditions in the north and drier conditions in the south, highlights the different hydroclimate response across west/northern Iberia compared to central/southern Iberia during the Northgrippian (Thatcher et al., 2020). A similar latitudinal pattern was described for the Central Mediterranean by Magny et al. (2013) signaling changes in the seasonality of precipitation as the main cause of differences between northern and southern Italy.

V.5.3.4   The 4.2 kyr BP event

The 4.2 kyr event might correspond to Bond event 3 (Fig. 5.6F), and there is an ongoing debate in the scientific community about the global extent of this cold, dry and locally also dusty multi-centennial event. Evidence of environmental and climatic deterioration around or coincident with the 4.2 kyr BP Event in the Mediterranean Basin is apparent but chronologically compromised considering a different selection of continental and marine records (Bini et al., 2019). According to Smith et al. (2016), based on the speleothem record from Asiul cave in northern Iberia, this dry interval was synchronous with North Atlantic cooling. In southern Spain, another speleothem record revealed a microhiatus at 4.16 kyr that might correspond to the 4.2 kyr event (Walczak et al., 2015). These findings are supported by a pollen record from the Doñana National Park in southwestern Spain that indicates a multi-centennial aridification trend centered at 4.0 kyr cal BP (Jiménez-Moreno et al., 2015). Furthermore, a speleothem record from Gueldaman Cave in northern Algeria revealed a multi-centennial dry phase that started around 4.4 kyr and was synchronous with the human abandonment of the cave (Ruan et al., 2016). Further, there is evidence of increased storm activity in the Mediterranean Basin between 4.4 and 4.0 kyr BP (Kaniewski et al., 2016). Therefore, this dry event was widespread in the Mediterranean region, even reaching the Atlantic part of Iberia.

The 4.2 kyr event is poorly expressed in the MEN $\delta^{18}O_c$ data (Fig. 5.6A and Supp. Material Fig. 8.4). It is likely that this event was more arid than previous events, such as the 8.2 or the 7.1 kyr BP event whereby the strongly negative $\delta^{18}O_c$ values point to cold temperatures. These arid conditions can act counteracting the MEN composite $\delta^{18}O$ variability. Therefore, the MEN composite recorded cold and very dry conditions during the 4.2 kyr event.

V.5.3.5   The 2.8 kyr BP event

In the middle of the Meghalayan period there was a 450-year interval (2850–2400 yr BP) of $\delta^{18}O_c$ values lower than the Holocene mean of the MEN composite record and stalagmites MEN-3, MEN-4, and MEN-5. This $\delta^{18}O_c$ anomaly is quite noticeable in the MEN-3 record and

more subordinate in the case of MEN-4 and MEN-5 (in which it is centered at 2.4 kyr BP) and suggests a period of cooler conditions that can be correlated with the first cold phase of the Subatlantic period, also called the "Iron Age Cold Epoch" (Van Geel et al., 1996). This period has been recognized by Desprat et al. (2003) in sediments from the Ría de Vigo on the northwestern coast of Spain, in a $\delta^{13}C_c$ record from northern Spain (Martín-Chivelet et al., 2011), from different areas and proxies in central and western Europe (e.g., Blaauw et al., 2004; Plunkett & Swindles, 2008; Speranza et al., 2003; Van Geel et al., 1996) and Greenland (O'Brien et al., 1995), and was also identified as the ice-rafted debris event 2 (~2700 yr BP) in Atlantic sediment cores (Bond, 1997; Bond et al., 2001) (Fig. 5.6F). Several hypothesis have considered to explain this cold event, but likely, changes in solar activity were one of the dominant forcings, as proposed by Zielhofer et al. (2017). Indeed, the onset of this episode coincided with a minimum in solar activity at ~2800 yr BP (e.g., Swindles et al., 2007; Usoskin et al., 2007).

V.6 Conclusions

The Mendukilo cave isotopic record, composed of four stalagmites dated at high precision, provides replicated and continuous speleothem information from the northern Iberian Peninsula for the YD and the entire Holocene able to capture centennial-multidecadal climate variability. Changes in the MEN $\delta^{13}C_c$ composite record are principally driven by climatic processes controlling soil pCO_2 and not by in-cave processes. This is supported by the variability of Sr/Ca (influenced by the growth rate) which is negatively correlated with the MEN $\delta^{13}C_c$ values. Carbon isotope values of the MEN composite display a high variability that correlates well with other records in the region with respect to changes in humidity and/or temperature related to insolation variability and North Atlantic climate. Thus, high MEN $\delta^{13}C_c$ values in the composite record during the YD indicate drier and colder conditions which resulted in low speleothem growth rates (low Sr/Ca ratios). The $\delta^{13}C_c$ data indicate a progressive change towards more humid conditions between the onset of the Holocene and 10-10.5 kyr BP, which represents a delayed signal with respect to climate warming at the Holocene onset (i.e., at 11.7 kyr BP). The onset of the Northgrippian marks the end of the climate optimum in the region and a tendency towards a drier climate which culminated in the Neoglacial, a cold and dry period between 6.0 and 2.5 kyr BP.

The oxygen isotope data of the MEN record show low variability, such as other speleothem records from the region, and especially negative values during some short events (e.g., 8.2 kyr BP) which are synchronous, within age uncertainties, with abrupt changes associated with AMOC perturbations and/or meltwater discharges into the North Atlantic and concomitant changes in the isotopic composition of the North Atlantic surface waters. This relationship between MEN $\delta^{18}O_c$ and $\delta^{18}O_{sw}$ is also evident at millennial scale at the beginning of the Holocene, where the progressive change towards less negative values correlates well with marine isotopic records in

the North Atlantic. Regarding the centennial scale, the MEN oxygen isotope composite records cold events at 8.2, 7.0-6.6, 5.5-4.8 and 2.8 kyr BP associated with major disturbances in the North Atlantic deep-water circulation and sometimes as result of meltwater input (at least for the first two events). Other two events, the 9.2 kyr and the 4.2 kyr events, are not captured by the MEN $\delta^{18}O_c$ profile but clearly expressed in the $\delta^{13}C_c$ profile. We interpret these events as dominated by dry and cold conditions (instead of wet and cold), where temperature and humidity changes have competing effects on the $\delta^{18}O_c$ signal.

Chapter VI

Paleotemperature reconstruction since last deglaciation in NE Iberian

VI.1 Introduction

The last deglaciation in the Northern Hemisphere (ca. 16.5 - 11.7 kyr BP) was punctuated by a series of abrupt climatic changes associated with changes in the extent of continental ice sheets, the concentration of greenhouse gases, and ocean circulation (Clark et al., 2012). On the other hand, the Holocene was more climatically invariant compared to the last deglaciation. Even so, the Holocene was not characterized by steady climate conditions in terms of temperature changes, precipitation seasonality, and extent of glaciers (Wanner et al., 2008, 2011). Unfortunately, many problems arise when reconstructing paleoclimate changes quantitatively because of the scarcity of robust techniques and the influence of different signals on the observed proxy variation, which precludes an accurate understanding of past temperature variations (Heiri et al., 2014b; Moreno et al., 2014a). These limitations greatly hinder the evaluation of whether the reconstructed paleotemperatures across different regions are related to different types of proxies, dissimilar analytical methodologies, climate variables, or a temperature gradient across the region. New and accurate quantitative temperature reconstructions presenting large and geographically extensive datasets and encompassing regional temperature patterns are essential to assess whether climate simulation models can adequately predict regionally divergent trends in climatic change and to understand global and regional climate mechanisms in the past (e.g., Affolter et al., 2019).

The last deglaciation in the Northern Hemisphere involved large shifts in climate associated with Greenland stadials (GS-2.1a and GS-1) and interstadials (GI-1 and the onset of the Holocene). The impact of these rapid climate changes on SW European environments has been recorded by temperature proxies, such as pollen, speleothems, planktonic foraminifera, and chironomids (Català et al., 2019; Cheng et al., 2020; González-Sampériz et al., 2017; Heiri et al., 2014a; Millet et al., 2012; Tarrats et al., 2018). However, the available temperature reconstructions show significant discrepancies and regional climate differences compared to other parts of Europe (Affolter et al., 2019; Heiri et al., 2014a; Renssen & Isarin, 2001). An example of these regional differences in temperature reconstructions is the chironomid study by Heiri et al. (2014a), which revealed that temperature variations during the last deglaciation were more pronounced in western Europe than in southwestern, central, and southeastern Europe. The same is the case for the Holocene, where the long-term evolution of variations in global and hemispheric temperatures remains a subject of debate, with climate models and proxy records showing different trends (Affolter et al., 2019). Given these uncertainties, quantitative studies of inorganic archives such as fluid inclusions (FI) in speleothems (Demény et al., 2016, 2021; Dublyansky & Spötl, 2009) are gaining increasing relevance (Affolter et al., 2019; Honiat et al., 2023; Wilcox et al., 2020) to complement existing studies based largely on biological archives. The strengths of this method include the (i) accurate and precise chronology provided by

speleothems, (ii) well-established link between the cave interior temperature and mean outside air temperature, and (iii) relationship between temperature and water isotopes, which is controlled by physical rather than biological processes. For the FI water isotope thermometry method to provide robust data, the following three aspects must be considered: (i) FIs must be of primary origin, well sealed, and sufficiently abundant. (ii) The choice of the transfer function converting the oxygen and/or hydrogen isotope signal ($\delta^{18}O_{FI}$ and δD_{FI}) into temperatures may bias the temperature estimates. (iii) The relationship between δD_{FI} and $\delta^{18}O_{FI}$, which may have changed over time.

Here, we assess the temperature evolution in northeastern Iberia during the last 16.5 kyr using a quantitative FI-based record of mean annual temperature from five well-dated and replicated stalagmites. This record, compared with other regional terrestrial data, allows for a better understanding of the temperature evolution in southern Europe during the last deglaciation and Holocene, disentangling the effects of temperature and humidity reported by previous studies using calcite stable isotope data (Bernal-Wormull et al., 2021, 2023). These paleotemperature data obtained from FIs in speleothems represent the first quantitative temperature reconstruction for northeastern Iberia for the last deglaciation and open the door for future studies to enhance our quantitative understanding of rapid regional climate change.

VI.2 Study site

The Ostolo (43°11'16"N, 1°43'56"W) and Mendukilo (42º58'25"N, 1º53'45"W) caves are located in northeastern Iberia (Fig. 6.1). Although they are only approximately 28 km apart, their geological, geomorphological, and climatic settings are different. Ostolo cave (248 m a.s.l.) is located in the Bidasoa River valley and is developed in the Carboniferous limestones of the Cinco Villas Massif (Basque Mountains, Western Pyrenees). Mendukilo cave (750 m a.s.l.) formed in reef limestones of the Lower Cretaceous age (Urgonian, Albian-Aptian) on the eastern boundary of the Basque-Cantabrian basin. Further information about the caves and location of the sampled stalagmites can be obtained from previous publications (Bernal-Wormull et al., 2021, 2023).

The climate of the study region is dominated by the Atlantic Ocean, with temperate summers, rainfall distributed throughout the year, and no dry season. The mean annual air temperature (MAAT) and the mean annual precipitation are higher at Ostolo cave ($13.5 \pm 0.8°C$; >2000 mm/year) than at Mendukilo ($12.2 \pm 0.4°C$; approximately 1365 mm/year). Vegetation outside the two caves is dominated by oaks (*Quercus robur* and *Quercus pyrenaica*), alders (*Alnus glutinosa*), beeches (*Fagus sylvatica*), Atlantic-type polycultures, ferns, and heather, and some parts are used for agriculture.

The nearest site where precipitation has been collected for stable isotope analysis is at the tourist cave "Las Güixas" (Fig. 6.1) in Villanúa, approximately 110 km southeast of the caves

located in the Central South Pyrenees (Huesca, Spain) (Giménez et al., 2021). At this location, precipitation is mainly controlled by westerly winds and the passage of Atlantic fronts (as in Ostolo and Mendukilo). Two years of stable isotope data for precipitation and air temperature are available from Villanúa, which were used to obtain monthly, seasonal, and long-term $\delta^{18}O_r/T$ and $\delta D_r/T$ relationships.
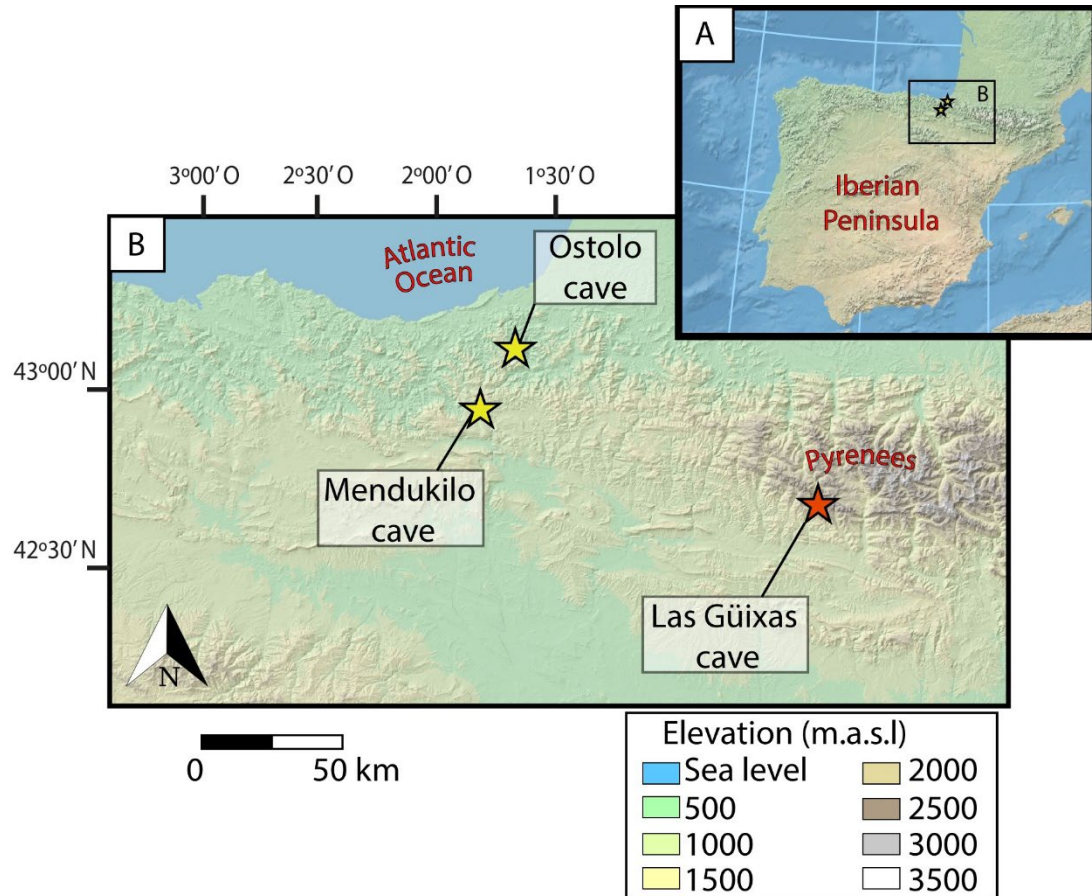
Fig 6.1. *A) Elevation map of the Iberian Peninsula that demarks the B) location of the study area in the NE of Iberia. Yellow stars indicate the locations of both caves, and red star indicate Las Güixas cave (rainfall monitoring site).*

VI.3 Methods

VI.3.1 Sampling and petrography

Stalagmites OST1, OST2, and OST3 were retrieved from the same gallery in the Ostolo cave. Active speleothem deposition was not observed in this cave. Stalagmites MEN-2 and MEN-5 were retrieved from the same gallery in Mendukilo cave. Active calcite precipitation was only observed at the original drip point of MEN-5. See (Bernal-Wormull et al., 2021, 2023) for more details on Ostolo and Mendukilo samples. All stalagmites were cut longitudinally and the central slab was polished. Small blocks were cut along the growth axis for thin sections. Thin sections were examined petrographically using a Nikon Eclipse microscope.

VI.3.2 Dating

10 to 150 mg subsamples were drilled from the stalagmites along discrete laminae. U and Th were separated from the carbonate matrix, purified in a clean-room laboratory, and prepared following the chemistry procedure as described in (Edwards et al., 1987). U and Th isotope measurements were performed using a MC-ICP-MS (Thermo-Finnigan Neptune) at the University of Xi'an and the University of Minneapolis, following the methodology of Cheng et al. (2013). A total of 102 dates were obtained, covering the Holocene and part of the last deglaciation. Age models were established using StalAge (Scholz & Hoffmann, 2011) and published by (Bernal-Wormull et al., 2021, 2023).

VI.3.3 Calcite stable isotope composition

Subsamples for oxygen isotope analyses ($\delta^{18}O_c$) were taken along the growth axes of all stalagmites using either a hand-held drilling device or a Merchantek micromill. A total of 1234 $\delta^{18}O_c$ samples were collected at 300 μm increments for OST2 and OST3. In the case of OST1, the samples were taken at 5 mm increments. A total of 915 samples were obtained for $\delta^{18}O_c$ analyses at 1 mm increments from stalagmites MEN-2 and MEN-5. Isotopic analyses were performed in the University of Innsbruck, using a ThermoFisher Delta V Plus linked to a GasBench II, following the methodology described in Spötl (2011). The long-term reproducibility (1 sigma) of the $\delta^{18}O_c$ analysis is 0.08‰ (Spötl, 2011). All values are reported in 'per mille' (‰) with respect to the Vienna Pee Dee Belemnite standard (VPDB). The $\delta^{18}O_c$ values were corrected for the ice-volume effect following Bintanja et al. (2005). The $\delta^{18}O_c$ profiles were previously published in (Bernal-Wormull et al., 2021, 2023).

VI.3.4 FI stable isotope composition

A total of 356 carbonate subsamples (including duplicates) were crushed and analyzed for δD_{FI} (287 subsamples of Mendukilo stalagmites and 69 of Ostolo samples). Between 0.3 and 2.5 g of calcite was used to ensure a sufficiently high water yield (between 0.2 and 1 μL). Stable isotope measurements were performed using a Delta V Advantage isotope ratio mass spectrometer as described by Dublyansky & Spötl (2009). δD_{FI} values are reported in per mil relative to Vienna Standard Mean Ocean Water (VSMOW). The average long-term precision of replicate measurements of the in-house calcite standard is ±2.4 ‰ for δD_{FI} for water amounts between 0.2 and 1 μL.

δD_{FI} is regarded as a more robust proxy of paleotemperatures than $\delta^{18}O_{FI}$ (which is influenced by climatic and non-climatic parameters) as there are no other sources of hydrogen once the water is entrapped in the calcite (Affolter et al., 2019; Demény et al., 2016, 2021). In addition, $\delta^{18}O_{FI}$ values obtained with the Innsbruck FI setup can be inaccurate for samples with low water content (Honiat et al., 2023). Therefore, we only used the δD_{FI} values in this study.

VI.3.5 Isotope temperature conversion

The composite paleotemperature records of Ostolo and Mendukilo speleothems are based on 356 FI samples (and replicates) applying a regional water isotope/temperature relationship using the monitoring data (isotopic values of drip waters and outside temperature) of both caves (Bernal-Wormull et al., 2021, 2023) and the precipitation dataset of "Las Güixas" tourist cave. The latter data provides the relationship between air temperature and the stable isotopic composition of rain ($\delta^{18}O_r$ and δD_r) between July 2017 to June 2019 (n = 216). MAAT and the weighted annual mean $\delta^{18}O_r$ at the Villanúa site are significantly correlated ($R^2 = 0.7$; p-value << 0.01). The δD_{FI} values were first corrected for the ice volume effect using the gradient obtained for $\delta^{18}O$ (Bintanja et al., 2005) converted to δD using a factor of eight. The paleotemperatures were then obtained using a linear $\delta D/T$ transfer function (see Supp. Material 8.4 for more information) anchored to the MAAT of both caves and the isotopic composition of drip waters (δD_d; Ostolo δD_d = -37.76‰; Mendukilo δD_d = -45.28‰), corrected for the elevation of the Villanua monitoring station (950 m a.s.l.). The modern δD_d values were corrected for the elevation difference, assuming a lapse rate of 0.2 ‰ per 100 m for $\delta^{18}O$, i.e., 1.6 ‰ per 100 m for δD_d (see Poage, 2001). The errors of the δD_{FI}, δD_d, $\delta D_r/T$, and MAAT values outside the cave, as well as the slope of the Local Meteoric Water Line (LMWL), were propagated through the different calculation steps. As there are no constraints on possible seasonal changes in precipitation and effective infiltration in the past, we assume that annual infiltration was constant over time.

VI.4 Results

VI.4.1 Last deglaciation and Holocene δ¹⁸O speleothem record

The Ostolo stalagmites cover much of the last deglaciation at high precision due to very high U concentrations (10-80 ppm), and the $\delta^{18}O_c$ profiles show a high degree of correlation among the three stalagmites (Fig. 6.2). OST1 and OST2 present more negative values (−5 to −8.9‰) during GS-1 and GS-2.1a and less negative ones (up to −3.4‰) during GI-1 and the onset of the Holocene. OST3 did not grow during the intervals characterized by the most negative $\delta^{18}O_c$ values covered by the other two stalagmites (Fig. 6.2). On the other hand, MEN stalagmites show low U concentrations (between 100 and 350 ppb) but also low detrital ^{232}Th contents, thus allowing robust age models for both stalagmites that cover different intervals of the Holocene and GS-1 with a good overlap (Fig. 6.2): (i) MEN-2 grew between 12.8 and 6.3 kyr BP and its $\delta^{18}O$ values remain stable during GS-1 (Fig. 6.3), but increase abruptly, reaching the highest values of the entire record at the GS-1/Holocene transition (from -5.2‰ in GS-1 to -4.3‰ at 11.6 kyr BP). (ii) MEN-5 spans the last 8.8 kyr and present especially negative values during some short events (e.g., 8.2 kyr BP with a value of -6.3 ‰, replicated in MEN-2) which are synchronous within age uncertainties with abrupt changes in the isotopic composition of the North Atlantic surface waters (Carlson et al., 2008) (Fig. 6.3). More details on the chronology and isotopic data of these speleothems are provided by (Bernal-Wormull et al., 2021, 2023).
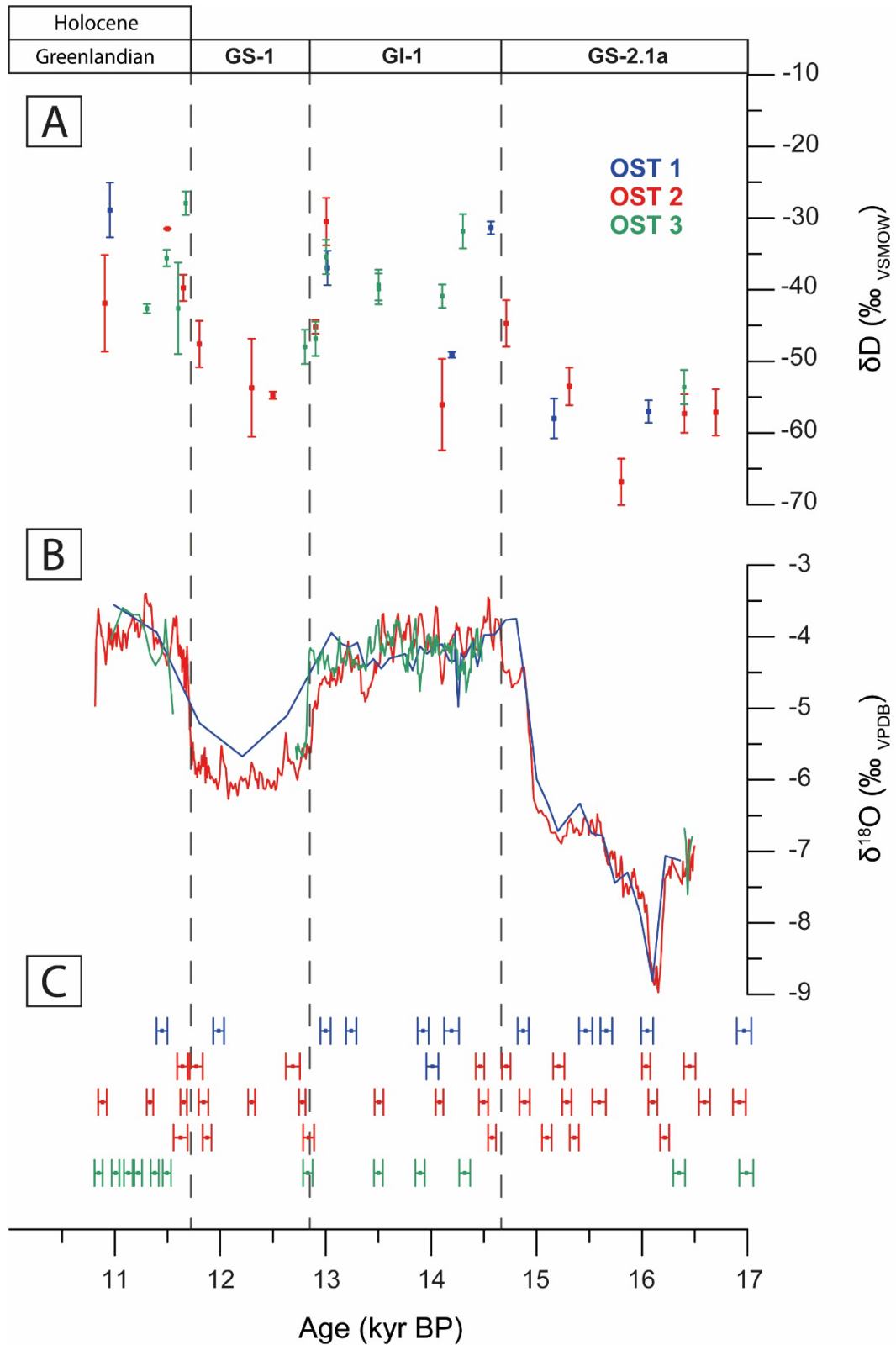
Fig 6.2. *A) δD_FI, B) δ¹⁸O_c, and C) dating values of Ostolo stalagmites (OST1 in blue, OST2 in red and OST3 in green). Deuterium isotopic composition of fluid-inclusion water are corrected for the ice-volume effect (Bintanja et al., 2005). Modeled U/Th ages of each stalagmite incorporate their 2σ uncertainties.*
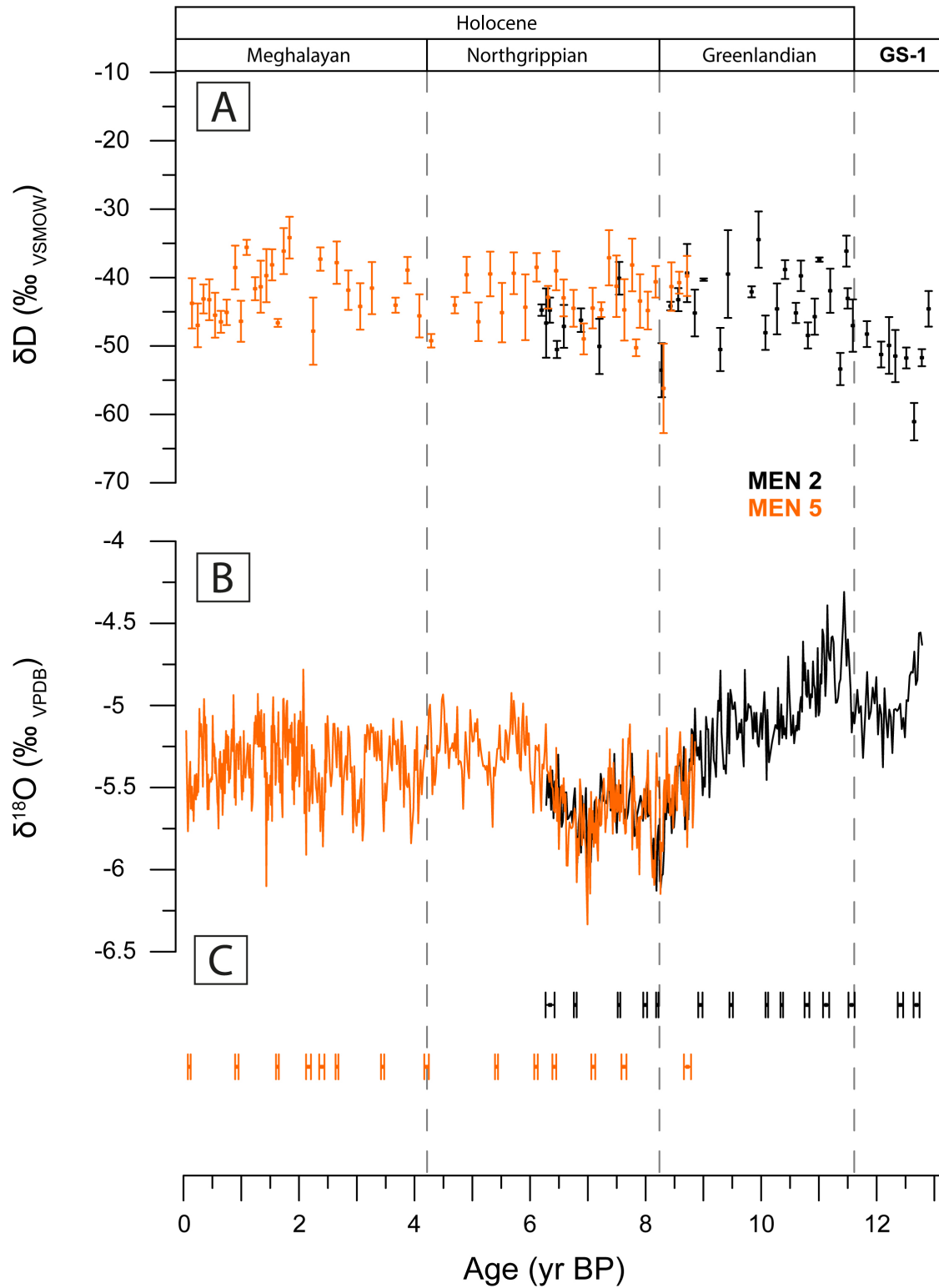
Fig 6.3. *A) δD_FI, B) δ¹⁸O_c, and C) dating values of Mendukilo stalagmites (MEN-5 in orange and MEN-2 in black). Deuterium isotopic composition of fluid-inclusion water are corrected for the ice-volume effect (Bintanja et al., 2005). Modeled U/Th ages of each stalagmite incorporate their 2σ uncertainties.*

VI.4.2 Fluid-inclusion isotopes

The stalagmites of Ostolo cave present greater variability in their amount of water throughout each record than those of Mendukilo. The replicates yielded a mean standard deviation of ±2.4 ‰ for δD_{FI}. We assigned this value to individual measurements and use it as an uncertainty estimate. All MEN samples were duplicated, triplicated, or even quadruplicated. Not every OST sample could be duplicated because of low water amounts, and there was insufficient material for sub-sampling individual growth layers several times. The δD_{FI} values of sub-samples of MEN-2 and MEN-5 (between -34 and -61 ‰) with water contents of 0.2 to 1 μL replicated within 2.7 ‰.

The δD_{FI} values for the Holocene and GI-1 are comparable to those of modern day at MEN and OST dripwaters (Fig. 6.2 and Fig. 6.3). On the other hand, values are more negative during GS-1 and GS-2.1a (Fig. 6.2): GS-2.1a is represented by seven OST subsamples with a mean δD_{FI} value of -58 ‰. One of these values at 15.80 ± 0.05 kyr BP is even more depleted (-66.8 ± 2.4 ‰). The values rapidly become less negative at 14.57 ± 0.05 kyr BP (Fig. 6.2; mean during GI-1: -40 ‰). This trend is interrupted in the three OST stalagmites at 14.13 ± 0.09 kyr BP leading to more negative values (between -40 and -56 ‰). During GS-1, δD_{FI} values decrease again (Fig. 6.2), reaching an average of -51 ‰ and showing a rapid rise at the onset of the Holocene (-36 ‰). The MEN-2 record also shows a mean of -51 ‰ during GS-1 (Fig. 6.3); however, the change at the onset of the Holocene is not sharp. Between 8.7 and 6.3 kyr BP MEN-2 and MEN-5 δD_{FI} values show an excellent correlation (Fig. 6.3). There is no significant variation between Greenlandian (-44‰), Northgrippian (-43‰), and Meghalayan (-42‰). Despite these fairly constant δD_{FI} values, short negative shifts were identified at 11.37 ± 0.08 (-53.4 ± 2.4‰), 9.29 ± 0.08 (-50.5 ± 3.2‰), 8.29 ± 0.07 (-54.9 ± 6.5‰) kyr BP.

VI.5 Discussion

VI.5.1 Interpretation of the $\delta^{18}O$ signal

Variations in the dripwater and stalagmite $\delta^{18}O$ records may reflect changes in $\delta^{18}O$ of the surface ocean in the moisture source area, as well as changes in atmospheric processes which together affect the fractionation of O isotopes between the ocean and the study site (Lachniet, 2009; McDermott, 2004). In Ostolo stalagmites, the $\delta^{18}O_c$ signal is coherent with air temperature changes throughout the entire deglaciation (Bernal-Wormull et al., 2021). The overall $\delta^{18}O_c$ pattern of these stalagmites is similar to that of speleothems from the Pyrenees (Bartolomé et al., 2015b; Cheng et al., 2020) and from the Alps (Li et al., 2020; Luetscher et al., 2015), which also receive predominantly Atlantic-derived moisture, and where $\delta^{18}O_c$ primarily reflects atmospheric temperature. Superimposed on the temperature effect are changes in the isotopic composition of

the moisture source, which may explain the negative excursion in the Ostolo $\delta^{18}O_c$ record during HE1 at 16.2–16.0 kyr BP, reaching values as low as −8.9‰ (Fig. 6.2).

In contrast, the MEN $\delta^{18}O_c$ record captured a signal that is primarily influenced by rainfall amount, as well as by changes in the isotopic composition of the ocean during the first part of the record (13-8 kyr) (Bernal-Wormull et al., 2023). A prominent feature of MEN-2 and MEN-5 $\delta^{18}O_c$ records (Fig. 6.3) is a -0.7‰ anomaly (relative to the Holocene mean of -5.4‰) that occured at 8.11 and 7.00 kyr BP. These two events of anomalously low $\delta^{18}O_c$ values were likely caused not by increased rainfall amount but rather record rapid and short-lived decreases in temperature and in $\delta^{18}O_{sw}$, as proposed in previous studies (e.g., Domínguez-Villar et al., 2009; García-Escárzaga et al., 2022; LeGrande & Schmidt, 2008; Matero et al., 2017).

VI.5.2 Paleothermometry using FI stable isotope data

Our δD_{FI} values represent a robust record because (i) part of the record is well replicated by samples from two caves with different climatic setting, (ii) stalagmites from the same cave are replicated (within their corresponding uncertainties), and (iii) a large percentage of the samples are replicated more than once. We investigated the temperature dependence of the hydrogen (and oxygen) isotope composition of precipitation water in the study region (i.e., multi-annual modern-day $\delta D_r/T$ and $\delta^{18}O_r/T$ gradients, respectively). This relationship, which may change over time, was examined by Rozanski et al. (1992) for Central Europe and applied by Affolter et al. (2019) for a 14 kyr record from Milandre cave (Switzerland). This approach was also applied to Last Interglacial records from Alpine caves (Honiat et al., 2023; Wilcox et al., 2020). The relationship between mean annual $\delta^{18}O_r$ and MAAT ($\delta^{18}O_r/T$) is 0.55 ± 0.03 ‰ °C−1 for the "Las Güixas" tourist cave in Villanúa. Compared to the average European $\delta^{18}O_r/T$ gradient of 0.59 ± 0.08 ‰ °C−1 (Rozanski et al., 1992), the gradient is within the combined uncertainties. The OST and MEN temperature transfer function (OM-FIT) calculated using the modern-day $\delta D_r/T$ gradient determined using the LMWL resulted in a paleotemperature record of the last 16.7 kyr BP (Fig. 6.4). The error propagation resulted in a combined paleotemperature uncertainty between 1.2 and 3.0 °C (see Supp. Material table 8.2).

VI.5.3 Temperature variability in European speleothem FI records

VI.5.3.1 Last deglaciation

The Ostolo cave $\delta^{18}O_c$ and δD_{FI} records (Fig. 6.2) and the OM-FIT (Fig. 6.4) show clear evidence of rapid temperature changes at GS-2.1a, GI-1, GS-1, and the onset of the Holocene. Their timing and amplitude are in excellent agreement with other European O isotope records from lake sediments (Grafenstein, 1999; Van Raden et al., 2013) and speleothems (Affolter et al.,

2019; Cheng et al., 2020; Li et al., 2020; Luetscher et al., 2015). The high degree of similarity between these records and NGRIP is a strong argument for a common North Atlantic climate forcing during the last deglaciation on millennial to decadal timescales.

The OM-FIT record suggests that the regional MAAT during GS-2.1a was slightly lower than during GS-1 and was marked by a negative excursion at 15.8 ± 0.1 kyr BP and an approximate drop of 2.0 °C compared to the average temperature determined for GS-2.1a (Fig. 6.4). This OM-FIT anomaly agrees with the last phase of the HE1, related to massive iceberg discharges from the Laurentide ice sheet, which collapsed around 16.2 ± 0.3 kyr BP (Landais et al., 2018). Regionally, a significant glacier advance occurred at that time in the Pyrenees and other Iberian mountains (García-Ruiz et al., 2023), and speleothems from Meravelles cave (NE Iberia) record a notable $\delta^{18}O_c$ anomaly between 16.2 and 15.9 kyr BP (Pérez-Mejías et al., 2021). This anomaly appears to have been part of the changes in the isotopic composition of the moisture source that led to the negative excursion in the OST2 $\delta^{18}O_c$ record between 16.2 and 16.0 kyr BP. This confirms that the OM-FIT record not only captured the temperature history on millennial time scales but also abrupt climate events on a centennial scale.

A rapid temperature increase of 6.0 ± 1.9 °C occurred at the onset of GI-1 (Fig. 6.4). This increase in the OM-FIT record occurred simultaneously with an important glacier retreat in the Iberian Mountains (García-Ruiz et al., 2023), an increase in the chironomid-inferred July air temperatures from the west-central Pyrenees (Millet et al., 2012), and an increase in MAAT recorded by branched glycerol dialkyl glycerol tetraethers in the Padul paleolake record (Sierra Nevada, southern Iberian Peninsula; Rodrigo-Gámiz et al., 2022). The onset of GI-1 in the OM-FIT was recorded by δD_{FI} data from the OST1 and OST3 stalagmites. The amplitude of this abrupt warming change is in agreement with other temperature records from Europe, such as temperature estimates based on $\delta^{18}O_c$ data of Alpine speleothems (Li et al., 2020; Luetscher et al., 2015). Von Grafenstein et al. (2013), using a combination of ostracod, mollusk and charophyte data, obtained an increase of about 6 °C in MAAT for this transition at the Gerzensee lake site. The warming at the onset of the Late Glacial interstadial recorded for the Ammersee record, using a coefficient suggested by a study of stalagmites from northern Switzerland (0.48‰/°C, Affolter et al., 2019), was about 5.5 °C (4.1–8.4 °C) (Li et al., 2020).
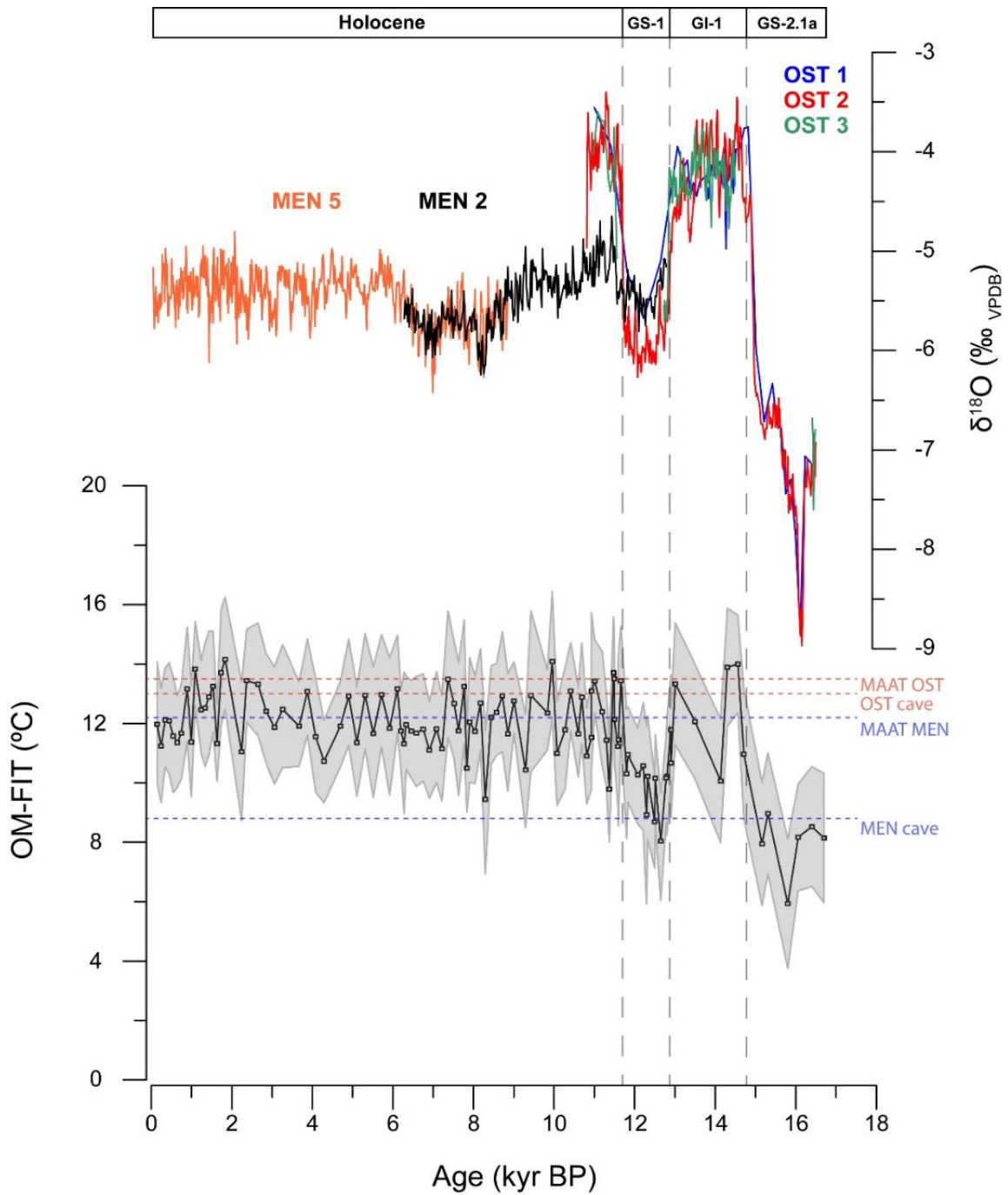
Fig 6.4. *Mendukilo and Ostolo $\delta^{18}O_c$ series (top) compared with the OM-FIT record (bottom). MAAT and temperature inside the cavity at each cave are highlighted.*

During GI-1, the δD_{FI} record is marked by higher δD values and similar temperatures in the OM-FIT record compared to the onset of the Holocene (Fig. 6.4). As in the OST $\delta^{18}O_c$ record, the δD_{FI} values follow a negative trend towards the end of GI-1. During this interstadial, a significant inflection point occurs with a negative anomaly at 14.1 ± 0.1 kyr BP in the OM-FIT record (Fig. 6.4). This suggests that this OM-FIT minimum during GI-1, also registered at 14.10 ± 0.03 kyr BP in the OST $\delta^{18}O_c$ record and equivalent to GI-1d in NGRIP (Rasmussen et al., 2014), involved the most pronounced cooling of GI-1 (between 2.0 and 3.8 ± 2.0 °C in the OM-FIT record), just after the GI-1e warm phase (Fig. 6.4). This colder spike recorded in OM-FIT (which almost lies in the range of the prediction error of the inference model) is coeval with glacier expansions in the Pyrenees (García-Ruiz et al., 2023) and a centennial-scale cooling at Ech paleolake (Millet et al., 2012), Lake Estanya (Vegas-Vilarrúbia et al., 2013), and in the El Portalet sedimentary sequence (González-Sampériz et al., 2006). This relatively small decrease in temperature during GI-1d, as quantified by the OM-FIT record and recorded in chironomid-inferred July air temperatures (Millet et al., 2012) in this region, resulted in: i) important vegetation response (González-Sampériz et al., 2017), with the decrease of juniper and expansion of steppe herbs during this cold and dry event, and ii) depositional processes with carbonate and massive organic-rich silt deposition during warm and humid interstadials alternating with siliciclastics when cold and arid conditions returned (González-Sampériz et al., 2006).

Between 12.9 and 12.6 kyr BP, the δD_{FI} decrease in Ostolo and Mendukilo (Fig. 6.2 and Fig. 6.3) resulted in a temperature decline in the OM-FIT record close to 5.3 ± 1.9 ºC (Fig. 6.4), which marks the first part of GS-1 (Rasmussen et al., 2014). Similar magnitudes of cooling were reported for the central Pyrenees (Bartolomé et al., 2015b). On the other hand, this change seems to have been slightly larger compared to summer air temperature records of the GI-1/GS-1 transition, such as lakes in NW Iberia (2-3 ºC - Muñoz Sobrino et al., 2013) and the central Pyrenees (1.5-2 ºC - Millet et al., 2012). This important change in the OM-FIT record also agrees in magnitude with the rapid cooling recorded by (i) speleothems from the Alps (around 4–5 °C; Li et al., 2020) and the Jura Mountains (4.3 ± 0.8 °C; Affolter et al., 2019) and (ii) a drop in SST of around 4 °C offshore Iberia at 12.9 kyr BP (Martrat et al., 2014; Rodrigues et al., 2010). Taken together, these observations suggest that records with an annual signal (e.g., OM-FIT) reflect the temperature change during the GI-1/GS-1 transition in central Europe compared to seasonal chironomid-based summer paleotemperature estimates (Heiri et al., 2014a; Millet et al., 2012; Muñoz Sobrino et al., 2013) (Fig. 6.5), refuting the absence of local interference in large-scale climate forcings (linking insolation, ocean, and atmosphere) and discarding a notable European S–N gradient in the magnitude of temperature changes.

The end of the GS-1 cold phase and the onset of the Holocene are marked by a rapid warming in the OM-FIT record of approximately 3-4 °C (Fig. 6.4), reaching a maximum at 11.66 ± 0.03 kyr BP. The variability of the MEN $\delta^{18}O_c$ data during the GI-1/GS-1 and GS-1/Holocene onset

transitions is small compared to that of the OST $\delta^{18}O_c$. This could be explained by the fact that Mendukilo cave is located closer to the Atlantic coast, with $\delta^{18}O_c$ being influenced not only by temperature but also by the amount effect, as already reported based on other speleothem records from this region (e.g., Baldini et al., 2019). In contrast, the $\delta^{18}O_c$ of speleothems from Pyrenean caves is controlled by temperature (Bartolomé et al., 2015b; Bernal-Wormull et al., 2021; Cheng et al., 2020). This leads to a "smoothed" temperature signal compared to the OST $\delta^{18}O_c$ record during GS-1, a cold and dry interval (Fletcher et al., 2010). Nevertheless, the MEN δD_{FI} records shows important changes during the GI-1/GS-1 and GS-1/Holocene onset transitions, and they correlate quite well with the δD_{FI} of OST (Fig. 6.2).

Fig 6.5. *(Next page)* *Comparison of different paleotemperature reconstructions for the 16.5 kyr BP (From Greenland to SW Europe) and other $\delta^{18}O_c$ records of the Iberian Peninsula. A) NGRIP $\delta^{18}O$ and $\delta^{15}N$ records (Kindler et al., 2014; Rasmussen et al., 2014). B) Milandre cave fluid-inclusion record, NW Switzerland (Affolter et al., 2019). C) Basa de la Mora Lake chironomid-inferred July temperature estimates (Tarrats et al., 2018). D) Stacked and spliced July Chironomid-inferred temperature record available for the SW Europe (Heiri et al., 2014a). E) OM-FIT (this study). F) Mendukilo and Ostolo $\delta^{18}O_c$ series. G) $\delta^{18}O_c$ record of LV5 stalagmite from northern Iberia (Kaite Cave) (Domínguez-Villar et al., 2017). H) GAR-01 $\delta^{18}O_c$ record from northern Iberia (La Garma Cave) (Baldini et al., 2019). I) SIR-14 $\delta^{18}O_c$ time series from north ern Iberia (El Soplao Cave) (Kilhavn et al., 2022).*
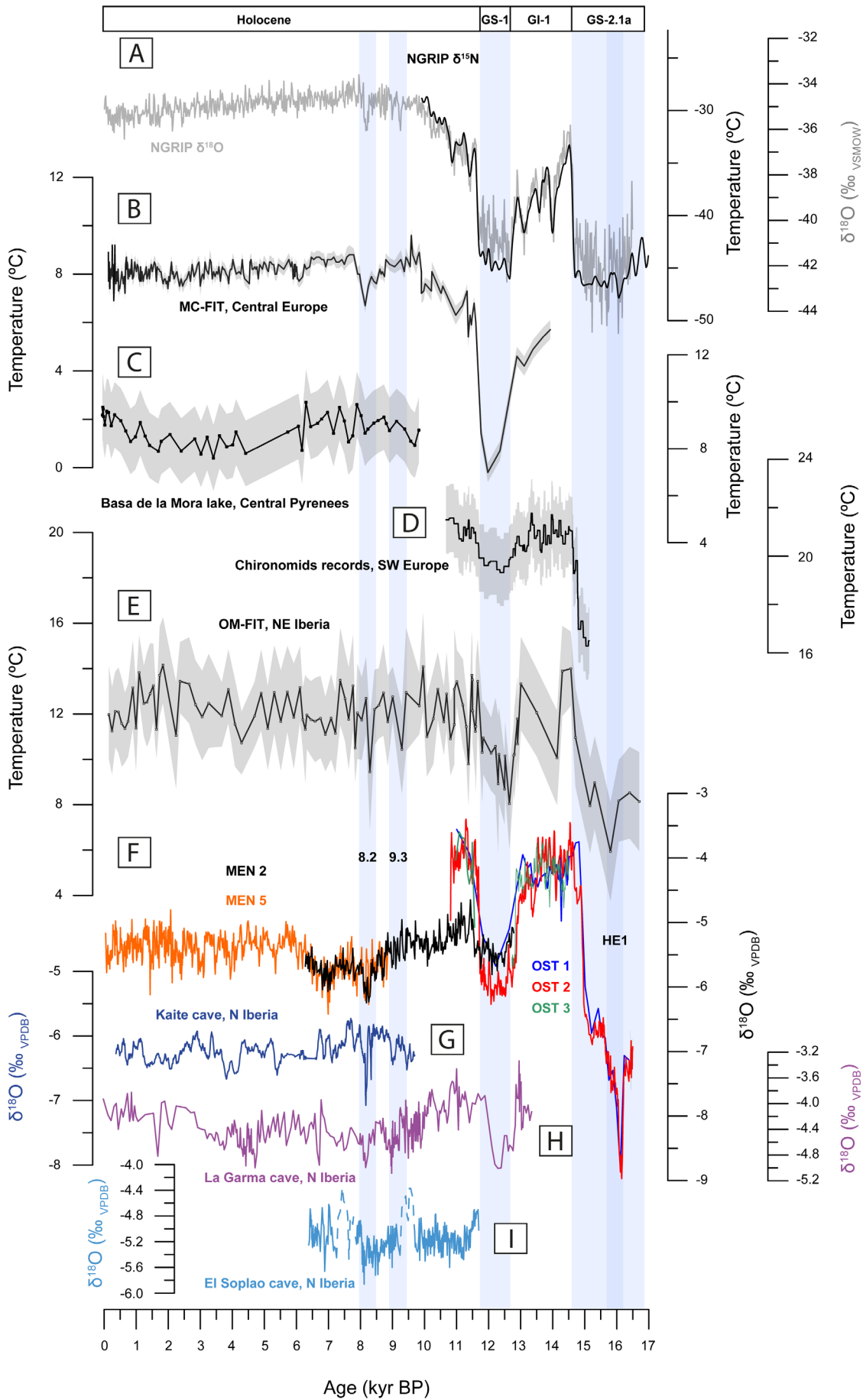
VI.5.3.2 Holocene

As mentioned above, the Holocene part of the OM-FIT record (Fig. 6.4) is based on δD_{FI} values of the MEN stalagmites (Fig. 6.3), a record that not only captures variability in its isotopic composition ($\delta^{18}O_c$ and $\delta^{13}C_c$) controlled by temperature but also past hydroclimatic conditions (Bernal-Wormull et al., 2023). This leads to a limitation in reconstructing a rather invariable period in terms of temperature, such as the Holocene, which is represented by a centennial OM-FIT temperature variability that can easily reach 2° in some parts of the Holocene, although these variations are close to the uncertainty of the OM-FIT record (between ± 1.2° and ± 2.6° for the Holocene). Therefore, these quantitative changes in temperature during the Holocene should be taken with caution. Throughout the Holocene, the OM-FIT record contrasts markedly not only with MEN $\delta^{18}O_c$ (Fig..6.5) but also with the MEN $\delta^{13}C_c$ composite (Bernal-Wormull et al., 2023), where millennial-scale variability is notable. MEN $\delta^{13}C_c$ has been shown to be mainly influenced by hydroclimate (and secondarily by temperature), suggesting a wetter climate during the Holocene Thermal Maximum (HTM) in this region (Bernal-Wormull et al., 2023; Morellón et al., 2018). On a millennial scale, OM-FIT does not record this feature, and instead records peak temperature during the onset of the Holocene (until ~10 kyr BP, but showing high centennial variability). This early rapid warming is also recorded by the hydroclimate-controlled isotopic signal of the SIR-1 stalagmite from NW Iberia (Rossi et al., 2018). This shows the importance of obtaining a temperature-sensitive record in regions where the isotopic signal of speleothems could also be influenced by local factors, as in the case of the MEN $\delta^{18}O_c$ record.

The OM-FIT record does not capture a clear cooling trend after the HTM compared to the $\delta^{18}O$ record from Greenland ice cores (Rasmussen et al., 2014) and the MC-FIT record from central Europe (Affolter et al., 2019) (Fig. 6.5), but rather suggest stable temperatures. This cooling is known throughout Europe (e.g., Ilyashuk et al., 2011; Larocque-Tobler et al., 2010) and Iberia (Català et al., 2019; García-Ruiz et al., 2020; Leunda et al., 2019; Sancho et al., 2018). The absence of this cooling (known as Neoglaciation (McKay et al., 2018)) in the OM-FIT is probably because this temperature reconstruction is partly masked by large centennial variability and the large errors for small temperature changes. MEN $\delta^{18}O_c$ and OM-FIT are different from the temperature trend captured by chironomids for the central Pyrenees (Tarrats et al., 2018), where a millennial-scale towards a colder middle Holocene compared to the HTM and the late Holocene is apparent (Fig. 6.5). This highlights again, as in the case of GS-1, the differences in temperature records obtained from speleothems (OM-FIT, recording an annual signal) and chironomids (recording summer air temperature). The most recent 2.5-3 kyr are not well resolved in the MEN $\delta^{18}O_c$ record (Bernal-Wormull et al., 2023). Therefore, no information on temperatures during this period is provided, as the inferences about climate are less robust than those for the earlier part of the record.

Despite the limited precision of OM-FIT, it is possible to identify abrupt centennial events, some of which can also be seen in the $\delta^{18}O_c$ values of MEN-2 and MEN-5 (Fig. 6.4). For example, one of the lowest OM-FIT temperatures (9.8 °C) occurred at 11.37 ± 0.08 kyr BP (mean temperature at the onset of the Holocene = 12.3 ± 1.8 °C), corresponding within age uncertainties to the Preboreal Oscillation (11.4 kyr) recorded in Greenland ice cores (11.27 ± 0.03 years BP, based on the new ice core chronology - (Seierstad et al., 2014) and by MC-FIT in Switzerland (11.37 ± 0.15 kyr BP - Affolter et al., 2019) (Fig. 6.5). Another example is the 9.2-kyr event that has been documented across the Northern Hemisphere (e.g., Fleitmann et al., 2008; Genty et al., 2006; Masson-Delmotte et al., 2005; Rasmussen et al., 2007), including terrestrial (Baldini et al., 2019; Carrión, 2002; Iriarte-Chiapusso, 2016; Mesa-Fernández et al., 2018; Vegas et al., 2010) and marine records from Spain (Nebout et al., 2009). This event is captured by a δD_{FI} value of -51‰ in MEN-2 and a temperature of 10.4 ± 1.9 °C in the OM-FIT record at 9.29 ± 0.08 kyr BP (Fig. 6.5). However, this event is not present in the $\delta^{18}O_c$ record of MEN-2, and previous research suggests that the conditions in northern Spain were likely considerably warmer and wetter at ~9 kyr BP (Baldini et al., 2019; Morellón et al., 2018; Tarrats et al., 2018). This confirms the suggestion by Bernal-Wormull et al. (2023) that the less-variable $\delta^{18}O_c$ signal in Mendukilo cave is not only influenced by short-lived decreases in $\delta^{18}O_{sw}$, but also by changes in humidity.

Catastrophic meltwater discharge during the '8.2 kyr event' from glacial lake Agassiz lowered the isotope composition of North Atlantic surface water by 0.4‰ (Carlson et al., 2008; Kleiven et al., 2008) and led to a wide spread cooling in the circum-North Atlantic realm. The isotopic signal of this meltwater event was transported by moisture and left an imprint in the isotopic composition of precipitation in Iberia (Bernal-Wormull et al., 2023; LeGrande & Schmidt, 2008). The 8.2-kyr event was superimposed on a cool multi-centennial period lasting from 8.29 to 8.10 ± 0.04 kyr BP recorded by MEN $\delta^{18}O_c$ and characterized by an abrupt drop in temperature of about ~2.8 °C at 8.29 ± 0.07 kyr BP in the OM-FIT record (Fig. 6.5). This drop in temperature within an interglacial period is another example of important vegetation change in the Iberian Peninsula (Allen et al., 1996; Carrión & Van Geel, 1999; González-Sampériz et al., 2006) during a short-lived event. This is important to assess future climate conditions in this region when changes in large parts of the climate system (climate tipping elements; McKay et al., 2022) amplify themselves beyond a warming threshold.

The temperature difference during the 8.2 kyr event recorded by OM-FIT seems to be higher than in other temperature (and precipitation) records from across the Northern Hemisphere, and proxy evidence across Europe indicates a cooling by ~ 1-1.7 °C during this event (Baldini et al., 2019; Davis et al., 2003; Morrill et al., 2013). Other terrestrial records in southwestern Europe offer important insights into the palaeoclimate during this event (e.g., Fletcher et al., 2013; González-Sampériz et al., 2017; Morellón et al., 2018; Zielhofer et al., 2019). This information is often contradictory in terms of humidity conditions as this region is influenced by both

Mediterranean air masses and those from the North Atlantic (Moreno et al., 2017, 2021). However, most of these terrestrial records show a longer-term change in climate but usually lack the resolution to appropriately constrain the regional response to the 8.2 kyr event. Therefore, it is likely that these long-term changes are more influenced by local summer insolation than by an Atlantic climatic anomaly, as suggested by Kilhavn et al. (2022). Thus, other stalagmite records from the region (Baldini et al., 2019; Benson et al., 2021; Bernal-Wormull et al., 2023; Kilhavn et al., 2022), the combination of carbonate isotopic series ($\delta^{18}O_c$ and $\delta^{13}C_c$), and the FI record from Mendukilo stalagmites, allow a better delineation of the regional response to this event when the climate conditions was colder compared to the average temperature of the Holocene (as shown quantitatively by the OM-FIT record), humid (MEN $\delta^{13}C_c$), and mainly associated with a change in the composition of the moisture source (MEN $\delta^{18}O_c$ signal; Bernal-Wormull et al., 2023; Domínguez-Villar et al., 2009; Kilhavn et al., 2022).

VI.6 Conclusions

The Ostolo and Mendukilo speleothems provide a well-replicated and precisely dated record of paleotemperatures in the NE Iberian region over the last 16.5 kyr BP. The OM-FIT record adds new and first non-biogenic evidence of rapid temperature transitions during the last deglaciation and the Holocene, accompanied by the identification of abrupt events. We report temperatures for GS-2.1a up to 6.0 ± 1.9 °C lower than for GI-1 and the present day and constrain the regional response of HE-1 to 16.2 to 15.8 kyr BP. The sharp rise in temperatures during the GS-2.1a/GI-1 transition was quantitatively similar to other records from SW and the rest of Europe. Temperatures during GI-1 were equivalent to those of the Holocene, and a minimum during GI-1d occurred at 14.1 ± 0.1 kyr BP. The rapid temperature changes during the beginning of GS-1 and the onset of the Holocene, as recorded by OM-FIT, are equivalent to those reported from other parts of Europe, but contrast with those recorded by chironomids from SW Europe (summer temperatures). Neither $\delta^{18}O_c$ nor OM-FIT show significant millennial-scale changes during the Holocene. The 8.2 kyr event is recorded between 8.29 and 8.10 ± 0.04 kyr in the $\delta^{18}O_c$ record and is centered at 8.29 ± 0.07 kyr in the OM-FIT record, synchronous with Greenland ice-core data and well-dated records from central and SW Europe.
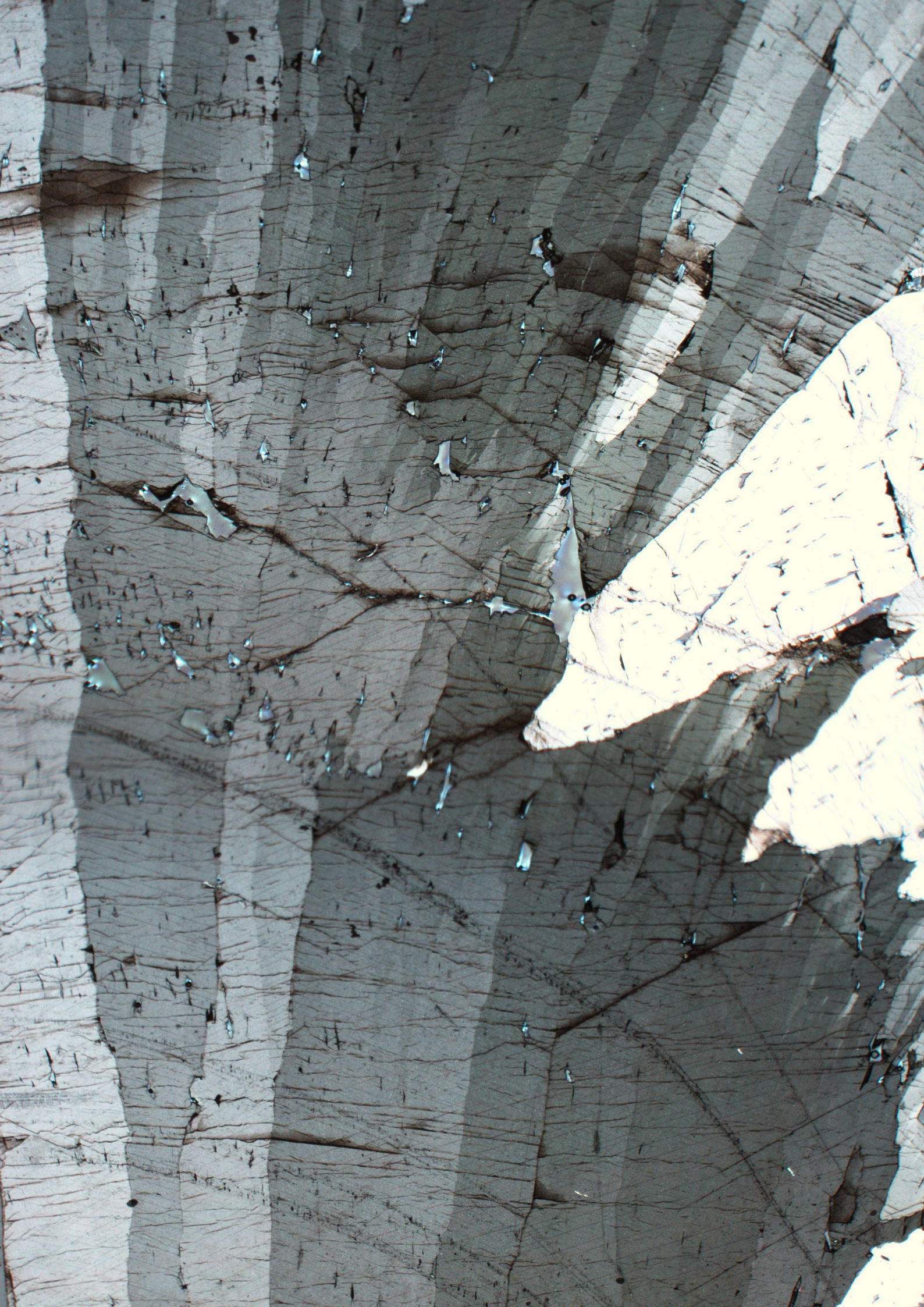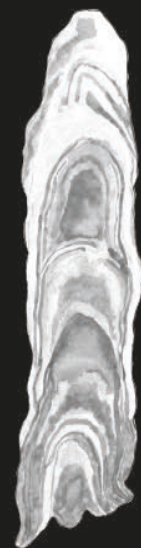
Chapter

VII

Epilogue

VII.1 Conclusions

> **Last deglaciation to the Holocene onset: Ostolo cave record**

- The Ostolo cave presents serious difficulties in correctly understanding cave present-day dynamics. Even so, the monitoring work inside the cavity allowed to determine that the $\delta^{18}O$ values in the dripwater and precipitated carbonates shows that there is no seasonal variation and that the carbonate precipitates year-round.

- The three stalagmites obtained from Ostolo cave are composed entirely of calcite and present similar petrography. Most stalagmites present fabrics that are suitable for paleoclimatic sampling and interpretation. The exception falls on the microcrystalline columnar fabric, in which the chronological (age reversals) and isotopic (lack of correlation between speleothems) results present a notable deviation in their values. This demonstrates the importance of carrying out a prior petrographic analysis, which allows certain problematic intervals to be ruled out before carrying out higher-resolution chronological and geochemical analyses of the speleothems.

- The chronology obtained from part of the Ostolo speleothems, which present an elevated uranium concentration, is of very high resolution and has low errors compared to any other last deglaciation record in the region. This allows the creation of age models that can capture rapid climate changes during that period.

- The $\delta^{18}O_c$ series of the three Ostolo stalagmites, corrected for ice volume changes and well correlated with each other, resemble in amplitude with other $\delta^{18}O$ records (between Greenland and southwestern Europe) directly influenced by changes in temperature during the last deglaciation.

- Light $\delta^{18}O_c$ values were observed during the cold stages (GS-1 and GS-2.1a), and higher values were observed during warm events (GI-1 and Holocene), indicating that air temperature was dominant in this signal.

- In addition to the effect of temperature, the $\delta^{18}O_c$ series of these speleothems are influenced by changes in the isotopic composition of the humidity source that affects these caves. This is due to the meltwater released into the North Atlantic Ocean by the discharge of massive ice sheets in the northern hemisphere during the Heinrich Event 1.

> **Since the YD to the present day: Mendukilo cave record**

- Extensive monitoring work has been carried out in Mendukilo cave, which has allowed us to understand the current dynamics in the transfer of the isotopic signal that takes place between rain, dripwater, and carbonate precipitation inside the cave. Therefore, it is determined that the amount of rainfall influences the $\delta^{18}O_p$ values in the precipitated carbonate samples on an interannual scale, but the seasonal impact is less pronounced. This appears to be true for the $\delta^{13}C_p$ values in the carbonate precipitates as well, although it also suggests greater degassing and possible pre-precipitation of calcite in the case of some drips.

- The record of speleothems from Mendukilo cave is made up of four stalagmites from the same gallery, composed of calcite, and with a similar petrography. As in the case of the Ostolo stalagmites, the few areas with a speleotemic fabric not particularly suitable for paleoclimatic work were discarded for the final interpretation.

- High-resolution U-Th dating of these four stalagmites revealed that they grew continuously during different intervals of the Holocene and Younger Dryas.

- The $\delta^{18}O_c$ and $\delta^{13}C_c$ series of the four Mendukilo stalagmites are remarkably well correlated with each other. This has allowed the creation of a single composite isotopic record from the Younger Dryas to the present.

- We infer that Sr/Ca values in these stalagmites may be influenced by the growth rate, whereas Mg/Ca may reflect variations due to previous calcite precipitation.

- By evaluating the composite $\delta^{13}C_c$ record from Mendukilo Cave in conjunction with trace element series and other records from the region, it was determined that higher (lower) $\delta^{13}C_c$ values are related to colder (warmer) and drier (wetter) intervals with reduced (improved) soil respiration and vegetation productivity.

- Petrographic and monitoring data suggest that the $\delta^{18}O_c$ record of the speleothems from Mendukilo captured an annual signal that was mainly influenced by i) the amount of rainfall, ii) changes in the isotopic composition of the ocean during the early part of the record (13-8 kyr), and iii) short-lived hydroclimate events throughout the Holocene.

- The dry and cold conditions during the Younger Dryas in this region resulted in slow growth (low Sr/Ca ratio), lower $\delta^{18}O_c$ values, and elevated $\delta^{13}C_c$ values. The $\delta^{18}O_c$ values recorded in Mendukilo during this period are higher than expected if cold temperatures were recorded. Changes in precipitation seasonality and ocean isotopic composition during the Younger Dryas may explain the different carbon and oxygen isotope patterns in Mendukilo speleothems.

- Both isotopic records, together with Sr/Ca ratios and growth rates, support the model of a progressive change towards wetter conditions between the beginning of the Holocene and 10.5-10.0 kyr (coinciding with the beginning of the Holocene Thermal Maximum at higher latitudes), which represents a delayed signal with respect to climate warming at the beginning of the Holocene.

- The onset of the Northgrippian (8.2 kyr) marks the end of the climate optimum in the region and a trend towards a drier climate (as recorded by the isotopic composite of $\delta^{13}C_c$) that culminated in the Neoglacial, a cold and dry period between 6.0 and 2.5 kyr.

- The Mendukilo oxygen isotope composite records, on a centennial scale, short-lived events at 8.2, 7.0-6.6, 5.5-4.8 and 2.8 kyr associated with major disturbances in North Atlantic deep-water circulation and sometimes as a result of meltwater intrusion (at least during the first two events). Two other events, 9.2 kyr and 4.2 kyr, are not captured by the $\delta^{18}O_c$ profile, but are clearly expressed in the $\delta^{13}C_c$ composite. We interpret these events to be dominated by dry and cold (rather than wet and cold) conditions, where changes in temperature and humidity have competing effects on the $\delta^{18}O_c$ signal.

> **Paleotemperature reconstruction since the last deglaciation in the northeast of the Iberian Peninsula**

- New series of stable isotopes are defined based on the δD_{FI} values from the analysis of fluid inclusions of Ostolo and Mendukilo stalagmites. These series are prepared in conjunction with high-resolution dating and compared with the $\delta^{18}O_c$ series described in previous chapters of this thesis.

- The δD_{FI} values of the Ostolo and Mendukilo stalagmites during the Holocene and GI-1 are comparable to those of modern day in each cave. In contrast, δD_{FI} values are more negative during GS-1 and GS-2.1a.

- Based on the monitoring results inside the Mendukilo and Ostolo caves (in conjunction with the rainwater monitoring results outside the Las Güixas cave), a transfer function was determined to convert the δD_{FI} values to a quantitative composite of temperature: the OM-FIT record.

- The OM-FIT record adds new and first non-biogenic evidence for the rapid temperature transitions during the last deglaciation and the Holocene period, accompanied by the identification of the most pronounced abrupt events that occurred during the last 16.5 kyr BP.

- Neither the $\delta^{18}O_c$ nor the OM-FIT records show important changes on a millennial scale during the Holocene. Even so, the OM-FIT allows us to identify short-lived climatic events that occurred during the Holocene.

- The 8.2 kyr event is recorded between 8.29 and 8.10 ± 0.04 kyr in the $\delta^{18}O_c$ record and is centered at 8.29 ± 0.07 kyr in the OM-FIT record, synchronous with Greenland ice-core data and well-dated records from central and SW Europe.

Conclusiones

> **Última deglaciación hasta el inicio del Holoceno: registro de la cueva de Ostolo**

- La cueva de Ostolo presenta serias dificultades para estudiar correctamente su dinámica actual por las dificultades de acceso. Aun así, los trabajos de monitorización al interior de la cavidad permitieron determinar que los valores de $\delta^{18}O$ en el agua de goteo y los carbonatos precipitados muestran que no existe variación estacional y que el carbonato precipita durante todo el año.

- Las tres estalagmitas obtenidas en la cueva de Ostolo están compuestas íntegramente de calcita y presentan petrografía similar. La mayoría de las estalagmitas muestran fabricas aptas para el muestreo e interpretación paleoclimática. La excepción recae en la fábrica columnar microcristalina, en la cual los resultados cronológicos (inversiones de edad) e isotópicos (falta de correlación entre espeleotemas) presentan una desviación notable en sus valores. Esto demuestra la importancia de realizar un análisis petrográfico previo, que permita descartar ciertos intervalos problemáticos antes de realizar análisis cronológicos y geoquímicos de mayor resolución en los espeleotemas.

- La cronología obtenida en los espeleotemas de Ostolo, los cuales presentan una elevada concentración de uranio, es de muy alta resolución y cuenta con bajos errores en comparación con cualquier otro registro de la última deglaciación en la región. Esto permite la creación de modelos de edad que pueden capturar los rápidos cambios climáticos durante el periodo de estudio.

- Las series de $\delta^{18}O_c$ de las tres estalagmitas de Ostolo, corregidas por cambios en el volumen de hielo y bien correlacionadas entre sí, se asemejan en amplitud a otros registros de $\delta^{18}O$ (en Groenlandia y el suroeste de Europa) directamente influenciados por cambios de temperatura durante la última deglaciación.

- Se observaron valores bajos de $\delta^{18}O_c$ durante las etapas frías (GS-1 y GS-2.1a), y valores más altos durante los eventos cálidos (GI-1 y Holoceno), lo que indica que la temperatura del aire fue dominante en esta señal isotópica.

- Además del efecto de la temperatura, las series $\delta^{18}O_c$ de estos espeleotemas están influenciadas por cambios en la composición isotópica de la fuente de humedad que afecta a estas cuevas. Un ejemplo ocurre durante el Evento Heinrich 1 cuando el agua de deshielo liberada al océano en el Atlántico Norte por la fusión de icebergs cambia la composición isotópica del océano.

> **Desde el YD hasta la actualidad: registro de la cueva de Mendukilo**

- En la cueva de Mendukilo se ha realizado un amplio trabajo de monitorización que ha permitido comprender la dinámica actual en la transferencia de la señal isotópica que se produce entre la lluvia, el agua de goteo y la precipitación de carbonatos en el interior de la cueva. Por lo tanto, se determina que la cantidad de lluvia influye en los valores de $\delta^{18}O_p$ en las muestras de carbonato precipitado a escala interanual, pero el impacto estacional es menos pronunciado. Esto parece ser cierto también para los valores de $\delta^{13}C_p$ en los precipitados de carbonato, aunque también sugiere una mayor desgasificación y un posible efecto de precipitación previa de la calcita en el caso de algunos goteos.

- El registro de espeleotemas de la cueva de Mendukilo está formado por cuatro estalagmitas de una misma galería, compuestas de calcita y con una petrografía similar. Como en el caso de las estalagmitas de Ostolo, las pocas zonas con una fábrica espeleotémica no especialmente adecuada para el trabajo paleoclimático fueron descartadas para la interpretación final.

- La datación U-Th de alta resolución de estas cuatro estalagmitas reveló que crecieron continuamente durante diferentes intervalos del Holoceno y el Younger Dryas.

- Las series $\delta^{18}O_c$ y $\delta^{13}C_c$ de las cuatro estalagmitas de Mendukilo están muy bien correlacionadas entre sí. Esto ha permitido la creación de un único registro isotópico compuesto que abarca desde el Younger Dryas hasta el presente.

- Inferimos que los valores de Sr/Ca en estas estalagmitas pueden estar influenciados por la tasa de crecimiento, mientras que Mg/Ca puede reflejar variaciones debido a la precipitación previa de calcita.

- Al evaluar el registro compuesto de $\delta^{13}C_c$ de la cueva Mendukilo junto con series de elementos traza y otros registros de la región, se determinó que los valores más altos (bajos) de $\delta^{13}C_c$ están relacionados con intervalos más fríos (cálidos) y más secos (húmedos) con intervalos reducidos (aumentados) de respiración del suelo y productividad de la vegetación.

- Los datos petrográficos y de monitorización sugieren que el registro $\delta^{18}O_c$ de los espeleotemas de Mendukilo captura una señal anual que fue influenciada principalmente por i) la cantidad de lluvia, ii) cambios en la composición isotópica del océano durante la primera parte del registro (13 -8 ka), y iii) eventos hidroclimáticos de corta duración a lo largo del Holoceno.

- Las condiciones secas y frías durante el Younger Dryas en esta región resultaron en un crecimiento lento (baja relación Sr/Ca), valores más bajos de $\delta^{18}O_c$ y valores

elevados de $\delta^{13}C_c$. Los valores de $\delta^{18}O_c$ registrados en Mendukilo durante este período son más altos de lo esperado si solo influyera el cambio de temperatura. Los cambios en la estacionalidad de las precipitaciones y la composición isotópica del océano durante el Younger Dryas pueden explicar los diferentes patrones de isótopos de carbono y oxígeno en los espeleotemas de Mendukilo.

- Ambos registros isotópicos, junto con las relaciones Sr/Ca y las tasas de crecimiento, apoyan el modelo de un cambio progresivo hacia condiciones más húmedas entre el inicio del Holoceno y los 10.5-10.0 ka (coincidiendo con el inicio del Máximo Térmico del Holoceno en latitudes superiores), lo que representa una señal retrasada con respecto al calentamiento climático a principios del Holoceno.

- El inicio del Northgrippian (8.2 ka) marca el final del óptimo climático en la región y una tendencia hacia un clima más seco (como lo registra el compuesto isotópico de $\delta^{13}C_c$) que culminó en el Neoglacial, un período frío y seco entre 6.0 y 2.5 ka.

- El compuesto de isótopos de oxígeno de Mendukilo registra, a escala centenaria, eventos de corta duración a 8.2, 7.0-6.6, 5.5-4.8 y 2.8 ka, los cuales están asociados con perturbaciones importantes en la circulación de aguas profundas del Atlántico norte y, a veces, como resultado de la intrusión de agua de deshielo (al menos durante los dos primeros eventos). Otros dos eventos, a 9.2 ka y 4.2 ka, no son capturados por el perfil de $\delta^{18}O_c$, pero se expresan claramente en el perfil compuesto de $\delta^{13}C_c$. Interpretamos que estos eventos están dominados por condiciones secas y frías (en lugar de húmedas y frías), donde los cambios de temperatura y humedad tienen efectos opuestos en la señal de $\delta^{18}O_c$.

> **Reconstrucción de paleotemperatura desde la última deglaciación en el noreste de la Península Ibérica**

- Se definen nuevas series de isótopos estables en base a los valores de δD_{FI} obtenidos del análisis de inclusiones fluidas de las estalagmitas de Ostolo y Mendukilo. Estas series se preparan junto con dataciones de alta resolución y se comparan con las series $\delta^{18}O_c$ descritas en capítulos anteriores de esta tesis.

- Los valores de δD_{FI} de las estalagmitas Ostolo y Mendukilo durante el Holoceno y GI-1 son comparables a los actuales determinados para cada cueva. Por el contrario, los valores de δD_{FI} son más negativos durante GS-1 y GS-2.1a.

- Gracias a los resultados de monitorización dentro de las cuevas de Mendukilo y Ostolo (en conjunto con los resultados de la monitorización de agua de lluvia fuera de la cueva de Güixas), se determinó una función de transferencia para convertir los valores de δD_{FI} a un compuesto cuantitativo de temperatura: el registro OM-FIT.

- El registro OM-FIT proporciona nueva y primera evidencia no biogénica cuantitativa de las rápidas transiciones de temperatura durante la última deglaciación y el Holoceno. Además, permite identificar y cuantificar su cambio térmico durante los eventos abruptos que ocurrieron en los últimos 16,5 ka antes del presente.

- Los registros de $\delta^{18}O_c$ y el OM-FIT no muestran cambios importantes a escala milenaria durante el Holoceno. Aun así, el OM-FIT nos permite identificar eventos climáticos de corta duración ocurridos durante el Holoceno.

- El evento de 8.2 ka se registró entre 8.29 y 8.10 ± 0.04 ka en el perfil de $\delta^{18}O_c$ y está centrado en 8.29 ± 0.07 ka en el OM-FIT, sincrónico con los datos de testigos de hielo de Groenlandia y registros bien datados de zona central y el suroeste de Europa.

VII.2 Future perspectives

The speleothem record of the Ostolo and Mendukilo caves is not limited to the results discussed in this thesis dissertation; in fact, it is not even half of the stalagmites dated at high resolution over the last five years that have been presented. Therefore, as a first point in future perspectives, the next efforts in these new stalagmites should be aimed at obtaining new isotopic and trace element series that cover new periods (e.g., with older ages within the last deglaciation) and replicate those recorded in this thesis (e.g., expanding the Ostolo record to the late Holocene).

The δ^{13}C series in the Ostolo stalagmites has not yet been correctly interpreted and is one of the great unknowns in the last years of this thesis. A first step in deciphering this mystery in the future is to expand the chronology of the Ostolo isotope and trace element series. Other perspectives to be resolved in the future are: i) understanding the speleogenesis of the Ostolo cave and the different flooding events during the past; ii) carrying out more extensive and periodic monitoring work inside and outside the cavity; iii) studying the variation of this δ^{13}C signal in the epikarst and its subsequent transfer in the speleothems inside the cave.

Working in this group with new techniques, such as fluid inclusions, has been a challenge, with complications during the analysis and subsequent interpretations. Therefore, the paleotemperature records presented in this thesis can be improved in three main ways: i) obtaining more analyses of fluid inclusions in other stalagmites from both caves; ii) monitoring the isotopic concentration of rainwater over several years in areas surrounding Ostolo and/or Mendukilo, which would allow us to better understand its variation and improve paleotemperature calculations in both caves; and iii) studying the petrographic changes in the distribution of fluid inclusions in these speleothems. New TEMPURE project to be developed in the IPE-CSIC will provide great opportunities to quantify temperature changes during abrupt climate transitions by using innovative techniques, such as biomarkers or clumped isotopes.

There are other speleothem records from different caves in NE Iberia that have also been dated. These unresolved records can help deciphering the different unknowns in this thesis and validate what was seen in Mendukilo and Ostolo in paleoclimatic terms.

VIII.   Supplementary Annex

VIII.1   Monitoring of rain events in northeastern Spain

To explore the relationship between the isotopic composition of rainfall and air temperature in northern Iberia, rainwater event sampling was conducted in the vicinity of the University of the Basque Country (Bilbao). The correlations (Fig. 8.1.A and Fig. 8.1.B) between daily temperature and precipitation with $\delta^{18}O_r$ are low but significant, with a correlation coefficient of 0.2. In the case of precipitation, only events with rainfall above 3 mm were considered. Dripwater isotopic values in Mendukilo cave display a water line that is very similar to the local meteoric water line established by the rainfall isotopic values ($\delta^{18}O_r$, δD_r), with much lower variability than that observed in the rainfall values. Therefore, the seasonality recorded in rainfall was also observed in the drip water, although it was much more reduced due to homogenization once water enters the epikarst (Fig. 5.7.C).

VIII.2   Types of drip sites in Mendukilo cave

Knowledge of dripwater hydrology is critical for speleothem-based paleoclimate studies (Baldini et al., 2006). To categorize vadose discharge in caves, the maximum discharge and the coefficient of variation of the latter are commonly used (Smart and Friederich, 1987). Four types of drip sites have been observed in Mendukilo cave (Fig. 8.2):

> **MEN-A:** Variability and maximum discharge of this drip site is very high, and they respond rapidly to rain events (i.e., low residence time within the karst system).
> **MEN-B:** Also shows significant variability following large rainfall events, but its discharge is lower.
> **MEN-D:** Medium variability and low maximum discharge.
> **MEN-E:** Low variability and low discharge.

The drips MEN D and MEN E, between seasonal and seepage, are the ones that give a better response to climatic changes in relation to the ones controlled by hydrological variations within the endokarst.
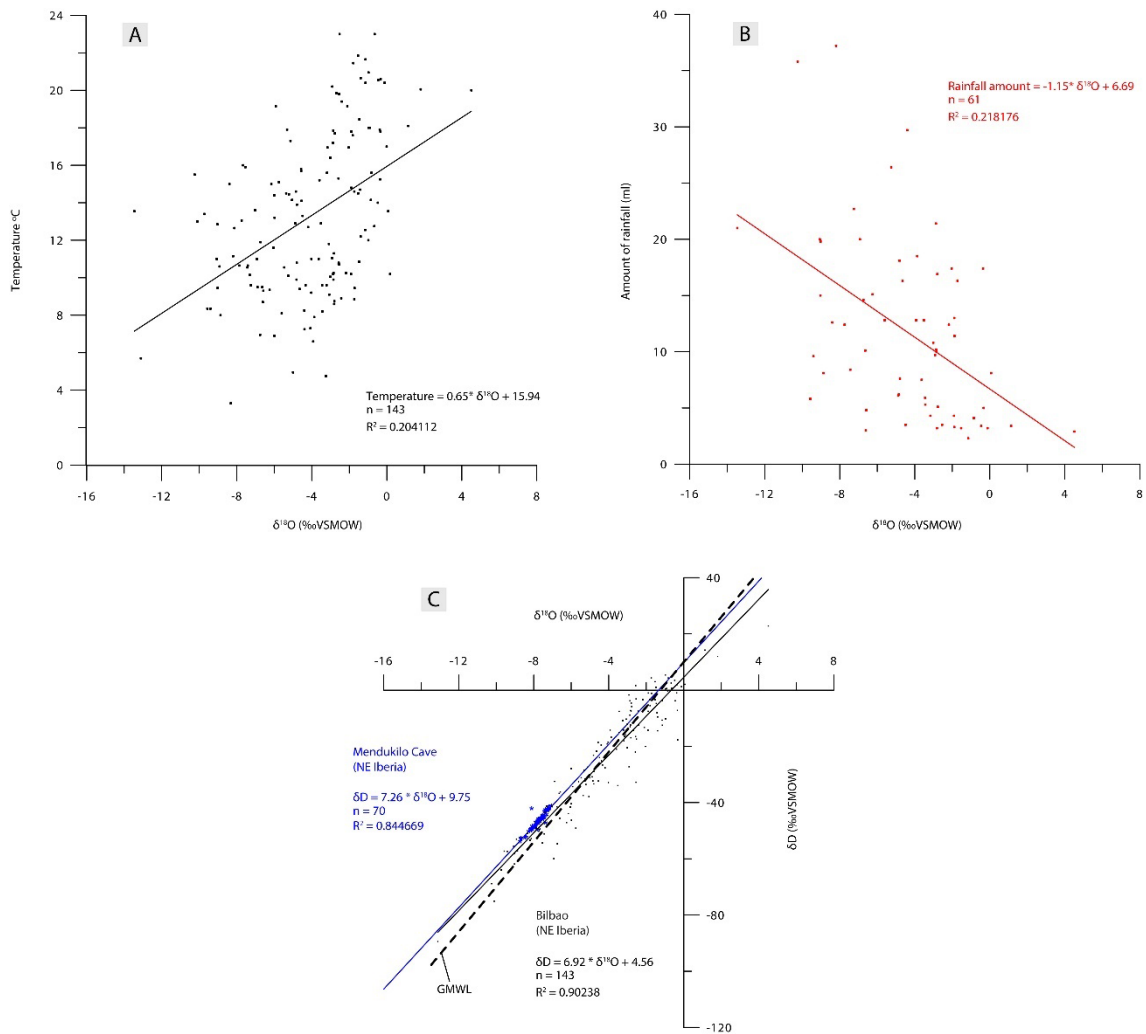
Fig 8.1. *A) Relationship between $\delta^{18}O_r$ and temperature for individual rainfall events. B) Relationship between $\delta^{18}O_r$ and amount of rainfall for individual rainfall events (only those with rainfall amount > 3mm). C) Relationship between $\delta^{18}O_r$ and δD_r in rainwater (black dots) and dripwater (blue stars). GMWL: Global Meteoric Water Line.*
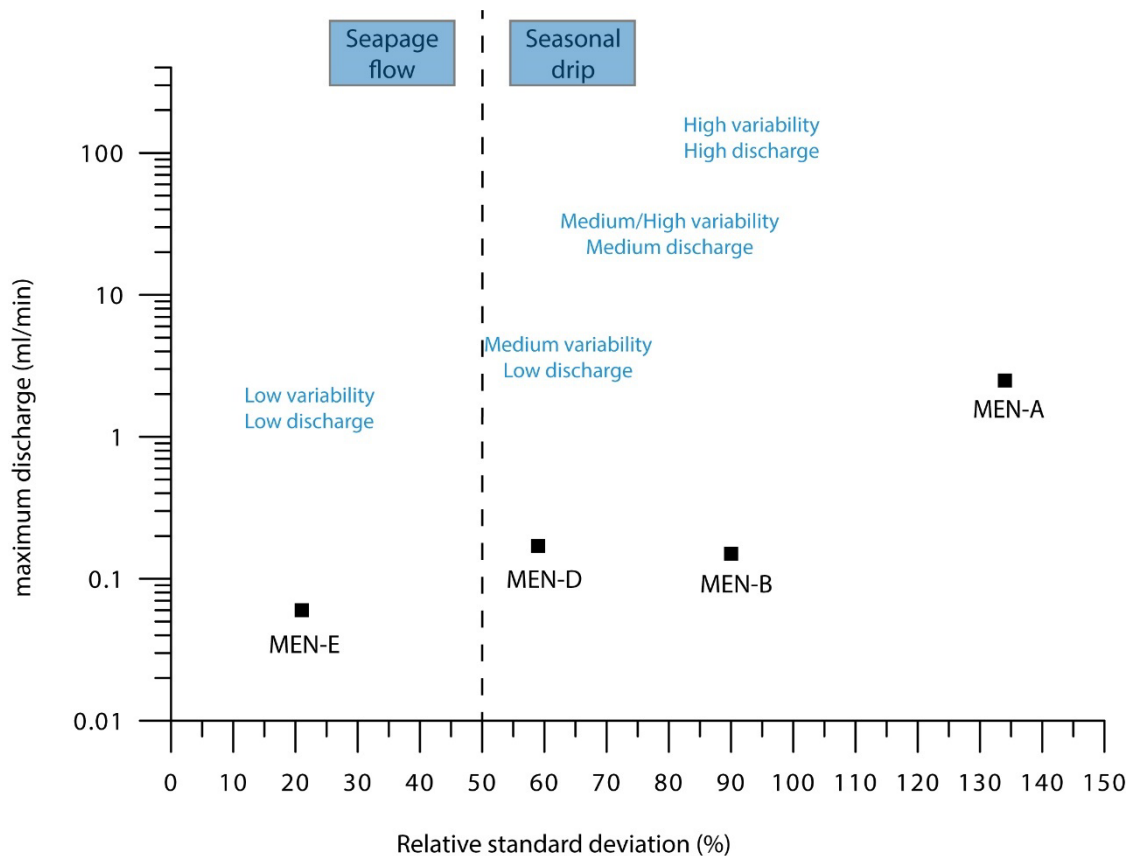
Fig 8.2. *Variability of the monitored drip sites in Mendukilo cave in relation to their maximum discharge (note logarithmic scale) using the classification scheme of Smart & Friederich (1987).*

VIII.3 Isotopic and trace element records of speleothems from Mendukilo cave

Splicing of the isotopic records of four speleothems (MEN-2, MEN-3, MEN-4, and MEN-5) (Fig. 8.3 and Fig. 8.4) was performed using Iscam (see the main text). The correlation between the different MEN stalagmite records is good, and they cover, with more than one record, the entire Holocene and the Younger Dryas (Fig. 8.3 and Fig. 8.4). The exception is the period 8.8-12.8 kyr BP, which is only represented by one stalagmite (MEN-2). The Mg and Sr records for the four stalagmites are shown in Fig. 8.5 and Fig. 8.6 respectively. As is the case for the isotope data, the individual Sr/Ca records correlate well with each other (Fig. 8.6). On the other hand, the Mg/Ca record is characterized by a low signal/noise ratio, and the correlation between the records is weak (Fig. 8.5). Sr/Ca can be conditioned by the growth rate of the stalagmites on a millennial time scale.
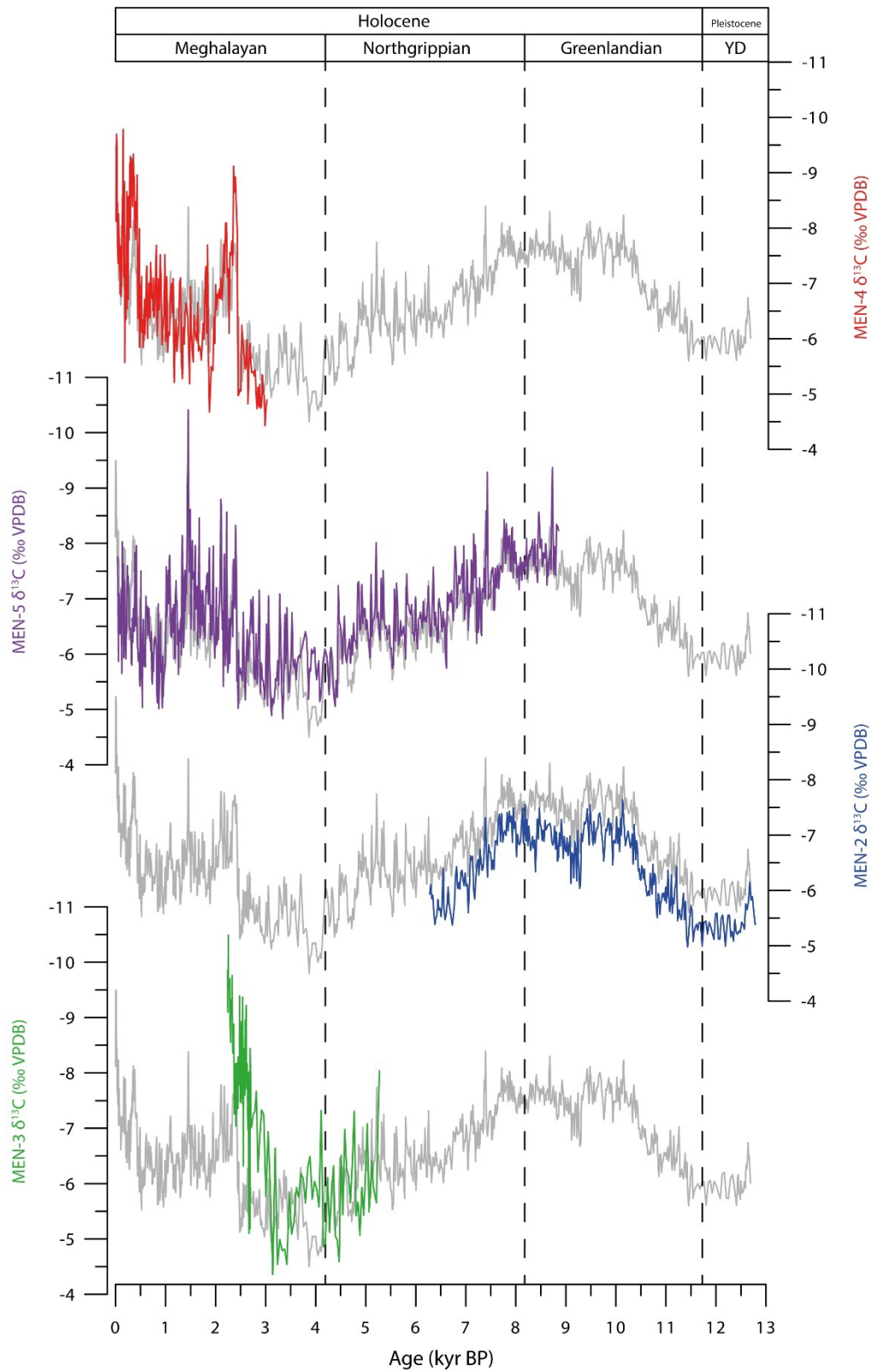
Fig 8.3. *Stable $\delta^{13}C_c$ isotope records of each of the four speleothems plotted on their age models. The $\delta^{13}C_c$ values of the MEN composite (grey lines) used in this work are shown behind the values of each stalagmite.*
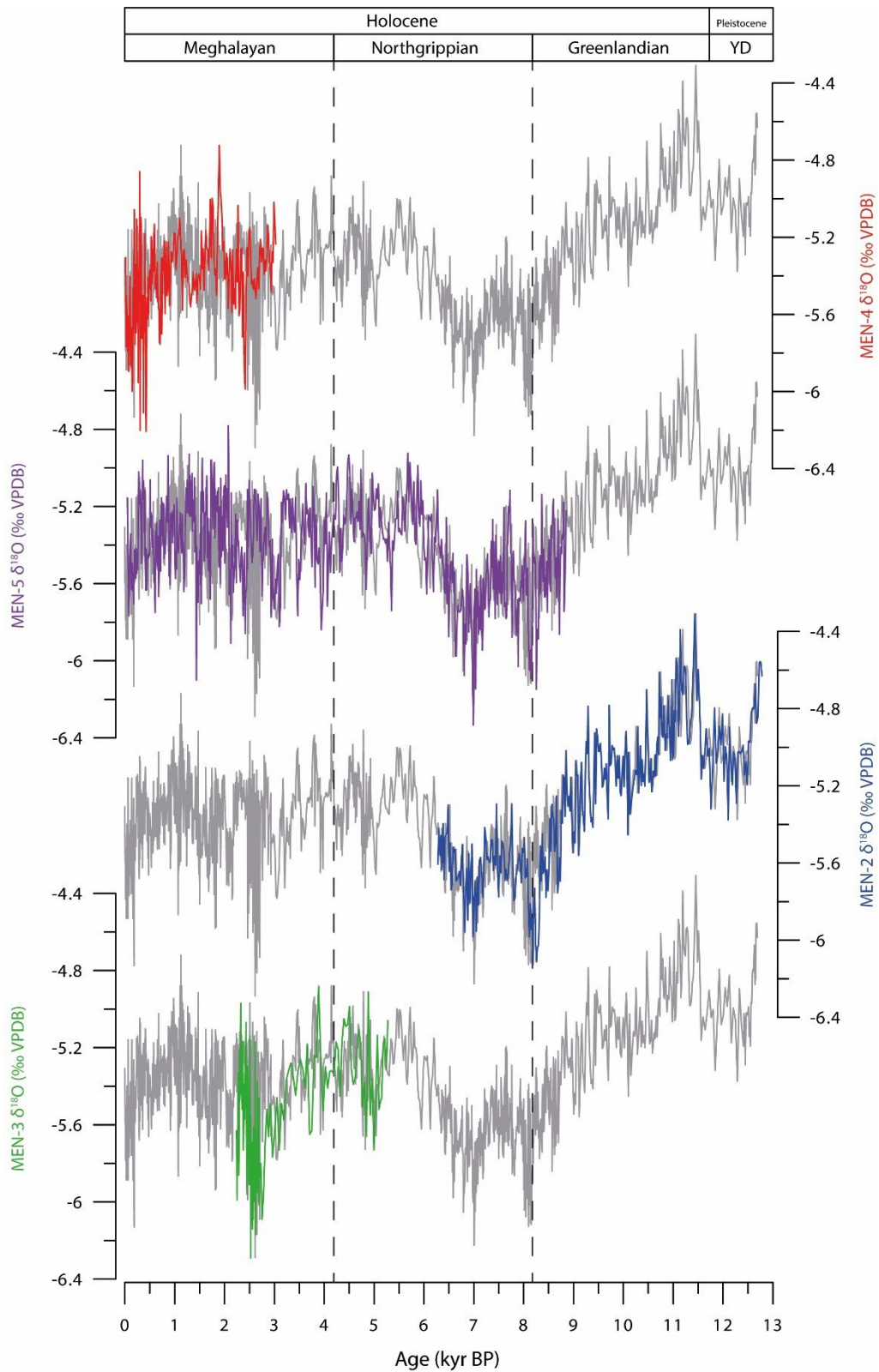
Fig 8.4. *Stable δ¹⁸Oc isotope records of each of the four speleothems plotted on their age models. The δ¹⁸Oc values of the MEN composite (grey lines) used in this work are shown behind the values of each stalagmite.*
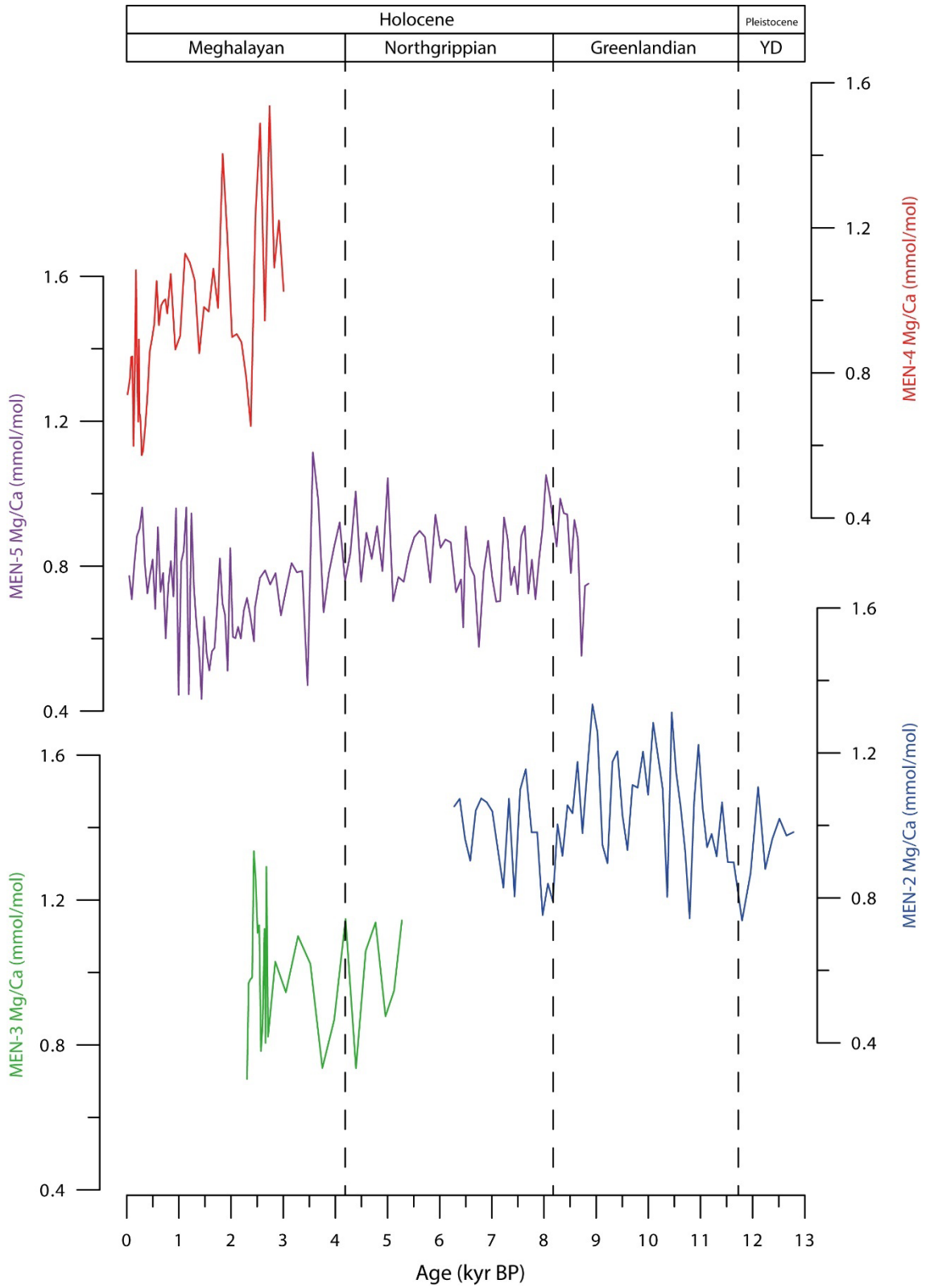
Fig 8.5. *Mg/Ca data (mmol/mol) of each MEN stalagmite.*
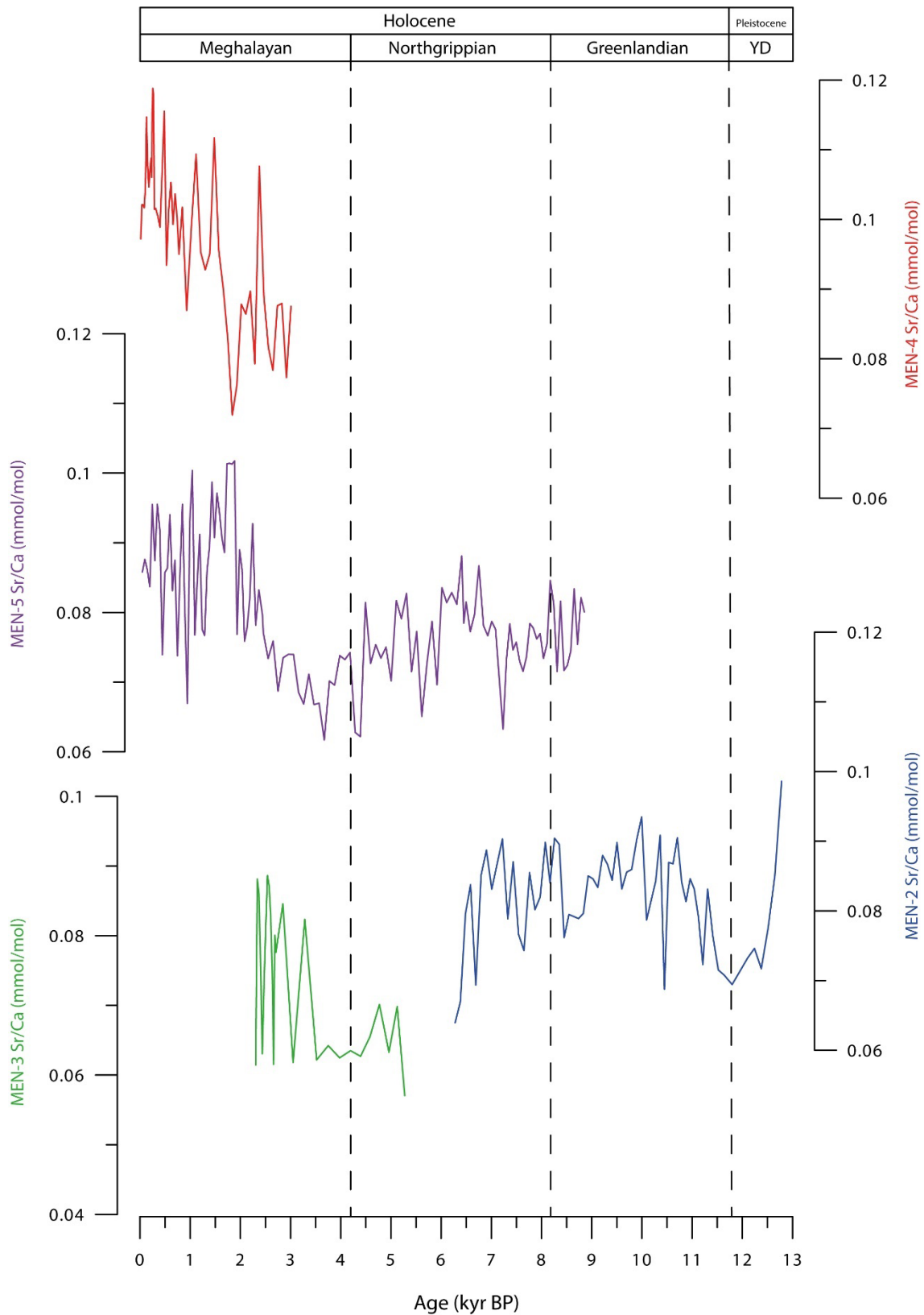
Fig 8.6. *Sr/Ca data (mmol/mol) of each MEN stalagmite.*

163

When the records are compared directly (Fig. 8.7), it appears that Sr/Ca is higher when $\delta^{13}C_c$ is more negative and correlates with variations in the growth rate of the MEN composite. This correlation allows PCP to be discarded as the main process controlling the variability.

To assess paleohydrological changes in the vadose karst system, isotope records are often compared with trace element data (e.g., Mg, Sr, and Ba) (Fairchild & Treble, 2009). For this purpose, $\delta^{13}C_c$ data are analyzed for PCP indicators, such as Mg/Ca. In Fig. 8.8, when there is a trend in the carbon isotopes, but the color of the sample points is the same (meaning you have the same PCP), it is an evidence that the carbon isotope trend is not driven by PCP. Between 9 and 3 kyr BP, the less negative trend of -3 ‰ in $\delta^{13}C_c$ is accompanied by Mg/Ca values between red and orange colors, which have similar values (between 0.7 to 1). Continuing with this idea, when the values become more negative between 2.5 and 1.5 kyr BP the colors of Mg/Ca vary from green to light blue (between 0.4 and 0.7). This low Mg/Ca variability between the $\delta^{13}C_c$ different trends confirm that the MEN $\delta^{13}C_c$ composite is not directly influenced by PCP variations.

A way to evaluate Sr/Ca data is to look at the Sr/Mg ratio of each stalagmite record (Fig. 8.9). Each MEN Sr/Mg record shows a good agreement with the corresponding growth rate, which indicates that Sr/Ca variations are controlled by changes in the growth rate (Fig. 8.9). This is because Mg/Ca is more variable between the different records and is certainly more affected by prior calcite precipitation (PCP) than Sr/Ca, while the Sr/Mg ratio allows to disentangle the growth rate effect.

We tested the relationship between the MEN $\delta^{18}O_c$ composite record and the seawater isotopic composition ($\delta^{18}O_{sw}$) derived from foraminifera in North Atlantic sediment cores (Fig. 8.10). Changes in seawater isotopic composition had a significant impact on the MEN $\delta^{18}O_c$ composite record in the early part of the Holocene (between 11.5 and 8.5 kyr) when melting of Northern Hemisphere ice sheets was still ongoing. Since 8 kyr $\delta^{18}O_{sw}$ and the MEN $\delta^{18}O_c$ composite record show smaller variations but short-term changes in ocean composition, not captured by the low resolution $\delta^{18}O_{sw}$ (e.g., the 8.2 kyr event) also contributed to variations in MEN $\delta^{18}O_c$.
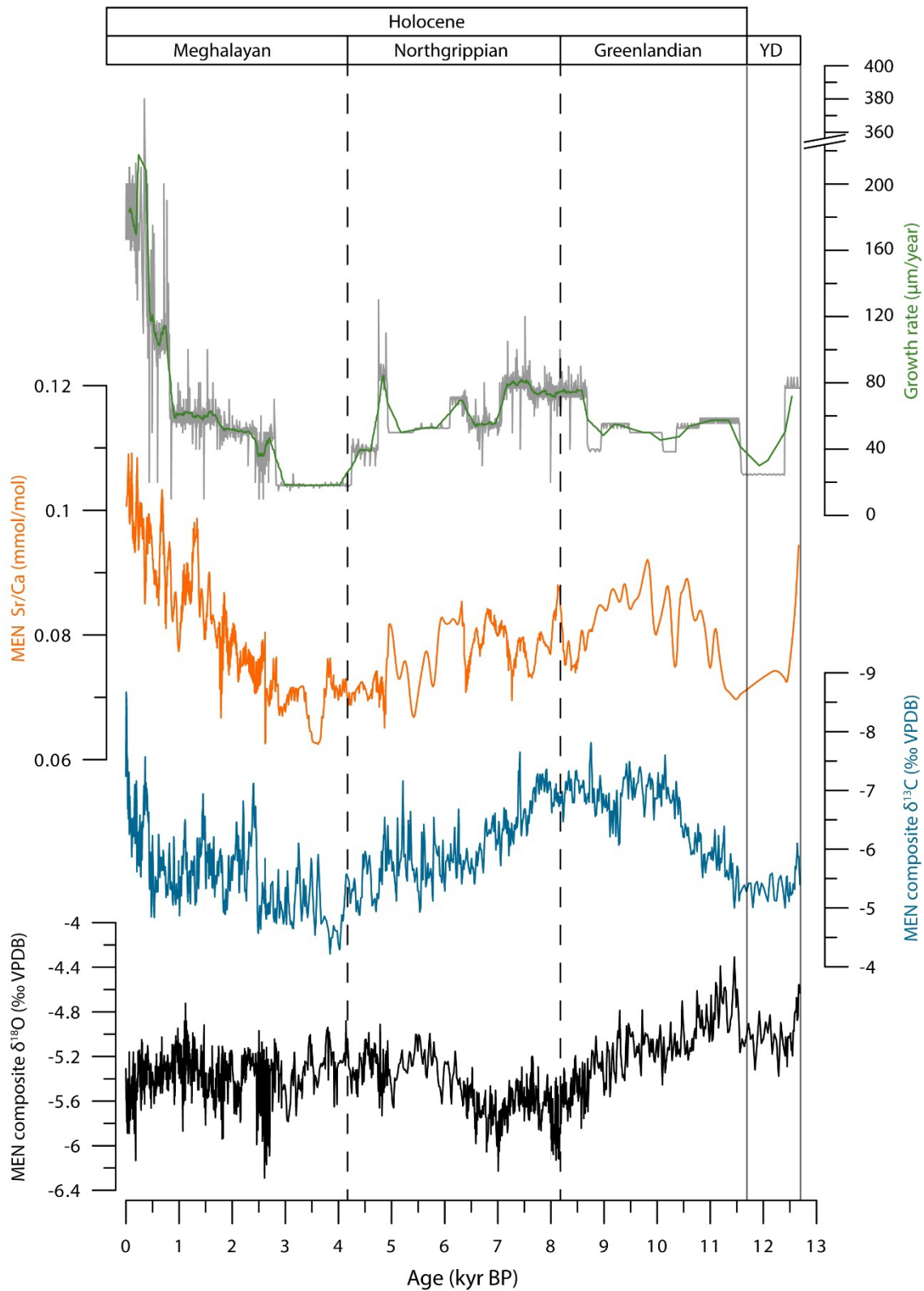
Fig 8.7. *Trace elements (Sr/Ca) composite series compared to growth rate and the MEN isotope composite δ¹³Cc and δ¹⁸Oc values.*
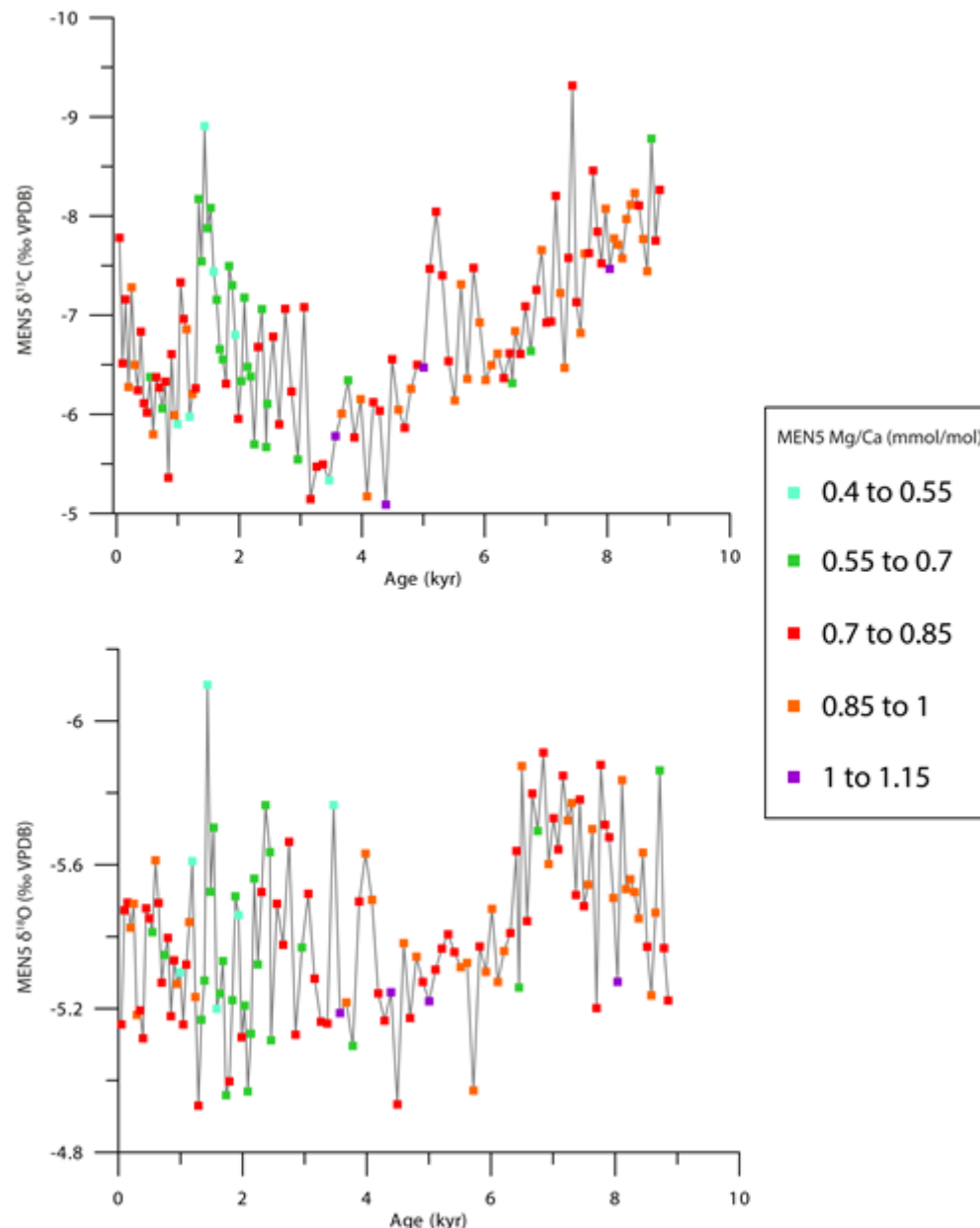
Fig 8.8. *MEN5 $\delta^{13}C_c$ and $\delta^{18}O_c$ data color-coded for Mg/Ca (grouped in 5 classes).*
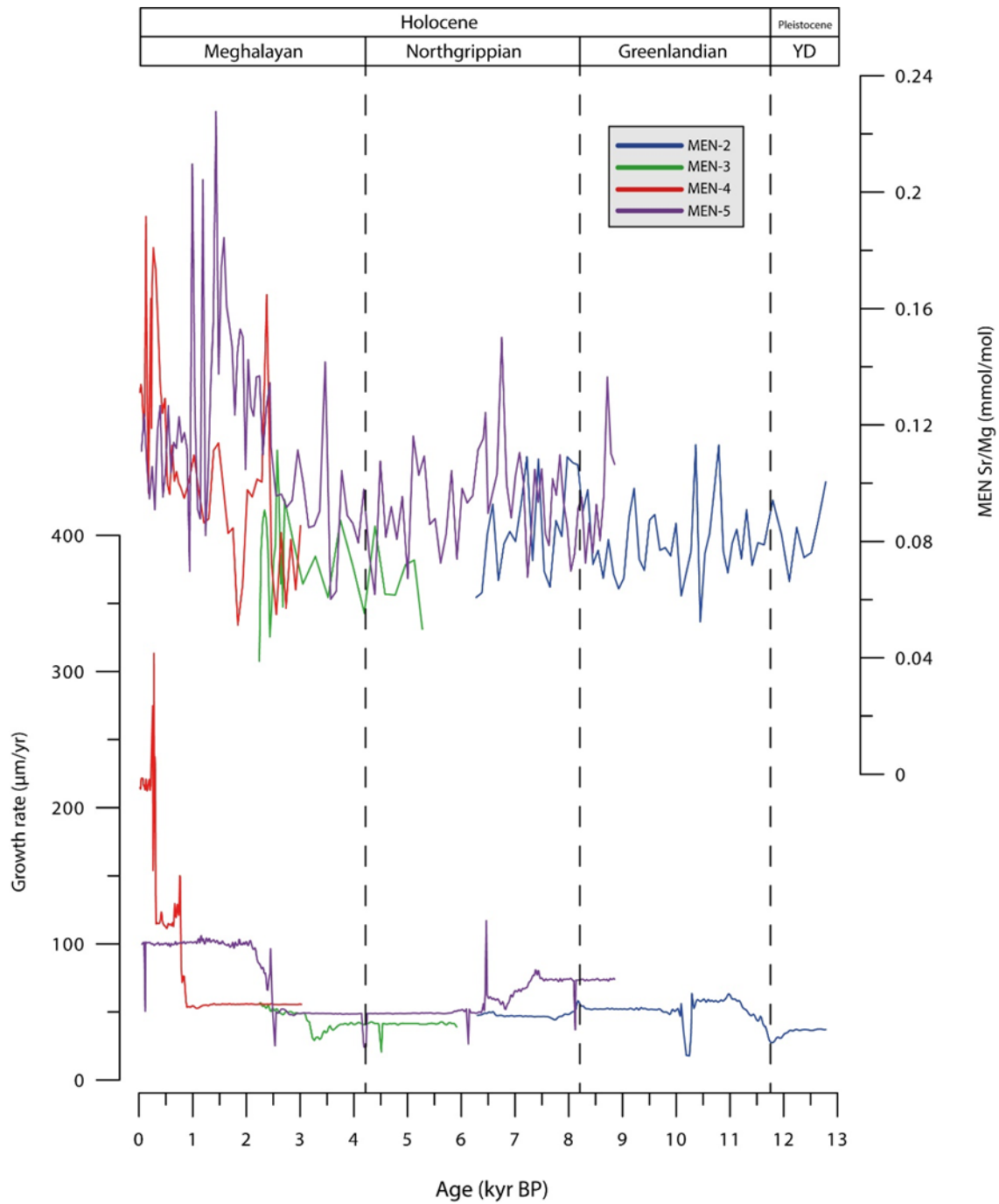
Fig 8.9. *Sr/Mg ratio of each stalagmite compared with the respective growth rate.*
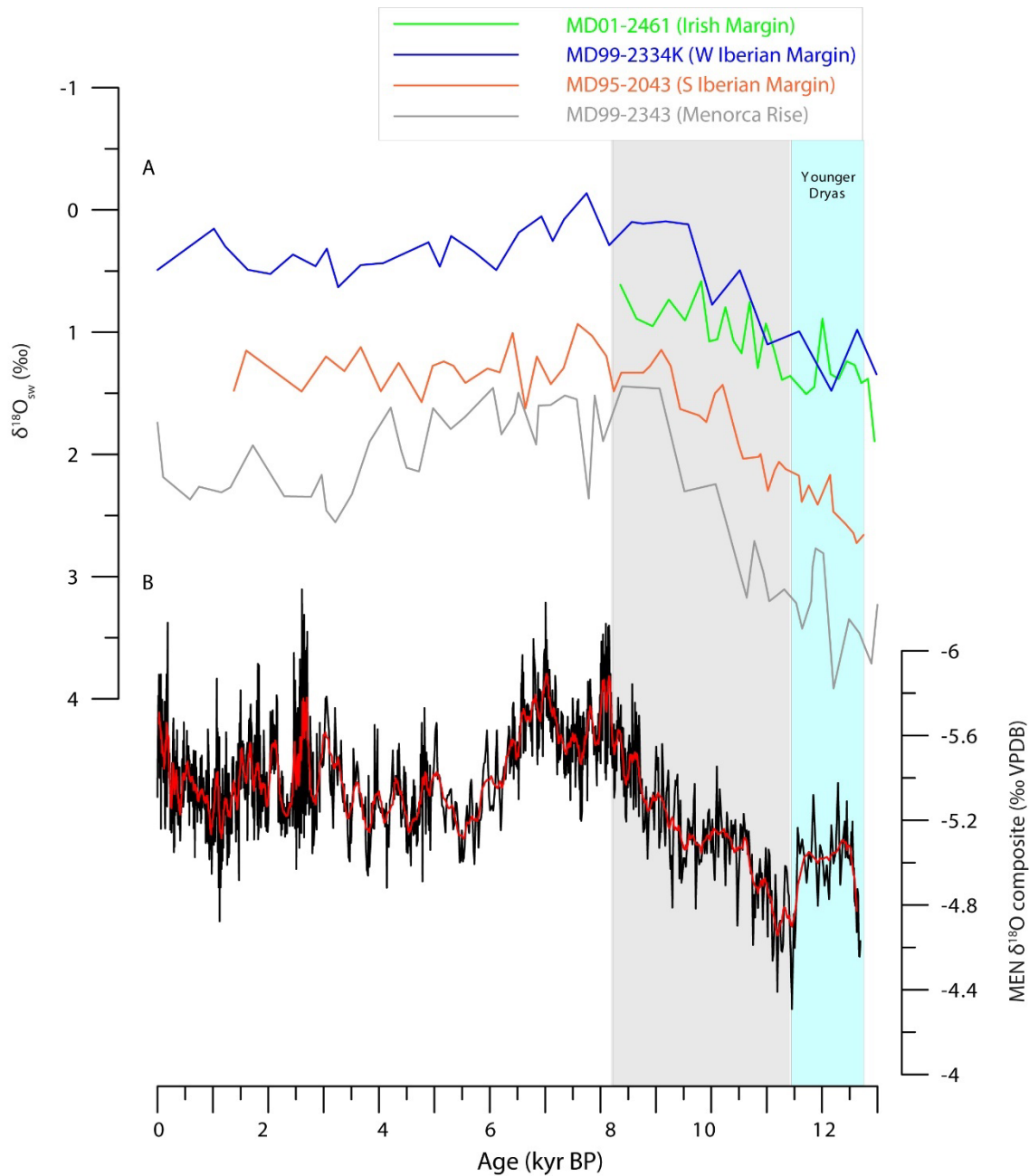
Fig 8.10. *Comparison of the seawater isotopic composition ($\delta^{18}O_{sw}$) and the $\delta^{18}O_c$*
MEN composite record. A) $\delta^{18}O_{sw}$ from paired Mg/Ca and $\delta^{18}O$ data of **Globigerina**
bulloides *from the W Iberian Margin (Skinner & Shackleton, 2006), Irish Margin*
(Peck et al., 2006), S Iberian Margin and the Menorca Rise (Català et al., 2019). B)
$\delta^{18}O_c$ MEN composite record (note inverted y axis).

VIII.4   Paleotemperatures and transfer function

Following Affolter et al. (2019) and (Honiat et al., 2023) the calculation of paleotemperatures (T_{past}) has been carried out with the following transfer function:

Table 8.1. *Summary of cave altitude, modern cave dripwater δD_d values (‰ VSMOW), modern MAAT (ºC) at each site and the gradient $\delta D_r/T$ determined outside of Güixas cave, Villanua. *Corrected in relation to the altitude of Villanua.*

Study site	Ostolo cave (250 m a.s.l.)	Mendukilo cave (750 m a.s.l.)	Güixas cave (950 m a.s.l.)
T_{modern}	10.0 ºC*	10.9 ºC*	10.0 ºC
δD_{modern}	-48.96 ‰	-48.48 ‰	
$\delta D/T_{gradient}$	4.4 ‰/ºC		

$$T_{past} = T_{modern} - \frac{\delta D_{modern} - \delta D_{FI\,corrected}}{\delta D / T_{gradient}}$$

Table 8.2. *(Next page) Paleotemperatures obtained from δD_{FI} data (calibrated average of individual values) using the OM-FIT transfer function. δD_{FI} was corrected for global ice-volume changes (Bintanja et al., 2005).*

Sample	Age	δD_{FI}	δD	T_{past}	Error
(in stratigraphic order)	*(kyr)*	*corrected (‰ VSMOW)*	*corrected error*	*(ºC)* *OM-FIT*	*± (ºC)*
OST2-16700	16.70	-57.1	2.4	8.1	2.2
OST2-16401	16.40	-57.3	2.7	8.5	2.0
OST3-16399		-53.6	2.4		
OST1-16061	16.06	-57.0	1.6	8.2	1.8
OST2-15803	15.80	-66.8	2.4	5.9	2.2
OST2-15309	15.31	-53.5	2.6	9.0	2.0
OST1-15164	15.16	-58.0	2.8	7.9	2.1
OST2-14711	14.71	-44.7	2.4	11.0	2.2
OST1-14565	14.57	-31.4	0.9	14.0	1.6
OST3-14301	14.30	-31.8	2.4	13.9	2.0
OST1-14196	14.14	-49.1	0.4	10.1	2.1
OST3-14105		-40.9	1.6		
OST2-14103		-56.0	6.4		
OST3-13501	13.50	-39.9	2.2	12.1	1.9
OST1-13015	13.08	-37.0	2.4	13.3	2.0
OST2-13005		-30.5	3.3		
OST3-13003		-35.4	2.4		
OST3-12903	12.90	-46.9	2.4	10.7	1.8
OST2-12902		-45.2	1.0		
MEN2-12900	12.90	-44.9	2.6	11.8	1.7
OST3-12802	12.80	-48.0	2.4	10.2	2.0
MEN2-12783	12.78	-52.0	1.3	10.2	1.5
MEN2-12649	12.65	-61.3	2.7	8.0	2.0
MEN2-12513	12.51	-52.0	1.5	10.2	1.6
OST2-12498	12.50	-54.7	0.5	8.7	1.6
MEN2-12323	12.32	-51.7	3.8	10.2	2.1
OST2-12297	12.30	-53.7	6.9	8.9	3.0
MEN2-12215	12.22	-50.1	4.2	10.6	2.2
MEN2-12078	12.08	-51.5	1.9	10.3	1.7
MEN2-11831	11.83	-48.5	1.9	11.0	1.6

OST2-11800	11.80	-47.6	2.4	10.3	2.2
OST3-11671	11.60	-27.9	1.6	13.4	1.8
OST2-11649		-39.7	1.8		
OST3-11599	11.60	-42.6	6.4	11.4	2.9
MEN2-11588	11.59	-47.2	3.8	11.2	2.1
MEN2-11499	11.50	-43.2	2.4	12.1	1.4
OST2-11497	11.49	-31.5	0.1	13.5	1.6
OST3-11491		-35.6	1.2		
MEN2-11476	11.48	-36.3	2.3	13.7	1.5
MEN2-11370	11.37	-53.5	1.5	9.8	1.8
OST3-11303	11.30	-42.6	0.6	11.4	1.6
MEN2-11196	11.20	-42.1	3.2	12.4	1.8
MEN2-11009	11.01	-37.5	0.3	13.4	1.1
OST1-10953	10.93	-28.9	3.8	13.1	2.6
OST2-10904		-41.9	6.8		
MEN2-10928	10.93	-45.9	2.6	11.5	1.8
MEN2-10810	10.81	-48.6	1.9	10.9	1.6
MEN2-10688	10.69	-39.9	2.2	12.9	1.6
MEN2-10602	10.60	-45.3	1.5	11.7	1.5
MEN2-10414	10.41	-39.0	1.4	13.1	1.3
MEN2-10275	10.28	-44.7	3.7	11.8	2.0
MEN2-10075	10.08	-48.2	2.5	11.0	1.8
MEN2-9956	9.96	-34.6	4.1	14.1	1.9
MEN2-9836	9.84	-42.2	0.8	12.4	1.3
MEN2-9426	9.43	-39.6	6.4	12.9	2.6
MEN2-9293	9.29	-50.6	3.2	10.4	1.9
MEN2-9006	9.01	-40.4	0.2	12.8	1.1
MEN2-8852	8.85	-45.3	3.4	11.7	1.9
MEN2-8718	8.72	-39.4	4.2	12.9	1.9
MEN5-8718		-39.8	2.9		
MEN5-8582	8.57	-40.8	1.6	12.4	1.5
MEN2-8565		-43.3	1.7		

MEN5-8447	8.44	-41.4	3.5	12.2	1.6
MEN2-8431		-44.2	0.6		
MEN5-8311	8.29	-56.3	6.5	9.5	2.5
MEN2-8278		-53.6	4.0		
MEN5-8175	8.18	-40.7	2.3	12.7	1.6
MEN5-8039	8.04	-44.9	2.8	11.7	1.8
MEN5-7904	7.90	-43.5	3.9	12.0	2.0
MEN5-7836	7.84	-50.3	1.2	10.5	1.5
MEN5-7767	7.77	-38.2	3.8	13.2	1.9
MEN5-7632	7.63	-44.8	4.5	11.8	2.2
MEN2-7542	7.53	-40.2	2.4	12.7	1.9
MEN5-7496		-41.3	4.5		
MEN5-7368	7.37	-37.2	4.0	13.5	2.0
MEN5-7233	7.23	-44.7	1.1	11.2	1.8
MEN5-7200		-50.1	4.0		
MEN5-7084	7.08	-44.5	3.0	11.8	1.8
MEN5-6929	6.91	-49.0	2.3	11.1	1.6
MEN2-6880		-46.3	1.7		
MEN5-6752	6.75	-44.5	2.7	11.8	1.7
MEN2-6586	6.58	-47.2	3.1	11.7	1.8
MEN5-6581		-43.0	2.7		
MEN2-6465	6.46	-50.6	1.3	11.7	1.6
MEN5-6451		-39.1	2.9		
MEN2-6342	6.33	-44.8	1.8	12.0	1.5
MEN5-6313		-42.9	1.7		
MEN2-6279	6.28	-46.7	5.1	11.3	2.4
MEN2-6200	6.20	-44.8	0.8	11.8	1.3
MEN5-6113	6.11	-38.54	2.1	13.2	1.5
MEN5-5919	5.92	-44.37	4.8	11.8	2.3
MEN5-5718	5.72	-39.40	3.1	13.0	1.8
MEN5-5513	5.51	-45.15	4.3	11.7	2.2
MEN5-5310	5.31	-39.50	3.3	12.9	1.8
MEN5-5106	5.11	-46.49	2.8	11.4	1.8

172

MEN5-4902	4.90	-39.62	2.6	12.9	1.7
MEN5-4697	4.70	-44.05	1.2	11.9	1.4
MEN5-4288	4.29	-49.26	1.0	10.7	1.4
MEN5-4083	4.08	-45.62	3.1	11.6	1.9
MEN5-3878	3.88	-38.93	1.9	13.1	1.5
MEN5-3672	3.67	-44.06	1.1	11.9	1.4
MEN5-3263	3.26	-41.56	3.8	12.5	2.0
MEN5-3059	3.06	-44.23	3.4	11.9	1.9
MEN5-2853	2.85	-41.85	2.9	12.4	1.7
MEN5-2653	2.65	-37.84	3.1	13.3	1.7
MEN5-2370	2.37	-37.31	1.7	13.4	1.4
MEN5-2245	2.25	-47.84	4.9	11.0	2.3
MEN5-1836	1.84	-34.18	3.1	14.2	1.7
MEN5-1735	1.74	-36.14	3.4	13.7	1.8
MEN5-1634	1.63	-46.64	0.6	11.3	1.3
MEN5-1534	1.53	-38.15	2.3	13.2	1.5
MEN5-1435	1.44	-39.73	3.9	12.9	2.0
MEN5-1337	1.34	-41.35	3.8	12.5	2.0
MEN5-1240	1.24	-41.64	1.7	12.5	1.5
MEN5-1094	1.09	-35.59	1.1	13.8	1.2
MEN5-995	1.00	-46.40	3.0	11.4	1.8
MEN5-896	0.90	-38.55	3.2	13.2	1.8
MEN5-747	0.75	-45.09	1.9	11.7	1.5
MEN5-648	0.65	-46.48	1.6	11.4	1.5
MEN5-547	0.55	-45.51	3.3	11.6	1.9
MEN5-447	0.45	-43.25	3.0	12.1	1.9
MEN5-347	0.35	-43.13	2.1	12.1	1.8
MEN5-247	0.25	-46.99	3.2	11.2	1.9
MEN5-147	0.15	-43.77	3.7	12.0	2.0

References

Ábalos, B. (2016). Geologic map of the Basque-Cantabrian Basin and a new tectonic interpretation of the Basque Arc. *International Journal of Earth Sciences*, *105*(8), Article 8. https://doi.org/10.1007/s00531-016-1291-6

Affolter, S., Fleitmann, D., & Leuenberger, M. (2014). New online method for water isotope analysis of speleothem fluid inclusions using laser absorption spectroscopy (WS-CRDS). *Climate of the Past*, *10*(4), Article 4. https://doi.org/10.5194/cp-10-1291-2014

Affolter, S., Häuselmann, A., Fleitmann, D., Edwards, R. L., Cheng, H., & Leuenberger, M. (2019). Central Europe temperature constrained by speleothem fluid inclusion water isotopes over the past 14,000 years. *Science Advances*, *5*(6), Article 6. https://doi.org/10.1126/sciadv.aav3809

Aguirre, E. (2008). *Cueva de Mendukilo: Valle del Larraun, Navarra = Mendukilo Lezea: Larraungo Bailaran, Nafarroa*. Lekunberri, Navarra Cuevas de Astitz.

Allen, J. R. M., Huntley, B., & Watts, W. A. (1996). The vegetation and climate of northwest Iberia over the last 14,000 years. *Journal of Quaternary Science*, *11*(2), Article 2. https://doi.org/10.1002/(SICI)1099-1417(199603/04)11:2<125::AID-JQS232>3.0.CO;2-U

Alley, R., & Agustsdottir, A. (2005). The 8k event: Cause and consequences of a major Holocene abrupt climate change. *Quaternary Science Reviews*, *24*(10-11), Article 10-11. https://doi.org/10.1016/j.quascirev.2004.12.004

Alley, R. B., Mayewski, P. A., Sowers, T., Stuiver, M., Taylor, K. C., & Clark, P. U. (1997). Holocene climatic instability: A prominent, widespread event 8200 yr ago. *Geology*, *25*(6), Article 6. https://doi.org/10.1130/0091-7613(1997)025<0483:HCIAPW>2.3.CO;2

Alonso-Zarza, A. M., & Martín-Pérez, A. (2008). Dolomite in caves: Recent dolomite formation in oxic, non-sulfate environments. Castañar Cave, Spain. *Sedimentary Geology*, *205*(3-4), Article 3-4. https://doi.org/10.1016/j.sedgeo.2008.02.006

Álvarez-Solas, J., Montoya, M., Ritz, C., Ramstein, G., Charbit, S., Dumas, C., Nisancioglu, K., Dokken, T., & Ganopolski, A. (2011). Heinrich event 1: An example of dynamical ice-sheet reaction to oceanic changes. *Climate of the Past*, *7*(4), Article 4. https://doi.org/10.5194/cp-7-1297-2011

Aranbarri, J., González-Sampériz, P., Valero-Garcés, B., Moreno, A., Gil-Romera, G., Sevilla-Callejo, M., García-Prieto, E., Di Rita, F., Mata, M. P., Morellón, M., Magri, D., Rodríguez-Lázaro, J., & Carrión, J. S. (2014). Rapid climatic changes and resilient vegetation during the Lateglacial and Holocene in a continental region of south-western Europe. *Global and Planetary Change*, *114*, 50-65. https://doi.org/10.1016/j.gloplacha.2014.01.003

Arienzo, M. M., Swart, P. K., & Vonhof, H. B. (2013). Measurement of $\delta^{18}O$ and δ^2H values of fluid inclusion water in speleothems using cavity ring-down spectroscopy compared with isotope ratio mass spectrometry: Analysis of fluid inclusion water isotopes in speleothems using CRDS. *Rapid Communications in Mass Spectrometry*, *27*(23), Article 23. https://doi.org/10.1002/rcm.6723

Armstrong McKay, D. I., Staal, A., Abrams, J. F., Winkelmann, R., Sakschewski, B., Loriani, S., Fetzer, I., Cornell, S. E., Rockström, J., & Lenton, T. M. (2022). Exceeding 1.5°C global warming could trigger multiple climate tipping points. *Science*, *377*(6611), Article 6611. https://doi.org/10.1126/science.abn7950

Asmerom, Y., Polyak, V. J., & Burns, S. J. (2010). Variable winter moisture in the southwestern United States linked to rapid glacial climate shifts. *Nature Geoscience*, *3*(2), Article 2. https://doi.org/10.1038/ngeo754

Atsawawaranunt, K., Comas-Bru, L., Amirnezhad Mozhdehi, S., Deininger, M., Harrison, S. P., Baker, A., Boyd, M., Kaushal, N., Ahmad, S. M., Ait Brahim, Y., Arienzo, M., Bajo, P., Braun, K., Burstyn, Y., Chawchai, S., Duan, W., Hatvani, I. G., Hu, J., Kern, Z., … SISAL Working Group Members. (2018). The SISAL database: A global resource to document oxygen and carbon isotope records from speleothems. *Earth System Science Data*, *10*(3), Article 3. https://doi.org/10.5194/essd-10-1687-2018

Ausín, B., Magill, C., Haghipour, N., Fernández, Á., Wacker, L., Hodell, D., Baumann, K.-H., & Eglinton, T. I. (2019). (In)coherent multiproxy signals in marine sediments: Implications for high-resolution paleoclimate reconstruction. *Earth and Planetary Science Letters*, *515*, 38-46. https://doi.org/10.1016/j.epsl.2019.03.003

Ayache, M., Swingedouw, D., Mary, Y., Eynaud, F., & Colin, C. (2018). Multi-centennial variability of the AMOC over the Holocene: A new reconstruction based on multiple proxy-derived SST records. *Global and Planetary Change*, *170*, 172-189. https://doi.org/10.1016/j.gloplacha.2018.08.016

Baker, A., Genty, D., Dreybrodt, W., Barnes, W. L., Mockler, N. J., & Grapes, J. (1998). Testing Theoretically Predicted Stalagmite Growth Rate with Recent Annually Laminated Samples: Implications for Past Stalagmite Deposition. *Geochimica et Cosmochimica Acta*, *62*(3), Article 3. https://doi.org/10.1016/S0016-7037(97)00343-8

Baker, A., Genty, D., & Fairchild, I. J. (2000). Hydrological characterisation of stalagmite dripwaters at Grotte de Villars, Dordogne, by the analysis of inorganic species and luminescent organic matter. *Hydrology and Earth System Sciences*, *4*(3), 439-449. https://doi.org/10.5194/hess-4-439-2000

Baker, A., Hartmann, A., Duan, W., Hankin, S., Comas-Bru, L., Cuthbert, M. O., Treble, P. C., Banner, J., Genty, D., Baldini, L. M., Bartolomé, M., Moreno, A., Pérez-Mejías, C., & Werner, M. (2019). Global analysis reveals climatic controls on the oxygen isotope composition of cave drip water. *Nature Communications*, *10*(1), Article 1. https://doi.org/10.1038/s41467-019-11027-w

Baker, A. J. (2014). *Lagrangian modelling of precipitation and speleothem proxy oxygen isotope systematics in the East Asian Summer Monsoon region.* https://doi.org/10.13140/RG.2.1.3953.1042/1

Baker, J. L., Lachniet, M. S., Chervyatsova, O., Asmerom, Y., & Polyak, V. J. (2017). Holocene warming in western continental Eurasia driven by glacial retreat and greenhouse forcing. *Nature Geoscience*, *10*(6), Article 6. https://doi.org/10.1038/ngeo2953

Bakke, J., Lie, Ø., Heegaard, E., Dokken, T., Haug, G. H., Birks, H. H., Dulski, P., & Nilsen, T. (2009). Rapid oceanic and atmospheric changes during the Younger Dryas cold period. *Nature Geoscience*, *2*(3), Article 3. https://doi.org/10.1038/ngeo439

Baldini, J. U. L., McDermott, F., & Fairchild, I. J. (2002). *Event Revealed by a Speleothem Trace Element Record. 296.*

Baldini, L. M., Baldini, J. U. L., McDermott, F., Arias, P., Cueto, M., Fairchild, I. J., Hoffmann, D. L., Mattey, D. P., Müller, W., Nita, D. C., Ontañón, R., Garciá-Moncó, C., & Richards, D. A. (2019). North Iberian temperature and rainfall seasonality over the Younger Dryas and Holocene. *Quaternary Science Reviews*, *226*, 105998. https://doi.org/10.1016/j.quascirev.2019.105998

Baldini, L. M., McDermott, F., Baldini, J. U. L., Arias, P., Cueto, M., Fairchild, I. J., Hoffmann, D. L., Mattey, D. P., Müller, W., Nita, D. C., Ontañón, R., Garciá-Moncó, C., & Richards, D. A. (2015). Regional temperature, atmospheric circulation, and sea-ice variability within the Younger Dryas Event constrained using a speleothem from northern Iberia. *Earth and Planetary Science Letters*, *419*, 101-110. https://doi.org/10.1016/j.epsl.2015.03.015

Banks, E. D., Taylor, N. M., Gulley, J., Lubbers, B. R., Giarrizzo, J. G., Bullen, H. A., Hoehler, T. M., & Barton, H. A. (2010). Bacterial Calcium Carbonate Precipitation in Cave Environments: A Function of Calcium Homeostasis. *Geomicrobiology Journal*, *27*(5), 444-454. https://doi.org/10.1080/01490450903485136

Barber, D. C., Dyke, A., Hillaire-Marcel, C., Jennings, A. E., Andrews, J. T., Kerwin, M. W., Bilodeau, G., McNeely, R., Southon, J., & Morehead, M. D. (1999). *Forcing of the cold event of 8,200 years ago by catastrophic drainage of Laurentide lakes. 400.*

Barker, S., & Knorr, G. (2021). Millennial scale feedbacks determine the shape and rapidity of glacial termination. *Nature Communications*, *12*(1), 2273. https://doi.org/10.1038/s41467-021-22388-6

Bar-Matthews, M., Ayalon, A., Kaufman, A., & Wasserburg, G. J. (1999). The Eastern Mediterranean paleoclimate as a reflection of regional events: Soreq cave, Israel. *Earth and Planetary Science Letters*, *166*(1-2), Article 1-2. https://doi.org/10.1016/S0012-821X(98)00275-1

Bartolomé, M. (2016). *La Cueva del Caserío de Seso (Pirineo Central): Espeleogénesis, dinámica actual y reconstrucción paleoambiental de los últimos 13000 años.*

Bartolomé, M., Cazenave, G., Luetscher, M., Spötl, C., Gázquez, F., Belmonte, Á., Turchyn, A. V., López-Moreno, J. I., & Moreno, A. (2023). Mountain permafrost in the Central Pyrenees: Insights from the Devaux ice cave. *The Cryosphere*, *17*(2), Article 2. https://doi.org/10.5194/tc-17-477-2023

Bartolomé, M., Moreno, A., Sancho, C., & Hellstrom, J. (2012). *Cambios climáticos cortos en el Pirineo central durante el final del Pleistoceno superior y Holoceno a partir del registro estalagmítico de la cueva de Seso (Huesca)*. 4.

Bartolomé, M., Moreno, A., Sancho, C., Stoll, H. M., Cacho, I., Spötl, C., Belmonte, Á., Edwards, R. L., Cheng, H., & Hellstrom, J. C. (2015). Hydrological change in Southern Europe responding to increasing North Atlantic overturning during Greenland Stadial 1. *Proceedings of the National Academy of Sciences*, *112*(21), Article 21. https://doi.org/10.1073/pnas.1503990112

Bartolomé, M., Sancho, C., Benito, G., Medialdea, A., Calle, M., Moreno, A., Leunda, M., Luetscher, M., Muñoz, A., Bastida, J., Cheng, H., & Edwards, R. L. (2021). Effects of glaciation on karst hydrology and sedimentology during the Last Glacial Cycle: The case of Granito cave, Central Pyrenees (Spain). *CATENA*, *206*, 105252. https://doi.org/10.1016/j.catena.2021.105252

Bartolomé, M., Sancho, C., Moreno, A., Oliva-Urcia, B., Belmonte, á., Bastida, J., Cheng, H., & Edwards, R. L. (2015). Upper Pleistocene interstratal piping-cave speleogenesis: The Seso Cave System (Central Pyrenees, Northern Spain). *Geomorphology*, *228*, 335-344. https://doi.org/10.1016/j.geomorph.2014.09.007

Bartolomé, M., Sancho, C., Osácar, M. C., Moreno, A., Leunda, M., Spötl, C., Luetscher, M., López-Martínez, J., & Belmonte, A. (2015). Characteristics of cryogenic carbonates in a Pyrenean ice cave (northern Spain). *Cuaternario y Geomorfología*.

Benson, A., Hoffmann, D. L., Daura, J., Sanz, M., Rodrigues, F., Souto, P., & Zilhão, J. (2021). A speleothem record from Portugal reveals phases of increased winter precipitation in western Iberia during the Holocene. *The Holocene*, 12.

Bernal-Wormull, J. L., Moreno, A., Bartolomé, M., Arriolabengoa, M., Pérez-Mejías, C., Iriarte, E., Osácar, C., Spötl, C., Stoll, H., Cacho, I., Edwards, R. L., & Cheng, H. (2023). New insights into the climate of northern Iberia during the Younger Dryas and Holocene: The Mendukilo multi-speleothem record. *Quaternary Science Reviews*, *305*, 108006. https://doi.org/10.1016/j.quascirev.2023.108006

Bernal-Wormull, J. L., Moreno, A., Pérez-Mejías, C., Bartolomé, M., Aranburu, A., Arriolabengoa, M., Iriarte, E., Cacho, I., Spötl, C., Edwards, R. L., & Cheng, H. (2021). Immediate temperature response in northern Iberia to last deglacial changes in the North Atlantic. *Geology*, *49*(8), Article 8. https://doi.org/10.1130/G48660.1

Bini, M., Zanchetta, G., Perşoiu, A., Cartier, R., Català, A., Cacho, I., Dean, J. R., Di Rita, F., Drysdale, R. N., Finnè, M., Isola, I., Jalali, B., Lirer, F., Magri, D., Masi, A., Marks, L., Mercuri, A. M., Peyron, O., Sadori, L., … Brisset, E. (2019). The 4.2 ka BP Event in the Mediterranean region: An overview. *Climate of the Past*, *15*(2), Article 2. https://doi.org/10.5194/cp-15-555-2019

Bintanja, R., van de Wal, R. S. W., & Oerlemans, J. (2005). Modelled atmospheric temperatures and global sea levels over the past million years. *Nature*, *437*(7055), Article 7055. https://doi.org/10.1038/nature03975

Blaauw, M., van Geel, B., & van der Plicht, J. (2004). Solar forcing of climatic change during the mid-Holocene: Indications from raised bogs in The Netherlands. *The Holocene*, *14*(1), Article 1. https://doi.org/10.1191/0959683604hl687rp

Boch, R., Cheng, H., Spötl, C., Edwards, R. L., Wang, X., & Häuselmann, Ph. (2011). NALPS: A precisely dated European climate record 120–60 ka. *Climate of the Past*, *7*(4), Article 4. https://doi.org/10.5194/cp-7-1247-2011

Bolland, A., Rey, F., Gobet, E., Tinner, W., & Heiri, O. (2020). Summer temperature development 18,000–14,000 cal. BP recorded by a new chironomid record from Burgäschisee, Swiss Plateau. *Quaternary Science Reviews*, *243*, 106484. https://doi.org/10.1016/j.quascirev.2020.106484

Bond, G. (1997). A Pervasive Millennial-Scale Cycle in North Atlantic Holocene and Glacial Climates. *Science*, *278*(5341), Article 5341. https://doi.org/10.1126/science.278.5341.1257

Bond, G. C., Showers, W., Elliot, M., Evans, M., Lotti, R., Hajdas, I., Bonani, G., & Johnson, S. (1999). The North Atlantic's 1–2 kyr climate rhythm: Relation to Heinrich events, Dansgaard/Oeschger

cycles and the Little Ice Age. En U. Clark, S. Webb, & D. Keigwin (Eds.), *Geophysical Monograph Series* (Vol. 112, pp. 35-58). American Geophysical Union. https://doi.org/10.1029/GM112p0035

Bond, G., Kromer, B., Beer, J., Muscheler, R., Evans, M. N., Showers, W., Hoffmann, S., Lotti-Bond, R., Hajdas, I., & Bonani, G. (2001). Persistent Solar Influence on North Atlantic Climate During the Holocene. *Science*, *294*(5549), Article 5549. https://doi.org/10.1126/science.1065680

Borsato, A., Frisia, S., Fairchild, I. J., Somogyi, A., & Susini, J. (2007). Trace element distribution in annual stalagmite laminae mapped by micrometer-resolution X-ray fluorescence: Implications for incorporation of environmentally significant species. *Geochimica et Cosmochimica Acta*, *71*(6), 1494-1512. https://doi.org/10.1016/j.gca.2006.12.016

Bradley, R. S., & Bakke, J. (2019). Is there evidence for a 4.2 ka BP event in the northern North Atlantic region? *Climate of the Past*, *15*(5), Article 5. https://doi.org/10.5194/cp-15-1665-2019

Brayshaw, D. J., Hoskins, B., & Black, E. (2010). Some physical drivers of changes in the winter storm tracks over the North Atlantic and Mediterranean during the Holocene. *Philosophical Transactions of the Royal Society A: Mathematical, Physical and Engineering Sciences*, *368*(1931), 5185-5223. https://doi.org/10.1098/rsta.2010.0180

Broecker, W. S. (1998). Paleocean circulation during the Last Deglaciation: A bipolar seesaw? *Paleoceanography*, *13*(2), Article 2. https://doi.org/10.1029/97PA03707

Budsky, A., Scholz, D., Wassenburg, J. A., Mertz-Kraus, R., Spötl, C., Riechelmann, D. F., Gibert, L., Jochum, K. P., & Andreae, M. O. (2019). Speleothem δ^{13} C record suggests enhanced spring/summer drought in south-eastern Spain between 9.7 and 7.8 ka – A circum-Western Mediterranean anomaly? *The Holocene*, *29*(7), Article 7. https://doi.org/10.1177/0959683619838021

Buizert, C., Keisling, B. A., Box, J. E., He, F., Carlson, A. E., Sinclair, G., & DeConto, R. M. (2018). Greenland-Wide Seasonal Temperatures During the Last Deglaciation. *Geophysical Research Letters*, *45*(4), Article 4. https://doi.org/10.1002/2017GL075601

Burns, S. J., Fleitmann, D., Matter, A., Kramers, J., & Al-Subbary, A. A. (2003). Indian Ocean Climate and an Absolute Chronology over Dansgaard/Oeschger Events 9 to 13. *Science*, *301*(5638), Article 5638. https://doi.org/10.1126/science.1086227

Burns, S. J., Fleitmann, D., Mudelsee, M., Neff, U., Matter, A., & Mangini, A. (2002). A 780-year annually resolved record of Indian Ocean monsoon precipitation from a speleothem from south Oman. *Journal of Geophysical Research*, *107*(D20), Article D20. https://doi.org/10.1029/2001JD001281

Cáceres, J. O., Pelascini, F., Motto-Ros, V., Moncayo, S., Trichard, F., Panczer, G., Marín-Roldán, A., Cruz, J. A., Coronado, I., & Martín-Chivelet, J. (2017). Megapixel multi-elemental imaging by Laser-Induced Breakdown Spectroscopy, a technology with considerable potential for paleoclimate studies. *Scientific Reports*, *7*(1), Article 1. https://doi.org/10.1038/s41598-017-05437-3

Cacho, I., Grimalt, J. O., Canals, M., Sbaffi, L., Shackleton, N. J., Schönfeld, J., & Zahn, R. (2001). Variability of the western Mediterranean Sea surface temperature during the last 25,000 years and its connection with the Northern Hemisphere climatic changes. *Paleoceanography*, *16*(1), Article 1. https://doi.org/10.1029/2000PA000502

Campbell, M., McDonough, L., Treble, P. C., Baker, A., Kosarac, N., Coleborn, K., Wynn, P. M., & Schmitt, A. K. (2023). A Review of Speleothems as Archives for Paleofire Proxies, With Australian Case Studies. *Reviews of Geophysics*, *61*(2), Article 2. https://doi.org/10.1029/2022RG000790

Camuera, J., Jiménez-Moreno, G., Ramos-Román, M. J., García-Alix, A., Jiménez-Espejo, F. J., Toney, J. L., & Anderson, R. S. (2021). Chronological control and centennial-scale climatic subdivisions of the Last Glacial Termination in the western Mediterranean region. *Quaternary Science Reviews*, *255*, 106814. https://doi.org/10.1016/j.quascirev.2021.106814

Carlson, A. E., LeGrande, A. N., Oppo, D. W., Came, R. E., Schmidt, G. A., Anslow, F. S., Licciardi, J. M., & Obbink, E. A. (2008). Rapid early Holocene deglaciation of the Laurentide ice sheet. *Nature Geoscience*, *1*(9), Article 9. https://doi.org/10.1038/ngeo285

Carrión, J. S. (2002). Patterns and processes of Late Quaternary environmental change in a montane region of southwestern Europe. *Quaternary Science Reviews*, *21*(18-19), Article 18-19. https://doi.org/10.1016/S0277-3791(02)00010-0

Carrión, J. S., Fernández, S., González-Sampériz, P., Gil-Romera, G., Badal, E., Carrión-Marco, Y., López-Merino, L., López-Sáez, J. A., Fierro, E., & Burjachs, F. (2010). Expected trends and surprises in the Lateglacial and Holocene vegetation history of the Iberian Peninsula and Balearic Islands. *Review of Palaeobotany and Palynology*, *162*(3), Article 3. https://doi.org/10.1016/j.revpalbo.2009.12.007

Carrión, J. S., & Van Geel, B. (1999). Fine-resolution Upper Weichselian and Holocene palynological record from Navarrés (Valencia, Spain) and a discussion about factors of Mediterranean forest succession. *Review of Palaeobotany and Palynology*, *106*(3-4), Article 3-4. https://doi.org/10.1016/S0034-6667(99)00009-3

Català, A., Cacho, I., Frigola, J., Pena, L. D., & Lirer, F. (2019). Holocene hydrography evolution in the Alboran Sea: A multi-record and multi-proxy comparison. *Climate of the Past*, *15*(3), Article 3. https://doi.org/10.5194/cp-15-927-2019

Chabaud, L., Sánchez Goñi, M. F., Desprat, S., & Rossignol, L. (2014). Land–sea climatic variability in the eastern North Atlantic subtropical region over the last 14,200 years: Atmospheric and oceanic processes at different timescales. *The Holocene*, *24*(7), Article 7. https://doi.org/10.1177/0959683614530439

Cheng, H., Edwards, R. L., Broecker, W. S., Denton, G. H., Kong, X., Wang, Y., Zhang, R., & Wang, X. (2009). Ice Age Terminations. *Science*, *326*(5950), Article 5950. https://doi.org/10.1126/science.1177840

Cheng, H., Edwards, R. L., Hoff, J., Gallup, C. D., Richards, D. A., & Asmerom, Y. (2000). The half-lives of uranium-234 and thorium-230. *Chemical Geology*, *169*(1-2), Article 1-2. https://doi.org/10.1016/S0009-2541(99)00157-6

Cheng, H., Edwards, R. L., Wang, Y., Kong, X., Ming, Y., Kelly, M. J., Wang, X., Gallup, C. D., & Liu, W. (2006). A penultimate glacial monsoon record from Hulu Cave and two-phase glacial terminations. *Geology*, *34*(3), Article 3. https://doi.org/10.1130/G22289.1

Cheng, H., Lawrence Edwards, R., Shen, C.-C., Polyak, V. J., Asmerom, Y., Woodhead, J., Hellstrom, J., Wang, Y., Kong, X., Spötl, C., Wang, X., & Calvin Alexander, E. (2013). Improvements in 230Th dating, 230Th and 234U half-life values, and U–Th isotopic measurements by multi-collector inductively coupled plasma mass spectrometry. *Earth and Planetary Science Letters*, *371-372*, 82-91. https://doi.org/10.1016/j.epsl.2013.04.006

Cheng, H., Spötl, C., Breitenbach, S. F. M., Sinha, A., Wassenburg, J. A., Jochum, K. P., Scholz, D., Li, X., Yi, L., Peng, Y., Lv, Y., Zhang, P., Votintseva, A., Loginov, V., Ning, Y., Kathayat, G., & Edwards, R. L. (2016). Climate variations of Central Asia on orbital to millennial timescales. *Scientific Reports*, *6*(1), Article 1. https://doi.org/10.1038/srep36975

Cheng, H., Zhang, H., Spötl, C., Baker, J., Sinha, A., Li, H., Bartolomé, M., Moreno, A., Kathayat, G., Zhao, J., Dong, X., Li, Y., Ning, Y., Jia, X., Zong, B., Ait Brahim, Y., Pérez-Mejías, C., Cai, Y., Novello, V. F., … Edwards, R. L. (2020). Timing and structure of the Younger Dryas event and its underlying climate dynamics. *Proceedings of the National Academy of Sciences*, *117*(38), Article 38. https://doi.org/10.1073/pnas.2007869117

Clark, I. D., & Fritz, P. (1997). *Environmental Isotopes in Hydrogeology* (0 ed.). CRC Press. https://doi.org/10.1201/9781482242911

Clark, P. U., Shakun, J. D., Baker, P. A., Bartlein, P. J., Brewer, S., Brook, E., Carlson, A. E., Cheng, H., Kaufman, D. S., Liu, Z., Marchitto, T. M., Mix, A. C., Morrill, C., Otto-Bliesner, B. L., Pahnke, K., Russell, J. M., Whitlock, C., Adkins, J. F., Blois, J. L., … Williams, J. W. (2012). Global climate evolution during the last deglaciation. *Proceedings of the National Academy of Sciences*, *109*(19), Article 19. https://doi.org/10.1073/pnas.1116619109

Crombé, P. (2018). Abrupt cooling events during the Early Holocene and their potential impact on the environment and human behaviour along the southern North Sea basin (NW Europe). *Journal of Quaternary Science*, *33*(3), 353-367. https://doi.org/10.1002/jqs.2962

Cruz, F. W., Karmann, I., Viana, O., Burns, S. J., Ferrari, J. A., Vuille, M., Sial, A. N., & Moreira, M. Z. (2005). Stable isotope study of cave percolation waters in subtropical Brazil: Implications for paleoclimate inferences from speleothems. *Chemical Geology*, *220*(3-4), Article 3-4. https://doi.org/10.1016/j.chemgeo.2005.04.001

Cruz, F. W., Vuille, M., Burns, S. J., Wang, X., Cheng, H., Werner, M., Lawrence Edwards, R., Karmann, I., Auler, A. S., & Nguyen, H. (2009). Orbitally driven east–west antiphasing of South American precipitation. *Nature Geoscience*, *2*(3), Article 3. https://doi.org/10.1038/ngeo444

Cruz, J. A., Martín-Chivelet, J., Marín-Roldán, A., Turrero, M. J., Edwards, R. L., Ortega, A. I., & Cáceres, J. O. (2015). Trace Elements in Speleothems as Indicators of Past Climate and Karst Hydrochemistry: A Case Study from Kaite Cave (N Spain). En B. Andreo, F. Carrasco, J. J. Durán, P. Jiménez, & J. W. LaMoreaux (Eds.), *Hydrogeological and Environmental Investigations in Karst Systems* (pp. 569-577). Springer. https://doi.org/10.1007/978-3-642-17435-3_64

Cruz, J. A., Turrero, M. J., Cáceres, J. O., Marín-Roldán, A., Ortega, A. I., Garralón, A., Sánchez, L., Gómez, P., Muñoz-García, M. B., Edwards, R. L., & Martín-Chivelet, J. (2015). Long-term hydrological changes in northern Iberia (4.9–0.9 ky BP) from speleothem Mg/Ca ratios and cave monitoring (Ojo Guareña Karst Complex, Spain). *Environmental Earth Sciences*, *74*(12), Article 12. https://doi.org/10.1007/s12665-015-4687-x

Dansgaard, W. (1964). Stable isotopes in precipitation. *Tellus*, *16*(4), Article 4. https://doi.org/10.1111/j.2153-3490.1964.tb00181.x

Davis, B. A. S., Brewer, S., Stevenson, A. C., & Guiot, J. (2003). The temperature of Europe during the Holocene reconstructed from pollen data. *Quaternary Science Reviews*, *22*(15-17), Article 15-17. https://doi.org/10.1016/S0277-3791(03)00173-2

Davis, P. T., Menounos, B., & Osborn, G. (2009). Holocene and latest Pleistocene alpine glacier fluctuations: A global perspective. *Quaternary Science Reviews*, *28*(21-22), Article 21-22. https://doi.org/10.1016/j.quascirev.2009.05.020

deMenocal, P. B. (2001). Cultural Responses to Climate Change During the Late Holocene. *Science*, *292*(5517), 667-673. https://doi.org/10.1126/science.1059287

deMenocal, P., Ortiz, J., Guilderson, T., Adkins, J., Sarnthein, M., Baker, L., & Yarusinsky, M. (2000). Abrupt onset and termination of the African Humid Period: Rapid climate responses to gradual insolation forcing. *Quaternary Science Reviews*, *19*(1-5), Article 1-5. https://doi.org/10.1016/S0277-3791(99)00081-5

Demény, A., Czuppon, G., Kern, Z., Leél-Őssy, S., Németh, A., Szabó, M., Tóth, M., Wu, C.-C., Shen, C.-C., Molnár, M., Németh, T., Németh, P., & Óvári, M. (2016). Recrystallization-induced oxygen isotope changes in inclusion-hosted water of speleothems – Paleoclimatological implications. *Quaternary International*, *415*, 25-32. https://doi.org/10.1016/j.quaint.2015.11.137

Demény, A., Rinyu, L., Kern, Z., Hatvani, I. G., Czuppon, G., Surányi, G., Leél-Őssy, S., Shen, C.-C., & Koltai, G. (2021). Paleotemperature reconstructions using speleothem fluid inclusion analyses from Hungary. *Chemical Geology*, *563*, 120051. https://doi.org/10.1016/j.chemgeo.2020.120051

Denton, G., Alley, R., Comer, G., & Broecker, W. (2005). The role of seasonality in abrupt climate change. *Quaternary Science Reviews*, *24*(10-11), Article 10-11. https://doi.org/10.1016/j.quascirev.2004.12.002

Denton, G. H., Anderson, R. F., Toggweiler, J. R., Edwards, R. L., Schaefer, J. M., & Putnam, A. E. (2010). The Last Glacial Termination. *Science*, *328*(5986), Article 5986. https://doi.org/10.1126/science.1184119

Deser, C., Knutti, R., Solomon, S., & Phillips, A. S. (2012). Communication of the role of natural variability in future North American climate. *Nature Climate Change*, *2*(11), Article 11. https://doi.org/10.1038/nclimate1562

Desprat, S., Sánchez Goñi, M. F., & Loutre, M.-F. (2003). Revealing climatic variability of the last three millennia in northwestern Iberia using pollen influx data. *Earth and Planetary Science Letters*, *213*(1-2), Article 1-2. https://doi.org/10.1016/S0012-821X(03)00292-9

Dickson. (1993). Crystal Growth Diagrams as an Aid to Interpreting the Fabrics of Calcite Aggregates. *SEPM Journal of Sedimentary Research*, *Vol. 63*. https://doi.org/10.1306/D4267A78-2B26-11D7-8648000102C1865D

Domínguez-Villar, D., Fairchild, I. J., Baker, A., Wang, X., Edwards, R. L., & Cheng, H. (2009). Oxygen isotope precipitation anomaly in the North Atlantic region during the 8.2 ka event. *Geology*, *37*(12), Article 12. https://doi.org/10.1130/G30393A.1

Domínguez-Villar, D., Wang, X., Cheng, H., Martín-Chivelet, J., & Edwards, R. L. (2008). A high-resolution late Holocene speleothem record from Kaite Cave, northern Spain: δ^{18}O variability and possible causes. *Quaternary International*, *187*(1), Article 1. https://doi.org/10.1016/j.quaint.2007.06.010

Domínguez-Villar, D., Wang, X., Krklec, K., Cheng, H., & Edwards, R. L. (2017). The control of the tropical North Atlantic on Holocene millennial climate oscillations. *Geology*, *45*(4), Article 4. https://doi.org/10.1130/G38573.1

Dorale, J. A., Onac, B. P., Fornós, J. J., Ginés, J., Ginés, A., Tuccimei, P., & Peate, D. W. (2010). Sea-Level Highstand 81,000 Years Ago in Mallorca. *Science*, *327*(5967), Article 5967. https://doi.org/10.1126/science.1181725

Dreybrodt, W. (1988). *Processes in Karst Systems* (Vol. 4). Springer Berlin Heidelberg. https://doi.org/10.1007/978-3-642-83352-6

Dreybrodt, W. (1999). Chemical kinetics, speleothem growth and climate. *Boreas*, *28*(3), Article 3. https://doi.org/10.1111/j.1502-3885.1999.tb00224.x

Drysdale, R. N., Hellstrom, J. C., Zanchetta, G., Fallick, A. E., Sánchez Goñi, M. F., Couchoud, I., McDonald, J., Maas, R., Lohmann, G., & Isola, I. (2009). Evidence for Obliquity Forcing of Glacial Termination II. *Science*, *325*(5947), Article 5947. https://doi.org/10.1126/science.1170371

Drysdale, R. N., Zanchetta, G., Hellstrom, J. C., Fallick, A. E., McDonald, J., & Cartwright, I. (2007). Stalagmite evidence for the precise timing of North Atlantic cold events during the early last glacial. *Geology*, *35*(1), Article 1. https://doi.org/10.1130/G23161A.1

Drysdale, R., Zanchetta, G., Hellstrom, J., Maas, R., Fallick, A., Pickett, M., Cartwright, I., & Piccini, L. (2006). Late Holocene drought responsible for the collapse of Old World civilizations is recorded in an Italian cave flowstone. *Geology*, *34*(2), 101. https://doi.org/10.1130/G22103.1

Dublyansky, Y. V., & Spötl, C. (2009). Hydrogen and oxygen isotopes of water from inclusions in minerals: Design of a new crushing system and on-line continuous-flow isotope ratio mass spectrometric analysis. *Rapid Communications in Mass Spectrometry*, *23*(17), Article 17. https://doi.org/10.1002/rcm.4155

Durán Valsero, J. J., López Martínez, J., Dallai, L., Bruschi, G., Caballero Mesa, E., Jiménez de Cisneros Vencelá, C., & Julià Brugués, R. (1999). Palaeoenvironmental reconstruction based on a detailed stable isotope analysis and dating of a Holocene speleothem from Valporquero Cave, Northern Spain. *Geogaceta*, *27*, Article 27.

Edwards, R. L., Chen, J. H., & Wasserburg, G. J. (1987). ^{238}U^{234}U^{230}Th^{232}Th systematics and the precise measurement of time over the past 500,000 years. *Earth and Planetary Science Letters*, *81*(2-3), Article 2-3. https://doi.org/10.1016/0012-821X(87)90154-3

Edwards, R. L., Gallup, C. D., & Cheng, H. (2003). *Uranium-series Dating of Marine and Lacustrine Carbonates*.

El-Shenawy, M. I., Kim, S.-T., Schwarcz, H. P., Asmerom, Y., & Polyak, V. J. (2018). Speleothem evidence for the greening of the Sahara and its implications for the early human dispersal out of sub-Saharan Africa. *Quaternary Science Reviews*, *188*, 67-76. https://doi.org/10.1016/j.quascirev.2018.03.016

Eynaud, F., Malaizé, B., Zaragosi, S., de Vernal, A., Scourse, J., Pujol, C., Cortijo, E., Grousset, F. E., Penaud, A., Toucanne, S., Turon, J.-L., & Auffret, G. (2012). New constraints on European glacial freshwater releases to the North Atlantic Ocean: EUROPEAN GLACIAL FRESHWATER RELEASES. *Geophysical Research Letters*, *39*(15), Article 15. https://doi.org/10.1029/2012GL052100

Fairchild, I. J., & Baker, A. (2012). *Speleothem science: From process to past environments*. Wiley.

Fairchild, I. J., Borsato, A., Tooth, A. F., Frisia, S., Hawkesworth, C. J., Huang, Y., McDermott, F., & Spiro, B. (2000). *Controls on trace element žSr–Mg/ compositions of carbonate cave waters: Implications for speleothem climatic records*. 15.

Fairchild, I. J., Frisia, S., Borsato, A., & F. Tooth, A. (2007). Speleothems. En D. J. Nash & S. J. McLaren (Eds.), *Geochemical Sediments and Landscapes* (pp. 200-245). Blackwell Publishing Ltd. https://doi.org/10.1002/9780470712917.ch7

Fairchild, I. J., Smith, C. L., Baker, A., Fuller, L., Spötl, C., Mattey, D., McDermott, F., & E.I.M.F. (2006). Modification and preservation of environmental signals in speleothems. *Earth-Science Reviews*, *75*(1-4), Article 1-4. https://doi.org/10.1016/j.earscirev.2005.08.003

Fairchild, I. J., & Treble, P. C. (2009). Trace elements in speleothems as recorders of environmental change. *Quaternary Science Reviews*, *28*(5-6), Article 5-6. https://doi.org/10.1016/j.quascirev.2008.11.007

Feinberg, J. M., & Johnson, K. R. (2021). Cave and Speleothem Science: From Local to Planetary Scales. *Elements*, *17*(2), Article 2. https://doi.org/10.2138/gselements.17.2.81

Finné, M., Woodbridge, J., Labuhn, I., & Roberts, C. N. (2019). Holocene hydro-climatic variability in the Mediterranean: A synthetic multi-proxy reconstruction. *The Holocene*, *29*(5), Article 5. https://doi.org/10.1177/0959683619826634

Fleitmann, D., Burns, S. J., Mangini, A., Mudelsee, M., Kramers, J., Villa, I., Neff, U., Al-Subbary, A. A., Buettner, A., Hippler, D., & Matter, A. (2007). Holocene ITCZ and Indian monsoon dynamics recorded in stalagmites from Oman and Yemen (Socotra). *Quaternary Science Reviews*, *26*(1-2), Article 1-2. https://doi.org/10.1016/j.quascirev.2006.04.012

Fleitmann, D., Burns, S. J., Mudelsee, M., Neff, U., Kramers, J., Mangini, A., & Matter, A. (2003). Holocene Forcing of the Indian Monsoon Recorded in a Stalagmite from Southern Oman. *Science*, *300*(5626), Article 5626. https://doi.org/10.1126/science.1083130

Fleitmann, D., Cheng, H., Badertscher, S., Edwards, R. L., Mudelsee, M., Göktürk, O. M., Fankhauser, A., Pickering, R., Raible, C. C., Matter, A., Kramers, J., & Tüysüz, O. (2009). Timing and climatic impact of Greenland interstadials recorded in stalagmites from northern Turkey. *Geophysical Research Letters*, *36*(19), Article 19. https://doi.org/10.1029/2009GL040050

Fleitmann, D., Mudelsee, M., Burns, S. J., Bradley, R. S., Kramers, J., & Matter, A. (2008). Evidence for a widespread climatic anomaly at around 9.2 ka before present: CLIMATIC ANOMALY AT AROUND 9.2 ka B.P. *Paleoceanography*, *23*(1), Article 1. https://doi.org/10.1029/2007PA001519

Fletcher, W. J., Debret, M., & Goñi, M. F. S. (2013). Mid-Holocene emergence of a low-frequency millennial oscillation in western Mediterranean climate: Implications for past dynamics of the North Atlantic atmospheric westerlies. *The Holocene*, *23*(2), Article 2. https://doi.org/10.1177/0959683612460783

Fletcher, W. J., & Sánchez Goñi, M. F. (2008). Orbital- and sub-orbital-scale climate impacts on vegetation of the western Mediterranean basin over the last 48,000 yr. *Quaternary Research*, *70*(3), Article 3. https://doi.org/10.1016/j.yqres.2008.07.002

Fletcher, W. J., Sánchez Goñi, M. F., Allen, J. R. M., Cheddadi, R., Combourieu-Nebout, N., Huntley, B., Lawson, I., Londeix, L., Magri, D., Margari, V., Müller, U. C., Naughton, F., Novenko, E., Roucoux, K., & Tzedakis, P. C. (2010). Millennial-scale variability during the last glacial in vegetation records from Europe. *Quaternary Science Reviews*, *29*(21-22), Article 21-22. https://doi.org/10.1016/j.quascirev.2009.11.015

Fohlmeister, J. (2012). A statistical approach to construct composite climate records of dated archives. *Quaternary Geochronology*, *14*, 48-56. https://doi.org/10.1016/j.quageo.2012.06.007

Fohlmeister, J., Voarintsoa, N. R. G., Lechleitner, F. A., Boyd, M., Brandstätter, S., Jacobson, M. J., & L. Oster, J. (2020). Main controls on the stable carbon isotope composition of speleothems. *Geochimica et Cosmochimica Acta*, *279*, 67-87. https://doi.org/10.1016/j.gca.2020.03.042

Foster, G., & Rahmstorf, S. (2011). Global temperature evolution 1979–2010. *Environmental Research Letters*, *6*(4), Article 4. https://doi.org/10.1088/1748-9326/6/4/044022

Franke, F. W. (1965). The theory behind stalagmite shapes. En *Studies in Speleology* (Vol. 1, pp. 89-95).

Frigola, J., Moreno, A., Cacho, I., Canals, M., Sierro, F. J., Flores, J. A., Grimalt, J. O., Hodell, D. A., & Curtis, J. H. (2007). Holocene climate variability in the western Mediterranean region from a deepwater sediment record: HOLOCENE CLIMATE VARIABILITY. *Paleoceanography*, *22*(2), Article 2. https://doi.org/10.1029/2006PA001307

Frisia, S. (1996). Petrographic evidences of diagenesis in speleothems: Some examples. *Speleochronos*, *7*, 21-30.

Frisia, S. (2015). Microstratigraphic logging of calcite fabrics in speleothems as tool for palaeoclimate studies. *International Journal of Speleology*, 17.

Frisia, S., & Borsato, A. (2010). Chapter 6 Karst. En *Developments in Sedimentology* (Vol. 61, pp. 269-318). Elsevier. https://doi.org/10.1016/S0070-4571(09)06106-8

Frisia, S., Borsato, A., Fairchild, I. J., & McDermott, F. (2000). Calcite Fabrics, Growth Mechanisms, and Environments of Formation in Speleothems from the Italian Alps and Southwestern Ireland. *Journal of Sedimentary Research*, *70*(5), Article 5. https://doi.org/10.1306/022900701183

Frisia, S., Borsato, A., Fairchild, I. J., McDermott, F., & Selmo, E. M. (2002). Aragonite-Calcite Relationships in Speleothems (Grotte De Clamouse, France): Environment, Fabrics, and Carbonate Geochemistry. *Journal of Sedimentary Research*, *72*(5), Article 5. https://doi.org/10.1306/020702720687

Frisia, S., Borsato, A., Fairchild, I. J., & Susini, J. (2005). Variations in atmospheric sulphate recorded in stalagmites by synchrotron micro-XRF and XANES analyses. *Earth and Planetary Science Letters*, *235*(3-4), 729-740. https://doi.org/10.1016/j.epsl.2005.03.026

Frisia, S., Borsato, A., Spötl, C., Villa, I. M., & Cucchi, F. (2005). Climate variability in the SE Alps of Italy over the past 17 000 years reconstructed from a stalagmite record. *Boreas*, *34*(4), Article 4. https://doi.org/10.1080/03009480500231336

García-Escárzaga, A., Gutiérrez-Zugasti, I., Marín-Arroyo, A. B., Fernandes, R., Núñez de la Fuente, S., Cuenca-Solana, D., Iriarte, E., Simões, C., Martín-Chivelet, J., González-Morales, M. R., & Roberts, P. (2022). Human forager response to abrupt climate change at 8.2 ka on the Atlantic coast of Europe. *Scientific Reports*, *12*(1), Article 1. https://doi.org/10.1038/s41598-022-10135-w

García-Mondéjar, J., Agirrezabala, L. M., Aranburu, A., Fernández-Mendiola, P. A., Gómez-Pérez, I., López-Horgue, M., & Rosales, I. (1996). Aptian—Albian tectonic pattern of the Basque—Cantabrian Basin (Northern Spain). *Geological Journal*, *31*(1), Article 1. https://doi.org/10.1002/(SICI)1099-1034(199603)31:1<13::AID-GJ689>3.0.CO;2-Y

García-Ruiz, J. M., Hughes, P. D., Palacios, D., & Andrés, N. (2023). The European glacial landscapes from the main deglaciation. En *European Glacial Landscapes* (pp. 243-259). Elsevier. https://doi.org/10.1016/B978-0-323-91899-2.00032-2

García-Ruiz, J. M., Palacios, D., Andrés, N., & López-Moreno, J. I. (2020). Neoglaciation in the Spanish Pyrenees: A multiproxy challenge. *Mediterranean Geoscience Reviews*, *2*(1), Article 1. https://doi.org/10.1007/s42990-020-00022-9

García-Ruiz, J. M., Palacios, D., González-Sampériz, P., de Andrés, N., Moreno, A., Valero-Garcés, B., & Gómez-Villar, A. (2016). Mountain glacier evolution in the Iberian Peninsula during the Younger Dryas. *Quaternary Science Reviews*, *138*, 16-30. https://doi.org/10.1016/j.quascirev.2016.02.022

Gascoyne, M. (1992). Palaeoclimate determination from cave calcite deposits. *Quaternary Science Reviews*, *11*(6), Article 6. https://doi.org/10.1016/0277-3791(92)90074-I

Gellatly, A. F., Grove, J. M., & Switsur, V. R. (1992). Mid-Holocene glacial activity in the Pyrenees. *The Holocene*, *2*(3), Article 3. https://doi.org/10.1177/095968369200200309

Genty, D., Baker, A., Massault, M., Proctor, C., Gilmour, M., Pons-Branchu, E., & Hamelin, B. (2001). Dead carbon in stalagmites: Carbonate bedrock paleodissolution vs. ageing of soil organic matter. Implications for 13 C variations in speleothems. *Geochimica et Cosmochimica Acta*, *65*(20), Article 20. https://doi.org/10.1016/S0016-7037(01)00697-4

Genty, D., Blamart, D., Ghaleb, B., Plagnes, V., Causse, Ch., Bakalowicz, M., Zouari, K., Chkir, N., Hellstrom, J., & Wainer, K. (2006). Timing and dynamics of the last deglaciation from European and North African δ13C stalagmite profiles—Comparison with Chinese and South Hemisphere stalagmites. *Quaternary Science Reviews*, *25*(17-18), Article 17-18. https://doi.org/10.1016/j.quascirev.2006.01.030

Genty, D., Combourieu-Nebout, N., Peyron, O., Blamart, D., Wainer, K., Mansuri, F., Ghaleb, B., Isabello, L., Dormoy, I., & von Grafenstein, U. (2010). Isotopic characterization of rapid climatic events during OIS3 and OIS4 in Villars Cave stalagmites (SW-France) and correlation with Atlantic and

Mediterranean pollen records. *Quaternary Science Reviews*, *29*(19-20), Article 19-20. https://doi.org/10.1016/j.quascirev.2010.06.035

Genty, D., Plagnes, V., Causse, C., Cattani, O., Stievenard, M., Falourd, S., Blamart, D., Ouahdi, R., & Van-Exter, S. (2002). Fossil water in large stalagmite voids as a tool for paleoprecipitation stable isotope composition reconstitution and paleotemperature calculation. *Chemical Geology*, *184*(1-2), Article 1-2. https://doi.org/10.1016/S0009-2541(01)00356-4

Genty, D., Vokal, B., Obelic, B., & Massault, M. (1998). Bomb 14C time history recorded in two modern stalagmites—Importance for soil organic matter dynamics and bomb 14C distribution over continents. *Earth and Planetary Science Letters*, *160*(3-4), Article 3-4. https://doi.org/10.1016/S0012-821X(98)00128-9

Gil-Romera, G., González-Sampériz, P., Lasheras-Álvarez, L., Sevilla-Callejo, M., Moreno, A., Valero-Garcés, B., López-Merino, L., Carrión, J. S., Pérez Sanz, A., Aranbarri, J., & García-Prieto Fronce, E. (2014). Biomass-modulated fire dynamics during the Last Glacial–Interglacial Transition at the Central Pyrenees (Spain). *Palaeogeography, Palaeoclimatology, Palaeoecology, 402*, 113-124. https://doi.org/10.1016/j.palaeo.2014.03.015

Giménez, R., Bartolomé, M., Gázquez, F., Iglesias, M., & Moreno, A. (2021). Underlying Climate Controls in Triple Oxygen (^{16}O, ^{17}O, ^{18}O) and Hydrogen (^{1}H, ^{2}H) Isotopes Composition of Rainfall (Central Pyrenees). *Frontiers in Earth Science*, *9*, 633698. https://doi.org/10.3389/feart.2021.633698

Goldstein, S. J., & Stirling, C. H. (2003). *Techniques for Measuring Uranium-series Nuclides: 1992-2002*.

Gómez, M., Vergés, J., & Riaza, C. (2002). Inversion tectonics of the northern margin of the Basque Cantabrian Basin. *Bulletin de La Société Géologique de France*, *173*(5), Article 5. https://doi.org/10.2113/173.5.449

Gonzalez, L. A., & Lohmann, K. C. (1988). Controls on Mineralogy and Composition of Spelean Carbonates: Carlsbad Caverns, New Mexico. En N. P. James & P. W. Choquette (Eds.), *Paleokarst* (pp. 81-101). Springer New York. https://doi.org/10.1007/978-1-4612-3748-8_4

González-Sampériz, P., Aranbarri, J., Pérez-Sanz, A., Gil-Romera, G., Moreno, A., Leunda, M., Sevilla-Callejo, M., Corella, J. P., Morellón, M., Oliva, B., & Valero-Garcés, B. (2017). Environmental and climate change in the southern Central Pyrenees since the Last Glacial Maximum: A view from the lake records. *CATENA*, *149*, 668-688. https://doi.org/10.1016/j.catena.2016.07.041

González-Sampériz, P., Valero-Garcés, B. L., Moreno, A., Jalut, G., García-Ruiz, J. M., Martí-Bono, C., Delgado-Huertas, A., Navas, A., Otto, T., & Dedoubat, J. J. (2006). Climate variability in the Spanish Pyrenees during the last 30,000 yr revealed by the El Portalet sequence. *Quaternary Research*, *66*(1), Article 1. https://doi.org/10.1016/j.yqres.2006.02.004

Goñi, M. F. S., Turon, J.-L., Eynaud, F., & Gendreau, S. (2000). European Climatic Response to Millennial-Scale Changes in the Atmosphere–Ocean System during the Last Glacial Period. *Quaternary Research*, *54*(3), Article 3. https://doi.org/10.1006/qres.2000.2176

Grachev, A. M., & Severinghaus, J. P. (2005). A revised +10±4°C magnitude of the abrupt change in Greenland temperature at the Younger Dryas termination using published GISP2 gas isotope data and air thermal diffusion constants. *Quaternary Science Reviews*, *24*(5-6), Article 5-6. https://doi.org/10.1016/j.quascirev.2004.10.016

Grafenstein, U. v. (1999). A Mid-European Decadal Isotope-Climate Record from 15,500 to 5000 Years B.P. *Science*, *284*(5420), Article 5420. https://doi.org/10.1126/science.284.5420.1654

Gregoire, L. J., Payne, A. J., & Valdes, P. J. (2012). Deglacial rapid sea level rises caused by ice-sheet saddle collapses. *Nature*, *487*(7406), Article 7406. https://doi.org/10.1038/nature11257

Griffiths, M. L., Drysdale, R. N., Vonhof, H. B., Gagan, M. K., Zhao, J., Ayliffe, L. K., Hantoro, W. S., Hellstrom, J. C., Cartwright, I., Frisia, S., & Suwargadi, B. W. (2010). Younger Dryas–Holocene temperature and rainfall history of southern Indonesia from δ18O in speleothem calcite and fluid inclusions. *Earth and Planetary Science Letters*, *295*(1-2), Article 1-2. https://doi.org/10.1016/j.epsl.2010.03.018

Griffiths, M. L., Fohlmeister, J., Drysdale, R. N., Hua, Q., Johnson, K. R., Hellstrom, J. C., Gagan, M. K., & Zhao, J. -x. (2012). Hydrological control of the dead carbon fraction in a Holocene tropical speleothem. *Quaternary Geochronology*, *14*, 81-93. https://doi.org/10.1016/j.quageo.2012.04.001

Grün, R. (1989). *ELECTRON SPIN RESONANCE (ESR) DATING*.

Haas, J. N., Richoz, I., Tinner, W., & Wick, L. (1998). Synchronous Holocene climatic oscillations recorded on the Swiss Plateau and at timberline in the Alps. *The Holocene*, *8*(3), Article 3. https://doi.org/10.1191/095968398675491173

Harmon, R. S., Schwarcz, H. P., Gascoyne, M., Hess, J. W., & Ford, D. C. (2004). Paleoclimate Information From Speleothems: The Present As A Guide To The Past. En I. D. Sasowsky & J. Mylroie (Eds.), *Studies of Cave Sediments* (pp. 199-226). Springer Netherlands. https://doi.org/10.1007/978-1-4020-5766-3_11

Harmon, R. S., Schwarcz, H. P., & O'Neil, J. R. (1979). D/H ratios in speleothem fluid inclusions: A guide to variations in the isotopic composition of meteoric precipitation? *Earth and Planetary Science Letters*, *42*(2), Article 2. https://doi.org/10.1016/0012-821X(79)90033-5

Heiri, O., Brooks, S. J., Renssen, H., Bedford, A., Hazekamp, M., Ilyashuk, B., Jeffers, E. S., Lang, B., Kirilova, E., Kuiper, S., Millet, L., Samartin, S., Toth, M., Verbruggen, F., Watson, J. E., van Asch, N., Lammertsma, E., Amon, L., Birks, H. H., … Lotter, A. F. (2014). Validation of climate model-inferred regional temperature change for late-glacial Europe. *Nature Communications*, *5*(1), Article 1. https://doi.org/10.1038/ncomms5914

Heiri, O., Koinig, K. A., Spötl, C., Barrett, S., Brauer, A., Drescher-Schneider, R., Gaar, D., Ivy-Ochs, S., Kerschner, H., Luetscher, M., Moran, A., Nicolussi, K., Preusser, F., Schmidt, R., Schoeneich, P., Schwörer, C., Sprafke, T., Terhorst, B., & Tinner, W. (2014). Palaeoclimate records 60–8 ka in the Austrian and Swiss Alps and their forelands. *Quaternary Science Reviews*, *106*, 186-205. https://doi.org/10.1016/j.quascirev.2014.05.021

Hellstrom, J., & Pickering, R. (2015). Recent advances and future prospects of the U–Th and U–Pb chronometers applicable to archaeology. *Journal of Archaeological Science*, *56*, 32-40. https://doi.org/10.1016/j.jas.2015.02.032

Hendy, C. H. (1971). The isotopic geochemistry of speleothems—I. The calculation of the effects of different modes of formation on the isotopic composition of speleothems and their applicability as palaeoclimatic indicators. *Geochimica et Cosmochimica Acta*, *35*(8), Article 8. https://doi.org/10.1016/0016-7037(71)90127-X

Hill, C., & Forti, P. (1997). *Cave Minerals of the World* (2nd edition). National Speleological Society. https://books.google.es/books?id=UCfwAAAAMAAJ

Hodge, E. J., Richards, D. A., Smart, P. L., Andreo, B., Hoffmann, D. L., Mattey, D. P., & González-Ramón, A. (2008). Effective precipitation in southern Spain (∼ 266 To 46 Ka) based on a speleothem stable carbon isotope record. *Quaternary Research*, *69*(03), Article 03. https://doi.org/10.1016/j.yqres.2008.02.013

Hoffmann, D. L., Prytulak, J., Richards, D. A., Elliott, T., Coath, C. D., Smart, P. L., & Scholz, D. (2007). Procedures for accurate U and Th isotope measurements by high precision MC-ICPMS. *International Journal of Mass Spectrometry*, *264*(2-3), Article 2-3. https://doi.org/10.1016/j.ijms.2007.03.020

Hoffmann, D. L., Spötl, C., & Mangini, A. (2009). Micromill and in situ laser ablation sampling techniques for high spatial resolution MC-ICPMS U-Th dating of carbonates. *Chemical Geology*, *259*(3-4), 253-261. https://doi.org/10.1016/j.chemgeo.2008.11.015

Honiat, C., Koltai, G., Dublyansky, Y., Edwards, R. L., Zhang, H., Cheng, H., & Spötl, C. (2023). A paleoprecipitation and paleotemperature reconstruction of the Last Interglacial in the southeastern Alps. *Climate of the Past*, *19*(6), Article 6. https://doi.org/10.5194/cp-19-1177-2023

Hoogakker, B. A. A., Chapman, M. R., McCave, I. N., Hillaire-Marcel, C., Ellison, C. R. W., Hall, I. R., & Telford, R. J. (2011). Dynamics of North Atlantic Deep Water masses during the Holocene. *Paleoceanography*, *26*(4), Article 4. https://doi.org/10.1029/2011PA002155

Ilyashuk, E. A., Koinig, K. A., Heiri, O., Ilyashuk, B. P., & Psenner, R. (2011). Holocene temperature variations at a high-altitude site in the Eastern Alps: A chironomid record from Schwarzsee ob Sölden, Austria. *Quaternary Science Reviews*, *30*(1-2), Article 1-2. https://doi.org/10.1016/j.quascirev.2010.10.008

Iriarte-Chiapusso, M. J. (2016). Reviewing the Lateglacial-Holocene transition in NW Iberia: A palaeoecological approach based on the comparison between dissimilar regions. *Quaternary International*, 26.

Isarin, R. F. B., & Bohncke, S. J. P. (1999). Mean July Temperatures during the Younger Dryas in Northwestern and Central Europe as Inferred from Climate Indicator Plant Species. *Quaternary Research*, *51*(2), Article 2. https://doi.org/10.1006/qres.1998.2023

Jaffey, A. H., Flynn, K. F., Glendenin, L. E., Bentley, W. C., & Essling, A. M. (1971). Precision Measurement of Half-Lives and Specific Activities of U 235 and U 238. *Physical Review C*, *4*(5), 1889-1906. https://doi.org/10.1103/PhysRevC.4.1889

Jalut, G., Dedoubat, J. J., Fontugne, M., & Otto, T. (2009). Holocene circum-Mediterranean vegetation changes: Climate forcing and human impact. *Quaternary International*, *200*(1-2), Article 1-2. https://doi.org/10.1016/j.quaint.2008.03.012

Jambrina-Enríquez, M., Rico, M., Moreno, A., Leira, M., Bernárdez, P., Prego, R., Recio, C., & Valero-Garcés, B. L. (2014). Timing of deglaciation and postglacial environmental dynamics in NW Iberia: The Sanabria Lake record. *Quaternary Science Reviews*, *94*, 136-158. https://doi.org/10.1016/j.quascirev.2014.04.018

Jamieson, R. A., Baldini, J. U. L., Frappier, A. B., & Müller, W. (2015). Volcanic ash fall events identified using principal component analysis of a high-resolution speleothem trace element dataset. *Earth and Planetary Science Letters*, *426*, 36-45. https://doi.org/10.1016/j.epsl.2015.06.014

Jaqueto, P., Trindade, R. I. F., Terra-Nova, F., Feinberg, J. M., Novello, V. F., Stríkis, N. M., Schroedl, P., Azevedo, V., Strauss, B. E., Cruz, F. W., Cheng, H., & Edwards, R. L. (2022). Stalagmite paleomagnetic record of a quiet mid-to-late Holocene field activity in central South America. *Nature Communications*, *13*(1), Article 1. https://doi.org/10.1038/s41467-022-28972-8

Jiménez De Cisneros, C., Caballero, E., Vera, J. A., Durán, J. J., & Juliá, R. (2003). A record of Pleistocene climate from a stalactite, Nerja Cave, southern Spain. *Palaeogeography, Palaeoclimatology, Palaeoecology*, *189*(1-2), Article 1-2. https://doi.org/10.1016/S0031-0182(02)00589-8

Jiménez de Cisneros, C., González-Ramón, A., Sequero, C., Andreo, B., & Fairchild, I. J. (2020). Isotopic and Petrographic Evidence as a Proxy in Paleoclimatic Reconstructions from Flowstones in Southern Spain. *Open Journal of Geology*, *10*(06), Article 06. https://doi.org/10.4236/ojg.2020.106027

Jiménez de Cisneros, C., Loncomilla, G., González-Ramón, A., & Liñán-Baena, C. (2023). Microstratigraphic Analysis of a Speleothem from the Nerja Cave (Málaga, Southern Spain). En B. Andreo, J. A. Barberá, J. J. Durán-Valsero, J. M. Gil-Márquez, & M. Mudarra (Eds.), *EuroKarst 2022, Málaga* (pp. 201-206). Springer International Publishing.

Jiménez-Moreno, G., Rodríguez-Ramírez, A., Pérez-Asensio, J. N., Carrión, J. S., López-Sáez, J. A., Villarías-Robles, J. J., Celestino-Pérez, S., Cerrillo-Cuenca, E., León, Á., & Contreras, C. (2015). Impact of late-Holocene aridification trend, climate variability and geodynamic control on the environment from a coastal area in SW Spain. *The Holocene*, *25*(4), Article 4. https://doi.org/10.1177/0959683614565955

Kaniewski, D., Marriner, N., Morhange, C., Faivre, S., Otto, T., & Van Campo, E. (2016). Solar pacing of storm surges, coastal flooding and agricultural losses in the Central Mediterranean. *Scientific Reports*, *6*(1), Article 1. https://doi.org/10.1038/srep25197

Kato, H., Mori, T., Amekawa, S., Wu, C.-C., Shen, C.-C., & Kano, A. (2023). Coevolutions of terrestrial temperature and monsoonal precipitation amounts from the latest Pleistocene to the mid-Holocene in Japan: Carbonate clumped isotope record of a stalagmite. *Chemical Geology*, *622*, 121390. https://doi.org/10.1016/j.chemgeo.2023.121390

Kaufman, D., McKay, N., Routson, C., Erb, M., Dätwyler, C., Sommer, P. S., Heiri, O., & Davis, B. (2020). Holocene global mean surface temperature, a multi-method reconstruction approach. *Scientific Data*, *7*(1), 201. https://doi.org/10.1038/s41597-020-0530-7

Kaufmann, G. (2003). Stalagmite growth and palaeo-climate: The numerical perspective. *Earth and Planetary Science Letters*, *214*(1-2), Article 1-2. https://doi.org/10.1016/S0012-821X(03)00369-8

Kendall, C., & Caldwell, E. A. (1998). Fundamentals of Isotope Geochemistry. En *Isotope Tracers in Catchment Hydrology* (pp. 51-86). Elsevier. https://doi.org/10.1016/B978-0-444-81546-0.50009-4

Kilhavn, H., Couchoud, I., Drysdale, R. N., Rossi, C., Hellstrom, J., Arnaud, F., & Wong, H. (2022). The 8.2 ka event in northern Spain: Timing, structure and climatic impact from a multi-proxy speleothem record. *Climate of the Past*, *18*(10), Article 10. https://doi.org/10.5194/cp-18-2321-2022

Kim, S.-T., & O'Neil, J. R. (1997). Equilibrium and nonequilibrium oxygen isotope effects in synthetic carbonates. *Geochimica et Cosmochimica Acta*, *61*(16), Article 16. https://doi.org/10.1016/S0016-7037(97)00169-5

Kindler, P., Guillevic, M., Baumgartner, M., Schwander, J., Landais, A., & Leuenberger, M. (2014). Temperature reconstruction from 10 to 120 kyr b2k from the NGRIP ice core. *Climate of the Past*, *10*(2), Article 2. https://doi.org/10.5194/cp-10-887-2014

Kleiven, H. (Kikki) F., Kissel, C., Laj, C., Ninnemann, U. S., Richter, T. O., & Cortijo, E. (2008). Reduced North Atlantic Deep Water Coeval with the Glacial Lake Agassiz Freshwater Outburst. *Science*, *319*(5859), Article 5859. https://doi.org/10.1126/science.1148924

Kobashi, T., Menviel, L., Jeltsch-Thömmes, A., Vinther, B. M., Box, J. E., Muscheler, R., Nakaegawa, T., Pfister, P. L., Döring, M., Leuenberger, M., Wanner, H., & Ohmura, A. (2017). Volcanic influence on centennial to millennial Holocene Greenland temperature change. *Scientific Reports*, *7*(1), Article 1. https://doi.org/10.1038/s41598-017-01451-7

Kong, Y., & Pang, Z. (2016). A positive altitude gradient of isotopes in the precipitation over the Tianshan Mountains: Effects of moisture recycling and sub-cloud evaporation. *Journal of Hydrology*, *542*, 222-230. https://doi.org/10.1016/j.jhydrol.2016.09.007

Koster, R. D., De Valpine, D. P., & Jouzel, J. (1993). Continental water recycling and H_2 ^{18}O concentrations. *Geophysical Research Letters*, *20*(20), Article 20. https://doi.org/10.1029/93GL01781

Kumar, R. (2011). Neoglaciation. *Encyclopedia of Snow, Ice and Glaciers. Springer,USA*.

Labuhn, I., Genty, D., Vonhof, H., Bourdin, C., Blamart, D., Douville, E., Ruan, J., Cheng, H., Edwards, R. L., Pons-Branchu, E., & Pierre, M. (2015). A high-resolution fluid inclusion δ18O record from a stalagmite in SW France: Modern calibration and comparison with multiple proxies. *Quaternary Science Reviews*, *110*, 152-165. https://doi.org/10.1016/j.quascirev.2014.12.021

Lachniet, M. S. (2004). A 1500-year El Niño/Southern Oscillation and rainfall history for the Isthmus of Panama from speleothem calcite. *Journal of Geophysical Research*, *109*(D20), Article D20. https://doi.org/10.1029/2004JD004694

Lachniet, M. S. (2009). Climatic and environmental controls on speleothem oxygen-isotope values. *Quaternary Science Reviews*, *28*(5-6), Article 5-6. https://doi.org/10.1016/j.quascirev.2008.10.021

Lachniet, M. S., Bernal, J. P., Asmerom, Y., & Polyak, V. (2012). Uranium loss and aragonite–calcite age discordance in a calcitized aragonite stalagmite. *Quaternary Geochronology*, *14*, 26-37. https://doi.org/10.1016/j.quageo.2012.08.003

Lachniet, M. S., Patterson, W. P., Burns, S., Asmerom, Y., & Polyak, V. (2007). Caribbean and Pacific moisture sources on the Isthmus of Panama revealed from stalagmite and surface water $\delta^{18}O$ gradients. *Geophysical Research Letters*, *34*(1), Article 1. https://doi.org/10.1029/2006GL028469

Lamare, P., Chabrol, A. ., & France. (1952). *Carte géologique détaillée 1:80 000. 238, St. Jean-Pied de Port* (2ème édition) [Map]. Service de la carte géologique de la France.

Landais, A., Capron, E., Masson-Delmotte, V., Toucanne, S., Rhodes, R., Popp, T., Vinther, B., Minster, B., & Prié, F. (2018). Ice core evidence for decoupling between midlatitude atmospheric water cycle and Greenland temperature during the last deglaciation. *Climate of the Past*, *14*(10), Article 10. https://doi.org/10.5194/cp-14-1405-2018

Larocque-Tobler, I., Heiri, O., & Wehrli, M. (2010). Late Glacial and Holocene temperature changes at Egelsee, Switzerland, reconstructed using subfossil chironomids. *Journal of Paleolimnology*, *43*(4), Article 4. https://doi.org/10.1007/s10933-009-9358-z

Lechleitner, F. A., Baldini, J. U. L., Breitenbach, S. F. M., Fohlmeister, J., McIntyre, C., Goswami, B., Jamieson, R. A., Van Der Voort, T. S., Prufer, K., Marwan, N., Culleton, B. J., Kennett, D. J., Asmerom, Y., Polyak, V., & Eglinton, T. I. (2016). Hydrological and climatological controls on radiocarbon concentrations in a tropical stalagmite. *Geochimica et Cosmochimica Acta*, *194*, 233-252. https://doi.org/10.1016/j.gca.2016.08.039

Lechleitner, F. A., Day, C. C., Kost, O., Wilhelm, M., Haghipour, N., Henderson, G. M., & Stoll, H. M. (2021). Stalagmite carbon isotopes suggest deglacial increase in soil respiration in western Europe driven by temperature change. *Climate of the Past*, *17*(5), Article 5. https://doi.org/10.5194/cp-17-1903-2021

LeGrande, A. N., & Schmidt, G. A. (2006). Global gridded data set of the oxygen isotopic composition in seawater. *Geophysical Research Letters*, *33*(12), Article 12. https://doi.org/10.1029/2006GL026011

LeGrande, A. N., & Schmidt, G. A. (2008). Ensemble, water isotope-enabled, coupled general circulation modeling insights into the 8.2 ka event: ENSEMBLE, δ^{18}O GCM OF THE 8.2 KA EVENT. *Paleoceanography*, *23*(3), Article 3. https://doi.org/10.1029/2008PA001610

Leunda, M., González-Sampériz, P., Gil-Romera, G., Aranbarri, J., Moreno, A., Oliva-Urcia, B., Sevilla-Callejo, M., & Valero-Garcés, B. (2017). The Late-Glacial and Holocene Marboré Lake sequence (2612 m a.s.l., Central Pyrenees, Spain): Testing high altitude sites sensitivity to millennial scale vegetation and climate variability. *Global and Planetary Change*, *157*, 214-231. https://doi.org/10.1016/j.gloplacha.2017.08.008

Leunda, M., González-Sampériz, P., Gil-Romera, G., Bartolomé, M., Belmonte-Ribas, Á., Gómez-García, D., Kaltenrieder, P., Rubiales, J. M., Schwörer, C., Tinner, W., Morales-Molino, C., & Sancho, C. (2019). Ice cave reveals environmental forcing of long-term Pyrenean tree line dynamics. *Journal of Ecology*, *107*(2), Article 2. https://doi.org/10.1111/1365-2745.13077

Li, H., Spötl, C., & Cheng, H. (2020). A high-resolution speleothem proxy record of the Late Glacial in the European Alps: Extending the NALPS19 record until the beginning of the Holocene. *Journal of Quaternary Science*, *36*(1), Article 1. https://doi.org/10.1002/jqs.3255

Li, Y.-X., Törnqvist, T. E., Nevitt, J. M., & Kohl, B. (2012). Synchronizing a sea-level jump, final Lake Agassiz drainage, and abrupt cooling 8200 years ago. *Earth and Planetary Science Letters*, *315-316*, 41-50. https://doi.org/10.1016/j.epsl.2011.05.034

Liu, Z., Otto-Bliesner, B. L., He, F., Brady, E. C., Tomas, R., Clark, P. U., Carlson, A. E., Lynch-Stieglitz, J., Curry, W., Brook, E., Erickson, D., Jacob, R., Kutzbach, J., & Cheng, J. (2009). Transient Simulation of Last Deglaciation with a New Mechanism for Bølling-Allerød Warming. *Science*, *325*(5938), 310-314. https://doi.org/10.1126/science.1171041

Liu, Z., Zhu, J., Rosenthal, Y., Zhang, X., Otto-Bliesner, B. L., Timmermann, A., Smith, R. S., Lohmann, G., Zheng, W., & Elison Timm, O. (2014). The Holocene temperature conundrum. *Proceedings of the National Academy of Sciences*, *111*(34), Article 34. https://doi.org/10.1073/pnas.1407229111

Lopez-Elorza, M., Muñoz-García, M. B., González-Acebrón, L., & Martín-Chivelet, J. (2021). Fluid-inclusion petrography in calcite stalagmites: Implications for entrapment processes. *Journal of Sedimentary Research*, *91*(11), Article 11. https://doi.org/10.2110/jsr.2021.016

López-Merino, L., Silva Sánchez, N., Kaal, J., López-Sáez, J. A., & Martínez Cortizas, A. (2012). Post-disturbance vegetation dynamics during the Late Pleistocene and the Holocene: An example from NW Iberia. *Global and Planetary Change*, *92-93*, 58-70. https://doi.org/10.1016/j.gloplacha.2012.04.003

Lorens, R. B. (1981). Sr, Cd, Mn and Co distribution coefficients in calcite as a function of calcite precipitation rate. *Geochimica et Cosmochimica Acta*, *45*(4), Article 4. https://doi.org/10.1016/0016-7037(81)90188-5

Ludwig, K. R., Simmons, K. R., Szabo, B. J., Winograd, I. J., Landwehr, J. M., Riggs, A. C., & Hoffman, R. J. (1992). Mass-Spectrometric ^{230}Th-^{234}U-^{238}U Dating of the Devils Hole Calcite Vein. *Science*, *258*(5080), Article 5080. https://doi.org/10.1126/science.258.5080.284

Luetscher, M., Boch, R., Sodemann, H., Spötl, C., Cheng, H., Edwards, R. L., Frisia, S., Hof, F., & Müller, W. (2015). North Atlantic storm track changes during the Last Glacial Maximum recorded by

Alpine speleothems. *Nature Communications*, *6*(1), Article 1. https://doi.org/10.1038/ncomms7344

Magny, M., Combourieu-Nebout, N., de Beaulieu, J. L., Bout-Roumazeilles, V., Colombaroli, D., Desprat, S., Francke, A., Joannin, S., Ortu, E., Peyron, O., Revel, M., Sadori, L., Siani, G., Sicre, M. A., Samartin, S., Simonneau, A., Tinner, W., Vannière, B., Wagner, B., … Wirth, S. (2013). North–south palaeohydrological contrasts in the central Mediterranean during the Holocene: Tentative synthesis and working hypotheses. *Climate of the Past*, *9*(5), Article 5. https://doi.org/10.5194/cp-9-2043-2013

Magny, M., Vannière, B., Calo, C., Millet, L., Leroux, A., Peyron, O., Zanchetta, G., La Mantia, T., & Tinner, W. (2011). Holocene hydrological changes in south-western Mediterranean as recorded by lake-level fluctuations at Lago Preola, a coastal lake in southern Sicily, Italy. *Quaternary Science Reviews*, *30*(19-20), Article 19-20. https://doi.org/10.1016/j.quascirev.2011.05.018

Magny, M., Vannière, B., De Beaulieu, J.-L., Bégeot, C., Heiri, O., Millet, L., Peyron, O., & Walter-Simonnet, A.-V. (2007). Early-Holocene climatic oscillations recorded by lake-level fluctuations in west-central Europe and in central Italy. *Quaternary Science Reviews*, *26*(15-16), Article 15-16. https://doi.org/10.1016/j.quascirev.2006.04.013

Marcott, S. A., Shakun, J. D., Clark, P. U., & Mix, A. C. (2013). A Reconstruction of Regional and Global Temperature for the Past 11,300 Years. *Science*, *339*(6124), Article 6124. https://doi.org/10.1126/science.1228026

Marsicek, J., Shuman, B. N., Bartlein, P. J., Shafer, S. L., & Brewer, S. (2018). Reconciling divergent trends and millennial variations in Holocene temperatures. *Nature*, *554*(7690), Article 7690. https://doi.org/10.1038/nature25464

Martín-Chivelet, J., Muñoz-García, M. B., Cruz, J. A., Ortega, A. I., & Turrero, M. J. (2017). Speleothem Architectural Analysis: Integrated approach for stalagmite-based paleoclimate research. *Sedimentary Geology*, *353*, 28-45. https://doi.org/10.1016/j.sedgeo.2017.03.003

Martín-Chivelet, J., Muñoz-García, M. B., Domínguez-Villar, D., Turrero, M. J., & Ortega, A. I. (2006). *COMPARATIVE ANALYSIS OF STALAGMITES FROM TWO CAVES OF NORTHERN SPAIN. IMPLICATIONS FOR HOLOCENE PALEOCLIMATE STUDIES.*

Martín-Chivelet, J., Muñoz-García, M. B., Edwards, R. L., Turrero, M. J., & Ortega, A. I. (2011). Land surface temperature changes in Northern Iberia since 4000yrBP, based on δ13C of speleothems. *Global and Planetary Change*, *77*(1-2), Article 1-2. https://doi.org/10.1016/j.gloplacha.2011.02.002

Martín-Chivelet, J., Turrero, M. J., Garralón, A., Gómez, P., Sánchez, L., & Ortega, A. I. (2007). *Geochemical evolution of drip-water and present-growing calcite at Kaite cave (N Spain). 2*, 1187-1190. Scopus. https://www.scopus.com/inward/record.uri?eid=2-s2.0-79956289428&partnerID=40&md5=98dcbafbc272b6b95bc65a73122085dc

Martín-García, R., Alonso-Zarza, A. M., Frisia, S., Rodríguez-Berriguete, Á., Drysdale, R., & Hellstrom, J. (2019). Effect of aragonite to calcite transformation on the geochemistry and dating accuracy of speleothems. An example from Castañar Cave, Spain. *Sedimentary Geology*, *383*, 41-54. https://doi.org/10.1016/j.sedgeo.2019.01.014

Martín-García, R., Alonso-Zarza, A. M., Martín-Pérez, A., Schröder-Ritzrau, A., & Ludwig, T. (2014). Relationships between colour and diagenesis in the aragonite-calcite speleothems in Basajaún Etxea cave, Spain. *Sedimentary Geology*, *312*, 63-75. https://doi.org/10.1016/j.sedgeo.2014.08.001

Martrat, B., Grimalt, J. O., Lopez-Martinez, C., Cacho, I., Sierro, F. J., Flores, J. A., Zahn, R., Canals, M., Curtis, J. H., & Hodell, D. A. (2004). Abrupt Temperature Changes in the Western Mediterranean over the Past 250,000 Years. *Science*, *306*(5702), Article 5702. https://doi.org/10.1126/science.1101706

Martrat, B., Grimalt, J. O., Shackleton, N. J., de Abreu, L., Hutterli, M. A., & Stocker, T. F. (2007). Four Climate Cycles of Recurring Deep and Surface Water Destabilizations on the Iberian Margin. *Science*, *317*(5837), Article 5837. https://doi.org/10.1126/science.1139994

Martrat, B., Jimenez-Amat, P., Zahn, R., & Grimalt, J. O. (2014). Similarities and dissimilarities between the last two deglaciations and interglaciations in the North Atlantic region. *Quaternary Science Reviews*, *99*, 122-134. https://doi.org/10.1016/j.quascirev.2014.06.016

Masson-Delmotte, V., Jouzel, J., Landais, A., Stievenard, M., Johnsen, S. J., White, J. W. C., Werner, M., Sveinbjornsdottir, A., & Fuhrer, K. (2005). GRIP Deuterium Excess Reveals Rapid and Orbital-Scale Changes in Greenland Moisture Origin. *Science*, *309*(5731), Article 5731. https://doi.org/10.1126/science.1108575

Matero, I. S. O., Gregoire, L. J., Ivanovic, R. F., Tindall, J. C., & Haywood, A. M. (2017). The 8.2 ka cooling event caused by Laurentide ice saddle collapse. *Earth and Planetary Science Letters*, *473*, 205-214. https://doi.org/10.1016/j.epsl.2017.06.011

Mattey, D. P., Fairchild, I. J., Atkinson, T. C., Latin, J.-P., Ainsworth, M., & Durell, R. (2010). Seasonal microclimate control of calcite fabrics, stable isotopes and trace elements in modern speleothem from St Michaels Cave, Gibraltar. *Geological Society, London, Special Publications*, *336*(1), 323-344. https://doi.org/10.1144/SP336.17

Mauri, A., Davis, B. A. S., Collins, P. M., & Kaplan, J. O. (2015). The climate of Europe during the Holocene: A gridded pollen-based reconstruction and its multi-proxy evaluation. *Quaternary Science Reviews*, *112*, 109-127. https://doi.org/10.1016/j.quascirev.2015.01.013

Mayewski, P. A., Rohling, E. E., Curt Stager, J., Karlén, W., Maasch, K. A., Meeker, L. D., Meyerson, E. A., Gasse, F., van Kreveld, S., Holmgren, K., Lee-Thorp, J., Rosqvist, G., Rack, F., Staubwasser, M., Schneider, R. R., & Steig, E. J. (2004). Holocene climate variability. *Quaternary Research*, *62*(3), Article 3. https://doi.org/10.1016/j.yqres.2004.07.001

McDermott, F. (2004). Palaeo-climate reconstruction from stable isotope variations in speleothems: A review. *Quaternary Science Reviews*, *23*(7-8), Article 7-8. https://doi.org/10.1016/j.quascirev.2003.06.021

McDermott, F., Mattey, D. P., & Hawkesworth, C. (2001). Centennial-Scale Holocene Climate Variability Revealed by a High-Resolution Speleothem δ^{18}O Record from SW Ireland. *Science*, *294*(5545), Article 5545. https://doi.org/10.1126/science.1063678

McGarry, S., Bar-Matthews, M., Matthews, A., Vaks, A., Schilman, B., & Ayalon, A. (2004). Constraints on hydrological and paleotemperature variations in the Eastern Mediterranean region in the last 140ka given by the δD values of speleothem fluid inclusions. *Quaternary Science Reviews*, *23*(7-8), Article 7-8. https://doi.org/10.1016/j.quascirev.2003.06.020

McKay, N. P., Kaufman, D. S., Routson, C. C., Erb, M. P., & Zander, P. D. (2018). The Onset and Rate of Holocene Neoglacial Cooling in the Arctic. *Geophysical Research Letters*, *45*(22), Article 22. https://doi.org/10.1029/2018GL079773

McManus, J. F., Francois, R., Gherardi, J.-M., Keigwin, L. D., & Brown-Leger, S. (2004). Collapse and rapid resumption of Atlantic meridional circulation linked to deglacial climate changes. *Nature*, *428*(6985), Article 6985. https://doi.org/10.1038/nature02494

Meckler, A. N., Affolter, S., Dublyansky, Y. V., Krüger, Y., Vogel, N., Bernasconi, S. M., Frenz, M., Kipfer, R., Leuenberger, M., Spötl, C., Carolin, S., Cobb, K. M., Moerman, J., Adkins, J. F., & Fleitmann, D. (2015). Glacial–interglacial temperature change in the tropical West Pacific: A comparison of stalagmite-based paleo-thermometers. *Quaternary Science Reviews*, *127*, 90-116. https://doi.org/10.1016/j.quascirev.2015.06.015

Medina-Elizalde, M., Burns, S. J., Lea, D. W., Asmerom, Y., Von Gunten, L., Polyak, V., Vuille, M., & Karmalkar, A. (2010). High resolution stalagmite climate record from the Yucatán Peninsula spanning the Maya terminal classic period. *Earth and Planetary Science Letters*, *298*(1-2), Article 1-2. https://doi.org/10.1016/j.epsl.2010.08.016

Medina-Elizalde, M., & Rohling, E. J. (2012). Collapse of Classic Maya Civilization Related to Modest Reduction in Precipitation. *Science*, *335*(6071), Article 6071. https://doi.org/10.1126/science.1216629

Mesa-Fernández, J. M., Jiménez-Moreno, G., Rodrigo-Gámiz, M., García-Alix, A., Jiménez-Espejo, F. J., Martínez-Ruiz, F., Anderson, R. S., Camuera, J., & Ramos-Román, M. J. (2018). Vegetation and geochemical responses to Holocene rapid climate change in the Sierra Nevada (southeastern

Iberia): The Laguna Hondera record. *Climate of the Past*, *14*(11), Article 11. https://doi.org/10.5194/cp-14-1687-2018

Meyer, M. C., Spötl, C., & Mangini, A. (2008). The demise of the Last Interglacial recorded in isotopically dated speleothems from the Alps. *Quaternary Science Reviews*, *27*(5-6), Article 5-6. https://doi.org/10.1016/j.quascirev.2007.11.005

Mickler, P. J., Banner, J. L., Stern, L., Asmerom, Y., Edwards, R. L., & Ito, E. (2004). Stable isotope variations in modern tropical speleothems: Evaluating equilibrium vs. kinetic isotope effects. *Geochimica et Cosmochimica Acta*, *68*(21), Article 21. https://doi.org/10.1016/j.gca.2004.02.012

Millet, L., Rius, D., Galop, D., Heiri, O., & Brooks, S. J. (2012). Chironomid-based reconstruction of Lateglacial summer temperatures from the Ech palaeolake record (French western Pyrenees). *Palaeogeography, Palaeoclimatology, Palaeoecology*, *315-316*, 86-99. https://doi.org/10.1016/j.palaeo.2011.11.014

Monnin, E., Indermühle, A., Dällenbach, A., Flückiger, J., Stauffer, B., Stocker, T. F., Raynaud, D., & Barnola, J.-M. (2001). Atmospheric CO_2 Concentrations over the Last Glacial Termination. *Science*, *291*(5501), Article 5501. https://doi.org/10.1126/science.291.5501.112

Moore, G. (1952). Speleothem—A new cave term. *National Speleological Society News*, *10*(6), 2.

Morellón, M., Aranbarri, J., Moreno, A., González-Sampériz, P., & Valero-Garcés, B. L. (2018). Early Holocene humidity patterns in the Iberian Peninsula reconstructed from lake, pollen and speleothem records. *Quaternary Science Reviews*, *181*, 1-18. https://doi.org/10.1016/j.quascirev.2017.11.016

Morellón, M., Valero-Garcés, B., Vegas-Vilarrúbia, T., González-Sampériz, P., Romero, Ó., Delgado-Huertas, A., Mata, P., Moreno, A., Rico, M., & Corella, J. P. (2009). Lateglacial and Holocene palaeohydrology in the western Mediterranean region: The Lake Estanya record (NE Spain). *Quaternary Science Reviews*, *28*(25-26), Article 25-26. https://doi.org/10.1016/j.quascirev.2009.05.014

Moreno, A., Iglesias, M., Azorin-Molina, C., Pérez-Mejías, C., Bartolomé, M., Sancho, C., Stoll, H., Cacho, I., Frigola, J., Osácar, C., Muñoz, A., Delgado-Huertas, A., Bladé, I., & Vimeux, F. (2021). Measurement report: Spatial variability of northern Iberian rainfall stable isotope values – investigating atmospheric controls on daily and monthly timescales. *Atmospheric Chemistry and Physics*, *21*(13), Article 13. https://doi.org/10.5194/acp-21-10159-2021

Moreno, A., Morellón, M., Martín-Puertas, C., Frigola, J., Canals, M., Cacho, I., Corella, J., Pérez, A., Belmonte, A., Vegas-Vilarrúbia, T., González-Sampériz, P., & Valero-Garcés, B. (2011). Was there a common hydrological pattern in the Iberian Peninsula region during the Medieval Climate Anomaly? *PAGES News*, *19*(1), Article 1. https://doi.org/10.22498/pages.19.1.16

Moreno, A., Pérez-Mejías, C., Bartolomé, M., Sancho, C., Cacho, I., Stoll, H., Delgado-Huertas, A., Hellstrom, J., Edwards, R. L., & Cheng, H. (2017). New speleothem data from Molinos and Ejulve caves reveal Holocene hydrological variability in northeast Iberia. *Quaternary Research*, *88*(2), Article 2. https://doi.org/10.1017/qua.2017.39

Moreno, A., Sancho, C., Bartolomé, M., Oliva-Urcia, B., Delgado-Huertas, A., Estrela, M. J., Corell, D., López-Moreno, J. I., & Cacho, I. (2014). Climate controls on rainfall isotopes and their effects on cave drip water and speleothem growth: The case of Molinos cave (Teruel, NE Spain). *Climate Dynamics*, *43*(1-2), Article 1-2. https://doi.org/10.1007/s00382-014-2140-6

Moreno, A., Stoll, H., Jiménez-Sánchez, M., Cacho, I., Valero-Garcés, B., Ito, E., & Edwards, R. L. (2010). A speleothem record of glacial (25–11.6kyr BP) rapid climatic changes from northern Iberian Peninsula. *Global and Planetary Change*, *71*(3-4), Article 3-4. https://doi.org/10.1016/j.gloplacha.2009.10.002

Moreno, A., Svensson, A., Brooks, S. J., Connor, S., Engels, S., Fletcher, W., Genty, D., Heiri, O., Labuhn, I., Perşoiu, A., Peyron, O., Sadori, L., Valero-Garcés, B., Wulf, S., & Zanchetta, G. (2014). A compilation of Western European terrestrial records 60–8 ka BP: Towards an understanding of latitudinal climatic gradients. *Quaternary Science Reviews*, *106*, 167-185. https://doi.org/10.1016/j.quascirev.2014.06.030

Morrill, C., Anderson, D. M., Bauer, B. A., Buckner, R., Gille, E. P., Gross, W. S., Hartman, M., & Shah, A. (2013). Proxy benchmarks for intercomparison of 8.2 ka simulations. *Climate of the Past*, *9*(1), Article 1. https://doi.org/10.5194/cp-9-423-2013

Moseley, G. E., Spötl, C., Brandstätter, S., Erhardt, T., Luetscher, M., & Edwards, R. L. (2020). NALPS19: Sub-orbital-scale climate variability recorded in northern Alpine speleothems during the last glacial period. *Climate of the Past*, *16*(1), Article 1. https://doi.org/10.5194/cp-16-29-2020

Muñoz, A., Bartolomé, M., Muñoz, A., Sancho, C., Moreno, A., Hellstrom, J. C., Osácar, M. C., & Cacho, I. (2015). Solar influence and hydrological variability during the Holocene from a speleothem annual record (Molinos Cave, NE Spain). *Terra Nova*, *27*(4), Article 4. https://doi.org/10.1111/ter.12160

Muñoz, A., Osácar Soriano, M. C., & Sancho Marcén, C. (2009). Estacionalidad de la laminación espeleotémica de las Cuevas de Oetigosa de Cameros (La Rioja): Aproximación expermental. *Geogaceta*, *46*, Article 46.

Muñoz, A., & Sancho, C. (2008). *MONITORIZACIÓN CLIMÁTICA DE LAS CUEVAS DE ORTIGOSA DE CAMEROS (LA RIOJA): APLICACIÓN A LA INTERPRETACIÓN DEL REGISTRO CLIMÁTICO DE LOS ESPELEOTEMAS HOLOCENOS.*

Muñoz Sobrino, C., Heiri, O., Hazekamp, M., van der Velden, D., Kirilova, E. P., García-Moreiras, I., & Lotter, A. F. (2013). New data on the Lateglacial period of SW Europe: A high resolution multiproxy record from Laguna de la Roya (NW Iberia). *Quaternary Science Reviews*, *80*, 58-77. https://doi.org/10.1016/j.quascirev.2013.08.016

Muñoz-García, M. B., Cruz, J., Martín-Chivelet, J., Ortega, A. I., Turrero, M. J., & López-Elorza, M. (2016). Comparison of speleothem fabrics and microstratigraphic stacking patterns in calcite stalagmites as indicators of paleoenvironmental change. *Quaternary International*, *407*, 74-85. https://doi.org/10.1016/j.quaint.2016.02.036

Muñoz-García, M. B., Martín Chivelet, J., & Rossi Nieto, C. (2004). Implicaciones paleoclimáticas de la distribución geocronológica de espeleotemas en la Cueva del Cobre (Palencia). *Geogaceta*, *35*, Article 35.

Muñoz-García, M. B., Martín-Chivelet, J., Rossi, C., Ford, D. C., & Schwarcz, H. P. (2007). Chronology of Termination II and the Last Interglacial Period in North Spain based on stable isotope records of stalagmites from Cueva del Cobre (Palencia). *Journal of Iberian Geology*.

Muschitiello, F., D'Andrea, W. J., Schmittner, A., Heaton, T. J., Balascio, N. L., deRoberts, N., Caffee, M. W., Woodruff, T. E., Welten, K. C., Skinner, L. C., Simon, M. H., & Dokken, T. M. (2019). Deep-water circulation changes lead North Atlantic climate during deglaciation. *Nature Communications*, *10*(1), Article 1. https://doi.org/10.1038/s41467-019-09237-3

Naughton, F., Costas, S., Gomes, S. D., Desprat, S., Rodrigues, T., Sanchez Goñi, M. F., Renssen, H., Trigo, R., Bronk-Ramsey, C., Oliveira, D., Salgueiro, E., Voelker, A. H. L., & Abrantes, F. (2019). Coupled ocean and atmospheric changes during Greenland stadial 1 in southwestern Europe. *Quaternary Science Reviews*, *212*, 108-120. https://doi.org/10.1016/j.quascirev.2019.03.033

Naughton, F., Sanchez Goñi, M. F., Rodrigues, T., Salgueiro, E., Costas, S., Desprat, S., Duprat, J., Michel, E., Rossignol, L., Zaragosi, S., Voelker, A. H. L., & Abrantes, F. (2016). Climate variability across the last deglaciation in NW Iberia and its margin. *Quaternary International*, *414*, 9-22. https://doi.org/10.1016/j.quaint.2015.08.073

Nebout, N. C., Peyron, O., Dormoy, I., Desprat, S., Beaudouin, C., Kotthoff, U., & Marret, F. (2009). Rapid climatic variability in the west Mediterranean during the last 25 000 years from high resolution pollen data. *Clim. Past*, 19.

Ng, H. C., Robinson, L. F., McManus, J. F., Mohamed, K. J., Jacobel, A. W., Ivanovic, R. F., Gregoire, L. J., & Chen, T. (2018). Coherent deglacial changes in western Atlantic Ocean circulation. *Nature Communications*, *9*(1), Article 1. https://doi.org/10.1038/s41467-018-05312-3

Nielsen, L. C., De Yoreo, J. J., & DePaolo, D. J. (2013). General model for calcite growth kinetics in the presence of impurity ions. *Geochimica et Cosmochimica Acta*, *115*, 100-114. https://doi.org/10.1016/j.gca.2013.04.001

References

O'Brien, S. R., Mayewski, P. A., Meeker, L. D., Meese, D. A., Twickler, M. S., & Whitlow, S. I. (1995). Complexity of Holocene Climate as Reconstructed from a Greenland Ice Core. *Science*, *270*(5244), Article 5244. https://doi.org/10.1126/science.270.5244.1962

Olagüe, V. (1951). *¿Acaban los pirineos en el río Oria?*

Olonscheck, D., & Notz, D. (2017). Consistently Estimating Internal Climate Variability from Climate Model Simulations. *Journal of Climate*, *30*(23), Article 23. https://doi.org/10.1175/JCLI-D-16-0428.1

Ortega, R., Maire, R., Devès, G., & Quinif, Y. (2005). High-resolution mapping of uranium and other trace elements in recrystallized aragonite–calcite speleothems from caves in the Pyrenees (France): Implication for U-series dating. *Earth and Planetary Science Letters*, *237*(3-4), 911-923. https://doi.org/10.1016/j.epsl.2005.06.045

Osácar, M. C., Sancho, C., Muñoz, A., Bartolomé, M., Moreno, A., Delgado-Huertas, A., & Cacho, I. (2014). Tracking the oxygen isotopic signature from the rainfall to the speleothems in Ortigosa de Cameros caves (La Rioja, Spain). *Estudios Geológicos*, *70*(2), Article 2. https://doi.org/10.3989/egeol.41730.319

Osete, M.-L., Martín-Chivelet, J., Rossi, C., Edwards, R. L., Egli, R., Muñoz-García, M. B., Wang, X., Pavón-Carrasco, F. J., & Heller, F. (2012). The Blake geomagnetic excursion recorded in a radiometrically dated speleothem. *Earth and Planetary Science Letters*, *353-354*, 173-181. https://doi.org/10.1016/j.epsl.2012.07.041

Otero, V. (2009). Tres años de estudios microclimáticos en la cueva de Mendukilo. *sociedad española de espeleología y ciencias del karst, boletin nº7*, 46-59.

Peck, V. L., Hall, I. R., Zahn, R., Elderfield, H., Grousset, F., Hemming, S. R., & Scourse, J. D. (2006). High resolution evidence for linkages between NW European ice sheet instability and Atlantic Meridional Overturning Circulation. *Earth and Planetary Science Letters*, *243*(3-4), Article 3-4. https://doi.org/10.1016/j.epsl.2005.12.023

Pellicer, X. M., Corella, J. P., Gutiérrez, F., Roqué, C., Linares, R., Carbonel, D., Zarroca, M., Guerrero, J., & Comas, X. (2016). Sedimentological and palaeohydrological characterization of Late Pleistocene and Holocene tufa mound palaeolakes using trenching methods in the Spanish Pyrenees. *Sedimentology*, *63*(6), Article 6. https://doi.org/10.1111/sed.12290

Peltier, W. R. (2004). GLOBAL GLACIAL ISOSTASY AND THE SURFACE OF THE ICE-AGE EARTH: The ICE-5G (VM2) Model and GRACE. *Annual Review of Earth and Planetary Sciences*, *32*(1), 111-149. https://doi.org/10.1146/annurev.earth.32.082503.144359

Pérez-Mejías, C. (2013). *La cueva de El Recuenco (Ejulve, Teruel): Espeleogénesis y registro de cambios climáticos rápidos durante el Holoceno*. Universidad de Zaragoza.

Pérez-Mejías, C. (2019). *The Ejulve cave speleothemic record:from monitoring control to abrupt climate changes during the Pleistocene in the Eastern Iberian Range (Teruel)*. Universidad de Zaragoza.

Pérez-Mejías, C., Moreno, A., Bernal-Wormull, J., Cacho, I., Osácar, M. C., Edwards, R. L., & Cheng, H. (2021). Oldest Dryas hydroclimate reorganization in the eastern Iberian Peninsula after the iceberg discharges of Heinrich Event 1. *Quaternary Research*, *101*, 67-83. https://doi.org/10.1017/qua.2020.112

Pérez-Mejías, C., Moreno, A., Sancho, C., Bartolomé, M., Stoll, H., Cacho, I., Cheng, H., & Edwards, R. L. (2017). Abrupt climate changes during Termination III in Southern Europe. *Proceedings of the National Academy of Sciences*, *114*(38), Article 38. https://doi.org/10.1073/pnas.1619615114

Pérez-Mejías, C., Moreno, A., Sancho, C., Bartolomé, M., Stoll, H., Osácar, M. C., Cacho, I., & Delgado-Huertas, A. (2018). Transference of isotopic signal from rainfall to dripwaters and farmed calcite in Mediterranean semi-arid karst. *Geochimica et Cosmochimica Acta*, *243*, 66-98. https://doi.org/10.1016/j.gca.2018.09.014

Pérez-Mejías, C., Moreno, A., Sancho, C., Martín-García, R., Spötl, C., Cacho, I., Cheng, H., & Edwards, R. L. (2019). Orbital-to-millennial scale climate variability during Marine Isotope Stages 5 to 3 in northeast Iberia. *Quaternary Science Reviews*, *224*, 105946. https://doi.org/10.1016/j.quascirev.2019.105946

Pérez-Mejías, C., Sancho, C., Gázquez, F., Moreno, A., Bartolomé, M., Osácar, M. C., & Cheng, H. (2019). Insights into the speleogenesis of Ejulve cave (Iberian Range, NE Spain): Quaternary

hydrothermal karstification? *Journal of Iberian Geology*, *45*(3), Article 3. https://doi.org/10.1007/s41513-019-00107-x

Pérez-Obiol, R., Bal, M.-C., Pèlachs, A., Cunill, R., & Soriano, J. M. (2012). Vegetation dynamics and anthropogenically forced changes in the Estanilles peat bog (southern Pyrenees) during the last seven millennia. *Vegetation History and Archaeobotany*, *21*(4-5), 385-396. https://doi.org/10.1007/s00334-012-0351-5

Pérez-Sanz, A., González-Sampériz, P., Moreno, A., Valero-Garcés, B., Gil-Romera, G., Rieradevall, M., Tarrats, P., Lasheras-Álvarez, L., Morellón, M., Belmonte, A., Sancho, C., Sevilla-Callejo, M., & Navas, A. (2013). Holocene climate variability, vegetation dynamics and fire regime in the central Pyrenees: The Basa de la Mora sequence (NE Spain). *Quaternary Science Reviews*, *73*, 149-169. https://doi.org/10.1016/j.quascirev.2013.05.010

Perry, C. A., & Hsu, K. J. (2000). Geophysical, archaeological, and historical evidence support a solar-output model for climate change. *Proceedings of the National Academy of Sciences*, *97*(23), 12433-12438. https://doi.org/10.1073/pnas.230423297

Peyron, O., Combourieu-Nebout, N., Brayshaw, D., Goring, S., Andrieu-Ponel, V., Desprat, S., Fletcher, W., Gambin, B., Ioakim, C., Joannin, S., Kotthoff, U., Kouli, K., Montade, V., Pross, J., Sadori, L., & Magny, M. (2017). Precipitation changes in the Mediterranean basin during the Holocene from terrestrial and marine pollen records: A model–data comparison. *Climate of the Past*, *13*(3), 249-265. https://doi.org/10.5194/cp-13-249-2017

Plunkett, G., & Swindles, G. T. (2008). Determining the Sun's influence on Lateglacial and Holocene climates: A focus on climate response to centennial-scale solar forcing at 2800cal.BP. *Quaternary Science Reviews*, *27*(1-2), Article 1-2. https://doi.org/10.1016/j.quascirev.2007.01.015

Poage, M. A. (2001). Empirical relationships between elevation and the stable isotope composition of precipitation and surface waters: Considerations for studies of paleoelevation change. *American Journal of Science*, *301*(1), 1-15. https://doi.org/10.2475/ajs.301.1.1

Polyak, V. J., & Asmerom, Y. (2001). Late Holocene Climate and Cultural Changes in the Southwestern United States. *Science*, *294*(5540), Article 5540. https://doi.org/10.1126/science.1062771

Railsback, L. B., Liang, F., Vidal Romaní, J. R., Grandal-d'Anglade, A., Vaqueiro Rodríguez, M., Santos Fidalgo, L., Fernández Mosquera, D., Cheng, H., & Edwards, R. L. (2011). Petrographic and isotopic evidence for Holocene long-term climate change and shorter-term environmental shifts from a stalagmite from the Serra do Courel of northwestern Spain, and implications for climatic history across Europe and the Mediterranean. *Palaeogeography, Palaeoclimatology, Palaeoecology*, *305*(1-4), Article 1-4. https://doi.org/10.1016/j.palaeo.2011.02.030

Rasmussen, S. O., Andersen, K. K., Svensson, A. M., Steffensen, J. P., Vinther, B. M., Clausen, H. B., Siggaard-Andersen, M.-L., Johnsen, S. J., Larsen, L. B., Dahl-Jensen, D., Bigler, M., Röthlisberger, R., Fischer, H., Goto-Azuma, K., Hansson, M. E., & Ruth, U. (2006). A new Greenland ice core chronology for the last glacial termination. *Journal of Geophysical Research*, *111*(D6), Article D6. https://doi.org/10.1029/2005JD006079

Rasmussen, S. O., Bigler, M., Blockley, S. P., Blunier, T., Buchardt, S. L., Clausen, H. B., Cvijanovic, I., Dahl-Jensen, D., Johnsen, S. J., Fischer, H., Gkinis, V., Guillevic, M., Hoek, W. Z., Lowe, J. J., Pedro, J. B., Popp, T., Seierstad, I. K., Steffensen, J. P., Svensson, A. M., … Winstrup, M. (2014). A stratigraphic framework for abrupt climatic changes during the Last Glacial period based on three synchronized Greenland ice-core records: Refining and extending the INTIMATE event stratigraphy. *Quaternary Science Reviews*, *106*, 14-28. https://doi.org/10.1016/j.quascirev.2014.09.007

Rasmussen, S. O., Vinther, B. M., Clausen, H. B., & Andersen, K. K. (2007). Early Holocene climate oscillations recorded in three Greenland ice cores. *Quaternary Science Reviews*, *26*(15-16), Article 15-16. https://doi.org/10.1016/j.quascirev.2007.06.015

Rat, P. (1988). The Basque-Cantabrian Basin Between The Iberian And European Plates Some Facts But Still Many Problems. *Revista de la Sociedad Geológica de España*, *1*(3-4), Article 3-4.

Regattieri, E., Zanchetta, G., Drysdale, R. N., Isola, I., Woodhead, J. D., Hellstrom, J. C., Giaccio, B., Greig, A., Baneschi, I., & Dotsika, E. (2016). Environmental variability between the penultimate deglaciation and the mid Eemian: Insights from Tana che Urla (central Italy) speleothem trace

element record. *Quaternary Science Reviews*, *152*, 80-92. https://doi.org/10.1016/j.quascirev.2016.09.027

Renssen, H., & Isarin, R. F. B. (2001). The two major warming phases of the last deglaciation at ~14.7 and ~11.5 ka cal BP in Europe: Climate reconstructions and AGCM experiments. *Global and Planetary Change*, *30*(1-2), Article 1-2. https://doi.org/10.1016/S0921-8181(01)00082-0

Renssen, H., Seppä, H., Heiri, O., Roche, D. M., Goosse, H., & Fichefet, T. (2009). The spatial and temporal complexity of the Holocene thermal maximum. *Nature Geoscience*, *2*(6), Article 6. https://doi.org/10.1038/ngeo513

Richards, D. A., & Dorale, J. A. (2003). *Uranium-series Chronology and Environmental Applications of Speleothems*.

Roberts, C. N., Woodbridge, J., Palmisano, A., Bevan, A., Fyfe, R., & Shennan, S. (2019). Mediterranean landscape change during the Holocene: Synthesis, comparison and regional trends in population, land cover and climate. *The Holocene*, *29*(5), Article 5. https://doi.org/10.1177/0959683619826697

Rodrigo-Gámiz, M., García-Alix, A., Jiménez-Moreno, G., Ramos-Román, M. J., Camuera, J., Toney, J. L., Sachse, D., Anderson, R. S., & Sinninghe Damsté, J. S. (2022). Paleoclimate reconstruction of the last 36 kyr based on branched glycerol dialkyl glycerol tetraethers in the Padul palaeolake record (Sierra Nevada, southern Iberian Peninsula). *Quaternary Science Reviews*, *281*, 107434. https://doi.org/10.1016/j.quascirev.2022.107434

Rodrigues, T., Grimalt, J. O., Abrantes, F., Naughton, F., & Flores, J.-A. (2010). The last glacial–interglacial transition (LGIT) in the western mid-latitudes of the North Atlantic: Abrupt sea surface temperature change and sea level implications. *Quaternary Science Reviews*, *29*(15-16), Article 15-16. https://doi.org/10.1016/j.quascirev.2010.04.004

Rossi, C., Bajo, P., Lozano, R. P., & Hellstrom, J. (2018). Younger Dryas to Early Holocene paleoclimate in Cantabria (N Spain): Constraints from speleothem Mg, annual fluorescence banding and stable isotope records. *Quaternary Science Reviews*, *192*, 71-85. https://doi.org/10.1016/j.quascirev.2018.05.025

Rossi, C., Mertz-Kraus, R., & Osete, M.-L. (2014). Paleoclimate variability during the Blake geomagnetic excursion (MIS 5d) deduced from a speleothem record. *Quaternary Science Reviews*, *102*, 166-180. https://doi.org/10.1016/j.quascirev.2014.08.007

Rozanski, K., Araguás-Araguás, L., & Gonfiantini, R. (1992). Relation Between Long-Term Trends of Oxygen-18 Isotope Composition of Precipitation and Climate. *Science*, *258*(5084), 981-985. https://doi.org/10.1126/science.258.5084.981

Rozanski, K., Araguás-Araguás, L., & Gonfiantini, R. (1993). Isotopic Patterns in Modern Global Precipitation. En P. K. Swart, K. C. Lohmann, J. Mckenzie, & S. Savin (Eds.), *Geophysical Monograph Series* (pp. 1-36). American Geophysical Union. https://doi.org/10.1029/GM078p0001

Ruan, J., Kherbouche, F., Genty, D., Blamart, D., Cheng, H., Dewilde, F., Hachi, S., Edwards, R. L., Régnier, E., & Michelot, J.-L. (2016). Evidence of a prolonged drought ca. 4200 yr BP correlated with prehistoric settlement abandonment from the Gueldaman GLD1 Cave, Northern Algeria. *Climate of the Past*, *12*(1), Article 1. https://doi.org/10.5194/cp-12-1-2016

Rudzka, D., McDermott, F., Baldini, L. M., Fleitmann, D., Moreno, A., & Stoll, H. (2011). The coupled δ13C-radiocarbon systematics of three Late Glacial/early Holocene speleothems; insights into soil and cave processes at climatic transitions. *Geochimica et Cosmochimica Acta*, *75*(15), Article 15. https://doi.org/10.1016/j.gca.2011.05.022

Sancho, C., Belmonte, Á., Bartolomé, M., Moreno, A., Leunda, M., & López-Martínez, J. (2018). Middle-to-late Holocene palaeoenvironmental reconstruction from the A294 ice-cave record (Central Pyrenees, northern Spain). *Earth and Planetary Science Letters*, *484*, 135-144. https://doi.org/10.1016/j.epsl.2017.12.027

Scholz, D., & Hoffmann, D. L. (2011). StalAge – An algorithm designed for construction of speleothem age models. *Quaternary Geochronology*, *6*(3-4), Article 3-4. https://doi.org/10.1016/j.quageo.2011.02.002

Schwarcz, H. P. (1986). Chapter 7—GEOCHRONOLOGY AND ISOTOPIC GEOCHEMISTRY OF SPELEOTHEMS. En P. Fritz & J. Ch. Fontes (Eds.), *The Terrestrial Environment, B* (pp. 271-303). Elsevier. https://doi.org/10.1016/B978-0-444-42225-5.50012-7

Schwarcz, H. P., Harmon, R. S., Thompson, P., & Ford, D. C. (1976). Stable isotope studies of fluid inclusions in speleothems and their paleoclimatic significance. *Geochimica et Cosmochimica Acta*, *40*(6), Article 6. https://doi.org/10.1016/0016-7037(76)90111-3

Seierstad, I. K., Abbott, P. M., Bigler, M., Blunier, T., Bourne, A. J., Brook, E., Buchardt, S. L., Buizert, C., Clausen, H. B., Cook, E., Dahl-Jensen, D., Davies, S. M., Guillevic, M., Johnsen, S. J., Pedersen, D. S., Popp, T. J., Rasmussen, S. O., Severinghaus, J. P., Svensson, A., & Vinther, B. M. (2014). Consistently dated records from the Greenland GRIP, GISP2 and NGRIP ice cores for the past 104 ka reveal regional millennial-scale δ18O gradients with possible Heinrich event imprint. *Quaternary Science Reviews*, *106*, 29-46. https://doi.org/10.1016/j.quascirev.2014.10.032

Severinghaus, J. P., & Brook, E. J. (1999). Abrupt Climate Change at the End of the Last Glacial Period Inferred from Trapped Air in Polar Ice. *Science*, *286*(5441), Article 5441. https://doi.org/10.1126/science.286.5441.930

Shah, A. M., Morrill, C., Gille, E. P., Gross, W. S., Anderson, D. M., Bauer, B. A., Buckner, R., & Hartman, M. (2013). Global Speleothem Oxygen Isotope Measurements Since the Last Glacial Maximum. *Dataset Papers in Geosciences*, *2013*, 1-9. https://doi.org/10.7167/2013/548048

Shakun, J. D., Clark, P. U., He, F., Marcott, S. A., Mix, A. C., Liu, Z., Otto-Bliesner, B., Schmittner, A., & Bard, E. (2012). Global warming preceded by increasing carbon dioxide concentrations during the last deglaciation. *Nature*, *484*(7392), Article 7392. https://doi.org/10.1038/nature10915

Sierro, F. J., Hodell, D. A., Curtis, J. H., Flores, J. A., Reguera, I., Colmenero-Hidalgo, E., Bárcena, M. A., Grimalt, J. O., Cacho, I., Frigola, J., & Canals, M. (2005). Impact of iceberg melting on Mediterranean thermohaline circulation during Heinrich events: IMPACT OF ICEBERG MELTING ON THE MEDITERRANEAN. *Paleoceanography*, *20*(2), Article 2. https://doi.org/10.1029/2004PA001051

Skinner, L. C., Fallon, S., Waelbroeck, C., Michel, E., & Barker, S. (2010). Ventilation of the Deep Southern Ocean and Deglacial CO$_2$ Rise. *Science*, *328*(5982), Article 5982. https://doi.org/10.1126/science.1183627

Skinner, L. C., & Shackleton, N. J. (2006). Deconstructing Terminations I and II: Revisiting the glacioeustatic paradigm based on deep-water temperature estimates. *Quaternary Science Reviews*, *25*(23-24), Article 23-24. https://doi.org/10.1016/j.quascirev.2006.07.005

Sliwinski, J. T., Kost, O., Endres, L., Iglesias, M., Haghipour, N., González-Lemos, S., & Stoll, H. M. (2023). Exploring soluble and colloidally transported trace elements in stalagmites: The strontium-yttrium connection. *Geochimica et Cosmochimica Acta*, *343*, 64-83. https://doi.org/10.1016/j.gca.2022.12.023

Smart, P. L., & Friederich, H. (1987). Water movement and storage in the unsaturated zone of a maturely karstified carbonate aquifer. *Proceedings of the conference on Environmenatl Problems in Karst Terranes and their Solutions, Dublin, Ohio*, 59-87.

Smith, A. C., Wynn, P. M., Barker, P. A., Leng, M. J., Noble, S. R., & Tych, W. (2016). North Atlantic forcing of moisture delivery to Europe throughout the Holocene. *Scientific Reports*, *6*(1), Article 1. https://doi.org/10.1038/srep24745

Speranza, A., van Geel, B., & van der Plicht, J. (2003). Evidence for solar forcing of climate change at ca. 850 cal BC from a Czech peat sequence. *Global and Planetary Change*, *35*(1-2), Article 1-2. https://doi.org/10.1016/S0921-8181(02)00091-7

Spötl, C. (2011). Long-term performance of the Gasbench isotope ratio mass spectrometry system for the stable isotope analysis of carbonate microsamples. *Rapid Communications in Mass Spectrometry*, *25*(11), Article 11. https://doi.org/10.1002/rcm.5037

Spötl, C., Fairchild, I. J., & Tooth, A. F. (2005). Cave air control on dripwater geochemistry, Obir Caves (Austria): Implications for speleothem deposition in dynamically ventilated caves. *Geochimica et Cosmochimica Acta*, *69*(10), 2451-2468. https://doi.org/10.1016/j.gca.2004.12.009

Spötl, C., & Mangini, A. (2002). Stalagmite from the Austrian Alps reveals Dansgaard–Oeschger events during isotope stage 3: *Earth and Planetary Science Letters*, *203*(1), Article 1. https://doi.org/10.1016/S0012-821X(02)00837-3

Spötl, C., Mangini, A., & Richards, D. A. (2006). Chronology and paleoenvironment of Marine Isotope Stage 3 from two high-elevation speleothems, Austrian Alps. *Quaternary Science Reviews*, *25*(9-10), Article 9-10. https://doi.org/10.1016/j.quascirev.2005.10.006

Spötl, C., Scholz, D., & Mangini, A. (2008). A terrestrial U/Th-dated stable isotope record of the Penultimate Interglacial. *Earth and Planetary Science Letters*, *276*(3-4), Article 3-4. https://doi.org/10.1016/j.epsl.2008.09.029

Staubwasser, M., Sirocko, F., Grootes, P. M., & Segl, M. (2003). Climate change at the 4.2 ka BP termination of the Indus valley civilization and Holocene south Asian monsoon variability: SOUTH ASIAN HOLOCENE CLIMATE CHANGE. *Geophysical Research Letters*, *30*(8). https://doi.org/10.1029/2002GL016822

Stoll, H. M., Cacho, I., Gasson, E., Sliwinski, J., Kost, O., Moreno, A., Iglesias, M., Torner, J., Perez-Mejias, C., Haghipour, N., Cheng, H., & Edwards, R. L. (2022). Rapid northern hemisphere ice sheet melting during the penultimate deglaciation. *Nature Communications*, *13*(1), Article 1. https://doi.org/10.1038/s41467-022-31619-3

Stoll, H. M., Day, C., Lechleitner, F., Kost, O., Endres, L., Sliwinski, J., Pérez-Mejías, C., Cheng, H., & Scholz, D. (2022). *Distinguishing the vegetation and soil component of $\delta^{13}C$ variation in speleothem records from degassing and prior calcite precipitation effects* [Preprint]. Proxy Use-Development-Validation/Terrestrial Archives/Pleistocene. https://doi.org/10.5194/cp-2022-77

Stoll, H. M., Moreno, A., Mendez-Vicente, A., Gonzalez-Lemos, S., Jimenez-Sanchez, M., Dominguez-Cuesta, M. J., Edwards, R. L., Cheng, H., & Wang, X. (2013). Paleoclimate and growth rates of speleothems in the northwestern Iberian Peninsula over the last two glacial cycles. *Quaternary Research*, *80*(02), Article 02. https://doi.org/10.1016/j.yqres.2013.05.002

Stoll, H. M., Müller, W., & Prieto, M. (2012). I-STAL, a model for interpretation of Mg/Ca, Sr/Ca and Ba/Ca variations in speleothems and its forward and inverse application on seasonal to millennial scales: I-STAL SPELEOTHEM TRACE ELEMENT MODEL. *Geochemistry, Geophysics, Geosystems*, *13*(9). https://doi.org/10.1029/2012GC004183

Stoll, H., Mendez-Vicente, A., Gonzalez-Lemos, S., Moreno, A., Cacho, I., Cheng, H., & Edwards, R. L. (2015). Interpretation of orbital scale variability in mid-latitude speleothem $\delta^{18}O$: Significance of growth rate controlled kinetic fractionation effects. *Quaternary Science Reviews*, *127*, 215-228. https://doi.org/10.1016/j.quascirev.2015.08.025

Swindles, G. T., Plunkett, G., & Roe, H. M. (2007). A delayed climatic response to solar forcing at 2800 cal. BP: Multiproxy evidence from three Irish peatlands. *The Holocene*, *17*(2), Article 2. https://doi.org/10.1177/0959683607075830

Tan, L., Shen, C.-C., Cai, Y., Lo, L., Cheng, H., & An, Z. (2014). Trace-element variations in an annually layered stalagmite as recorders of climatic changes and anthropogenic pollution in Central China. *Quaternary Research*, *81*(2), Article 2. https://doi.org/10.1016/j.yqres.2013.12.001

Tang, J., Köhler, S. J., & Dietzel, M. (2008). Sr2+/Ca2+ and $^{44}Ca/^{40}Ca$ fractionation during inorganic calcite formation: I. Sr incorporation. *Geochimica et Cosmochimica Acta*, *72*(15), Article 15. https://doi.org/10.1016/j.gca.2008.05.031

Tang, K., & Feng, X. (2001). The effect of soil hydrology on the oxygen and hydrogen isotopic compositions of plants' source water. *Earth and Planetary Science Letters*.

Tarrats, P., Heiri, O., Valero-Garcés, B., Cañedo-Argüelles, M., Prat, N., Rieradevall, M., & González-Sampériz, P. (2018). Chironomid-inferred Holocene temperature reconstruction in Basa de la Mora Lake (Central Pyrenees). *The Holocene*, *28*(11), Article 11. https://doi.org/10.1177/0959683618788662

Taylor, K. C., Hammer, C. U., Alley, R. B., Clausen, H. B., Dahl-Jensen, D., Gow, A. J., Gundestrup, N. S., Kipfstuh, J., Moore, J. C., & Waddington, E. D. (1993). Electrical conductivity measurements from the GISP2 and GRIP Greenland ice cores. *Nature*, *366*(6455), Article 6455. https://doi.org/10.1038/366549a0

Teller, J. T., Leverington, D. W., & Mann, J. D. (2002). Freshwater outbursts to the oceans from glacial Lake Agassiz and their role in climate change during the last deglaciation. *Quaternary Science Reviews*, *21*(8-9), Article 8-9. https://doi.org/10.1016/S0277-3791(01)00145-7

Tesoriero, A. J., & Pankow, J. F. (1996). Solid solution partitioning of Sr^{2+}, Ba^{2+}, and Cd^{2+} to calcite. *Geochimica et Cosmochimica Acta*, *60*(6), Article 6. https://doi.org/10.1016/0016-7037(95)00449-1

Thatcher, D. L., Wanamaker, A. D., Denniston, R. F., Asmerom, Y., Polyak, V. J., Fullick, D., Ummenhofer, C. C., Gillikin, D. P., & Haws, J. A. (2020). Hydroclimate variability from western Iberia (Portugal) during the Holocene: Insights from a composite stalagmite isotope record. *The Holocene*, *30*(7), Article 7. https://doi.org/10.1177/0959683620908648

Thomas, E. R., Wolff, E. W., Mulvaney, R., Steffensen, J. P., Johnsen, S. J., Arrowsmith, C., White, J. W. C., Vaughn, B., & Popp, T. (2007). The 8.2ka event from Greenland ice cores. *Quaternary Science Reviews*, *26*(1-2), Article 1-2. https://doi.org/10.1016/j.quascirev.2006.07.017

Törnqvist, T. E., & Hijma, M. P. (2012). Links between early Holocene ice-sheet decay, sea-level rise and abrupt climate change. *Nature Geoscience*, *5*(9), Article 9. https://doi.org/10.1038/ngeo1536

Toucanne, S., Zaragosi, S., Bourillet, J. F., Naughton, F., Cremer, M., Eynaud, F., & Dennielou, B. (2008). Activity of the turbidite levees of the Celtic–Armorican margin (Bay of Biscay) during the last 30,000 years: Imprints of the last European deglaciation and Heinrich events. *Marine Geology*, *247*(1-2), Article 1-2. https://doi.org/10.1016/j.margeo.2007.08.006

Treble, P., Chappell, J., Gagan, M., Mckeegan, K., & Harrison, T. (2005). In situ measurement of seasonal δ18O variations and analysis of isotopic trends in a modern speleothem from southwest Australia. *Earth and Planetary Science Letters*, *233*(1-2), Article 1-2. https://doi.org/10.1016/j.epsl.2005.02.013

Treble, P., Shelley, J. M. G., & Chappell, J. (2003). Comparison of high resolution sub-annual records of trace elements in a modern (1911–1992) speleothem with instrumental climate data from southwest Australia. *Earth and Planetary Science Letters*, *216*(1-2), Article 1-2. https://doi.org/10.1016/S0012-821X(03)00504-1

Tremaine, D. M., Froelich, P. N., & Wang, Y. (2011). Speleothem calcite farmed in situ: Modern calibration of δ18O and δ13C paleoclimate proxies in a continuously-monitored natural cave system. *Geochimica et Cosmochimica Acta*, *75*(17), Article 17. https://doi.org/10.1016/j.gca.2011.06.005

Tugend, J., Manatschal, G., Kusznir, N. J., Masini, E., Mohn, G., & Thinon, I. (2014). Formation and deformation of hyperextended rift systems: Insights from rift domain mapping in the Bay of Biscay-Pyrenees. *Tectonics*, *33*(7), Article 7. https://doi.org/10.1002/2014TC003529

Uemura, R., Kina, Y., Shen, C.-C., & Omine, K. (2020). Experimental evaluation of oxygen isotopic exchange between inclusion water and host calcite in speleothems. *Climate of the Past*, *16*(1), Article 1. https://doi.org/10.5194/cp-16-17-2020

Uemura, R., Nakamoto, M., Asami, R., Mishima, S., Gibo, M., Masaka, K., Jin-Ping, C., Wu, C.-C., Chang, Y.-W., & Shen, C.-C. (2016). Precise oxygen and hydrogen isotope determination in nanoliter quantities of speleothem inclusion water by cavity ring-down spectroscopic techniques. *Geochimica et Cosmochimica Acta*, *172*, 159-176. https://doi.org/10.1016/j.gca.2015.09.017

Usoskin, I. G., Solanki, S. K., & Kovaltsov, G. A. (2007). Grand minima and maxima of solar activity: New observational constraints. *Astronomy & Astrophysics*, *471*(1), Article 1. https://doi.org/10.1051/0004-6361:20077704

Van Geel, B., Buurman, J., & Waterbolk, H. T. (1996). Archaeological and palaeoecological indications of an abrupt climate change in The Netherlands, and evidence for climatological teleconnections around 2650 BP. *Journal of Quaternary Science*, *11*(6), Article 6. https://doi.org/10.1002/(SICI)1099-1417(199611/12)11:6<451::AID-JQS275>3.0.CO;2-9

Van Raden, U. J., Colombaroli, D., Gilli, A., Schwander, J., Bernasconi, S. M., Van Leeuwen, J., Leuenberger, M., & Eicher, U. (2013). High-resolution late-glacial chronology for the Gerzensee lake record (Switzerland): δ18O correlation between a Gerzensee-stack and NGRIP. *Palaeogeography, Palaeoclimatology, Palaeoecology*, *391*, 13-24. https://doi.org/10.1016/j.palaeo.2012.05.017

Vansteenberge, S., De Winter, N. J., Sinnesael, M., Verheyden, S., Goderis, S., Van Malderen, S. J. M., Vanhaecke, F., & Claeys, P. (2020). Reconstructing seasonality through stable-isotope and trace-element analyses of the Proserpine stalagmite, Han-sur-Lesse cave, Belgium: Indications for climate-driven changes during the last 400 years. *Climate of the Past*, *16*(1), Article 1. https://doi.org/10.5194/cp-16-141-2020

Vegas, J., Ruiz-Zapata, B., Ortiz, J. E., Galán, L., Torres, T., García-Cortés, Á., Gil-García, M. J., Pérez-González, A., & Gallardo-Millán, J. L. (2010). Identification of arid phases during the last 50 cal. ka BP from the Fuentillejo maar-lacustrine record (Campo de Calatrava Volcanic Field, Spain): ARID PHASES DURING THE LAST 50 KA FROM THE FUENTILLEJO MAAR-LAKE RECORD, SPAIN. *Journal of Quaternary Science*, *25*(7), Article 7. https://doi.org/10.1002/jqs.1262

Vegas-Vilarrúbia, T., González-Sampériz, P., Morellón, M., Gil-Romera, G., Pérez-Sanz, A., & Valero-Garcés, B. (2013). Diatom and vegetation responses to Late Glacial and Early Holocene climate changes at Lake Estanya (Southern Pyrenees, NE Spain). *Palaeogeography, Palaeoclimatology, Palaeoecology*, *392*, 335-349. https://doi.org/10.1016/j.palaeo.2013.09.011

Vesica, P. L., Tuccimei, P., Turi, B., Fornós, J. J., Ginés, A., & Ginés, J. (2000). Late Pleistocene Paleoclimates and sea-level change in the Mediterranean as inferred from stable isotope and U-series studies of overgrowths on speleothems, Mallorca, Spain. *Quaternary Science Reviews*, *19*(9), Article 9. https://doi.org/10.1016/S0277-3791(99)00026-8

Vinther, B. M., Buchardt, S. L., Clausen, H. B., Dahl-Jensen, D., Johnsen, S. J., Fisher, D. A., Koerner, R. M., Raynaud, D., Lipenkov, V., Andersen, K. K., Blunier, T., Rasmussen, S. O., Steffensen, J. P., & Svensson, A. M. (2009). Holocene thinning of the Greenland ice sheet. *Nature*, *461*(7262), Article 7262. https://doi.org/10.1038/nature08355

Voelker, A. H. L., De Abreu, L., Schönfeld, J., Erlenkeuser, H., & Abrantes, F. (2009). Hydrographic conditions along the western Iberian margin during marine isotope stage 2: IBERIAN MARGIN HYDROGRAPHY DURING MIS 2. *Geochemistry, Geophysics, Geosystems*, *10*(12), Article 12. https://doi.org/10.1029/2009GC002605

Von Grafenstein, U., Belmecheri, S., Eicher, U., Van Raden, U. J., Erlenkeuser, H., Andersen, N., & Ammann, B. (2013). The oxygen and carbon isotopic signatures of biogenic carbonates in Gerzensee, Switzerland, during the rapid warming around 14,685years BP and the following interstadial. *Palaeogeography, Palaeoclimatology, Palaeoecology*, *391*, 25-32. https://doi.org/10.1016/j.palaeo.2013.08.018

Vonhof, H. B., van Breukelen, M. R., Postma, O., Rowe, P. J., Atkinson, T. C., & Kroon, D. (2006). A continuous-flow crushing device for on-lineδ2H analysis of fluid inclusion water in speleothems. *Rapid Communications in Mass Spectrometry*, *20*(17), Article 17. https://doi.org/10.1002/rcm.2618

Walczak, I. W., Baldini, J. U. L., Baldini, L. M., McDermott, F., Marsden, S., Standish, C. D., Richards, D. A., Andreo, B., & Slater, J. (2015). Reconstructing high-resolution climate using CT scanning of unsectioned stalagmites: A case study identifying the mid-Holocene onset of the Mediterranean climate in southern Iberia. *Quaternary Science Reviews*, *127*, 117-128. https://doi.org/10.1016/j.quascirev.2015.06.013

Walker, M., Head, M. J., Lowe, J., Berkelhammer, M., BjÖrck, S., Cheng, H., Cwynar, L. C., Fisher, D., Gkinis, V., Long, A., Newnham, R., Rasmussen, S. O., & Weiss, H. (2019). Subdividing the Holocene Series/Epoch: Formalization of stages/ages and subseries/subepochs, and designation of GSSPs and auxiliary stratotypes. *Journal of Quaternary Science*, *34*(3), Article 3. https://doi.org/10.1002/jqs.3097

Wang, S., Ge, Q., Wang, F., Wen, X., & Huang, J. (2013). Abrupt climate changes of Holocene. *Chinese Geographical Science*, *23*(1), 1-12. https://doi.org/10.1007/s11769-013-0591-z

Wang, Y. J., Cheng, H., Edwards, R. L., An, Z. S., Wu, J. Y., Shen, C.-C., & Dorale, J. A. (2001). A High-Resolution Absolute-Dated Late Pleistocene Monsoon Record from Hulu Cave, China. *Science*, *294*(5550), 2345-2348. https://doi.org/10.1126/science.1064618

Wanner, H., Beer, J., Bütikofer, J., Crowley, T. J., Cubasch, U., Flückiger, J., Goosse, H., Grosjean, M., Joos, F., Kaplan, J. O., Küttel, M., Müller, S. A., Prentice, I. C., Solomina, O., Stocker, T. F.,

Tarasov, P., Wagner, M., & Widmann, M. (2008). Mid- to Late Holocene climate change: An overview. *Quaternary Science Reviews*, *27*(19-20), Article 19-20. https://doi.org/10.1016/j.quascirev.2008.06.013

Wanner, H., Solomina, O., Grosjean, M., Ritz, S. P., & Jetel, M. (2011). Structure and origin of Holocene cold events. *Quaternary Science Reviews*, *30*(21-22), Article 21-22. https://doi.org/10.1016/j.quascirev.2011.07.010

Warken, S. F., Fohlmeister, J., Schröder-Ritzrau, A., Constantin, S., Spötl, C., Gerdes, A., Esper, J., Frank, N., Arps, J., Terente, M., Riechelmann, D. F. C., Mangini, A., & Scholz, D. (2018). Reconstruction of late Holocene autumn/winter precipitation variability in SW Romania from a high-resolution speleothem trace element record. *Earth and Planetary Science Letters*, *499*, 122-133. https://doi.org/10.1016/j.epsl.2018.07.027

Webb, M., Dredge, J., Barker, P. A., Müller, W., Jex, C., Desmarchelier, J., Hellstrom, J., & Wynn, P. M. (2014). Quaternary climatic instability in south-east Australia from a multi-proxy speleothem record: Quaternary CLIMATIC INSTABILITY IN SE AUSTRALIA. *Journal of Quaternary Science*, *29*(6), Article 6. https://doi.org/10.1002/jqs.2734

Weiss, H., & Bradley, R. S. (2001). What Drives Societal Collapse? *Science*, *291*(5504), 609-610. https://doi.org/10.1126/science.1058775

Weiss, H., Courty, M.-A., Wetterstrom, W., Guichard, F., Senior, L., Meadow, R., & Curnow, A. (1993). The Genesis and Collapse of Third Millennium North Mesopotamian Civilization. *Science*, *261*(5124), 995-1004. https://doi.org/10.1126/science.261.5124.995

Weissbach, T., Kluge, T., Affolter, S., Leuenberger, M. C., Vonhof, H., Riechelmann, D. F. C., Fohlmeister, J., Juhl, M.-C., Hemmer, B., Wu, Y., Warken, S. F., Schmidt, M., Frank, N., & Aeschbach, W. (2023). Constraints for precise and accurate fluid inclusion stable isotope analysis using water-vapour saturated CRDS techniques. *Chemical Geology*, *617*, 121268. https://doi.org/10.1016/j.chemgeo.2022.121268

Wilcox, P. S., Honiat, C., Trüssel, M., Edwards, R. L., & Spötl, C. (2020). Exceptional warmth and climate instability occurred in the European Alps during the Last Interglacial period. *Communications Earth & Environment*, *1*(1), Article 1. https://doi.org/10.1038/s43247-020-00063-w

Williams, P. W., King, D. N. T., Zhao, J.-X., & Collerson, K. D. (2005). Late Pleistocene to Holocene composite speleothem 18O and 13C chronologies from South Island, New Zealand—Did a global Younger Dryas really exist? *Earth and Planetary Science Letters*, *230*(3-4), Article 3-4. https://doi.org/10.1016/j.epsl.2004.10.024

Wirth, S. B., Glur, L., Gilli, A., & Anselmetti, F. S. (2013). Holocene flood frequency across the Central Alps – solar forcing and evidence for variations in North Atlantic atmospheric circulation. *Quaternary Science Reviews*, *80*, 112-128. https://doi.org/10.1016/j.quascirev.2013.09.002

Wong, C. I., & Breecker, D. O. (2015). Advancements in the use of speleothems as climate archives. *Quaternary Science Reviews*, *127*, 1-18. https://doi.org/10.1016/j.quascirev.2015.07.019

Woodhead, J., & Pickering, R. (2012). Beyond 500 ka: Progress and prospects in the U Pb chronology of speleothems, and their application to studies in palaeoclimate, human evolution, biodiversity and tectonics. *Chemical Geology*, *322-323*, 290-299. https://doi.org/10.1016/j.chemgeo.2012.06.017

Yuan, D., Cheng, H., Edwards, R. L., Dykoski, C. A., Kelly, M. J., Zhang, M., Qing, J., Lin, Y., Wang, Y., Wu, J., Dorale, J. A., An, Z., & Cai, Y. (2004). Timing, Duration, and Transitions of the Last Interglacial Asian Monsoon. *Science*, *304*(5670), Article 5670. https://doi.org/10.1126/science.1091220

Zanchetta, G., Drysdale, R. N., Hellstrom, J. C., Fallick, A. E., Isola, I., Gagan, M. K., & Pareschi, M. T. (2007). Enhanced rainfall in the Western Mediterranean during deposition of sapropel S1: Stalagmite evidence from Corchia cave (Central Italy). *Quaternary Science Reviews*, *26*(3-4), Article 3-4. https://doi.org/10.1016/j.quascirev.2006.12.003

Zielhofer, C., Fletcher, W. J., Mischke, S., De Batist, M., Campbell, J. F. E., Joannin, S., Tjallingii, R., El Hamouti, N., Junginger, A., Stele, A., Bussmann, J., Schneider, B., Lauer, T., Spitzer, K., Strupler, M., Brachert, T., & Mikdad, A. (2017). Atlantic forcing of Western Mediterranean winter rain minima during the last 12,000 years. *Quaternary Science Reviews*, *157*, 29-51. https://doi.org/10.1016/j.quascirev.2016.11.037

References

Zielhofer, C., Köhler, A., Mischke, S., Benkaddour, A., Mikdad, A., & Fletcher, W. J. (2019). Western Mediterranean hydro-climatic consequences of Holocene ice-rafted debris (Bond) events. *Climate of the Past*, *15*(2), Article 2. https://doi.org/10.5194/cp-15-463-2019